Directional seismic source signature deconvolution

Roberts, Gordon Anthony

Directional Seismic Source Signature Deconvolution

by

Gordon Anthony Roberts

A thesis submitted in partial fulfilment
of the requirements for the degree of
Doctor of Philosophy

Department of Geological Sciences

The University of Durham
1989

Abstract

Directional Seismic Source Signature Deconvolution
by
Gordon Anthony Roberts

Marine seismic source arrays are directional. Source directivity is used to attenuate coherent noise, but primary reflected data may be degraded. Source directivity is ignored in a standard processing sequence, so directional source signature deconvolution may be required.

In the frequency-wavenumber (f-k) directional deconvolution method, a filter is calculated from far-field source signatures and is applied to the f-k transform of common-receiver gathers. Reflections on common-receiver gathers are often spatially aliased, and this causes practical problems with the technique.

Directional deconvolution may also be performed in combination with prestack migration because the prestack Kirchhoff summation migration operator is a function of source take-off angle. The constant-offset section is deconvolved separately with a full range of filters for source signatures radiated in different directions; then the migration summation operator sums across the deconvolved sections, selecting the section which has been deconvolved for the correct source signature at each point.

Physical model data, which were acquired over simple models using a directional source, are used to evaluate directional deconvolution assuming constant velocity. Reflector continuity and resolution are improved by using directional deconvolution.

Directional deconvolution combined with prestack migration is extended to media in which the velocity varies with depth, and is applied to two datasets from the Southern North Sea. The second dataset, which has shallow steeply dipping reflectors, is improved by using directional deconvolution. Directional deconvolution may be combined with a Kirchhoff migration technique which assumes a linear velocity-depth model. Results are superior to conventional Kirchhoff migration because ray bending is honoured.

Directional deconvolution cannot synthesise fully point-source equivalent data from data acquired with a source array without excessive noise amplification. Source arrays with a short in-line dimension should be used where possible. For data which have been acquired with a long source array, directional deconvolution is desirable.

Acknowledgements

I cannot possibly acknowledge by name everyone who has influenced the progress of this thesis. To those I have omitted, I apologise.

Firstly I would like to thank my supervisor Neil Goulty. This work would never have been completed without his depth of understanding, enthusiasm and guidance.

I would also like to thank those in the department who have helped: the computer gurus, both past and present (Adrian Bowen, Dave Stevenson, Mike Smith, and Stefan Thatcher), for their subroutines; my room mates (Tracey, Joao, Samsudin and Stuart), for putting up with me; and the technicians, led by Dave Asbery, for their willingness to help.

Horizon Exploration Ltd and Merlin Geophysical both gave their valuable time and data; particular thanks are due to Mike Hall (Horizon) and to Mark Loveridge (Merlin).

I acknowledge the financial support of NERC who gave me enough money to live on and to conduct research for three years.

Finally, thanks to my family and friends, who are an important part of my life. Particular thanks are due to my grandfather, Professor R.D.Preston FRS, for setting a fine example and for always encouraging my studies. Special thanks to my proof-reader, my wife Chris, with whom the future lies.

Contents

Chapter I

Seismic Source Directivity

1.1 Introduction

In a uniform medium only a spherically symmetrical source will radiate the same waveform in all directions. In practice, all marine seismic sources are directional. Their directivity is due to the use of arrays of source elements and to the free surface 'ghost' effect. Simple array theory can be used to calculate directivity for non-interacting source elements. For airgun arrays source interactions between the individual airguns must be considered. Directivity may be used to attenuate coherent noise, but may also have adverse effects on the data. The effects of directivity are not considered in a standard processing sequence.

1.2 Directivity

1.2.1 Simple source arrays

For a point source in an infinite isotropic medium there will be no directivity. In reflection seismology this will never be the case due to the surface 'ghost' and to the use of spatial source arrays. In order to demonstrate directivity effects, two simple source arrays will be considered: one horizontal and the other vertical. Each array consists of a pair of identical point oscillators with angular frequency ω separated by a distance d. Directivity effects in the 'far-field' will be examined. 'Far-field' implies that distances are great compared to the size of the array. Sources can thus be treated as radiating plane-waves, so only time delays between sources need be considered. The calculated signatures will be normalised to remove absolute amplitude effects.

The horizontal array is shown in figure 1.1.a. The signal measured in the far-field at a take-off angle from the source ϕ in the vertical plane containing both source positions will be proportional to D_h, given by

$$D_h = \cos(\omega(t+\tau)) + \cos(\omega(t-\tau))$$

$$= 2\cos\omega\tau\cos\omega t$$

where τ is the time delay of an arrival from an individual source relative to the arrival time from the centre of the array, given by

$$\tau = \frac{d\sin\phi}{2V}$$

and V is velocity. The angular frequency ω and the velocity V are related by

$$V = \frac{\omega\lambda}{2\pi} = \frac{\omega}{2\pi k}$$

where λ is the wavelength and k the wavenumber.

Let k_x be the horizontal wavenumber:

$$k_x = k\sin\phi$$

Then the measured signal may be written as

$$D_h = 2\cos\pi d k_x \cos\omega t \qquad 1.1$$

Thus the directivity of the horizontal array is a simple function of the horizontal wavenumber.

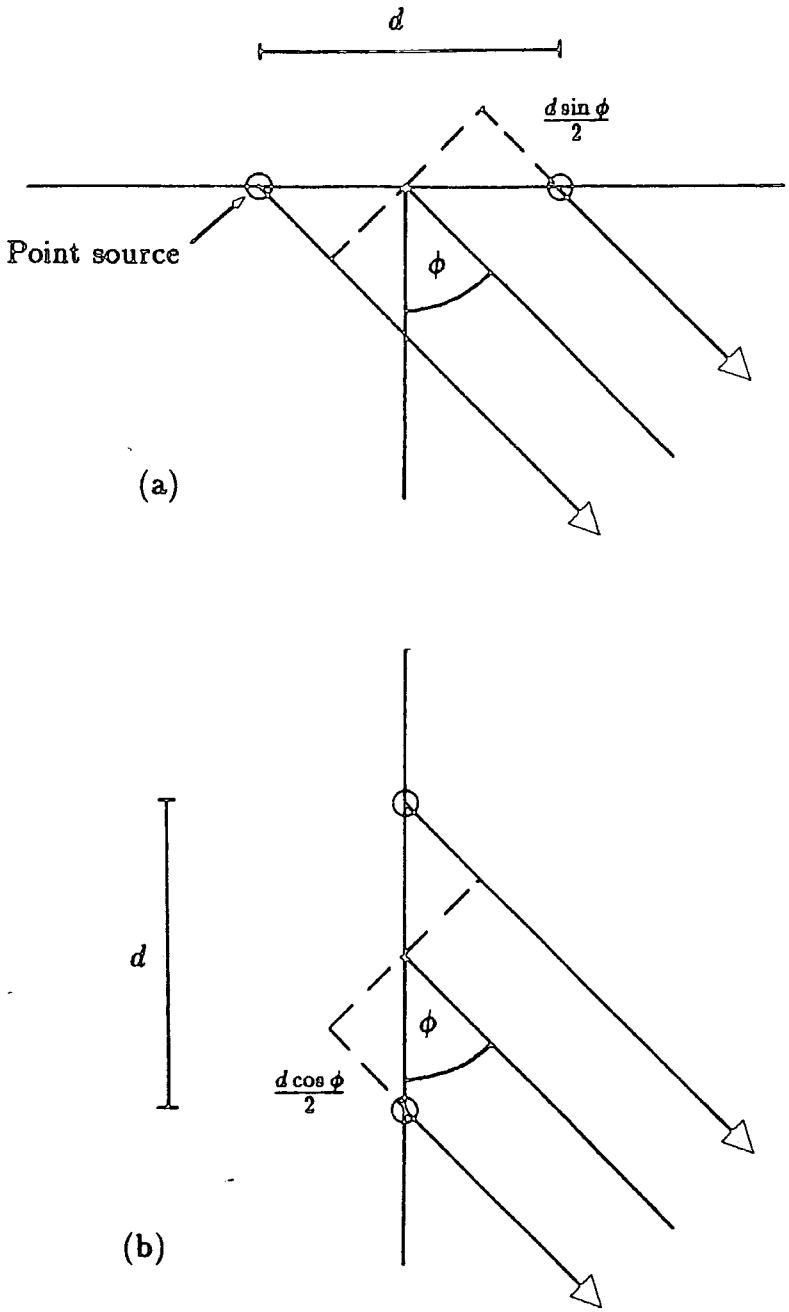

Figure 1.1. Arrays of two point sources, (a) horizontal and (b) vertical.

The vertical source array is shown in figure 1.1.b. The signal measured at a take-off angle ϕ will be D_v, given by

$$D_v = \cos(\omega(t+\tau)) + \cos(\omega(t-\tau))$$

$$= 2\cos\omega\tau\cos\omega t$$

where τ, the time delay relative to the centre of the array, is now

$$\tau = \frac{d\cos\phi}{2V}$$

Thus the measured signal is

$$D_v = 2\cos\pi d k_z \cos\omega t$$

The horizontal and vertical wavenumbers are related as follows:

$$k^2 = k_x^2 + k_z^2 = \left(\frac{\omega}{2\pi V}\right)^2$$

Therefore the measured directivity is

$$D_v = 2\cos\pi d\sqrt{\left(\frac{\omega}{2\pi V}\right)^2 - {k_x}^2}\cos\omega t \qquad 1.2$$

Thus the directivity of the vertical array is not a function of horizontal wavenumber alone because the angular frequency ω also appears in the amplitude of the measured signal.

These two results (1.1 and 1.2) demonstrate that even simple source arrays are directional. A more general solution is needed for arrays of more than two elements.

1.2.2 Source arrays

Equation 1.1 gives the directivity for an in-line source array with two identical point sources. It may be extended to an in-line source array of N identical point sources, spaced equal distances apart, giving the directivity function (Waters, 1978)

$$\frac{\sin\frac{N\gamma}{2}}{sin\frac{\gamma}{2}} \qquad 1.3$$

where

$$\gamma = \frac{\omega b \sin\phi}{V} = 2\pi b k_x$$

N is the number of elements in the array, and

b is the separation of individual elements.

Destructive interference occurs when

$$\sin\frac{N\gamma}{2} = 0$$

This causes notches in the wavenumber spectrum. The first notch will occur when

$$\frac{N\gamma}{2} = \pi$$

i.e.

$$Nbk_x = 1$$

As an example, if the array consists of 8 point sources spaced evenly over 50 m,

$$b = \frac{50}{7}\,\mathrm{m}$$

and

$$N = 8$$

Therefore

$$k_x = 0.0175\,\mathrm{m}^{-1}$$

Result 1.3 can be extended to include non-identical sources and uneven spacing of elements of the array. Provided that the individual sources are at the same depth, the directivity function can still be expressed as a function of the horizontal wavenumber variable only. This gives added flexibility in array design to pass certain parts of the wavenumber spectrum and to suppress other parts.

Using this simple model of linear superposition it is possible to calculate the actual source signatures at all take-off angles, given the signatures of the individual elements and the layout of the array.

When airgun sources are fired simultaneously near to each other, their bubbles interact. Because of this interaction, linear superposition is not adequate for the calculation of airgun array signatures and an extension to the method must be used (Ziolkowski et al., 1982). This involves calculating 'notional' signatures from each element in the airgun array, which may then be superimposed exactly as the individual signatures from non-interacting elements.

1.2.3 The 'ghost'

'Ghost' reflections (Lindsey, 1960) are caused by the large acoustic impedance discontinuity at the air-water interface. Equation 1.2 may be modified to give

the directivity resulting from the ghost effect. For a perfect free surface, the ghost is a negative virtual image at a distance $2z_s$ above the source, where z_s is the depth of the source below the surface. The signature measured at an angle ϕ will be given by

$$\cos\left(\omega(t+\tau)\right) - \cos\left(\omega(t-\tau)\right)$$

where

$$\tau = \frac{z_s \cos\phi}{V}$$

Following the derivation of equation 1.2, directivity due to the ghost may be written as

$$2\sin 2\pi z_s \sqrt{\left(\frac{\omega}{2\pi V}\right)^2 - {k_x}^2}\,\sin\omega t \qquad 1.4$$

The above derivation assumes a surface reflection coefficient of -1. This is an over simplification because energy breaks through the surface; the surface is not planar (especially in bad weather !); and air bubbles are present in the near surface. Loveridge (1985) considered these effects, and concluded that the resulting lower surface reflection coefficient will cause notches in the wavenumber spectra to be shallower. This will be seen to be beneficial when deconvolution is considered.

1.2.4 Variation of source signature with source take-off angle

Typical marine seismic data will thus have source directivity due to the ghost and to the use of arrays. This will manifest itself as a variation in source signature with take-off angle from the source. The main features will be a decrease in signature amplitude and a loss of high frequencies with increasing take-off angle

from the vertical. Results of modelling by Loveridge et al.(1984) are shown in figure 1.2.

Additional directivity will result from the use of receiver arrays. This thesis will concentrate principally on source directivity because source arrays tend to have a longer in-line dimension than receiver arrays and hence are more directional. The techniques developed could equally be applied to receiver directivity.

The surface ghost will always be present in marine seismic data. Source arrays are, however, optional. The reasons for their use will be examined in the next section.

1.3 Reasons for the deployment of source arrays

Source arrays have been used since the earliest days of seismic exploration. There are two main reasons for their deployment: suppression of noise and signature optimisation.

1.3.1 Suppression of noise

Seismic data are contaminated with noise of many types. Noise suppression is a subject which has been much studied (e.g. Larner et al., 1983). Examples of marine seismic noise are tow (mechanical) noise, guided waves, multiples in the water layer and scattering of energy from sea-bottom diffractors, both in and out of the recording plane. Much of this noise is coherent in that there is a 'systematic phase relationship between adjacent traces' (Sheriff, 1984). The apparent velocity of these coherent noise arrivals is usually different from that of primary reflected energy. This has lead to the design of arrays to attenuate the noise by careful tailoring of the notches in the wavenumber spectra. An additional benefit of directive arrays is that a larger part of the available acoustic power is directed towards the target (Safar, 1985).

In order to attenuate side-scattered noise, cross-line arrays are needed, and to attenuate noise in all directions, areal arrays. Lynn and Larner (1989) report

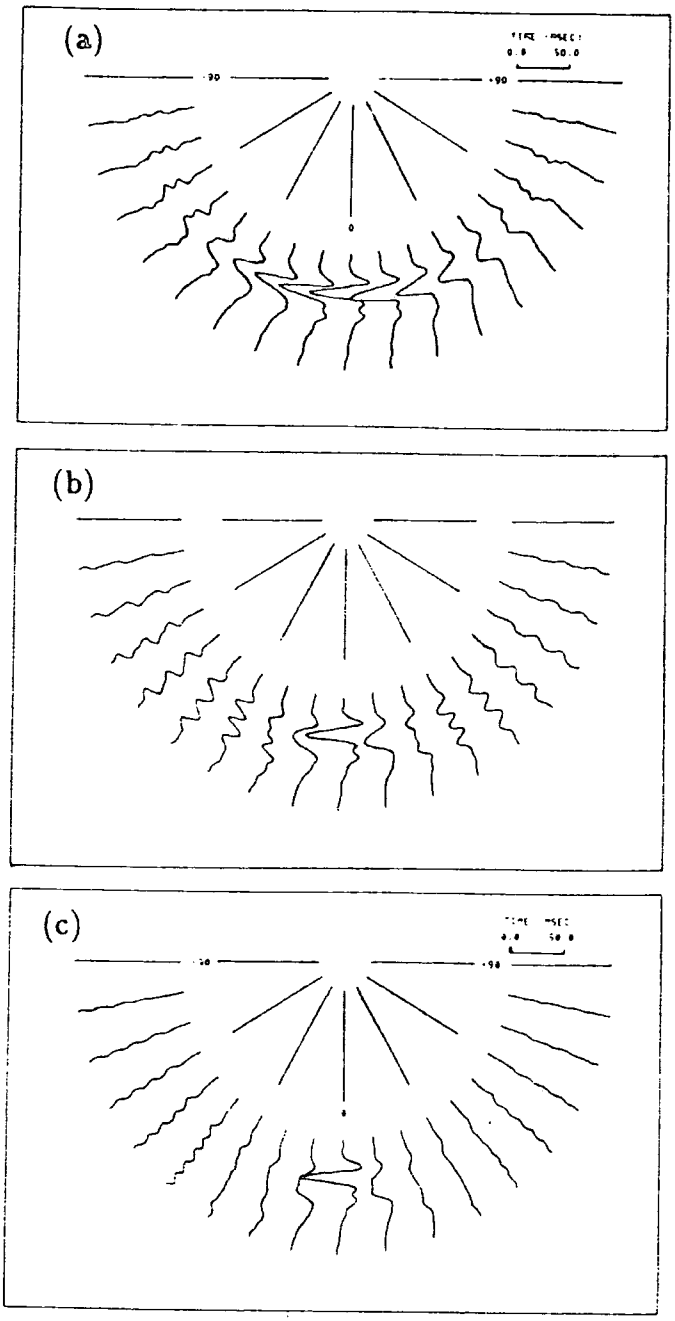

Figure 1.2. Variation of source signature with take-off angle, for airgun source arrays with an in-line dimension of, (a) 40m, (b) 110m and (c) 170m. (Loveridge et al., 1984).

that the CMP process itself is efficient in attenuating scattered noise from outside the recording plane, so that arrays with a large cross-line dimension need only be used in areas where out-of-plane noise is a major problem.

In the late 1970s 'super-long ' arrays (Ursin, 1978) became fashionable in an attempt to attenuate greatly energy leaving the source at large take-off angles from the vertical, because this generates much of the noise. In section 1.4 it will be shown that primary data are affected adversely for such a directive source. Today the trend is towards much shorter arrays, which exhibit less directivity.

For data acquired on land, source arrays are used for a similar purpose: to attenuate ground roll. 'Noise spreads' are shot prior to the survey to determine the dominant characteristics of the noise.

1.3.2 Signature optimisation

Airguns are the most popular marine energy source because of their reliability and signature repeatability. Single airguns have signatures which are far from ideal because bubble pulses follow the main energy peak. The period of the bubble pulse depends on the airgun size. To suppress these bubble pulses, arrays are designed with guns of different sizes so that the bubble pulses destructively interfere (Giles and Johnston, 1973). To further tune the array, the spread of bubble pulse periods may be increased by placing certain guns just close enough for their bubble pulses to coalesce (Safar, 1976).

Waterguns do not suffer from the bubble pulse problem because energy is concentrated in a sharp peak (Tree at al., 1986).

Thus arrays perform two important roles in data acquisition. They can be tuned to give directivity and to optimise source signatures. If primary reflected data are affected by directivity, this must be considered when arrays are used.

1.4 The effects of source directivity on primary data

As discussed in section 1.2.2, arrays cause notches in the wavenumber spectrum and this may be used to attenuate coherent noise. If some of the primary reflected energy falls within these notches it will also be attenuated. A schematic frequency-wavenumber plot of a common-receiver gather is shown in figure 1.3. The source array response is also shown. The reasons for considering a common-receiver gather will be explained in chapter II. Much of the noise energy falls within the array notch and is thus attenuated. At lower apparent velocities, primary reflected signal also falls within the notch and is attenuated. Apparent velocity is given by

$$V_{apparent} = \frac{f}{k_x} = \frac{V}{\sin\phi} \qquad 1.5$$

As the apparent velocity of the reflected arrivals decreases, so more of the high frequency energy is attenuated. The effect that this has on the source signatures is shown in figure 1.2. As the take-off angle from the source increases, more of the high frequencies are lost, leaving lower frequency signatures.

For directivity effects to be evident in primary reflected data, arrivals originating from large take-off angles from the source must be present. Loveridge (1985) has used model and real datasets to assess the directivity effect. His conclusions are summarised below.

- Directivity effects are dependent on reflector geometry. For a plane-layered earth, the effects of directivity will be negligble for most data except for shallow reflectors. In the presence of dip, the source take-off angles will increase or decrease depending on whether the shooting is in the up- or down-dip direction, respectively. Directivity could have an important effect on the data in the former case.

- Directivity is dependent on the length of the source array (figure 1.2). Data

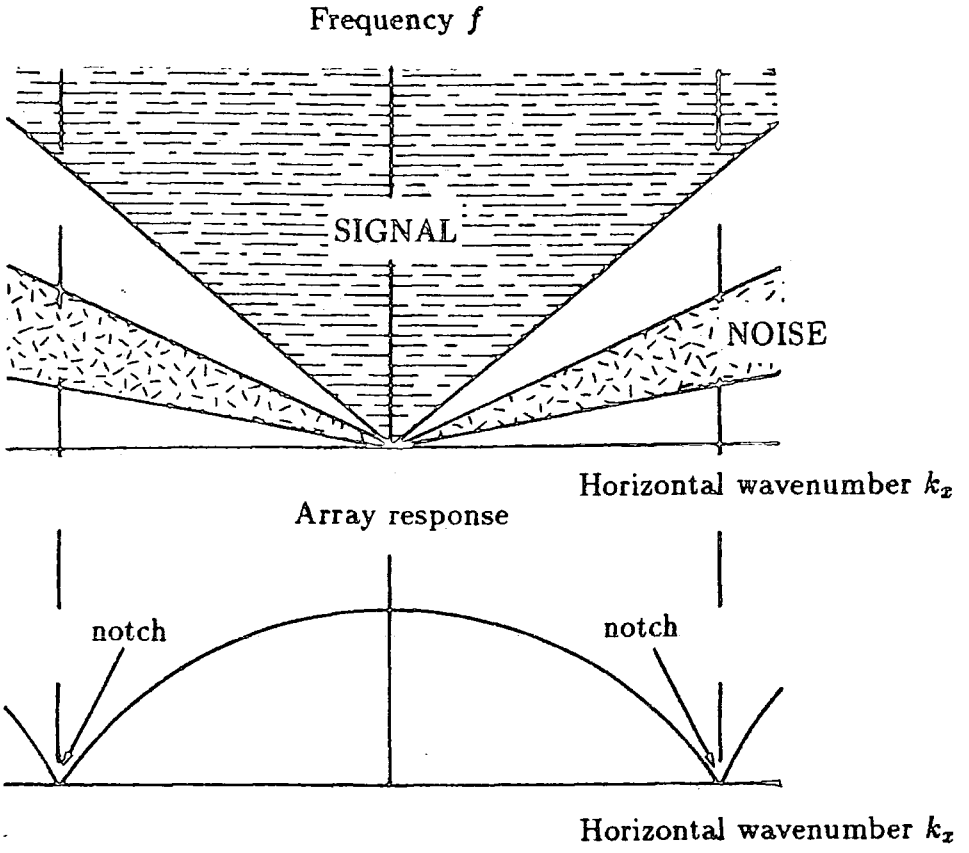

Figure 1.3. Schematic f-k plot of a common-receiver gather and source array response.

acquired with 'super-long' arrays (Ursin, 1978) will exhibit directivity effects at typical target traveltimes for horizontal reflectors.

- Directivity effects are less important if there is anelastic absorption of the propagating seismic energy, because absorption is greater for higher frequencies. As directivity is most evident at high frequencies, this will reduce the effect.

- Critical reflection at the sea floor limits the take-off angle from the source at which a ray can penetrate the sea bed. For a high-velocity sea bed, energy from large source take-off angles will be totally internally reflected within the sea-water layer. Thus directivity effects will be minimal in the primary reflected signal from below the sea bed.

The effect of source directivity on real data is illustrated by Brummitt (1989). A dataset was acquired with two source arrays of different in-line dimensions. Other acquisition parameters were identical. The dataset acquired with the longer array is of lower resolution at intermediate and long source-receiver offsets.

In summary, for the majority of seismic reflection data directivity may not be a great problem. However, in some cases primary reflections will display directivity effects. Standard seismic processing assumes a point source model, and this model will be incorrect for directional data.

1.5 Seismic processing of directional data

Figure 1.4 shows a typical processing sequence. The following processes are those whose efficacy will be affected by source directivity: signature deconvolution, predictive deconvolution, velocity analysis and CMP stacking.

1.5.1 Signature deconvolution

Deterministic signature deconvolution (Robinson and Treitel, 1980) can be used when the source signature is known. Calculation of such a shaping filter

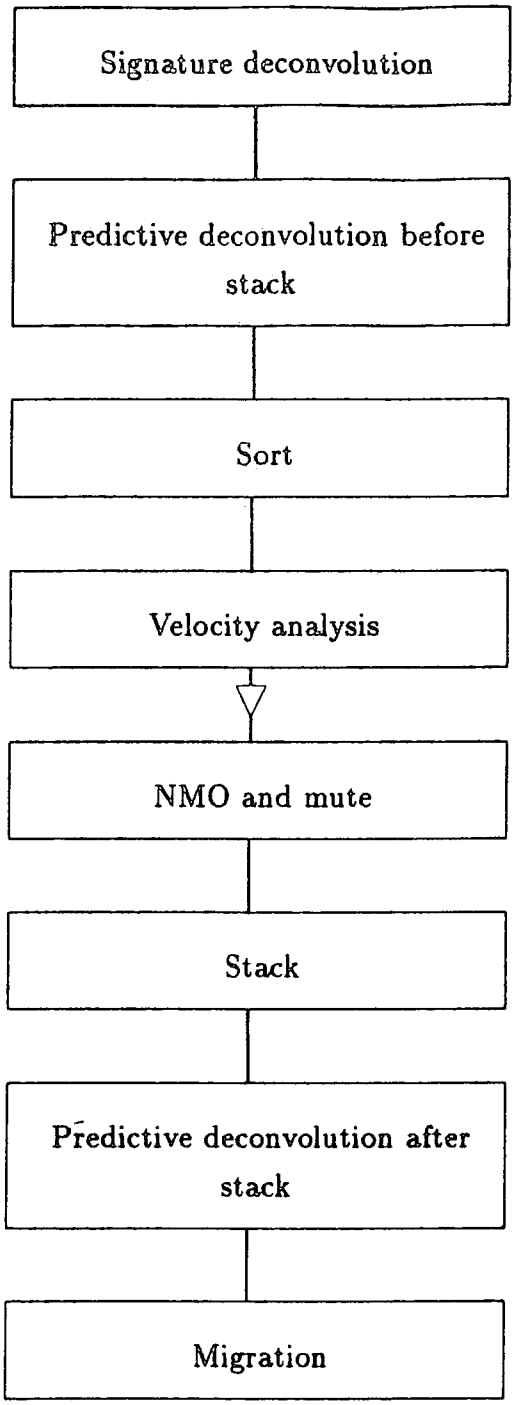

Figure 1.4. Simple seismic processing sequence.

requires an input wavelet and a desired output wavelet. When designing the filter, the energy difference between the desired and actual outputs is minimised to give the optimum filter of some chosen length.

Signature deconvolution is often used to compress the long signature of an airgun source to a shorter minimum-phase or zero-phase wavelet. The far-field source signature is read from a catalogue of calculated or measured far-field signatures, but recently has been calculated from field measurements. This involves making near-field measurements using hydrophones within the source array and subsequently calculating the far-field signatures. Because of interference between sources, simple linear superposition is not adequate for this task for airgun arrays, and the technique of calculating 'notional' signatures must be used (Ziolkowski et al., 1982). If this is done for every shot, the quality control of the calculated source signature is excellent, but filter design becomes very time consuming. Dragoset et al.(1987) have studied the effect of airgun source instabilities on calculated and measured source signatures. Possible causes of source instability include changes in gun positions, firing times and pressures, gun failures and scattering from the fluctuating rough ocean surface. They report that the far-field signature only changes significantly if there is a gun dropout. For other possible instabilities, the signature does not change enough to affect the performance of signature deconvolution. Thus the expensive process of continuous signature monitoring and filter update is not usually necessary. The far-field signature, and corresponding deconvolution filter, need only be calculated once for a particular source array, as long as shooting ceases if there is gun dropout.

Signature deconvolution may also be used as a de-ghosting filter (Jovanovich et al., 1983). The ghost may be calculated approximately if the source depth and sea conditions are known. Deconvolution will be unable to fully restore frequencies in the notch.

Conventional (1-D) signature deconvolution does not take directivity into account. The filter is designed using the vertically travelling, or near-vertically

travelling, signature as an input wavelet. Loveridge et al.(1984) show that such a filter does not perform well for large take-off angles, i.e. when the signature to be deconvolved differs significantly from the input wavelet used to design the filter (figure 1.5).

1.5.2 Predictive deconvolution

Predictive deconvolution (Peacock and Treitel, 1969) is used universally to broaden the frequency spectrum and to attenuate multiples. It is very robust, even though some of the assumptions implicit in its use are often violated (Jurkevics and Wiggins, 1984). One assumption is that the source waveform does not change with time. This is not true for data acquired with a directional source, as a single seismic trace consists of arrivals originating from different take-off angles at the source (figure 1.6).

A more familiar cause of nonstationarity is the attenuation of high frequencies by the earth (Yilmaz, 1987). This causes arrivals later in the record to be deficient in high frequencies. Thus, over any window in the seismic trace, arrivals differ in amplitude and spectral shape. As a result, the estimate of the wavelet from the auto-correlation function of the data in the window is not representative of the entire window. This leads to poor performance of the deconvolution. Small deconvolution windows may be used to reduce nonstationarity within each window, but small windows reduce the reliability of estimates of the coefficients in the auto-correlation function at long lags. Even if small windows are used, spectral whitening will not be the same over the whole record due to the absence of high frequencies at later traveltimes. This problem has lead to the development of inverse-Q filters (Hale, 1982).

Nonstationarity is also a problem for directional data. For a horizontally stratified medium, earlier arrivals will be deficient in high frequencies because of their larger source take-off angles. The situation will be further complicated in the presence of dipping reflectors. The degree of nonstationarity will depend on

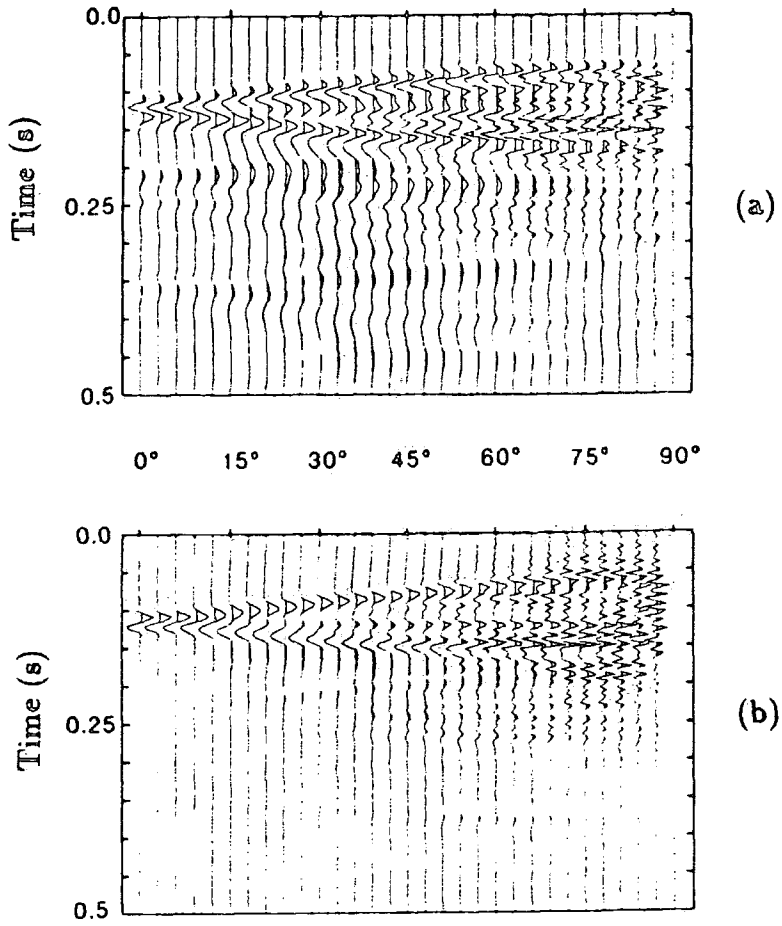

Figure 1.5. Variation of source signature with take-off angle for a 100m array. (a) Raw signatures. (b) After signature deconvolution using a filter designed for the vertically travelling signature. Traces are individually scaled. (Loveridge et al., 1984).

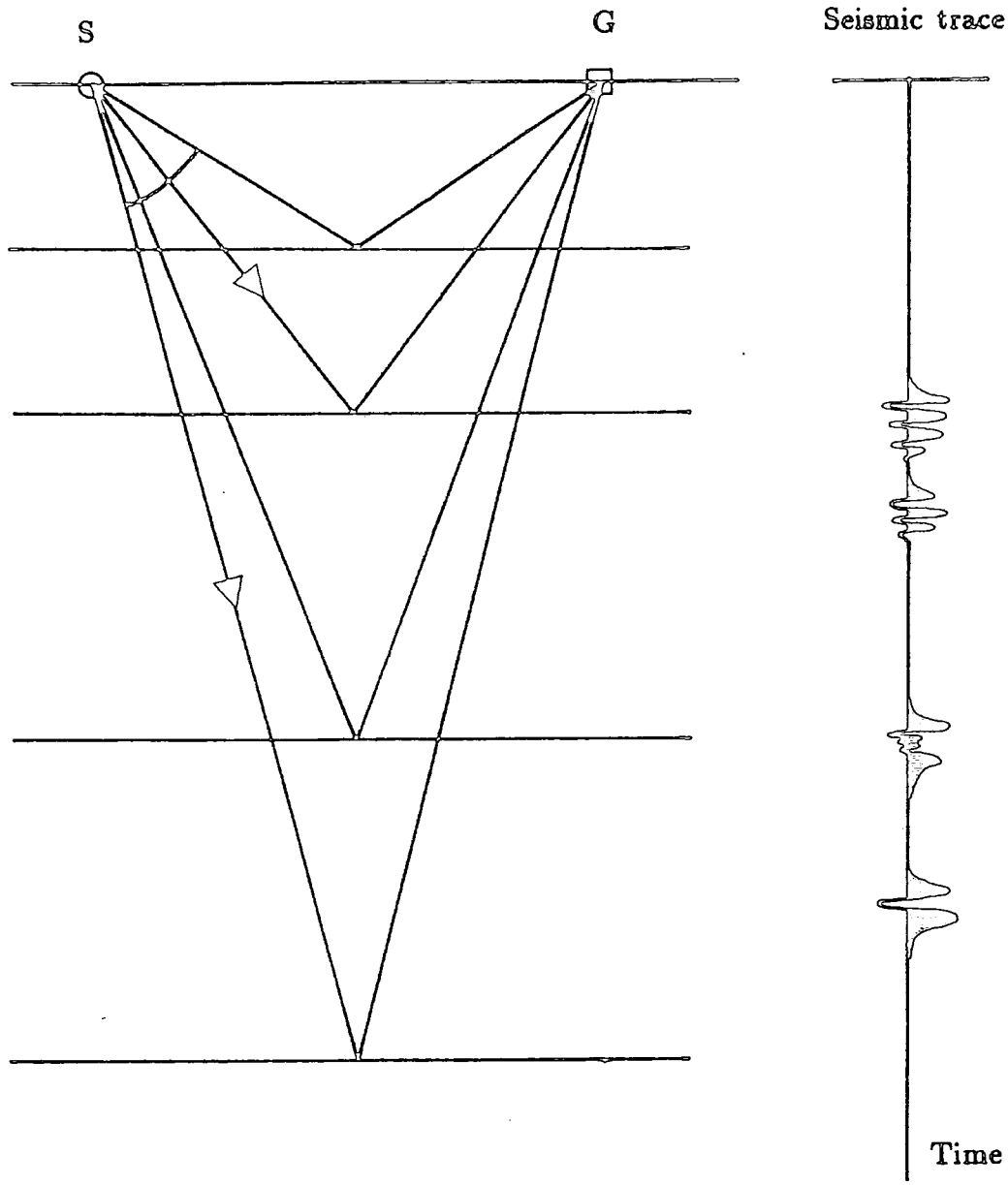

Figure 1.6. Schematic diagram, showing a seismogram of primary reflections only from a horizontally layered medium. The wavelet changes down the seismogram because of source directivity.

acquisition and reflector geometry, and may be significant.

1.5.3 Velocity analysis

The normal moveout (NMO) equation is the basis for determining velocities from seismic data. For a common-midpoint gather (CMP),

$$t_x{}^2 = t_0{}^2 + \frac{x^2}{V^2} \tag{1.6}$$

for a constant velocity medium , where t_x is the two-way traveltime at an offset between the source and receiver x and t_0 is the traveltime at zero offset.

The NMO equation can be extended for a horizontally stratified medium by making a small-offset approximation (Dix, 1955), which gives

$$t_x{}^2 = t_0{}^2 + \frac{x^2}{V_{rms}{}^2} \tag{1.7}$$

where V_{rms} is the r.m.s velocity.

Normal moveout is the time shift which must be applied to a reflection at offset x to shift it to the traveltime which would have been recorded at zero offset.

Velocity analyses are performed to calculate the 'NMO velocities' necessary for the application of NMO. The most widely used technique is the velocity spectrum (Taner and Koehler, 1969) . Coherence is measured along a suite of hyperbolic trajectories for each traveltime. These hyperbolae are defined by the NMO equation. The correct stacking velocity should give a trajectory corresponding to a true reflection event, thus giving a high coherence measure. Summation along the hyperbolae is the simplest coherence measure, but semblance (Neidell and Taner, 1971) is the most widely used.

For data acquired with a directional source, the waveform will change along the reflection hypebolae as the take-off angle from the source changes. Thus the coherency along such a hyperbola will be less than that for data acquired with a point source, where the waveform will be the same for all take-off angles. A poorer signal-to-noise ratio in the velocity spectrum will result.

The longer offsets of the CMP gather will be most affected by source directivity, and it is just this part of the CMP gather which is particularly important in discriminating between primary reflected data and multiple arrivals. This is because there is more differential moveout between multiples and primaries at longer offsets than there is at shorter offsets.

1.5.4 CMP stacking

After application of NMO, based on the results of velocity analysis, CMP gathers are stacked to improve the signal-to-noise ratio. The maximum signal-to-noise improvement for a conventional (mean amplitude) stack is $M^{\frac{1}{2}}$, where M is the number of traces. This maximum assumes that the same signal is present in all traces of the gather, and that the noise is random. For directional data, the waveform will change across the gather. The signal-to-noise improvement will thus be less than for point-source data.

Prior to the application of NMO and stacking, data are muted for early traveltimes and long offsets because these areas would degrade the stack due to NMO stretch and the dominance of direct arrivals and refracted energy. Arrivals most affected by source directivity effects will lie in this mute zone and hence may be ignored. If directivity effects extend to useful parts of the gather then standard processing will fail to take this into account. Primary reflected data may be processed incorrectly. Acquisition and reflector geometry will determine the severity of the problem.

1.6 Reducing the effect of source directivity

1.6.1 Array design

Arrays must be designed with subsequent processing in mind, as well as attenuation of coherent noise in the field. Once data are recorded with notches in the wavenumber spectra, deconvolution cannot fully recover the signal from corresponding areas in the f-k spectrum. If directivity is going to be a problem, it must be asked whether it is better to use large source arrays in the field, or whether acquistion with a shorter array followed by computer array simulation would be better. This second approach gives more flexibility to examine whether useful signal will be affected by array forming, and to allow the use of beam steering and filtering approaches not viable in the field. The available dynamic range of the recording equipment and cost considerations will determine whether this approach is possible. Larner et al.(1983) have investigated the use of processing techniques to suppress the types of coherent noise seen on marine records, and conclude that such an approach is viable. A disadvantage with this method is that, in general, field source arrays appear to perform better than simulated arrays (Roksandić, 1986). This observation has not yet been fully explained (Eiken, 1987).

For 2-D data, cross-line directivity cannot be simulated at the processing stage. If out-of-plane noise is a major problem, wide field arrays will have to be used (Lynn and Larner, 1989). Cross-dipping primary events could be degraded.

The use of source arrays for signature optimisation was described in section 1.3.2. Larner et al.(1982) conclude that only coarse tuning of the array is needed at the acquisition stage, with predictive or signature deconvolution to follow. This approach is motivated mainly by cost considerations.

Reflection data will usually be acquired with a source array. If attenuation of coherent noise in the field was considered to be of paramount importance (frequently the case for old data), the array is likely to be large and primary

reflections may show directivity effects. Once recorded, if data exhibit directivity effects some attempt may be necessary to reduce them. This is the subject of this dissertation. Further discussion on the amount of directivity desirable at the acquisition stage will be left until the final conclusions.

1.6.2 Directional deconvolution

Figure 1.6 shows that a single seismic trace contains arrivals which have originated from a range of take-off angles from the source. These take off-angles are not known unless the reflector geometry is known. Directional signature deconvolution is needed to deconvolve all the different wavelets originating from different take-off angles to one desired output, i.e. to remove directivity effects. Intuitively, some form of two-dimensional filter is needed. Two approaches are documented in the literature, a tau-p method (Van der Schans and Ziolkowski, 1983), and a frequency-wavenumber (f-k) method (Hubbard et al., 1984). Neither has gained acceptance by the seismic industry. A third method has been developed in this study, the prestack migration method (Roberts and Goulty, 1988). Tau-p and f-k transforms are closely related, both being plane-wave decompositions. The frequency-wavenumber method will be discussed in chapter II. This was chosen because the forward and inverse transforms are relatively easy to perform. The prestack migration method will be explained in chapter III, and both methods will be evaluated on model data in chapter IV. The new method of directional deconvolution combined with prestack migration will be applied to real data from the Southern North Sea in chapter V, and the final chapter will discuss whether directional deconvolution is necessary.

Chapter II

Directional Deconvolution in the Frequency-Wavenumber Domain

2.1 Introduction

Source directivity is ignored by one-dimensional source signature deconvolution. Some form of 2-D deconvolution is needed. Hubbard et al.(1984) describe a method for implementing directional deconvolution in the f-k domain. Data are sorted into common-receiver gathers and a deconvolution filter is then applied in the f-k domain. The filter may be designed directly from near-field measurements, or from calculated far-field source signatures at a range of take-off angles from the source.

Efficient filtering in the f-k domain is made possible by the fast Fourier transform (FFT), (Cooley and Tukey, 1965). Problems exist with the processing of edges of the data, and with aliasing.

2.2 F-k directional deconvolution

2.2.1 Filter design: direct calculation

Source directivity was described in chapter I, and is due to the use of source arrays and to the ghost. Parts of the f-k spectrum will be attenuated. The f-k source spectrum can be calculated if acquisition parameters and individual source signatures are known. For an airgun source array, Hubbard et al.(1984) show that the spectrum may be calculated directly from near-field measurements using the method of notional signatures (Ziolkowski et al., 1982).

A deconvolution filter may be designed to be the inverse of the calculated f-k spectrum. If the f-k spectrum of the source is $G(f, k_x)$ then the filter will be $H(f, k_x)$, where

$$H(f,k_x) = \frac{1}{G(f,k_x)}$$

It is thus possible to design a deconvolution filter directly from the acquisition parameters.

A one-dimensional example of a deconvolution filter is shown in figure 2.1. The input spectrum $G(f)$ has a notch at a frequency of f_{notch}. The filter $H(f)$ is the inverse of $G(f)$. The result of applying the filter to the original spectrum is an amplitude spectrum of constant value at all frequencies. The filter is thus a 'spiking' deconvolution filter. The filter compensates for the lack of energy at the notch frequency, so it has large amplification at this frequency. If there is no energy at the notch frequency, the filter amplitude will tend to infinity.

Seismic data are noisy. If the noise is 'white', energy is present at all frequencies. Application of the filter shown in figure 2.1 will cause amplification of the noise at the notch frequency. To prevent excessive amplification, 'white noise' may be added to the original spectrum before filter design. The notch will appear to be shallower, and the resulting filter will have lower amplification around that frequency. If the power of the added white noise is ${\sigma_n}^2$ then the filter will be

$$H(f,k_x) = \frac{G^*(f,k_x)}{|G(f,k_x)|^2 + {\sigma_n}^2}$$

For spiking deconvolution, the desired output of deconvolution is an amplitude spectrum of a constant value at all frequencies. If some other desired output were chosen, the deconvolution would be a 'shaping' deconvolution. The desired output may be chosen to have a similar energy distribution over the range of frequencies as the input spectrum. The resulting filter will be more stable because amplification at all frequencies will be closer to unity.

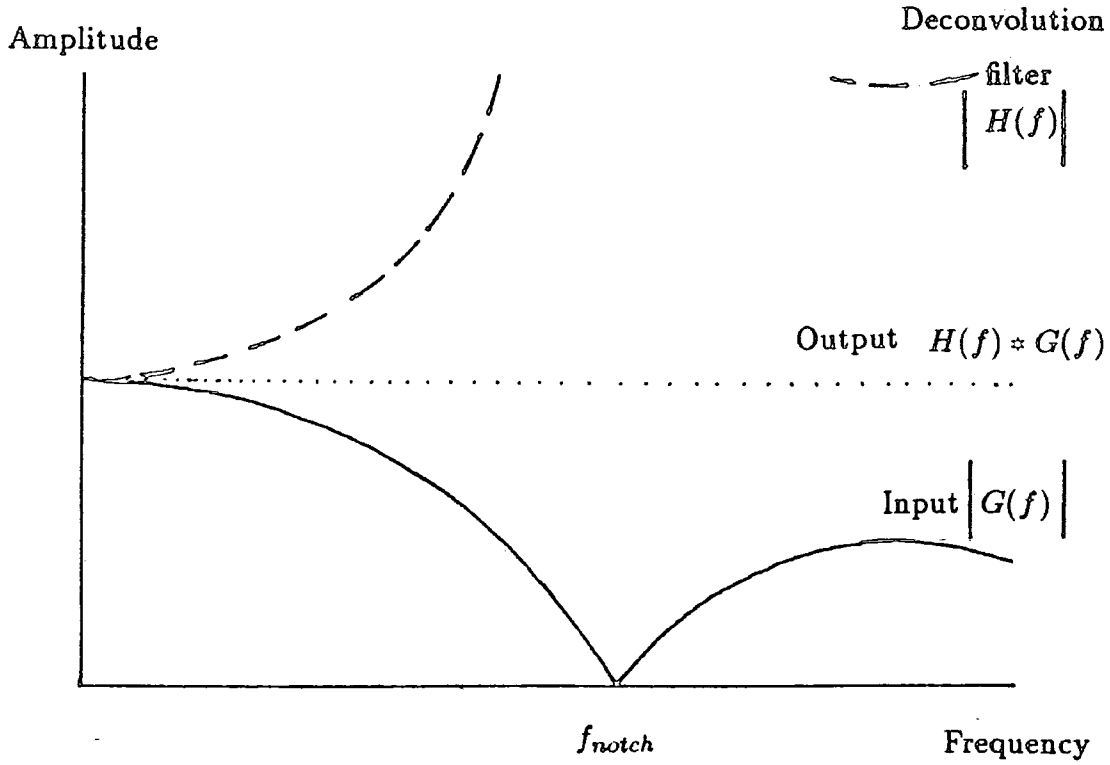

Figure 2.1. Deconvolution filter design in the frequency domain.

Thus a directional deconvolution filter may be designed in the f-k domain directly from the acquisition parameters. The filter may be a spiking or shaping deconvolution filter. An alternative method of filter design uses the source signatures at different take-off angles from the source.

2.2.2 Filter design: the 'mapping' method

Far-field source signatures at all take-off angles from a source array may be calculated or measured. The ghost effect can be included. Examples were shown in figure 1.2. The source signatures can each be transformed into the frequency domain, and the one-dimensional spectra may then be mapped on to the f-k plane (Confurius, 1987). Each spectrum is mapped onto a radial line in f-k space, governed by the equation

$$k_x = \frac{f \sin \phi}{V} \qquad 2.1$$

Thus each component at frequency f from each spectrum may be placed at the correct point (f, k_x) on the f-k plane.

The resulting f-k spectrum must be regularly sampled in both frequency and wavenumber. If the sampling in frequency is the same as for the one-dimensional spectra, interpolation along the frequency axis is not required. The mapping will result in an irregular sampling in wavenumber, so interpolation is necessary. This may be performed as a series of one-dimensional interpolations along the wavenumber axis, at each frequency value.

The resulting f-k source spectrum will be identical to that calculated by the direct calculation method (section 2.1.1) if the interpolation is perfect. The deconvolution filter may thus be designed in the same way. The mapping method will prove useful when only the source signatures are available, which will be the case for ultrasonic model data in chapter IV.

The mapping method has another advantage. Filters may be designed in the time domain for source signatures radiated at different take-off angles. These filters may then be transformed to the frequency domain, and mapped on to the f-k plane to give the f-k filter. Time domain filter design minimises the error energy between the desired output and the actual output (Robinson and Treitel, 1980). The presence of notches in the spectrum of the input wavelet implies the need for a long deconvolution filter. The shorter the filter in the time domain, the less it will compensate for the notch. If the filter is designed in the frequency domain by spectral division it will completely compensate for the notch, but it will have a large amplification at the notch frequency, whereas the short filter designed in the time domain will have a lower amplification. The actual output from the filter designed in the frequency domain will have the same spectral characteristics as the desired output, but the filter will greatly amplify noise at the notch frequency. The filter designed in the time-domain will leave a residual notch, but will be more stable. Model examples of filter design will be given in chapter IV.

Thus an f-k filter suitable for directional source signature deconvolution may be designed. Two closely related techniques are available, and these are summarised in figure 2.2.

In order to perform directional deconvolution, the filter must be applied to the f-k transform of the data. This is performed as a complex number multiplication.

2.2.3 Filter application

The f-k transform is a plane-wave decomposition. Each point in f-k space represents a plane-wave of a particular frequency, f, travelling at an angle to the vertical of ϕ (equation 2.1). Considering the f-k transform of a common-shot gather, ϕ would be the angle at which the plane-wave arrives at the receivers. Only for a horizontally stratified medium would this be equal to the angle at which it left the source. To perform directional source signature deconvolution,

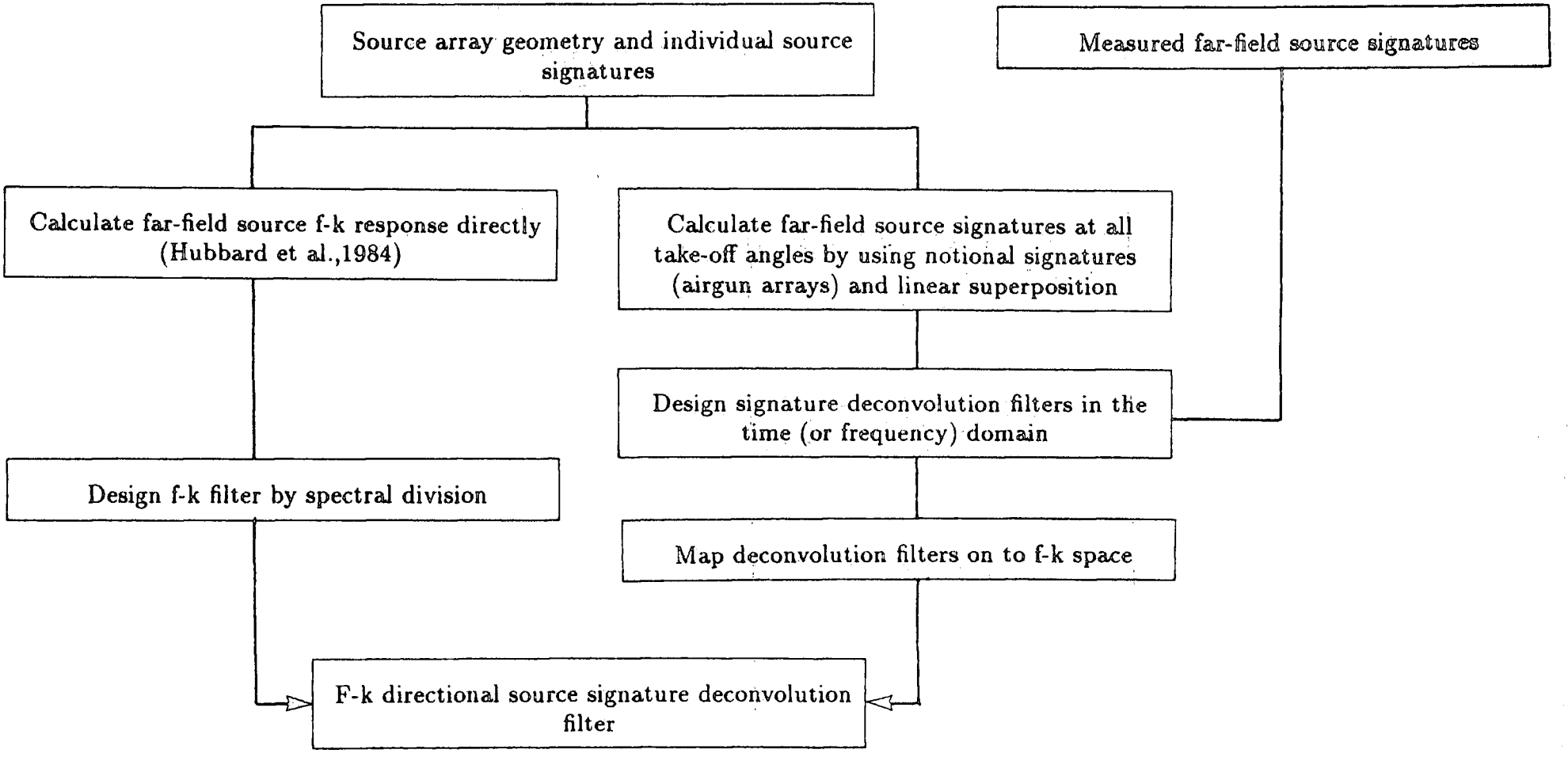

Figure 2.2. Flow chart of f-k directional deconvolution filter design.

it is the take-off angle at the source which is important. Thus common-receiver gathers must be used.

The need to use common-receiver gathers can be illustrated by considering the response to a point diffractor (figure 2.3) where

x_s is the distance to the source from the origin,

x_g is the distance to the receiver from the origin,

x_0 is the distance to the point diffractor from the origin,

z_0 is the depth to the point diffractor,

V is velocity and

ϕ is the take-off angle from the source.

The traveltime curve is given by

$$t(x_s, x_g) = \frac{1}{V}((z_0{}^2 + (x_s - x_0)^2)^{\frac{1}{2}} + (z_0{}^2 + (x_g - x_0)^2)^{\frac{1}{2}})$$

For a common-receiver gather, the apparent slowness is the partial derivative of the traveltime curve $t(x_s, x_g)$ with respect to source position (Hampson, 1987)

$$\frac{\partial t}{\partial x_s} = \frac{1}{V}\frac{(x_s - x_0)}{(z_0{}^2 + (x_s - x_0)^2)^{\frac{1}{2}}} = \frac{\sin\phi}{V}$$

Thus

$$V_{apparent} = \frac{V}{\sin\phi} \qquad 2.2$$

Thus a point on the f-k transform of a common-receiver gather represents a plane wave of frequency f which has left the source at a take-off angle ϕ.

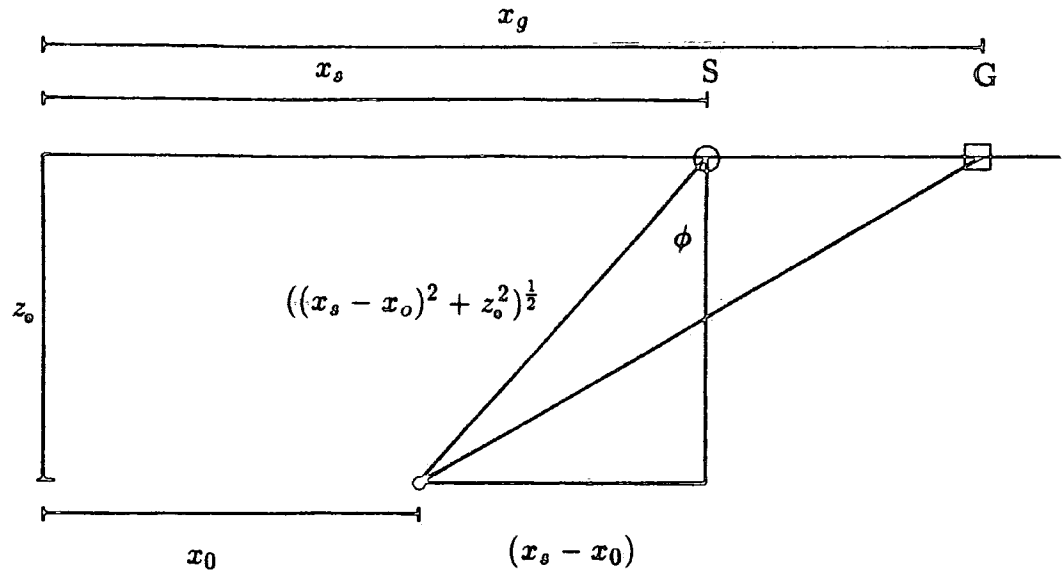

Figure 2.3. Geometry of a point diffractor (at (x_0, z_0)), source $(S)$and receiver (G).

Apparent velocity can be calculated for other types of gather. For a common-shot gather, the apparent slowness is the partial derivative of $t(x_s, x_g)$ with respect to receiver position x_g. The resulting angle in the equivalent formula to equation 2.2 will be the angle at which the plane-wave arrives at the receivers. If it is desired to compensate for the directional response of the receivers, this may be done in the f-k domain for each common-shot gather. As it is the take-off angle at the source which is needed for directional source signature deconvolution, the f-k filter must be applied to the f-k transform of common-receiver gathers.

The f-k method for directional deconvolution is summarised in figure 2.4. Data are not usually processed as common-receiver gathers, so additional sorting is required. This is time consuming and costly. A suite of programs has been written for the evaluation of f-k directional deconvolution (Appendix A).

The f-k transform has inherent problems which lead to incorrect processing of parts of the data. The next section will review Fourier theory, and these problems will then be examined.

2.3 The 2-D Fourier transform

Reviews of Fourier theory are given by Bracewell (1978) and Brigham (1974). Fourier theory was first developed for the continuous one-dimensional case. The discrete case is an approximation and the 2-D case an extension of the basic method. The Fourier transform of a function $h(t)$ is defined as

$$H(f) = \int_{-\infty}^{\infty} h(t) e^{-2\pi i f t}\, dt$$

The inverse transform is

$$h(t) = \int_{-\infty}^{\infty} H(f) e^{2\pi i f t}\, df$$

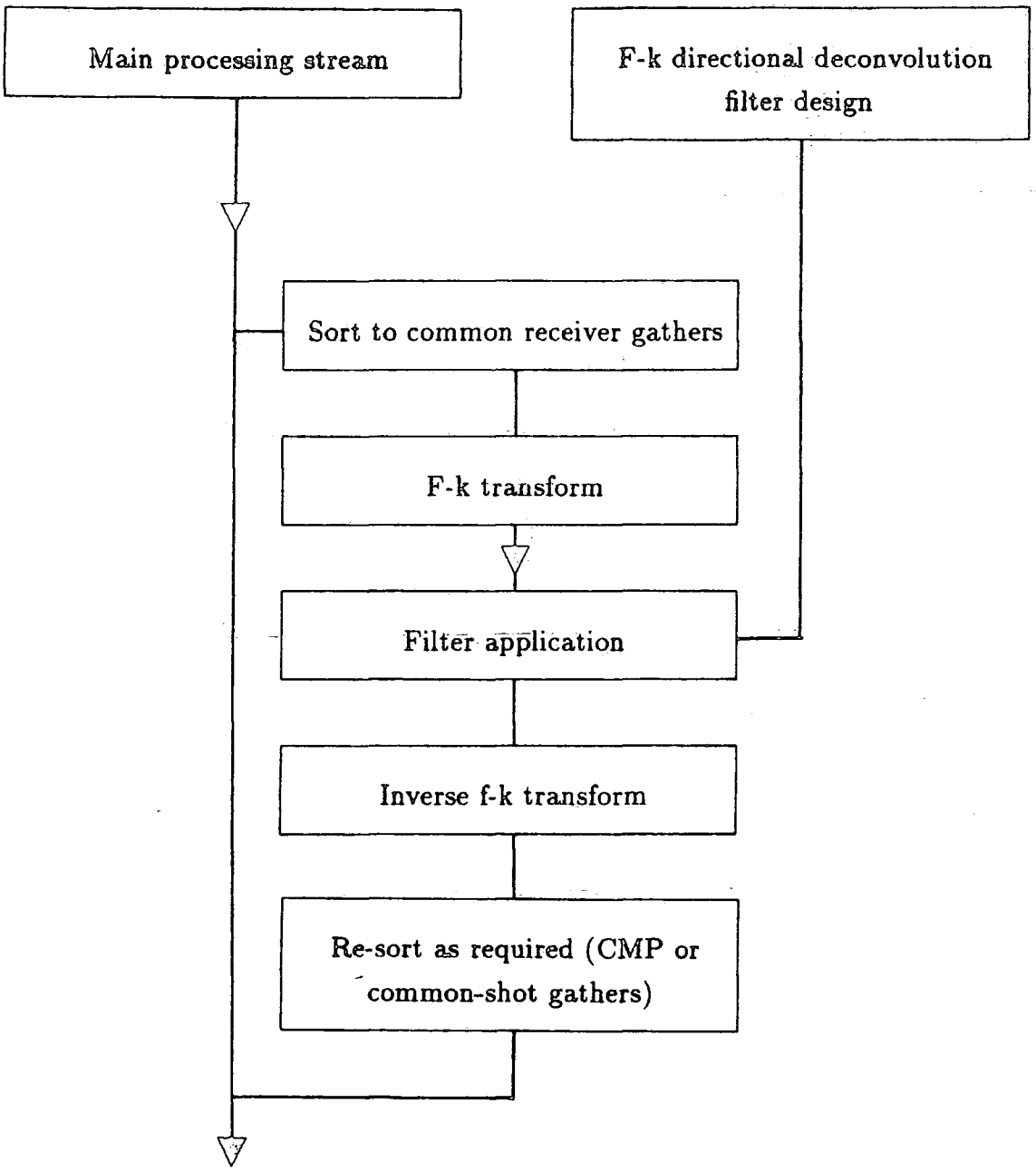

Figure 2.4. F-k directional deconvolution processing sequence.

If the unit of t is time (s), then the unit of f is frequency (Hz). If the unit of t is distance (m), then the unit of f is wavenumber (m^{-1}). These integrals enable transformation from one domain to the other. $H(f)$ and $h(t)$ are said to form a 'Fourier transform pair'.

The convolution theorem is important for deconvolution. The convolution of two functions, denoted as $g * h$ is defined as

$$g * h = \int_{-\infty}^{\infty} g(\tau)h(t-\tau)\,d\tau$$

Representing the transform pair by

$$h(t) \rightleftharpoons H(f)$$

the convolution theorem states that a convolution in one domain is equivalent to a multiplication in the other:

$$g(t) * h(t) \rightleftharpoons G(f).H(f) \qquad 2.3$$

A convolutional model is assumed for source signature deconvolution. Thus deconvolution filters may be designed and applied in either the time, or frequency domain.

Fourier theory may be extended to the discrete case, i.e. sampled data. This involves a discrete approximation of the integral. The resulting discrete Fourier transform (DFT) is

$$H_l = \frac{1}{L}\sum_{r=0}^{L-1} h(r)e^{-2\pi i\frac{l}{L}r}$$

The DFT is periodic with period L. The DFT provides a good spectral representation providing that the sampling criterion is obeyed. If the sampling period is Δt, the Nyquist frequency, f_{nyq}, is

$$f_{nyq} = \frac{1}{2\Delta t} \qquad 2.4$$

A function that is bandlimited to frequencies below the Nyquist frequency is completely determined by its samples. If frequencies are present above the Nyquist, they are said to be aliased. Because of the periodic nature of the DFT they will wrap around in Fourier space.

Calculation of the DFT can be made very efficiently using a fast Fourier transform (FFT) (Cooley and Tukey, 1965).

The 2-D DFT involves extending the basic formulae to two dimensions. The FFT can be similarly extended. In seismology it is usual to transform one spatial and one temporal axis. This gives an f-k transform. Hatton et al.(1986) and March and Bailey (1983) give excellent intuitive insights into the f-k transform. Figure 2.5, adapted from Hatton et al.(1986) shows a sketch of a seismic section and its f-k transform. Frequency is shown varying from zero to the temporal Nyquist frequency, and wavenumber varying between plus and minus the spatial Nyquist wavenumber. A linearly dipping event in the x-t domain transforms to a linearly dipping event which passes through the origin in the f-k domain. Event E shows spatial aliasing. The f-k transform is periodic in time and space, so transform space can be visualised as a series of adjacent boxes. Aliased energy continues across these boxes. The f-k transform plot, e.g. figure 2.5.b, is a superposition of all of the boxes, so the aliased arrival appears as wrapped around energy.

2.4 Filtering using the 2-D FFT: data edges

Until the mid 1970s, 2-D filtering was performed by a convolution operation

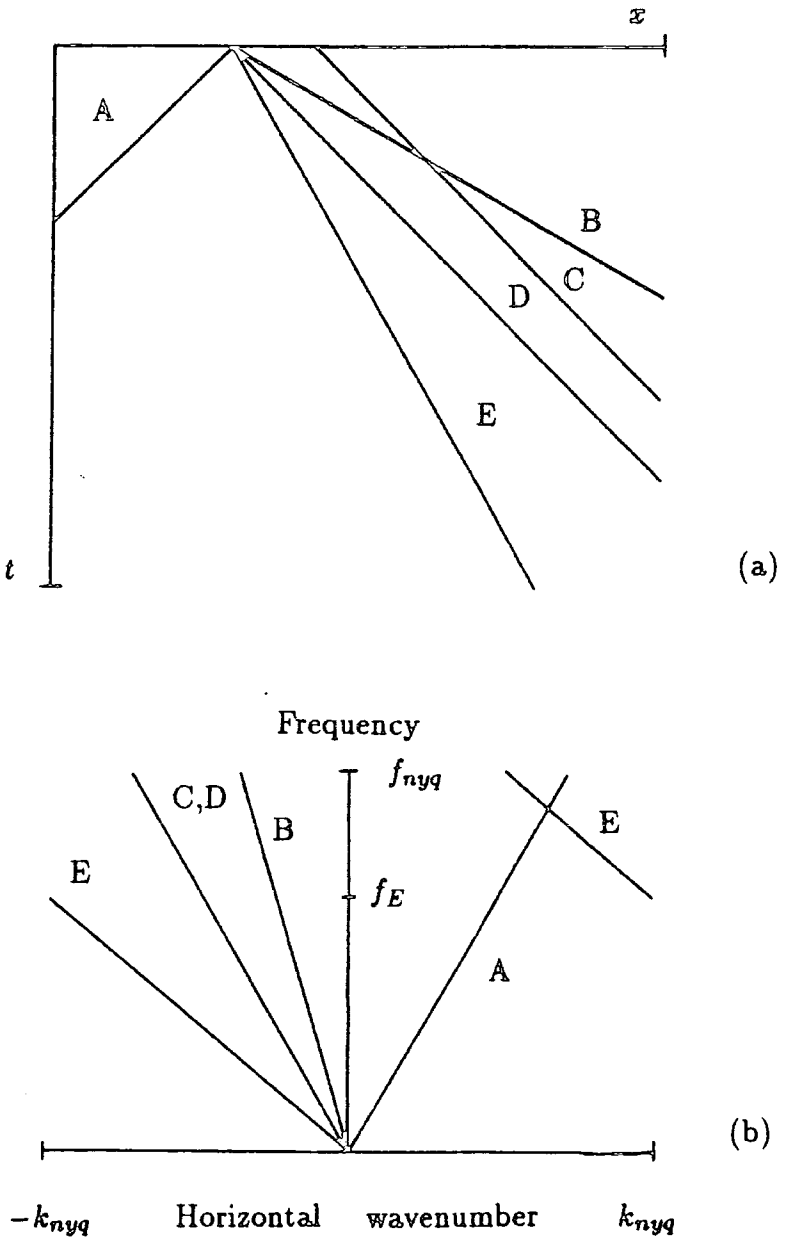

Figure 2.5. Equivalent responses in the t-x and f-k domains (adapted from Hatton et al., 1986).

in the time domain. Specification of the filters, however, often started with frequency domain considerations (e.g. Embree et al., 1963). With the advent of the fast Fourier transform (Cooley and Tukey, 1965), filtering became viable in the more natural frequency domain. Today the technique is widely used, with examples from gravity data processing (Ku et al., 1971), velocity filtering of seismic data (Christie et al., 1983), and VSP wave-field separation (Suprajitno and Greenhalgh, 1985).

Filtering in the Fourier domain involves a complex number multiplication. The convolution theorem (equation 2.3) states that this is equivalent to a convolution in the time domain. Figure 2.6.a from March and Bailey (1983) shows a velocity filter which was designed in the f-k domain. The same filter is shown transformed to the space-time (x-t) domain (figure 2.6.b). Application of the velocity filter in the f-k domain is equivalent to a convolution of the data with the x-t impulse response shown. The x-t impulse response has both temporal and spatial extent. The side lobes of the impulse response are caused by Gibb's phenomenon. A discontinuity, or steep slope, in the f-k domain causes ringing in the x-t domain.

2-D seismic data usually taper to zero temporally but not spatially, because the finite recording aperture in space is a boxcar window parallel to the x-axis. The sharp edges of the boxcar window are discontinuities which lead to Gibb's phenomenon, i.e ringing, in the wavenumber domain. Tapering the edges of the data before the f-k transform provides a partial solution, and the edges may then be amplified on return to the x-t domain. This is not a complete solution, as the tapered outer traces will be affected by the convolution of the impulse response of the filter with the inner traces. This noise will then be artificially amplified when the taper is removed at a later stage (March and Bailey, 1983).

The implied periodicity of the f-k transform further adds to the problem near the edges of the data. The data input to the FFT are recorded over a finite range, but the FFT regards it them being periodic. Thus a multiplication in the

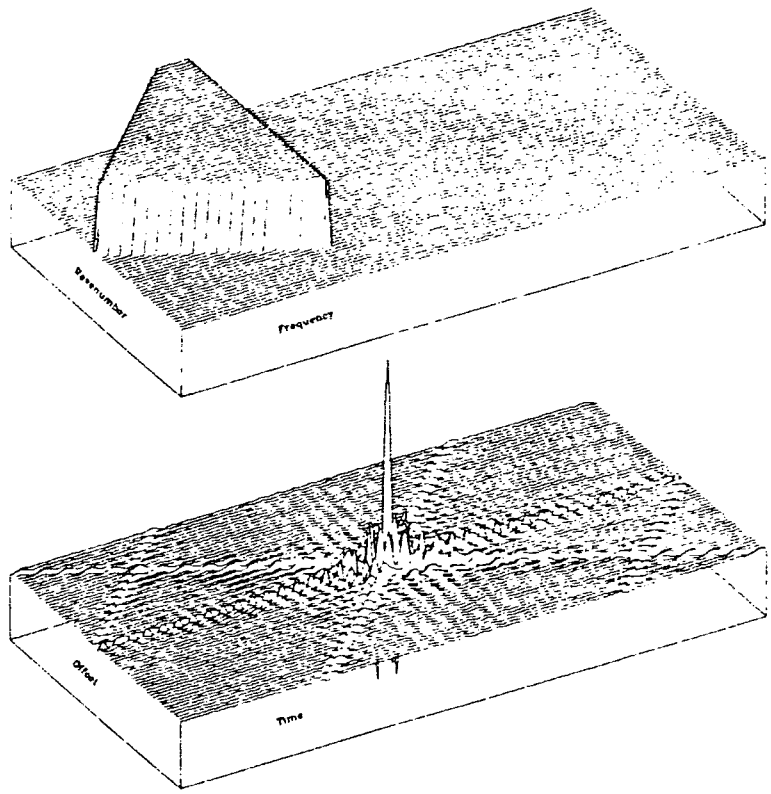

Figure 2.6. An f-k filter and the equivalent t-x response (March and Bailey, 1983).

f-k domain is equivalent to a cyclic convolution, and not a transient convolution (Clement, 1973). Convolution in the time domain results in an output equal to the length of the data plus the length of the filter. Because of the cyclicity inherent in Fourier methods, the extra output will appear as wrapped around noise on the outer traces after the inverse transform. This leakage can be prevented if the data are padded with blank traces before the f-k transform. The contamination of the padded traces by wrap around is unimportant as they will later be discarded. As most FFTs require the number of traces to be a power of two, it is convenient to pad to the next power of two, or more if necessary.

Despite these measures, edges of the data will still not be completely processed. An outer trace of the gather will only be affected by the convolution of the impulse response of the filter with itself and with the inner traces. An inner trace of the gather will be affected by convolutions from itself and with traces on both sides of it. Thus, as no data exist outside the recording window, outer traces are not completely processed. The spatial extent of the filter will determine how many traces are affected.

The spatial and temporal extent of the filter is dependent on the nature of the f-k response. Discontinuities in the f-k domain will result in ringing in the time domain. If the f-k filter has gentle slopes, the x-t impulse response will have a small temporal and spatial extent. It may be necessary to design the f-k filter with steep slopes. An example is a velocity filter with a sharp reject zone. To minimise the ringing effect on the data, the velocity filter may be tailored to fit low amplitude channels in the spectra (Christie et al., 1983), which also has the advantage that linear velocity cut-offs will be replaced with curves, so the energy previously in long tails of the impulse response will become more evenly spread. For VSP wave-field separation, a similar approach has been suggested (Suprajitno and Greenhalgh, 1985).

F-k directional deconvolution filters may have steep slopes in the f-k domain. These occur where the filter is compensating for notches in the f-k spectrum of

the source function. The impulse responses of f-k directional deconvolution filters will need to be examined to assess their stability before application.

2.5 Filtering using the 2-D FFT: aliasing

Seismic data can contain spatially aliased events because no spatial equivalent of a temporal anti-alias filter is applied during acquisition. Spatial aliasing occurs if the time moveout per trace of an event is greater than half the period of the maximum frequency being considered (Figure 2.7). The Nyquist wavenumber is given by

$$k_{nyq} = \frac{1}{2\Delta x}$$

where Δx is the trace spacing, as implied by equation 2.4. Spatially aliased events will wrap around in the f-k domain (figure 2.5). To filter an aliased event correctly, the f-k filter would need to wrap around to the same degree. The filter would then process non-aliased events incorrectly. A better approach is to remove the spatial aliasing prior to the f-k transform. Several means are available: recording the data with finer spatial sampling; spatial interpolation; high-cut filtering; applying linear moveout; and muting aliased events.

- Finer spatial sampling

  Spatial aliasing is due to insufficient spatial sampling. Figure 2.7.b shows an event which is just aliased. If the spatial sampling interval were smaller, for example half the interval shown, the event would not be aliased. Thus adequate spatial sampling in the field will ensure no spatial aliasing.

- Spatial interpolation

  Spatial interpolation aims to emulate finer spatial sampling. If data are recorded with spatial aliasing, trace interpolation is a major problem. Most methods of spatial interpolation attempt to determine the local dip at all

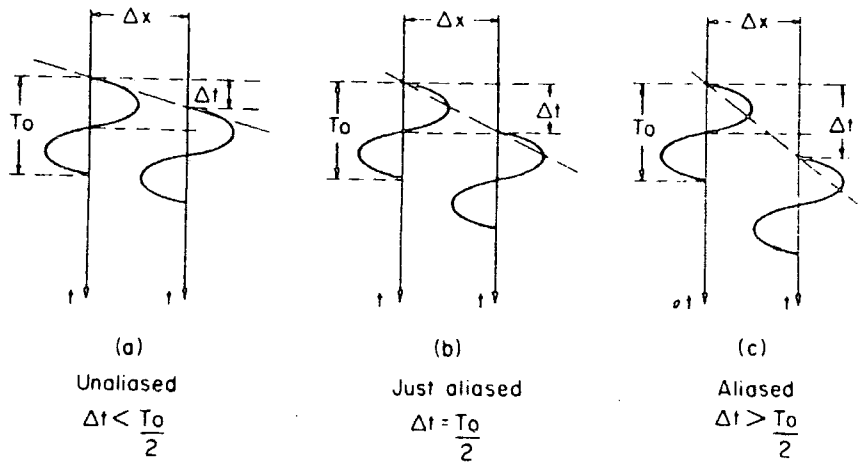

Figure 2.7. Condition for spatial aliasing (Christie et al., 1983).

points on the dataset by measuring coherence over a range of dips. The data are then interpolated along the local dips which show maximum coherence. Spatially aliased data exhibit conflicting dips (e.g. Hatton et al., 1986), so the interpolation method may be unable to distinguish between true dips and apparent dips. Thus spatially aliased data may be interpolated incorrectly. Trace interpolation does not improve lateral resolution; it just avoids the aliasing problem.

- High-cut filtering

  Figure 2.5 showed an event which is spatially aliased (event E). It wraps around to the right-hand quadrant at frequencies greater than f_E. If frequencies above f_E were removed by high-cut filtering, the event would not be aliased, but valuable high frequencies would be lost from the data.

- Linear-moveout (Yilmaz, 1987)

  Time shifts may be applied to data so that steeply dipping events appear to have shallower dips. For example, linear-moveout could be applied to event E in figure 2.5 to alter the dip to that of event D. Event E would then no longer be spatially aliased and could be filtered. Events which were not spatially aliased could become so after the application of linear-moveout. Thus the method is highly data-dependent.

- Muting

  A commonly occurring steeply dipping event on a common-receiver gather is the direct wave. This will usually be spatially aliased, but may be muted prior to the f-k transform.

F-k directional source signature deconvolution filters are applied to the f-k transforms of common-receiver gathers. If there are aliased events in the gather, these events will be incorrectly processed. For a common-receiver gather, the

shot spacing determines the spatial sampling. A typical marine shot spacing is 25 m, so the Nyquist wavenumber is (equation 2.4)

$$k_{nyq} = \frac{1}{2\Delta x} = 0.02\,\mathrm{m}^{-1}$$

The source take-off angle for a common-receiver gather is given by

$$\sin\phi = \frac{V k_x}{f}$$

If the highest frequency of interest is 80 Hz, and the velocity of water is 1480 m s^{-1}, the maximum angle at which energy can be radiated from the source without being aliased on a common-receiver gather is 22°. Energy radiated at larger take-off angles will be aliased, and it is this energy which will exhibit directivity when a moderate length source array (e.g. figure 1.2.a) is used. Spatially aliased events will be incorrectly processed by application of directional deconvolution by filtering in the f-k domain. Therefore spatial aliasing must be dealt with before directional deconvolution. Hubbard et al.(1984) spatially interpolate each common-receiver gather to reduce the shot interval to 12.5 m. The need for spatial interpolation is a major short coming of the f-k directional deconvolution method.

Chapter III

Directional Deconvolution Combined with Prestack Migration

3.1 Introduction

Prestack migration can almost completely be understood by geometrical considerations. Additional weighting factors are needed to provide a complete solution consistent with Kirchhoff diffraction theory (Schneider, 1978). Approximations must be made to the Kirchhoff integral due to the discrete nature of seismic data.

A new method of directional source signature deconvolution has been developed (Roberts and Goulty, 1988). Directional deconvolution is performed as a series of one-dimensional source signature deconvolutions in a Kirchhoff summation prestack migration scheme. A processing scheme has been written to evaluate the technique. Physical model data have been used (chapter IV). Extensions to the method are necessary for real data, which have been recorded over variable-velocity media (chapter V).

3.2 Prestack migration

The aim of migration is to relocate reflection events to their true subsurface positions. Migration is usually applied to stacked data as one of the last processes in the processing sequence. The stacked section is assumed to be equivalent to a zero-offset section. The assumptions implicit in the application of normal moveout (NMO) and stacking are violated for certain situations and, for these situations, the stacked section will not equal a true zero-offset section. Post-stack migration will not perform correctly.

The main area where NMO fails is when conflicting dips are present. Stacking velocities are dip dependent (Levin, 1971). Only one stacking velocity may be

chosen for each traveltime. Thus if reflectors of conflicting dip are present at the same traveltime, only one will be stacked correctly. Migration velocities, however, are independent of dip, so prestack migration will correctly image structurally complex areas where NMO assumptions break down.

Prestack migration is still not widely used despite this advantage. Migration requires a knowledge of the velocity structure of the subsurface, but at early stages of the processing sequence there is little velocity information. This is a major problem, as prestack migration is very sensitive to velocity errors. Recently, advances in computer technology have enabled prestack migration itself to be used as a velocity analysis tool. This approach was first suggested by Gardner et al.(1974), and is used in chapter V. Prestack migration is also a relatively expensive process because the volume of data before stack is much greater than post-stack.

The problems associated with knowledge of the velocity field and cost considerations have lead to the development of 'prestack partial migration' methods. One such method, Dip Moveout (DMO) (Deregowski and Rocca, 1981), has gained wide acceptance by the seismic processing industry.

Migration may be performed in several different domains (e.g. Stolt and Benson, 1986). The method used to incorporate directional deconvolution is Kirchhoff summation migration (Schneider, 1978). This is an extension of one of the earliest methods, diffraction stack migration.

3.2.1 Diffraction stack migration

Diffraction stack migration was one of the earliest types of migration to become commercially available. It is based on simple geometrical considerations and follows from the work of Huygens and Fresnel. For zero-offset (i.e post-stack) data, diffraction stack migration is performed by summing along hyperbolic trajectories. For prestack data the summation operator is slightly more complicated. Consider a constant-offset section with only an isolated impulsive arrival, (Figure

3.1.a). If a constant velocity medium is assumed, the reflector configuration must be the depth ellipse in Figure 3.1.b. When the source and receiver are at the position shown, reflections are recorded from all points on the ellipse at the same traveltime. For any other source and receiver position, no reflections are recorded. The equation of the ellipse is a function of traveltime, velocity and offset between source and receiver. Conceptually, migration may be performed by taking the event from the constant-offset section and distributing it around the appropriate ellipse. To migrate a complete constant-offset section, this operation must be performed for every data sample on the section. Alternatively, migration may be performed directly by summing over trajectories on the constant-offset section. This summation is defined by the 'migration summation operator', whose geometrical shape also depends on traveltime, velocity and source-receiver offset. For zero-offset data the summation operator is a hyperbola. In two dimensions for non-zero-offset data, the summation is over vertical slices through the surface of a Cheops pyramid (Claerbout, 1985). The migration summation operator approximates to a hyperbola for small source-receiver offsets and large traveltimes, but is actually a 'flattened' hyperbola.

3.2.2 Kirchhoff extensions to diffraction stack migration

Schneider (1978) solved the wave equation to obtain a Kirchhoff integral solution suitable for the migration of zero-offset sections. A full derivation is given by Devey (1979). The resulting two-dimensional Kirchhoff integral formula suitable for migration, assuming constant velocity V, is

$$P(x_m, t_m) \simeq K \int_{-\infty}^{\infty} \frac{\cos\alpha}{(V^2 t_0)^{\frac{1}{2}}} \left(\frac{\partial^{\frac{1}{2}} P}{\partial t^{\frac{1}{2}}}(x, t_0) \right) dx \qquad 3.1$$

$P(x_m, t_m)$ is the pressure at a coincident source and receiver position x_m and at a migrated vertical traveltime t_m.

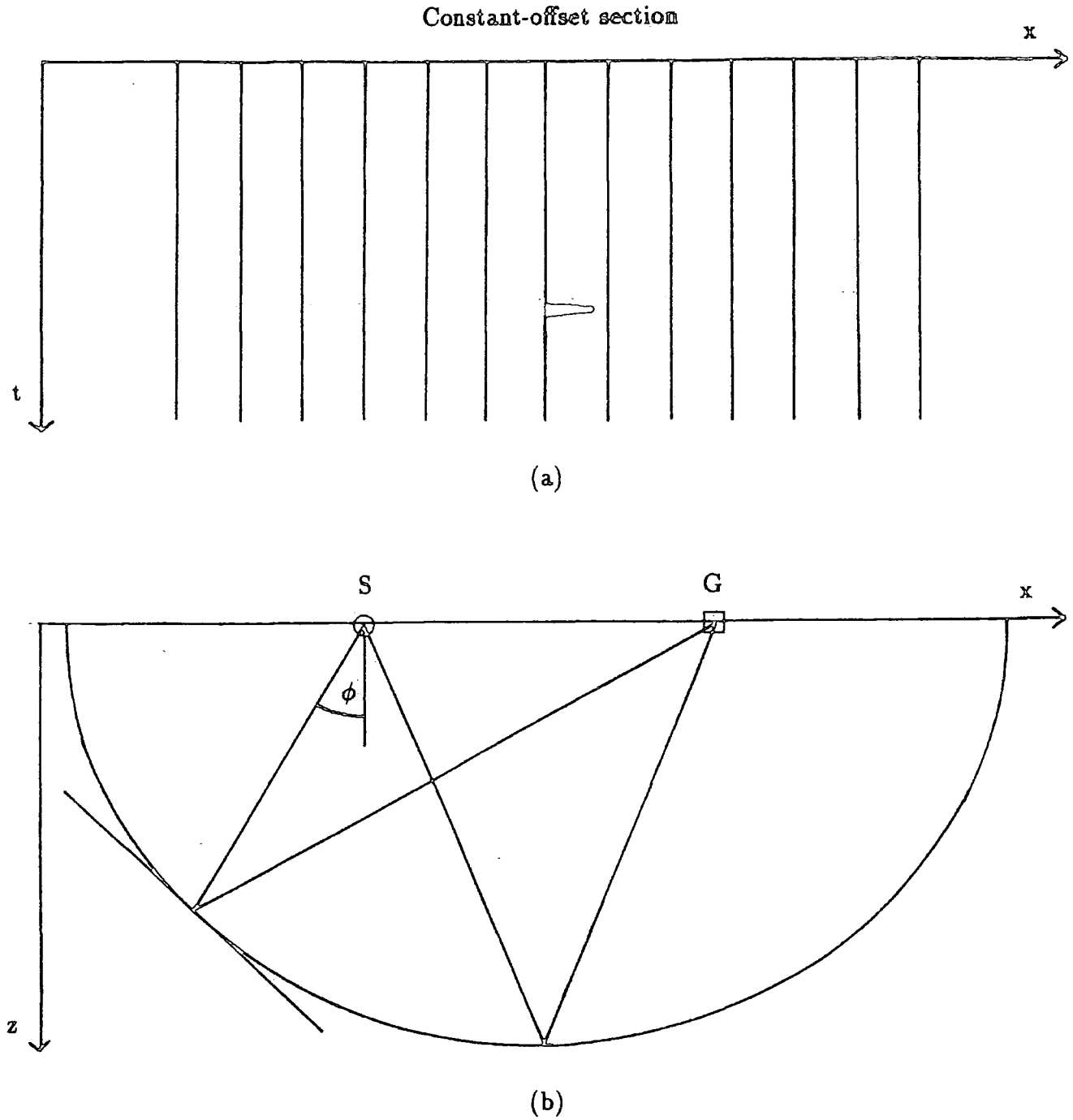

Figure 3.1. Principle of prestack migration. (a) Constant-offset section with a single arrival. (b) The depth ellipse in a constant-velocity medium which would give rise to the section in (a).

K is a constant which can be evaluated, but in practice is adjusted for convenience of output signal amplitude scale.

t_0 is the traveltime on the zero-offset section. It is calculated using raypaths to the point (x_m, t_m) and is given by

$$t_0 = \left({t_m}^2 + \frac{(x_m - x)^2}{V^2} \right)^{\frac{1}{2}}$$

$P(x, t_0)$ is the pressure at a traveltime t_0 on the zero-offset section with source and receiver coincident at x.

The operations implied by equation 3.1 are an integration over a hyperbola, i.e diffraction stack migration, with additional weighting and phase shifting factors. These additional factors are a directivity factor, a true amplitude scaling factor and the Newman filter (Newman, 1975).

The directivity factor, often called the obliquity factor, is

$$\cos \alpha = \frac{t_m}{t_0}$$

The factor is unity at the apex of the summation hyperbola and decreases gradually on the flanks. More severe directivity factors have been tried by Kuhn (1979).

The true amplitude scaling factor is given by

$$\frac{1}{(V^2 t_0)^{\frac{1}{2}}}$$

This factor is explained in figure 3.2 (Hatton et al., 1986), which shows a zero-offset section with two horizontal reflectors. The migration operator sums over the zero-offset section. When the summation operator encompasses a reflector,

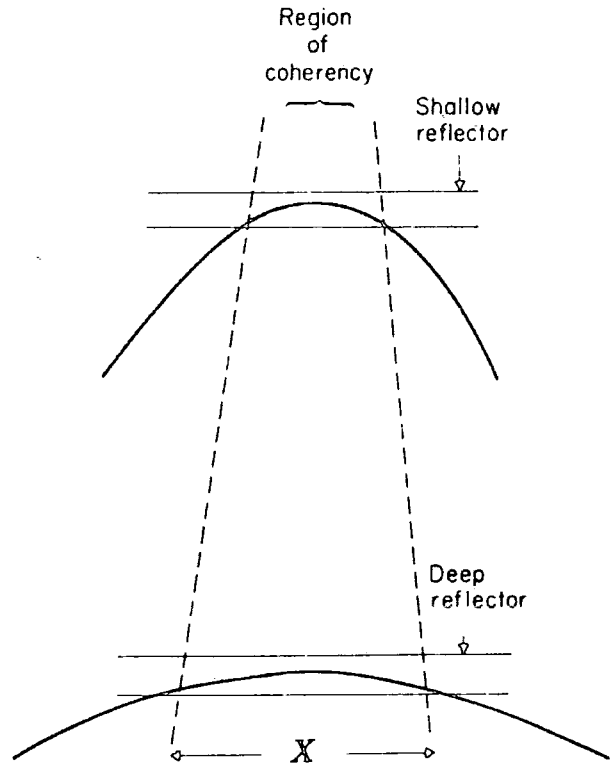

$$X \sim (V^2 t_0)^{\frac{1}{2}}$$

Figure 3.2. Spread in the region of summation coherency (stationary phase) with increasing time (Hatton et al., 1986).

there will be a region of coherency which will result in a significant migrated output value. The region of coherency increases with traveltime so that the output from a deep reflector will be greater than for a shallow reflector. The true amplitude scaling factor corrects for this effect.

The directivity and true amplitude scaling factors can be combined to give a computationally efficient weighting scheme for Kirchhoff summation migration (Hosken, 1979). The combined weighting factor is

$$\frac{t_m}{V(t_0)^{\frac{3}{2}}}$$

The Newman filter (Newman, 1975) is given by

$$\frac{\partial^{\frac{1}{2}} P}{\partial t^{\frac{1}{2}}}$$

The filter has a 45 degree phase lag and a 3dB per octave rise in amplitude. It is equivalent to multiplication in the frequency domain by $\sqrt{i\omega}$. The filter may be applied in the time domain (Hosken, 1979).

The Kirchhoff integral in equation 3.1 was derived for zero-offset data. It is an extension of diffraction stack migration. For the migration of constant-offset sections, the summation method can be extended similarly (e.g. Stolt and Benson, 1986). The weighting function is more complicated for constant-offset data than for zero-offset data because the finite source-receiver offset must be normalised. A simpler weighting function will often suffice (Stolt and Benson, 1986). The Newman filter is still appropriate for constant-offset migration (Hood, 1981).

3.3 Practical Kirchhoff summation migration

3.3.1 Interpolation in time

Seismic data are recorded at discrete intervals of space and time so the integral in equation 3.1 must be approximated by a summation. The migration summation operator sums across many traces to calculate a single migrated output value. It is likely to pass between samples on each trace that it crosses; thus interpolation is necessary.

3.3.2 'Discretisation' noise (Hosken, 1979)

'Discretisation' noise is also known as 'aliasing' noise. This latter term is confusing as discretisation noise may occur even if the data are not aliased. Data are discretely sampled in space. Figure 3.3.a shows how a single migrated output trace is formed by summation migration for a horizontal reflector. For each point above the reflector, the migration operator sums over the reflector which it intersects at two points. The sum of the reflector amplitudes at these points, each weighted by the appropriate weighting factor, is placed at the correct point on the migrated trace. If the data are finely sampled, the contributions from all operators coalesce to form an elongated pulse which appears as a precursor to the reflection event. The Newman filter is designed to collapse such a pulse back to the wavelet shape of the reflection before migration. Due to the discrete sampling interval in space, contributions to the migrated trace from the more remote traces do not coalesce, but form individual pulses. The Newman filter does not filter these individual pulses correctly; thus discretisation noise occurs. The situation is further aggravated for dipping reflectors (Figure 3.3.b). Contributions to the migrated trace from the up-dip side of the dipping reflector are separated further than they were for the horizontal reflector. For zero-offset data, discretisation noise appears above a dipping reflector if the highest frequency on the input traces is greater than f_{max}, where

$$f_{max} = \frac{V}{4\Delta x \sin \alpha_{max}} \qquad 3.2$$

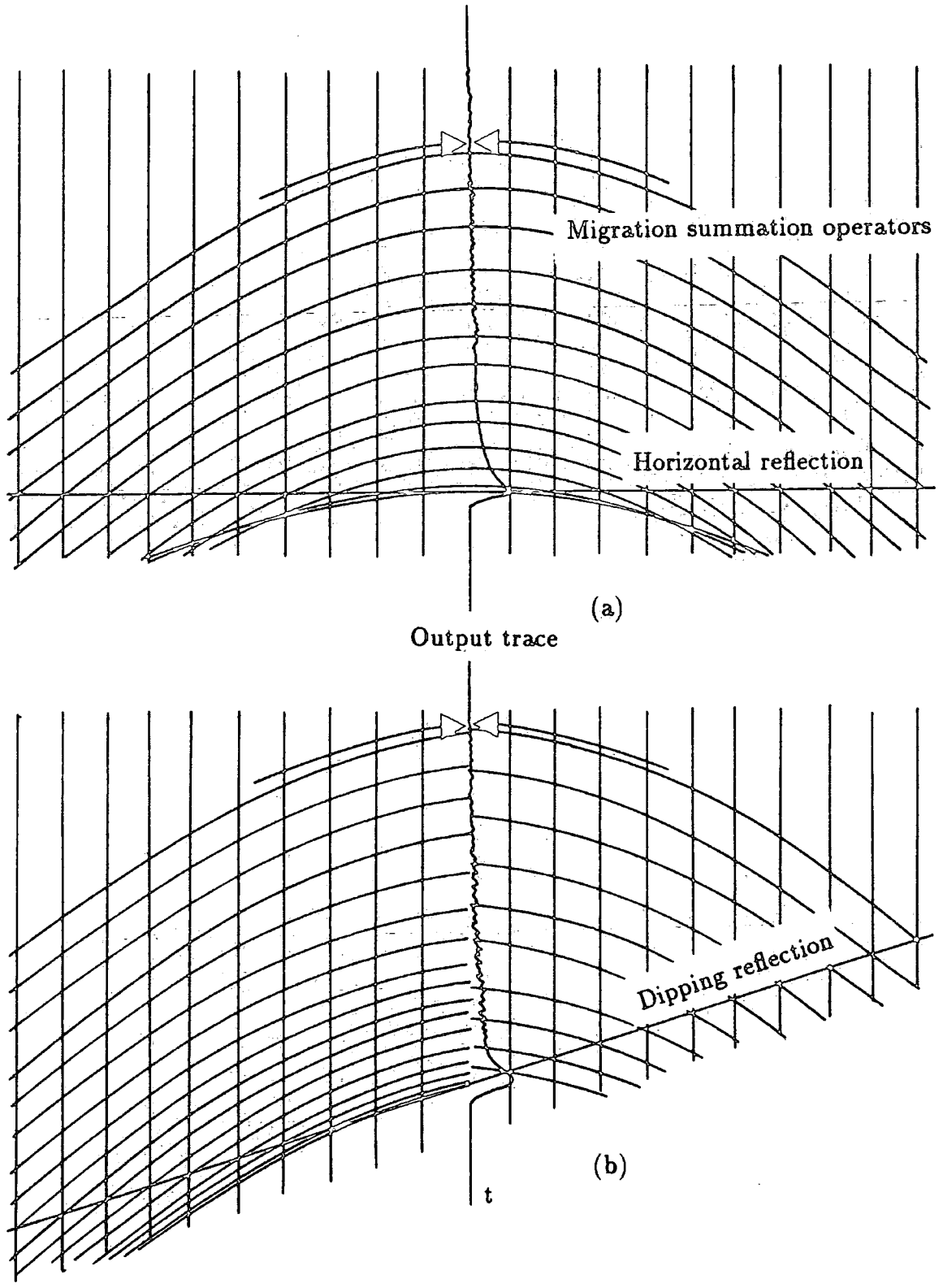

Figure 3.3. Kirchhoff summation migration of (a) a single horizontal reflection and (b) a single dipping reflection (adapted from Hosken, 1979).

(Hosken, 1979). Equation 3.2 assumes that the migration operator has been truncated so that the maximum dip which can be migrated is α_{max}. The true dip α_{max} is related to the dip on the input traces θ_{max}, calculated after values on the time axis have been multiplied by $V/2$, by

$$\tan \theta_{max} = \sin \alpha_{max}$$

Thus if the time moveout per trace of the migration operator is greater than half the period of the maximum frequency, discretisation noise will occur. This is equivalent to the criterion for wavenumber aliasing (section 2.5). To reduce discretisation noise, several options are available.

- The migration operator may be truncated. The maximum dip which can be migrated is decreased.
- A high-cut filter may be applied to the input data so that frequencies above f_{max} are removed. High frequency data are then lost.
- The spatial sampling interval (Δx) may be reduced by spatial interpolation.

Equation 3.2 was derived by Hosken (1979) for zero-offset migration. For finite-offset migration, the equivalent formula would not be such a simple function of dip, frequency and spatial sampling. The approaches outlined above, when applied to finite-offset migration, should still reduce discretisation noise.

3.3.3 Truncation error

The migration summation operator must be truncated to include only a limited number of traces. The size of the operator is limited ultimately by the temporal and spatial extent of the dataset, but in practice it is desirable to truncate the summation operator further. This has several advantages:

- discretisation noise is reduced,

- noise energy is not distributed as far over the section, and
- computer run time, and hence cost, is reduced.

Truncating the operator will also have disadvantages:

- the maximum dip which can be migrated is reduced,
- diffraction hyperbolae are not collapsed fully,
- random noise becomes organised as dominantly horizontally spurious events (Yilmaz, 1987), and
- truncation noise occurs (Hosken, 1979).

Despite these disadvantages, the migration summation operator should be truncated as much as possible. The operator should be chosen to migrate the maximum dip present in the section. Truncation noise may be minimised by tapering the migration operator to zero at the ends of the aperture.

3.3.4 Data aliasing

Migration will perform poorly if data are aliased. This is explained in figure 3.4. Aliased events appear as conflicting dips. The migration summation operator cannot distinguish between the true dip of the event and the apparent aliased dip, so coherent migrated events result from both. Events are thus migrated incorrectly and the section is noisy. Examples are shown by Bardan (1987) and Yilmaz (1987). Prevention of spatial aliasing was discussed in chapter II.

Spatial sampling for a constant-offset section is determined by the shot spacing. Spatial sampling for a stacked section is the CMP interval, which is half of the receiver interval. Thus for the usual case of the shot and receiver intervals being equal, a constant-offset section is twice as coarsely sampled as a stacked section, so an event with a particular time-dip may be unaliased on a stacked section but aliased on a constant-offset section. Bardan (1987) notes that as offset

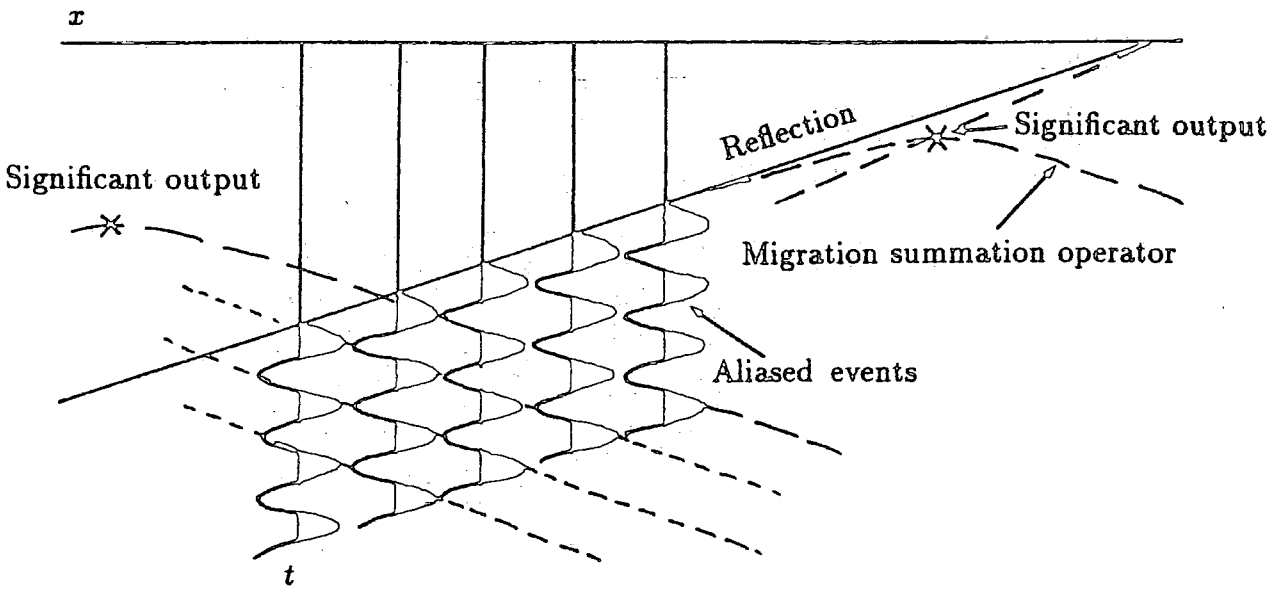

Figure 3.4. Kirchhoff summation migration of spatially aliased events.

increases, the time-dip of a reflection event on a constant-offset section decreases. An event which is aliased on a stacked (zero-offset) section could therefore be unaliased on a constant-offset section. Data are usually acquired so that events on the stacked section will not be spatially aliased. Whether they are aliased on a constant-offset section is dependent on reflector geometry and acquisition parameters.

3.3.5 Stretch

NMO is implicit in prestack migration (Hood, 1980). NMO causes wavelets to be stretched at large source-receiver offsets and low traveltimes. A mute region may be designed to avoid excessive pulse stretching.

3.3.6 Computer algorithms

Kirchhoff summation migration is widely used. A prestack migration scheme is given by Jain and Wren (1980). Kirchhoff migration can be visualised as having two data 'boxes'. One 'box' contains the input data which, for prestack-migration, is a constant-offset section. The other, which is initially empty, contains the migrated output. For each output sample, the appropriate migration summation operator is calculated. The operator then sums across the input data and the weighted sum is placed at the output sample. This operation is repeated for all samples on the migrated output, which may be a limited window of interest. Computer memory limitations may make it necessary for the data to be read and processed in subsets.

For prestack migration, each constant-offset section is migrated individually and the sections are then stacked to build up the 'fold of cover'. In order to economise, groups of constant-offset sections may be stacked prior to migration. Differential normal moveout is applied to each trace in the substack to reduce the range of offsets to a single offset. If the range of offsets is small the time shifts involved are small, hence the process is relatively insensitive to velocity errors and to problems with NMO assumptions. Partial stacking before prestack

migration reduces the number of migrations, but the substacks, and hence the final results, may be degraded in areas where NMO assumptions break down.

3.4 Incorporation of directional deconvolution into prestack migration

Figure 3.1.b shows the elliptical prestack migration impulse response for a constant-velocity medium. To perform prestack migration, energy from each sample on the constant-offset section is distributed over the appropriate ellipse. The take-off angle at the source determines the position on the ellipse.

Migration is usually performed as a summation rather than a 'smearing' operation (section 3.2.1). The geometrical shape of the operator is calculated by considering raypaths to a point diffractor (figure 3.5.a), and is a vertical slice through a Cheops pyramid (Claerbout, 1985). A prestack migration summation operator is shown in figure 3.5.b. There is also a one-for-one correspondence between source take-off angle and location on the summation operator. This provides the basis for performing directional deconvolution.

For a directional source, the source signature will change with source take-off angle (chapter I). Thus each point on constant-offset section along the migration summation operator should be deconvolved with a filter designed for the appropriate take-off angle. If the constant-offset section is deconvolved for the source signature radiated at one particular take-off angle, only the part of the summation operator corresponding to that take-off angle should be included. To perform directional deconvolution, the constant-offset section must be deconvolved separately with a full range of filters for the source signatures radiated in different directions. For each portion of the operator, the source take-off angle is calculated. The deconvolved section which has been deconvolved with the correct angular filter is selected, and the contribution from this section is summed to the migrated output. Thus each migrated sample is obtained by summing across the set of deconvolved sections, selecting the appropriate section for each part of the migration summation operator. This method appears to require massive

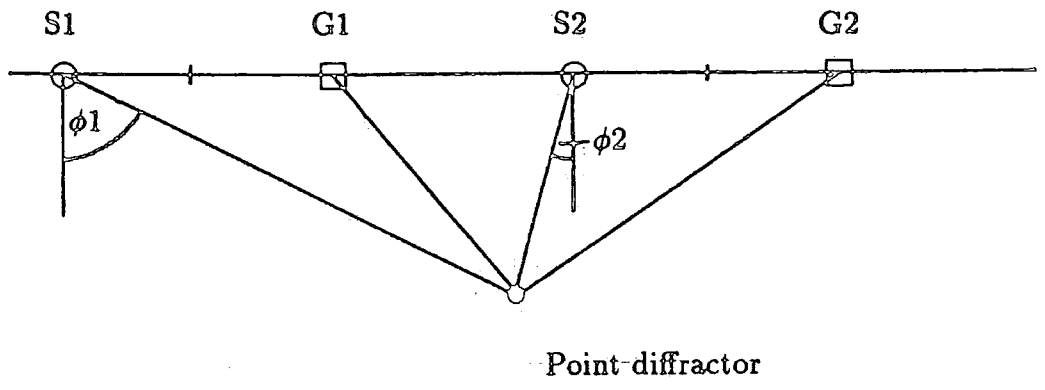

(a)

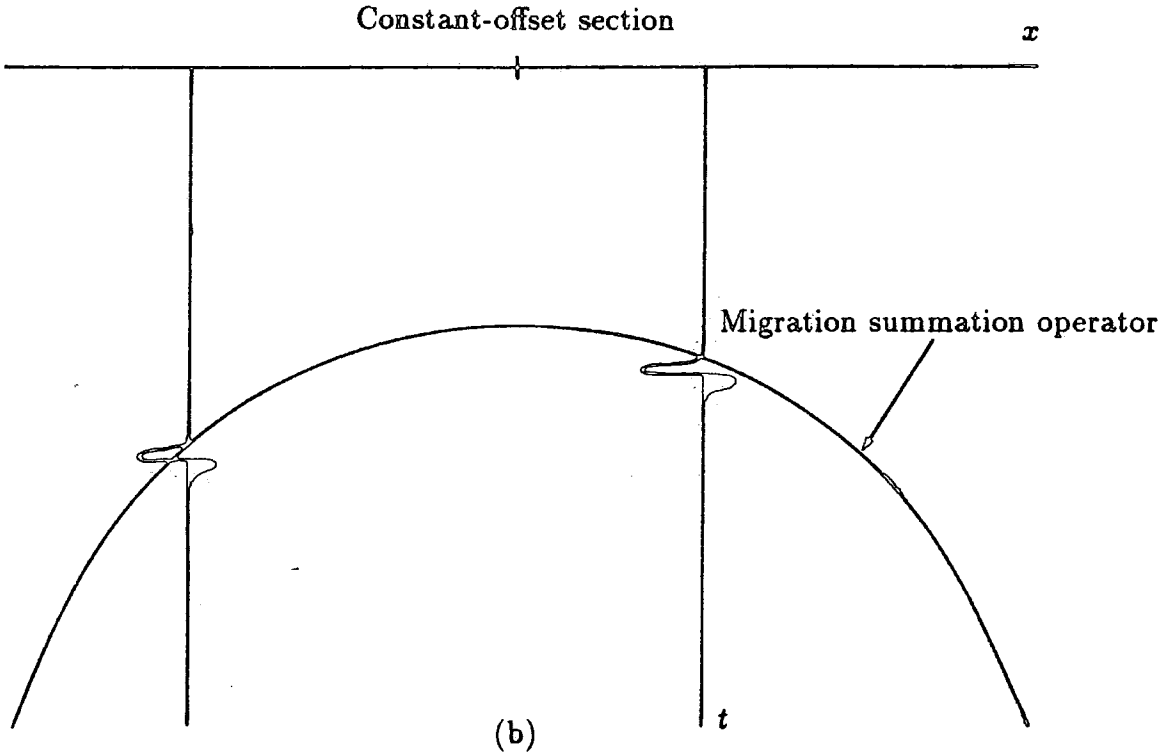

(b)

Figure 3.5. Prestack Kirchhoff summation migration. (a) Geometry of a constant-offset section over a single diffraction point. Raypaths for two source-receiver positions are shown. (b) Constant-offset section from the point diffractor. Seismograms for the two raypaths in (a) are superimposed.

computer storage because the constant-offset sections have been deconvolved for many source take-off angles. To avoid storing all these sections the ordering of the steps in the process can be changed.

In practice, the deconvolutions may be applied sequentially so that only one deconvolved section needs to be stored. The constant-offset section is deconvolved with a filter designed for the first source take-off angle to be considered. For each migrated output sample, summation takes place only over the appropriate part of the migration summation operator. The constant-offset section is then deconvolved with a filter designed for the next source take-off angle. The summation operation is then repeated for each output sample, now summing over that part of the migration summation operator which is appropriate for the new take-off angle. This is repeated for the full range of source take-off angles, after which the section has been migrated fully. Thus each migrated output sample is not calculated in the usual manner, by one application of a complete migration summation operator. They are built up sequentially, by using the relevant parts of the summation operators as the section is deconvolved for each source take-off angle.

To implement the method, a suite of deconvolution filters must be designed for the far-field source signatures radiated at different take-off angles. A discrete increment in angle for successive filters must be chosen, and also the maximum angle to the vertical which needs to be considered.

3.5 The processing scheme

A processing scheme has been written to perform directional deconvolution combined with prestack migration. It is part of a complete processing package which is described in Appendix A.

The first step in the scheme is to calculate the migration and deconvolution parameters.

3.5.1 Calculation of parameters

The migration summation operator is calculated as a function of source take-off angle. This enables deconvolution to be performed efficiently by the computer algorithm. Angular limits and a discrete angular increment for calculating deconvolution operators are chosen. Signature deconvolution filters are designed for the source signatures radiated at the full range of take-off angles chosen.

Angular limits for the summation operator are specified as the maximum source take-off angle either side of the vertical. For simplicity, one limit is used for the whole dataset. Time and spatially varying limits could be incorporated. Limiting the source take-off angles to be considered is equivalent to truncating the migration operator, so the angular aperture should be chosen to migrate the steepest dips present on the section. This aperture may be calculated as follows. Figure 3.6 shows the raypaths from a source and receiver to a point (x_m, z_m) on a dipping reflector. Point (x_m, z_m) is the true subsurface, and hence migrated, position. To migrate reflectors with a dip of α degrees, the migration operator must include source take-off angles up to ϕ degrees, where

$$\phi = \alpha + \beta$$

Hood (1981) shows that the angle of incidence β is given by

$$\beta = \tan^{-1}\left\{\frac{-Vt_m + \left((Vt_m)^2 + 4h^2(1-\cos^2 2\alpha)\right)^{\frac{1}{2}}}{2h(1-\cos 2\alpha)}\right\}$$

where

t_m, the migrated time, is given by

$$t_m = \frac{2z_m}{V}$$

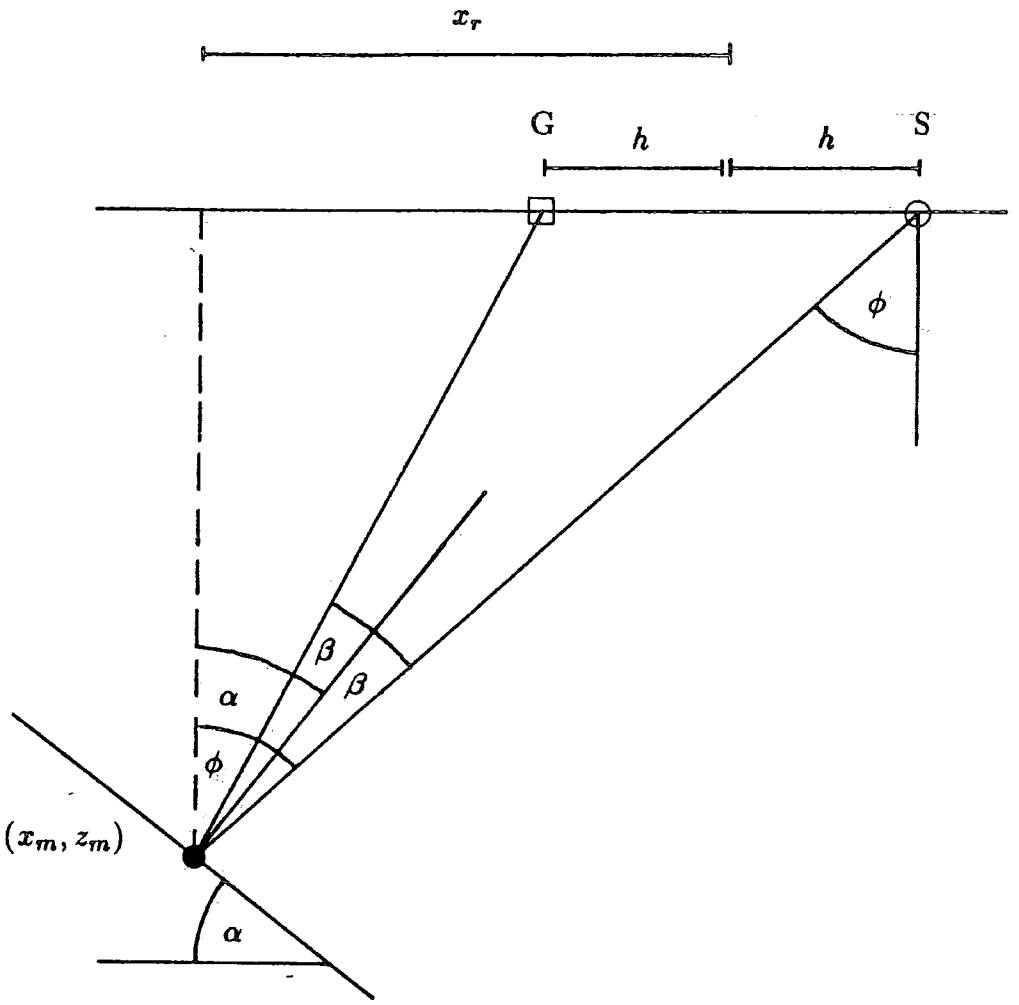

Figure 3.6. Geometry of a dipping reflector, source (S) and receiver (G).

V is velocity, and

h is half the source-receiver offset.

By specifying the maximum geological dip to be migrated at a particular traveltime, the maximum source take-off angle from the vertical which needs to be considered in the prestack migration is calculated.

The angular increment for deconvolution must be chosen. If the increment is small, there will be many deconvolutions for a given angular aperture. The computer run time and hence the cost will be great. If the deconvolution increment is too coarse, events could be deconvolved with a filter designed for a very different source signature. Trials on model and real data show that a deconvolution filter performs well for a range of angular signatures around the one for which it was designed. This range depends on the directivity of the source. The deconvolution increment should chosen to be within this range. A small increment is unnecessary as the source take-off angles used to determine the position on the migration summation operator will be in error if the velocity field is not known precisely.

Source signature deconvolution filters must be designed for the range of take-off angles needed for the migration at the chosen incremental value of take-off angle. They are designed from the far-field source signatures.

3.5.2 Processing algorithm

A flow chart for directional deconvolution combined with prestack migration is shown in figure 3.7. The different stages will now be explained.

1. The parameters for the migration and the directional deconvolution have been calculated and are read from a control file. The complete constant-offset section is read into memory from magnetic tape. The tape must be in SEG-Y (Society of Exploration Geophysicists, 1980) format. Alternatively,

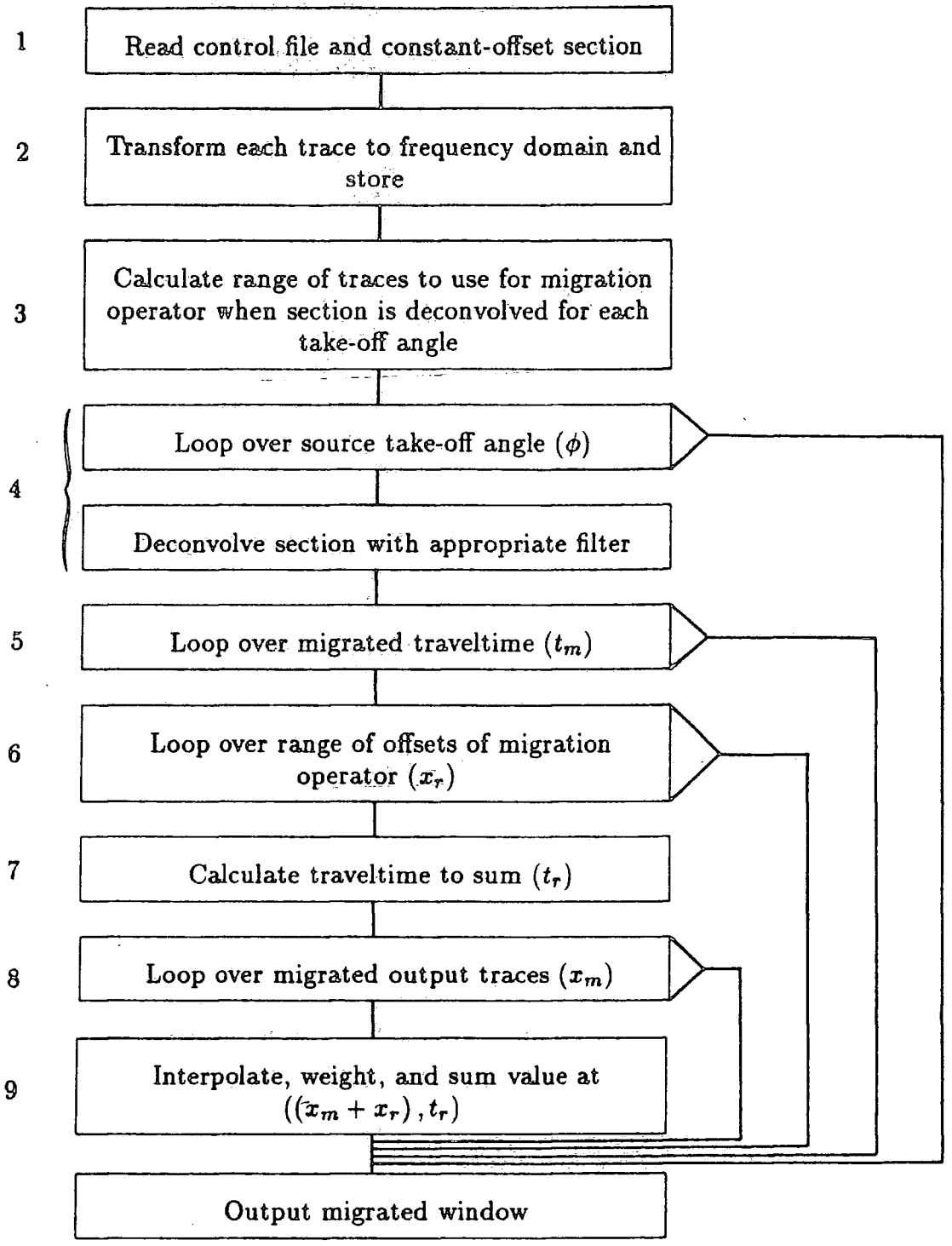

Figure 3.7. Directional deconvolution combined with prestack migration. Computer flow chart.

the constant-offset section may be read directly from a file on disc. The traces on the section may be bandpass filtered.

2. Each trace on the constant-offset section is transformed into the frequency domain, using a one-dimensional FFT, and stored. Storage in the frequency domain will enable rapid deconvolution of the constant-offset section at a later stage. The data and signature deconvolution filters are padded with zeros to the same length prior to the FFT so that the discrete frequency values of the data and filters are the same.

3. The migration summation operator will be applied in several stages as a function of source take-off angle. The operator is a function of migrated traveltime, velocity and source-receiver offset, and so must be calculated for each migrated sample. For a laterally homogeneous medium, the migration summation operator is spatially invariant. Thus the operator calculated for each traveltime may be used for all traces on the migrated output. In addition to calculating the operator, the portion of the operator to employ when the constant-offset section has been deconvolved for a particular take-off angle must be calculated. At this stage, the traveltimes of each point on the operator are not calculated. This avoids unnecessary storage. Only the range of traces, expressed as the range from the apex of the summation operator to the points to be summed (x_r), are calculated and stored. From figure 3.6

$$x_r = z_m \tan\phi - h$$

Now

$$z_m = \frac{V t_m}{2}$$

so

$$x_r = \frac{V t_m}{2} \tan\phi - h$$

Thus, for a particular migrated traveltime t_m, the portion of the migration summation operator to use when the section has been deconvolved for a particular source take-off angle ϕ is calculated. This calculation is performed for all traveltimes and the results stored.

4. This loop is the first of four 'nested FORTRAN DO-loops'. DO-loops allow the repetition of a number of statements a predetermined number of times. The loops are shown schematically in figure 3.8.

   The first source take-off angle is considered. Take-off angles vary from the maximum to the minimum chosen, and increment by the chosen amount. The constant-offset section is deconvolved with the appropriate signature deconvolution filter. The filters are read from file, and deconvolution is performed by multiplication in the frequency domain. The constant-offset section is now correctly deconvolved for a small range of source take-off angles, which is assumed to equal the chosen angular deconvolution increment.

5. The first migrated traveltime is considered. Traveltimes vary from the minimum to the maximum traveltimes in the migrated window.

6. The section has been correctly deconvolved for a small range of take-off angles (stage 4), and the portion of the migration operator to use for the particular traveltime (stage 5) and take-off angle being considered has been calculated (stage 3). Thus the range of traces over which the summation operator is to sum is known. The first offset within the range is considered. The range varies from the maximum to the minimum previously calculated, expressed as the offset of the trace from the apex of the summation operator.

7. For the first offset to be included in the summation, the traveltime of the operator is calculated. From figure 3.6, the traveltime on the constant-offset

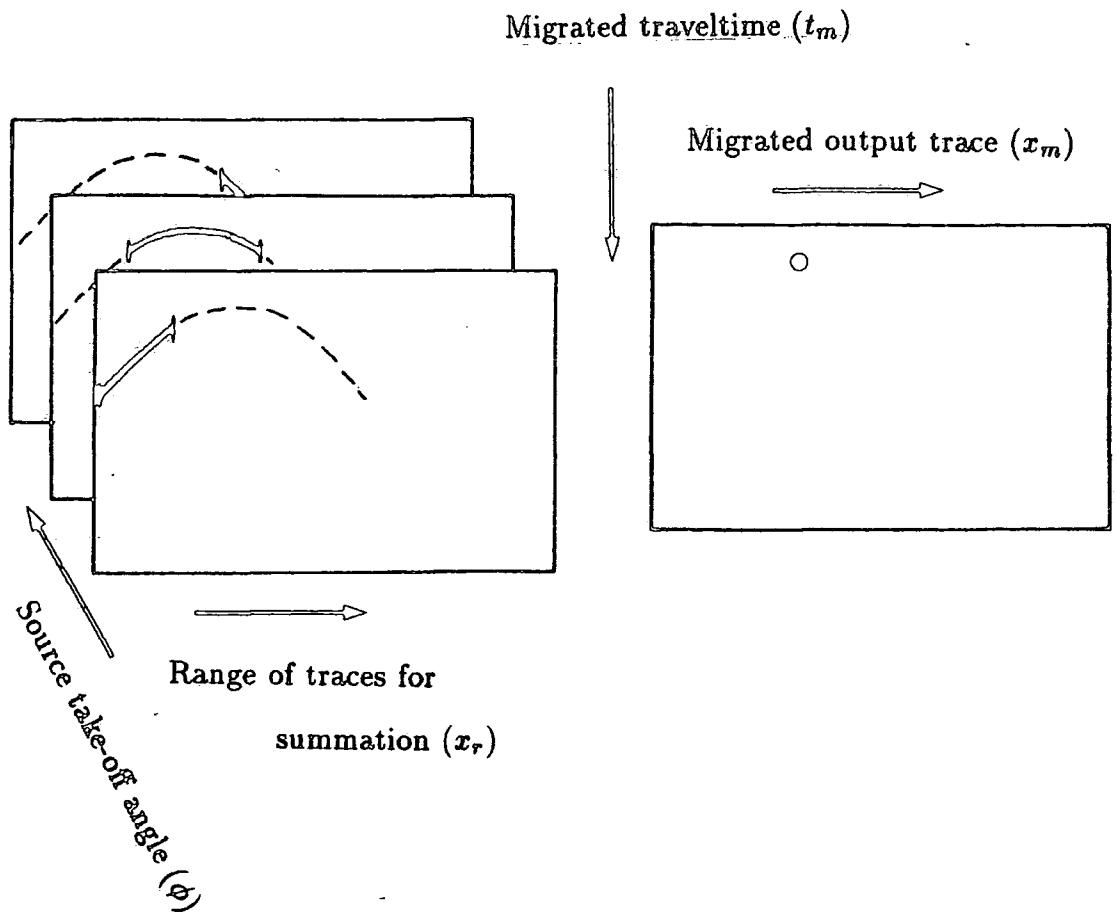

Figure 3.8. Directional deconvolution combined with prestack migration. Schematic diagram.

section (t_r) will be the sum of the traveltimes from the source and from the receiver to the point (x_m, z_m). Therefore

$$t_r = \frac{1}{V}\left\{((x_r - h)^2 + z_m^2)^{\frac{1}{2}} + ((x_r + h)^2 + z_m^2)^{\frac{1}{2}}\right\}$$

8. The first trace on the migrated output is considered. Output traces vary from the first to the last in the migration window.

9. The correct trace to use for the summation is given by

$$x_m + x_r$$

The correct traveltime (t_r) to use has been calculated. The value is interpolated, weighted and summed to the migrated output sample.

The DO-loops then proceed in the usual manner, as shown in figure 3.8. The values are calculated and summed to all of the traces in the migrated window, while the variables in loop 4 (ϕ), loop 5 (t_m) and loop 6 (x_r) are kept constant. Then the process is repeated for each of the traces to be included in the migration operator (each defined by a particular value of x_r), for the first migrated traveltime and the first source take-off angle. The process is then repeated for the next migrated traveltime (t_m). The section has now been migrated for the small range of take-off angles, defined by the deconvolution increment and the first take-off angle. The constant-offset section is then deconvolved for the next take-off angle and the whole process repeated. Once all take-off angles have been considered, the window is migrated fully and is written to file. The Newman filter is then applied by multiplication in the frequency domain.

The program may also be used with standard signature deconvolution rather than directional deconvolution. The constant-offset section is deconvolved with the filter designed for the vertically travelling wavelet on the first entry to loop 4,

after which no further deconvolution is performed. This will enable a comparison of directional deconvolution with standard one-dimensional deconvolution.

The program outlined above has been written to evaluate the technique of directional deconvolution combined with prestack migration. It has been written for use on the University of Durham Amdahl 470/V8 mainframe computer. The aim of the program has been to keep the number of deconvolution operations to a minimum which will minimise CPU time. This has been achieved, but at the expense of large storage requirements because the whole constant-offset section must be stored. If computer memory limitations dictate that the data must be processed in subsets, the number of deconvolutions will increase. Storage of the deconvolved constant-offset sections on disc or magnetic tape is an alternative method, but read and write times will be greater.

In the present scheme, interpolation (stage 9) is performed by use of a bicubic spline. A smooth curve is fitted to several samples either side of the point to be interpolated, and then the value is calculated. This operation must be performed every time a value is summed and is therefore time consuming. The standard approach to interpolation is to resample data to a finer sampling interval. The nearest sample to the point to be interpolated is then used as the interpolated value. This resampling technique is very popular, for example for the application of NMO and for velocity analysis. Resampling is most efficiently performed in the frequency domain. Data are transformed to the frequency domain and padded with zeros before the inverse transform. Resampling to eight times the original sampling is often performed. For the present prestack migration algorithm, resampling is not feasible because if the whole constant-offset section were resampled, the required storage space would exceed computer memory limitations.

There are many permutations of how directional deconvolution combined with prestack migration may be programmed. The present scheme has been employed sucessfully on the Durham University computer where keeping the run

time to a minimum is of paramount importance. The technique is now tested on physical model data before being applied to real data.

Chapter IV

Directional Deconvolution of Model Data

4.1 Introduction

Physical and synthetic modelling techniques were available for testing the directional deconvolution methods described in chapters II and III. Two physical model datasets were used. Dataset 1 was acquired over a steeply dipping wedge model to evaluate the prestack migration method (chapter III). A second dataset was acquired over a less steeply dipping model to test the f-k method (chapter II), to compare the two methods and to examine a dataset with less directivity effects than the first.

4.2 Seismic modelling

Evaluation of a seismic processing technique using real data is highly subjective, because the earth's reflectivity sequence is not known. Model seismic data are employed widely for testing processing software. Test datasets are generated cheaply, over known models, using physical or synthetic modelling techniques.

Physical modelling has been used over many years to study seismic wave propagation (e.g. Angona, 1960, Purnell, 1986). Recently, the main role of physical modelling has been to generate test datasets for processing techniques (e.g. Tatham et al., 1983, Wapenaar and Berkhout, 1987). Several institutions have modelling facilities; the most prominent is the Seismic Acoustic Laboratory at Houston (McDonald et al., 1983).

In most modern modelling systems, data are acquired over solid models submerged in a water-tank. Model making is a highly specialised operation if geologically realistic models are required. Energy sources which generate frequencies

in the ultrasonic range are used so that data may be scaled to geological proportions. Piezoelectric transducers are the most efficient sources and receivers.

Physical model data are close in 'character' to real data. All arrivals, including 3-D effects, are correctly modelled. Noise is also present. Disadvantages of physical modelling are that certain geological features (e.g. velocity gradients) are difficult to model, and certain dimensions (e.g. source size) do not scale correctly.

Synthetic modelling is reviewed by Kennett and Harding (1985) and by Mooney (1983). There are five basic categories;

- asymptotic ray theory (ART) (Červený et al., 1977),
- Gaussian beam modelling (Červený et al., 1982),
- integral methods (Trorey, 1977),
- reflectivity modelling (Fuchs and Müller, 1971), and
- numerical methods (e.g. Kelly et al., 1976).

The five categories and physical modelling are compared in table 4.1.

All synthetic modelling methods involve some form of approximation which leads to incorrect modelling of certain features. Incorrect modelling can be predicted theoretically, and can be illustrated by comparison with physical model data (Howson, 1982). Physical modelling generates realistic datasets, similar in most respects to real data; therefore this method was used to test directional deconvolution.

4.3 University of Durham physical modelling system

The ultrasonic seismic modelling system at the University of Durham is designed to acquire reflection data in common-midpoint (CMP) gathers from solid

Feature	Ray tracing	Gaussian beam	Kirchhoff	Reflectivity	Numerical	Physical
Plane layers						
Pre-critical reflections	1	1	1	1	1	1
Near-critical reflections	0	1	1	1	1	1
Post-critical reflections	1	1	1	1	1	1
Head waves	0	0	0	1	1	1
Thin layers	0	0	0	1	1	1
Multiples	1	1	1	1	1	1
Dipping layers	1	1	1	0	1	1
Diffractions	0	0	1	0	1	1
Cusps and caustics	0	1	1	0	1	1
Frequency dependent effects	0	0	0	1	1	1

(a)

Feature	Ray tracing	Gaussian beam	Kirchhoff	Reflectivity	Numerical	Physical
Cost of modelling	low	low	high	high	very high	low
Time taken to model	low	low	high	high	very high	high
Availability of package	very good	poor	good	good	poor	poor
Packages at Durham	SEIS83 AIMS	BEAM87	AIMS	SYNSEI	-	TANK

(b)

Table 4.1. Seismic modelling. (a) Capabilities of modelling methods (1: features are correctly modelled. 0: features are not correctly modelled. Some packages may have additional features.). (b) Practical aspects.

models submerged in a water tank (Sharp et al., 1985). A range of silicone rubbers and epoxy resins, with different acoustic and elastic properties, are available for model making. Often simple perspex models are adequate.

Data acquisition is controlled by a PDP 11-23+ computer. Acquisition parameters are input manually, after which acquisition is fully automated. Data are written to magnetic tape in SEG-Y (Society of Exploration Geophysicists, 1980) format.

To measure source directivity, a 'test-rig' was used. The receiver transducer was held at one end of a rigid arm, which pivoted about the source transducer position. The arm was long enough to ensure that far-field signatures were measured. A directivity test dataset was generated by rotating the arm manually, and recording the source signature at each angular increment. Increments were read from a protractor scale. To measure receiver directivity the transducer positions were reversed, with the receiver transducer at the pivot.

Source directivity is illustrated in figure 4.1.a, and receiver directivity in figure 4.1.b. The source transducer is highly directional. There is a decrease in amplitude, and change of signature shape with increasing take-off angle. The receiver is less directional than the source. Receiver directivity has been ignored in directional deconvolution tests.

4.4 Directional deconvolution filter design

Directional deconvolution is an extension of one-dimensional signature deconvolution. Far-field signatures are measured directly for physical model data. A desired output is chosen which is the same for signatures radiated at all source take-off angles. Deconvolution filters are designed for each signature in the time domain (Robinson and Treitel, 1980), or in the frequency domain (section 2.2.1). 'Directional deconvolution combined with prestack migration' (chapter III) uses these filters directly. 'Directional deconvolution in the frequency-wavenumber

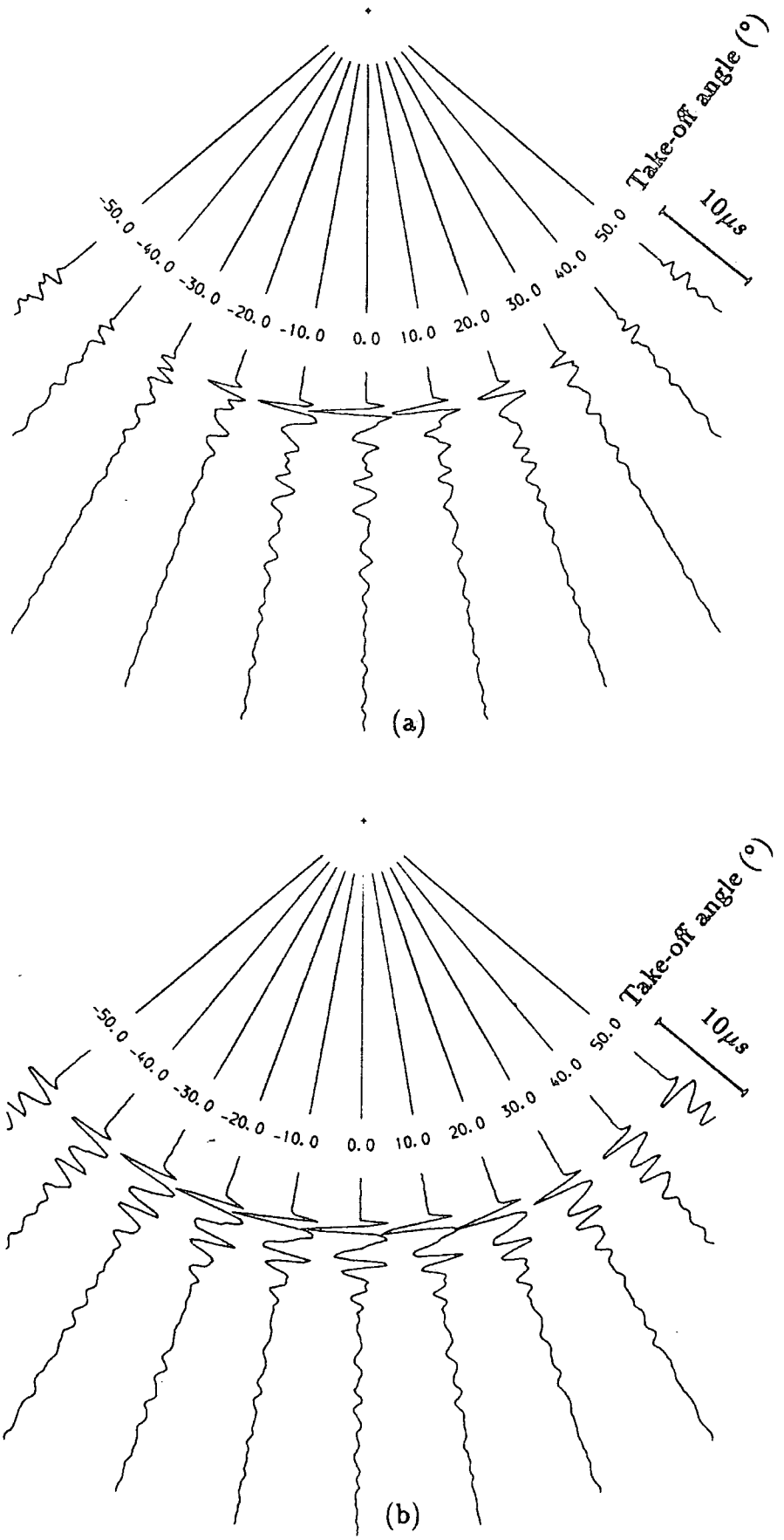

Figure 4.1. Directivity of ultrasonic transducers, (a) source and (b) receiver. Far-field measured signatures are shown .

domain' (chapter II) requires filters to be mapped on to the f-k plane (section 2.2.2).

Selected measured far-field source transducer signatures are shown in figure 4.2. Amplitude spectra are also displayed. Choice of a desired output for deconvolution is arbitrary, but a wavelet with similar spectral content to the signatures is desirable because amplification of the deconvolution filters will be close to unity for all frequencies. The phase of the desired output is also arbitrary. A zero-phase wavelet was chosen because it has the shortest time duration of any wavelet with the same amplitude spectrum. Four desired outputs were considered (figure 4.3).

Figure 4.3.a shows the zero-phase version of the vertically travelling wavelet. Directional deconvolution using this wavelet as a desired output would synthesise a source which radiates this waveform in all directions. An ideal source would radiate a waveform with all energy concentrated in a central peak. This wavelet (figure 4.3.a) has energy in 'side lobes', because the spectrum is not smooth. Smoothing of the spectrum reduces side-lobe energy (figure 4.3.b). Deconvolution filters were designed using the 'smoothed vertically travelling wavelet' (figure 4.3.b) as a desired output, and are shown in figure 4.4. Filters were designed in the time domain. At large take-off angles the deconvolution filters amplify high frequencies. This is because the desired output (figure 4.3.b) has higher frequency content than the source signatures (figure 4.2) at large take-off angles. These large take-off angle filters (figure 4.4) are unstable and will cause noise amplification. A desired output with less high frequency content should stabilise the filters.

The 'average signature' (figure 4.3.c) and 'smoothed average signature' (figure 4.3.d) have less high frequency content than the 'smoothed vertically travelling wavelet' (figure 4.3.b). The average signature was calculated by summing all of the measured angular signatures shown in figure 4.2. Deconvolution filters designed with the smoothed average wavelet as the desired output are shown

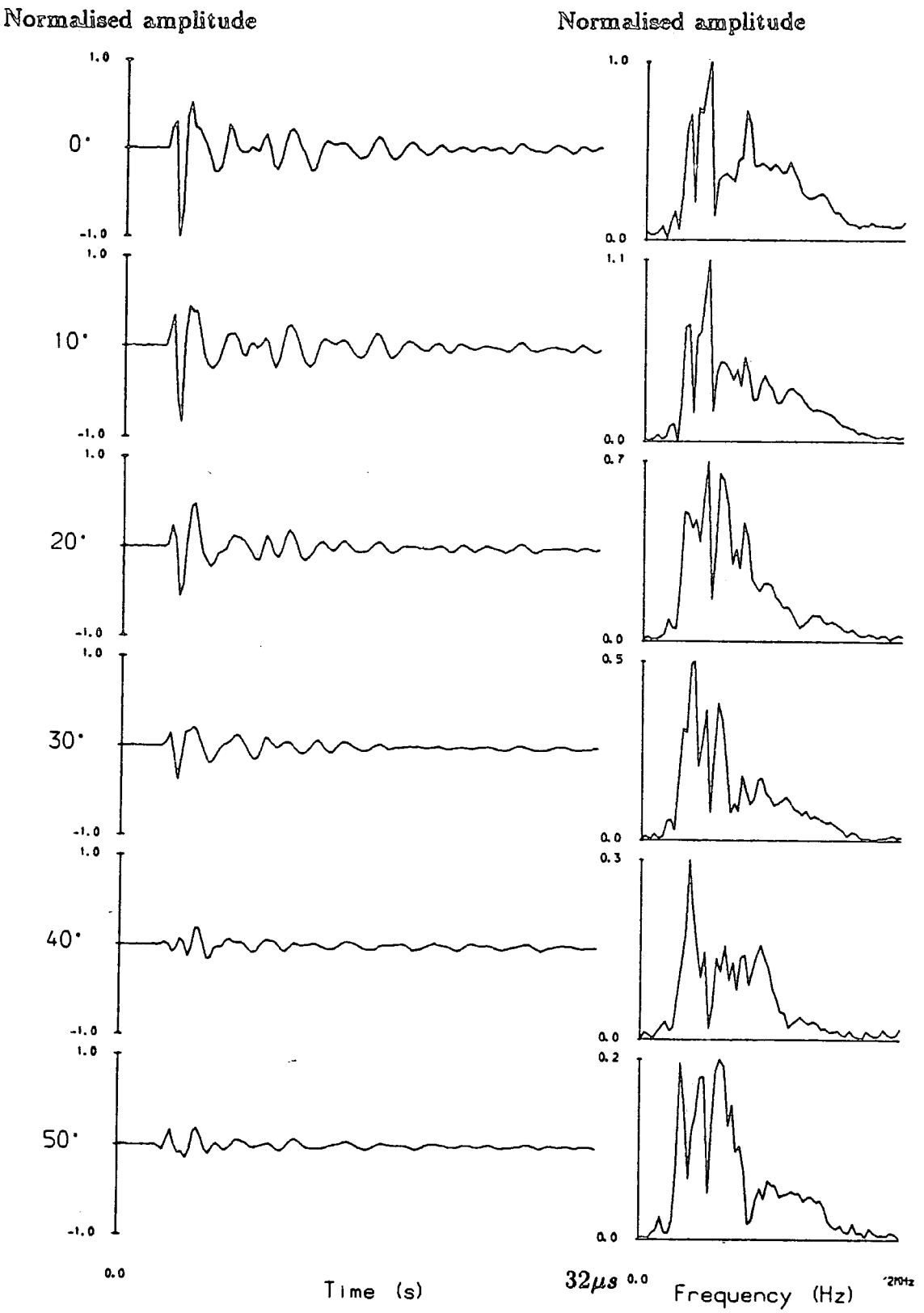

Figure 4.2. Far-field source transducer signatures and amplitude spectra. Take-off angles vary from 0° (vertical) to 50° from vertical.

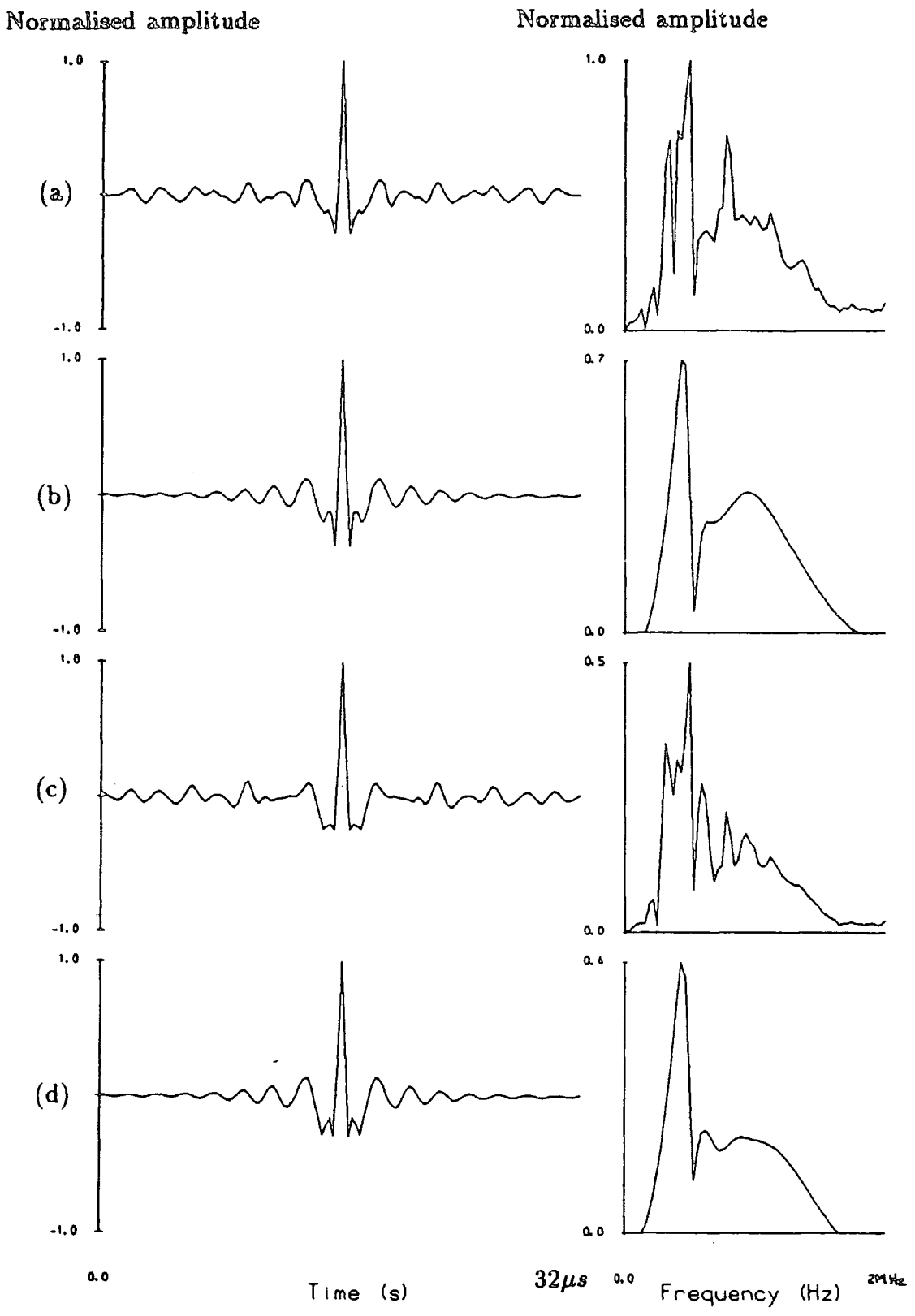

Figure 4.3. Desired outputs for deconvolution. (a) Zero-phase equivalent of the vertically travelling signature. (b) Waveform with smoothed amplitude spectrum of signature (a). (c) Average signature. (d) Waveform with smoothed amplitude spectrum of signature (c).

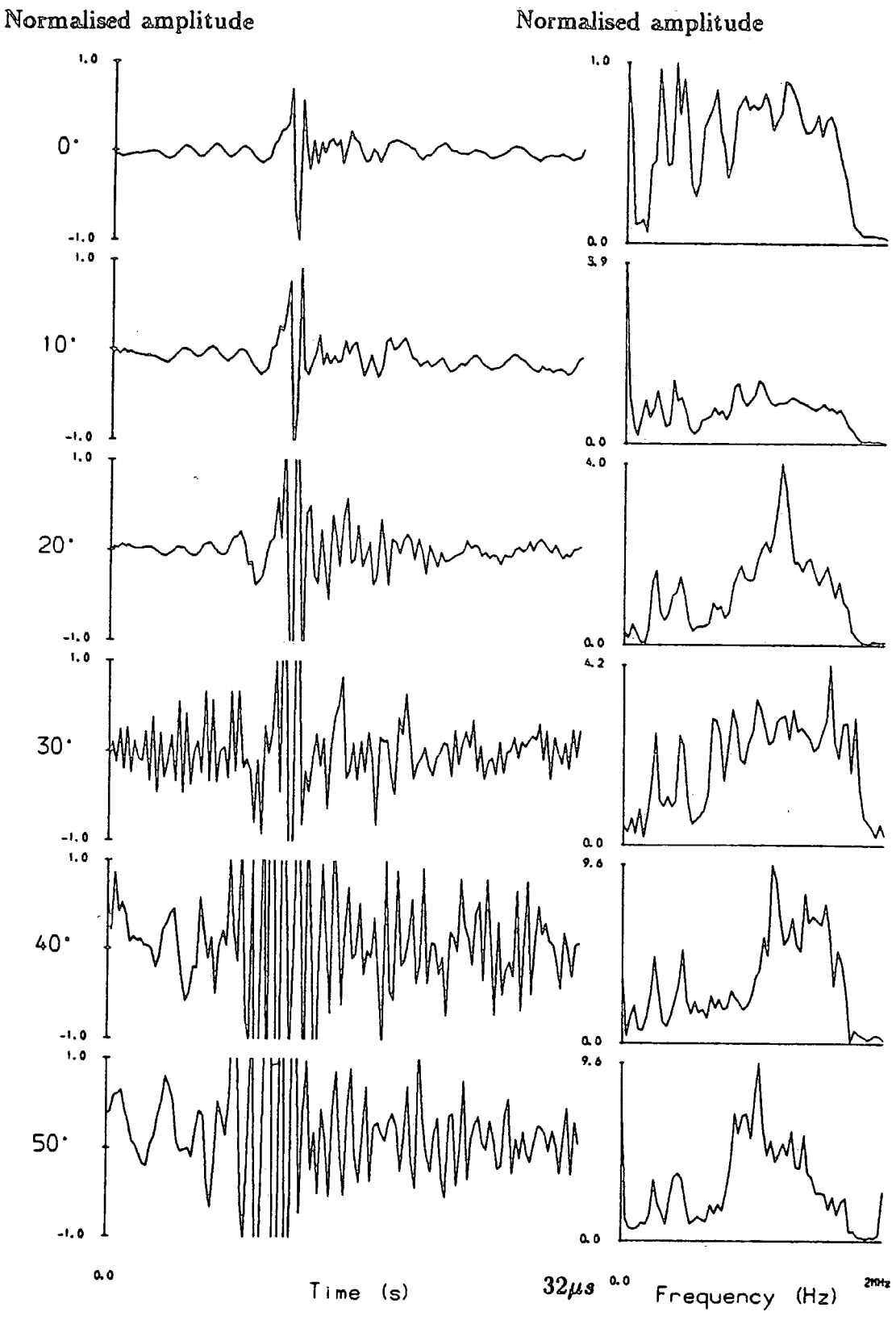

Figure 4.4. Directional deconvolution filters designed for the far-field signatures shown in figure 4.2, and the desired output in figure 4.3.b.

in figure 4.5. These have lower amplification at high frequencies than figure 4.4. Thus the filters are more stable, but large take-off angle filters still have excessive amplification of high frequencies. More severe high-cut filtering of the desired output would stabilise the filters further. As directional deconvolution aims to preserve high frequencies, this would be counter-productive.

An alternative method of reducing amplification of high frequencies at large take-off angles is to taper the amplitude of the desired output with take-off angle in approximate agreement with the reduction in amplitude of the source signature. The desired output shown in figure 4.3.b was used. The energy of each source signature was calculated, and the desired output was modified so that it had similar energy to each of the angular signatures for filter design. Filters designed for the tapered desired output are shown in figure 4.6. Several ~~filters~~ filters still have excessive amplification at certain frequencies. This was suppressed by the addition of 1.0% white noise in filter design (figure 4.7). The result of applying these filters (figure 4.7) to the source signatures (figure 4.2), is to synthesise a source which radiates waveforms of the same spectral content at all take-off angles, but radiates energy in a similar manner to the original source signatures. This is shown by the actual outputs in figure 4.8. The actual outputs are not identical to the desired output (figure 4.3.b) because of the finite length of the deconvolution filters. The results of standard signature deconvolution using a filter designed for the vertically travelling wavelet are shown in figure 4.9. Directional deconvolution (figure 4.8) is superior, especially at large take-off angles.

For the highly directive source transducer, directional deconvolution is unable to remove directivity without excessive noise amplification. The synthesised source is still directional because a lower energy signal is radiated at large take-off angles. Directional deconvolution does, however, restore high frequencies of large take-off angle signatures, so that these signatures become a scaled version of the vertically travelling signature. Directional deconvolution was performed using the filters shown in figure 4.7.

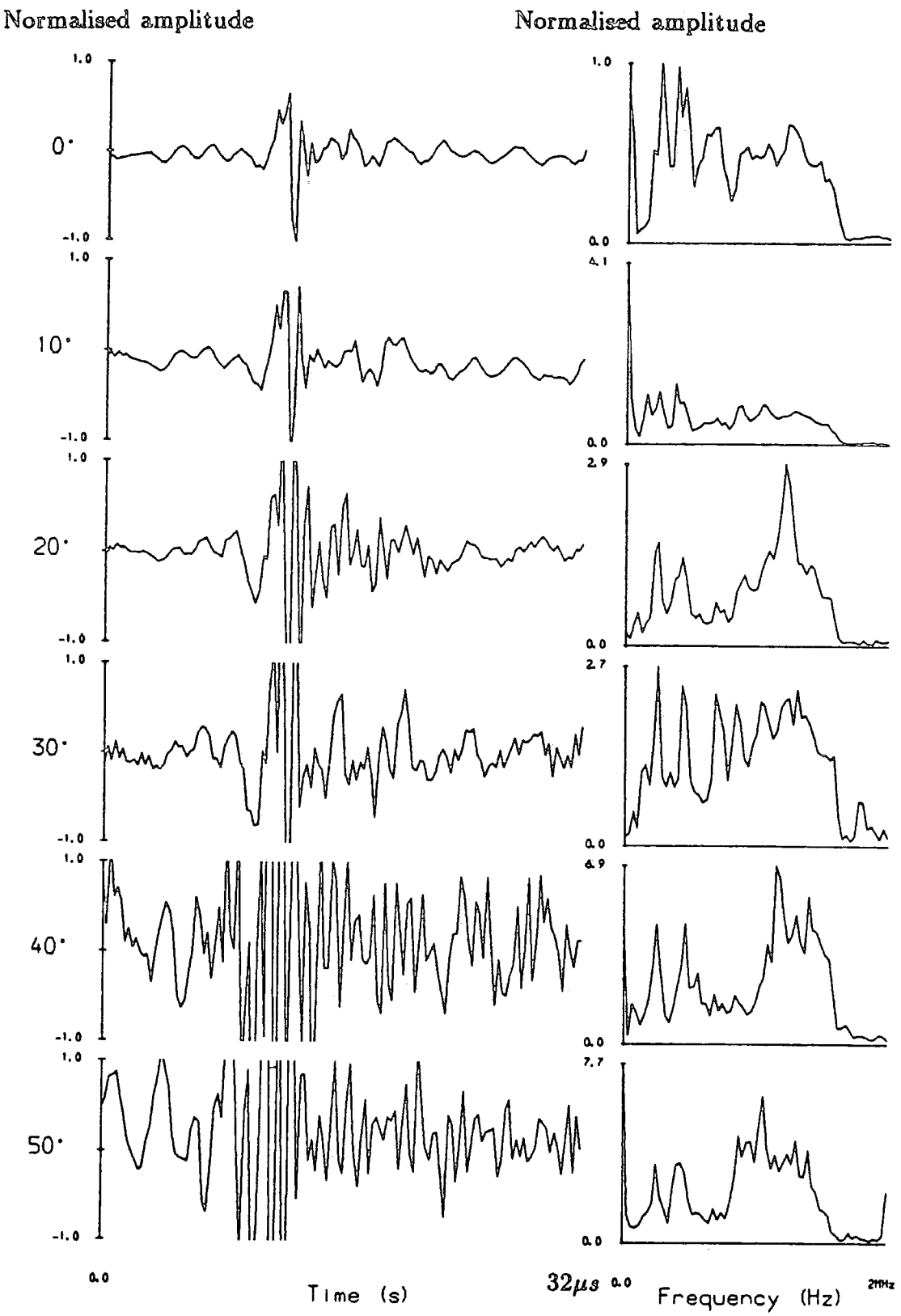

Figure 4.5. Directional deconvolution filters as for figure 4.4 but designed for the desired output in figure 4.3.d.

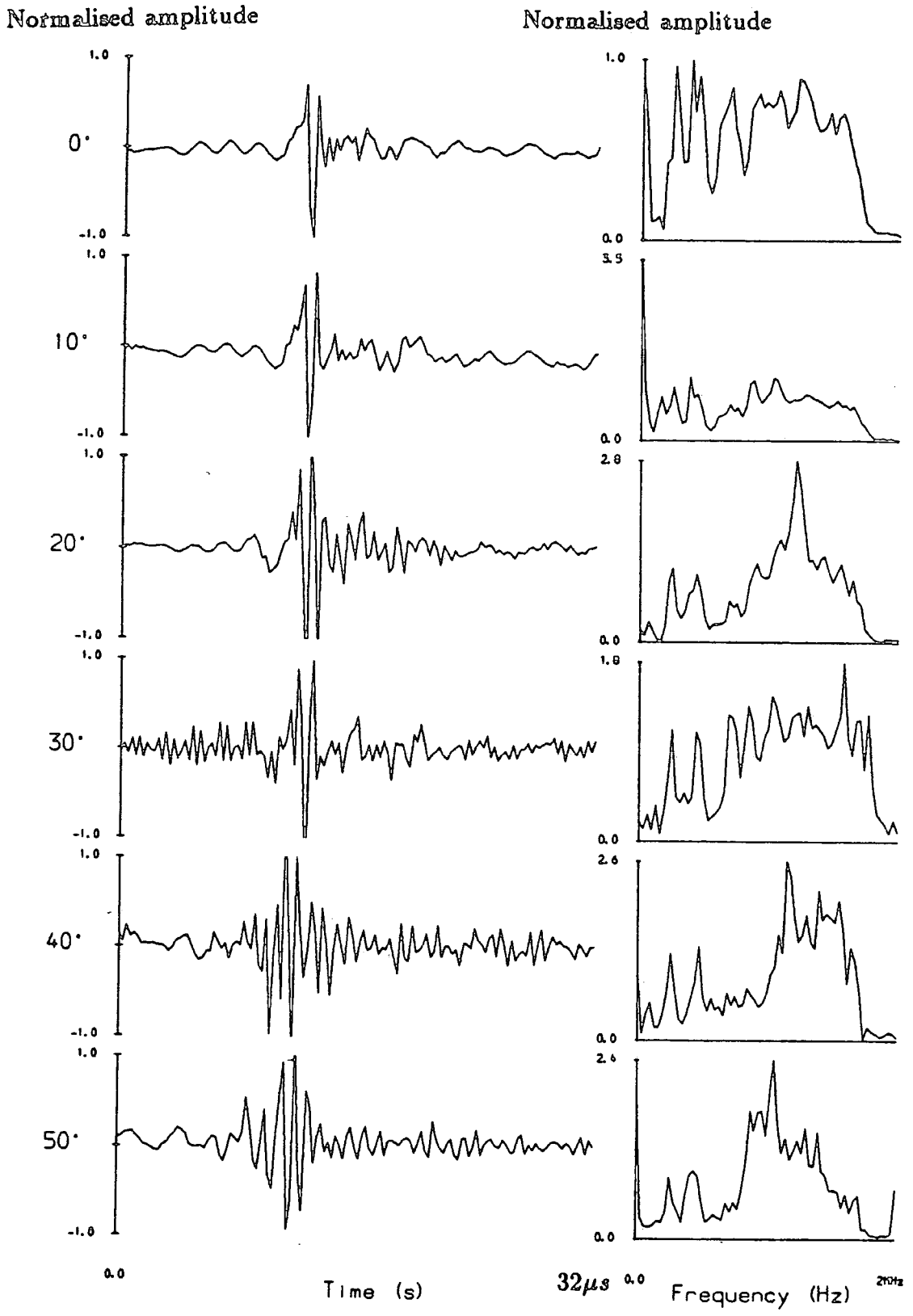

Figure 4.6. Directional deconvolution filters designed as for figure 4.5 but designed with a tapered desired output.

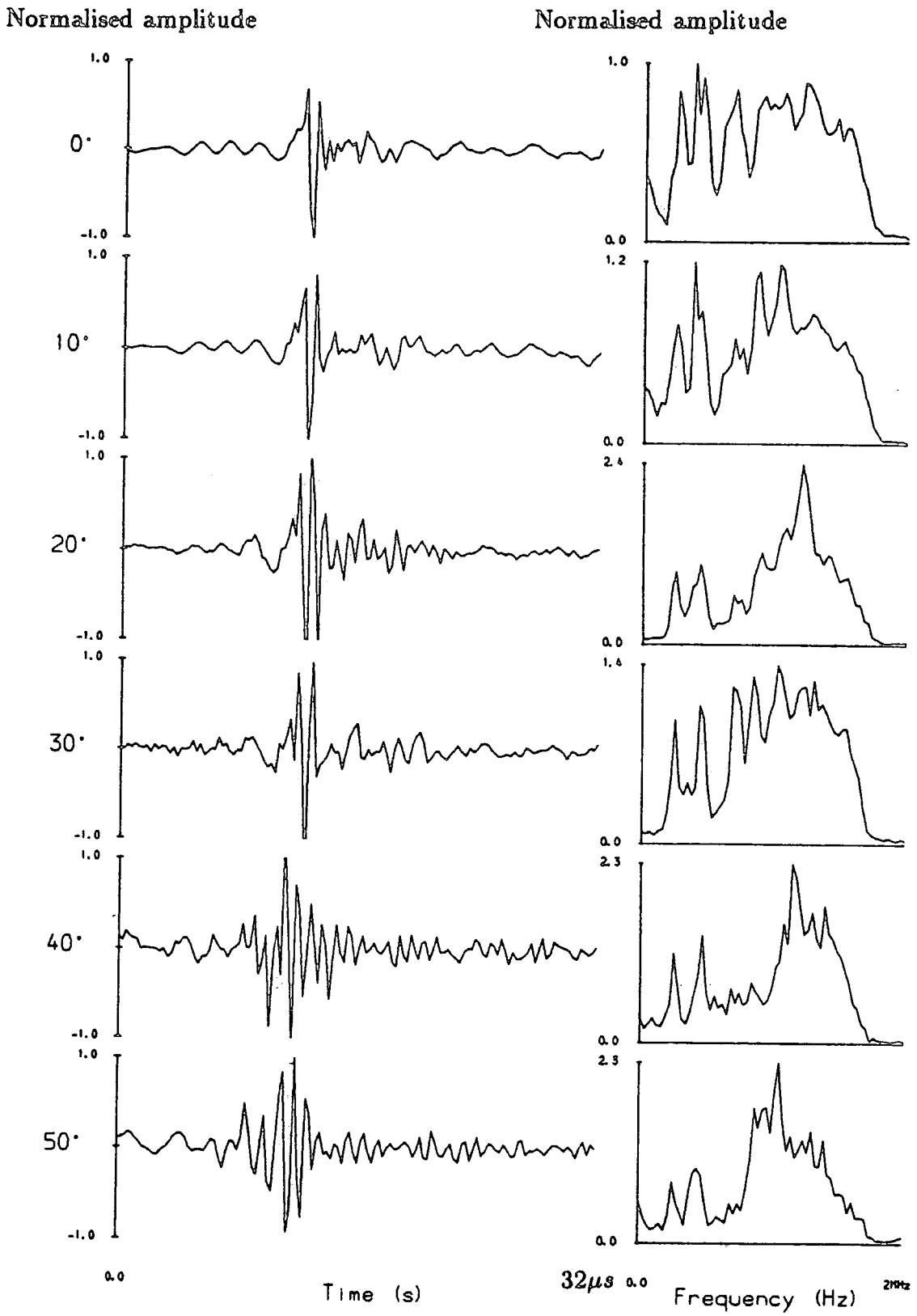

Figure 4.7. Directional deconvolution filters designed as for figure 4.6 but designed with the addition of 1.0% white noise.

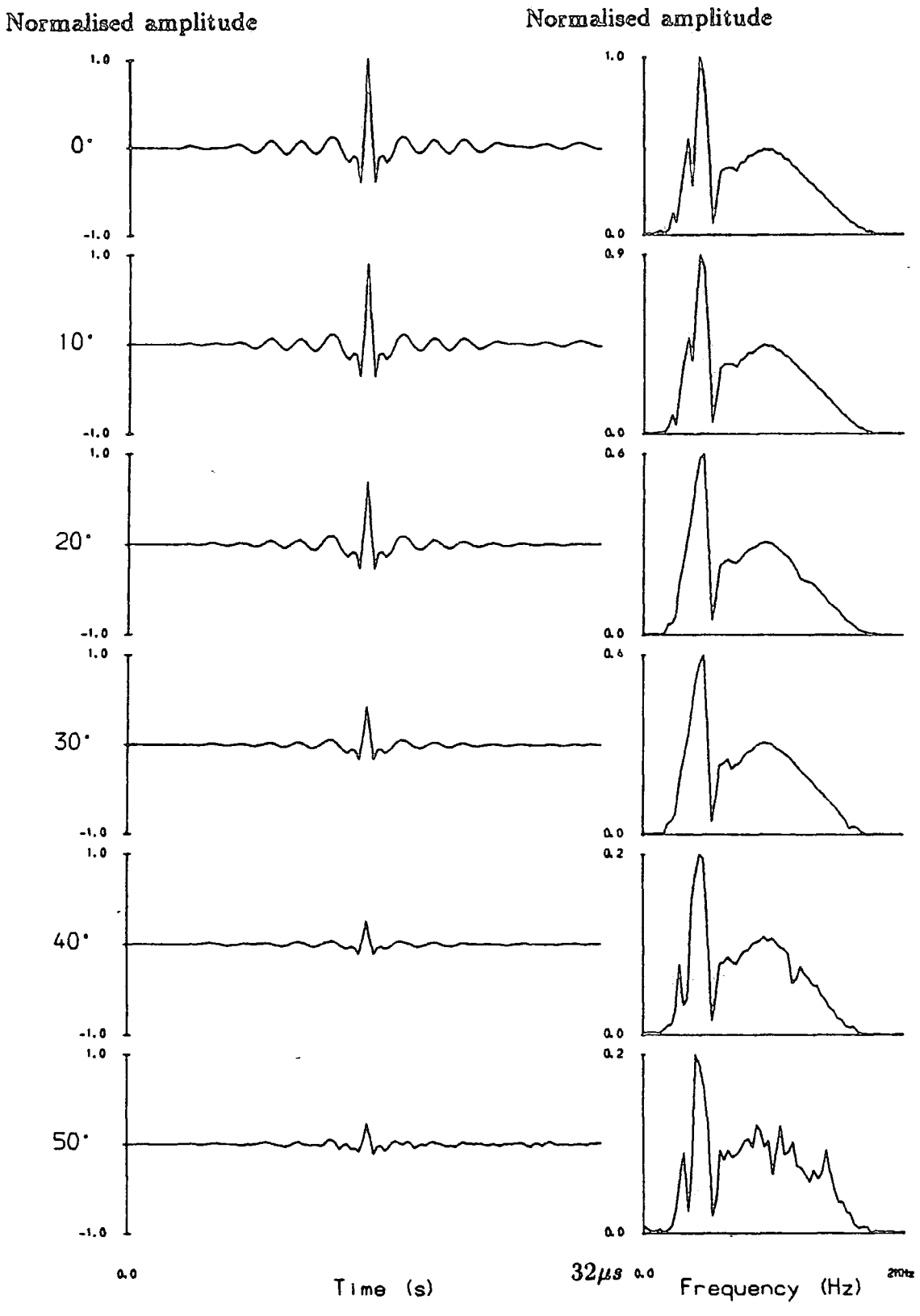

Figure 4.8. Actual outputs when the directional deconvolution filters (figure 4.7) were applied to the source signatures (figure 4.2).

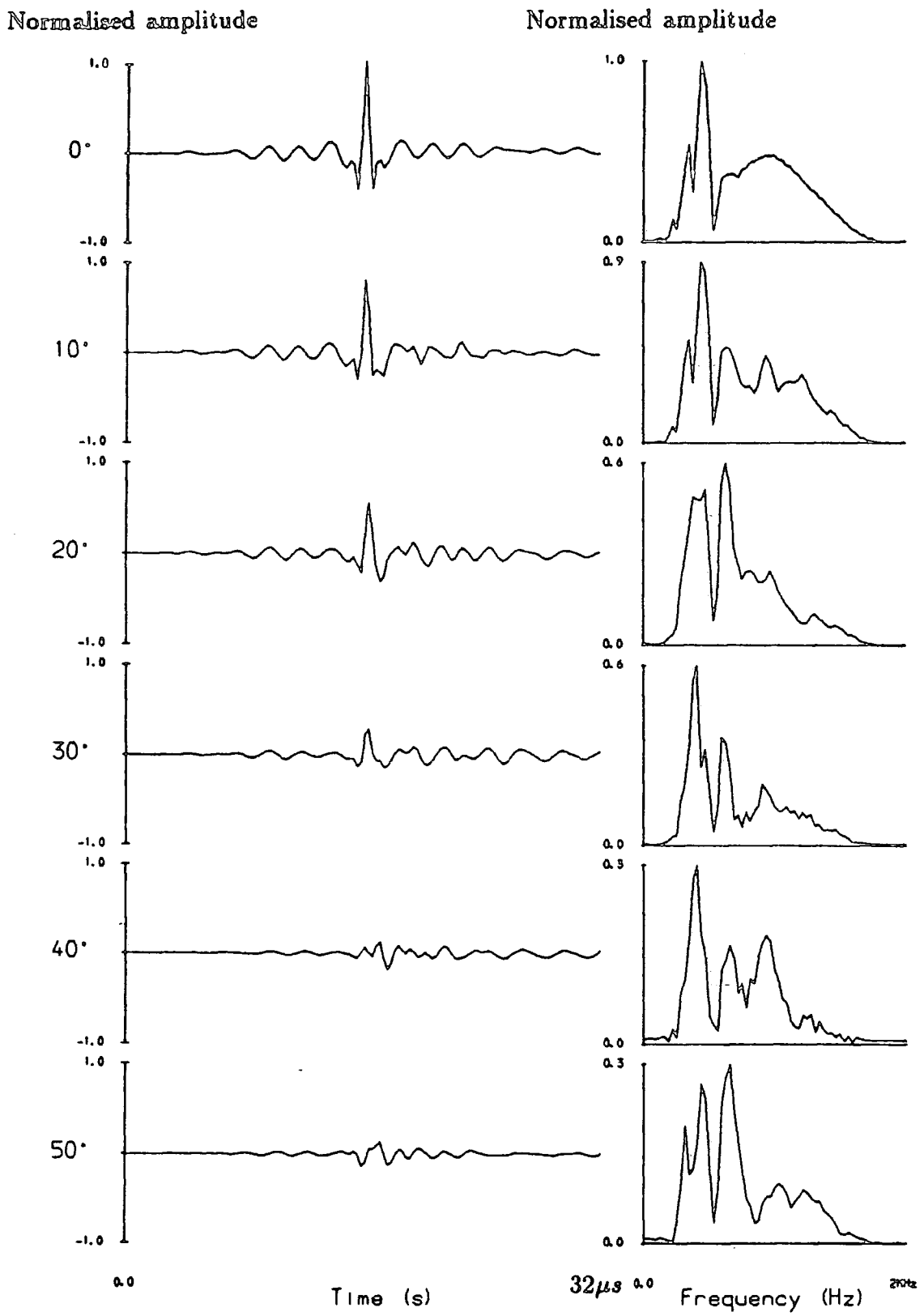

Figure 4.9. Actual outputs when the filter designed for the vertically travelling signature (top of figure 4.7) was applied to the source signatures (figure 4.2).

For the f-k method of directional deconvolution (chapter II), filters must be mapped on to the f-k plane. For simplicity, the source response was considered to be symmetrical about the vertical (horizontal waveneumber = 0). The Nyquist wavenumber of the filter is appropriate for a spatial sampling interval of 1.0 mm. Figure 4.10 shows the resulting f-k filter. The velocity cut-offs are defined by the maximum source take-off angle considered ($\pm 50°$ from the vertical). Areas of highest amplification (shaded grey) are at high frequencies and high wavenumbers, which correspond to large take-off angles. The f-k filter has fairly gentle slopes because of the careful time domain design. Thus problems at the edges of the data (section 2.4) should not be too severe.

4.5 Physical model dataset 1

Dataset 1 was acquired over a perspex wedge model suspended in water (figure 4.11). The transducers were at a sufficient depth to ensure that there was no interference from the ghost reflection at the water surface. The top of the perspex sheet was 11.5 cm below the transducers, and 2.1 cm thick. The sloping face of the wedge had a dip of 27°.

Two hundred four-fold CMP gathers were acquired at a CMP spacing of 0.1 cm, with offsets of 1.5, 2.5, 3.5, and 4.5 cm. Using a scaling factor of 20000 applied to distances, traveltimes and frequencies, without adjusting the velocity this experiment simulates a seismic reflection profile with dimensions appropriate for oil exploration. The target depth scales to between 2 and 3 km, the streamer length to 1 km and the centre of the data bandwidth to 20 Hz. The velocity of the overburden (water, V=1480 m s^{-1}) is less than typical rock velocities but this may be readily compensated. If the rock velocity is assumed to be twice the water velocity, then a scaling factor of 20000 applied to distances and 10000 applied to traveltimes and frequencies would simulate the same target depth and streamer length with the centre of the signal bandwidth at 40 Hz.

The constant-offset section for the third offset (3.5 cm) is shown in figure

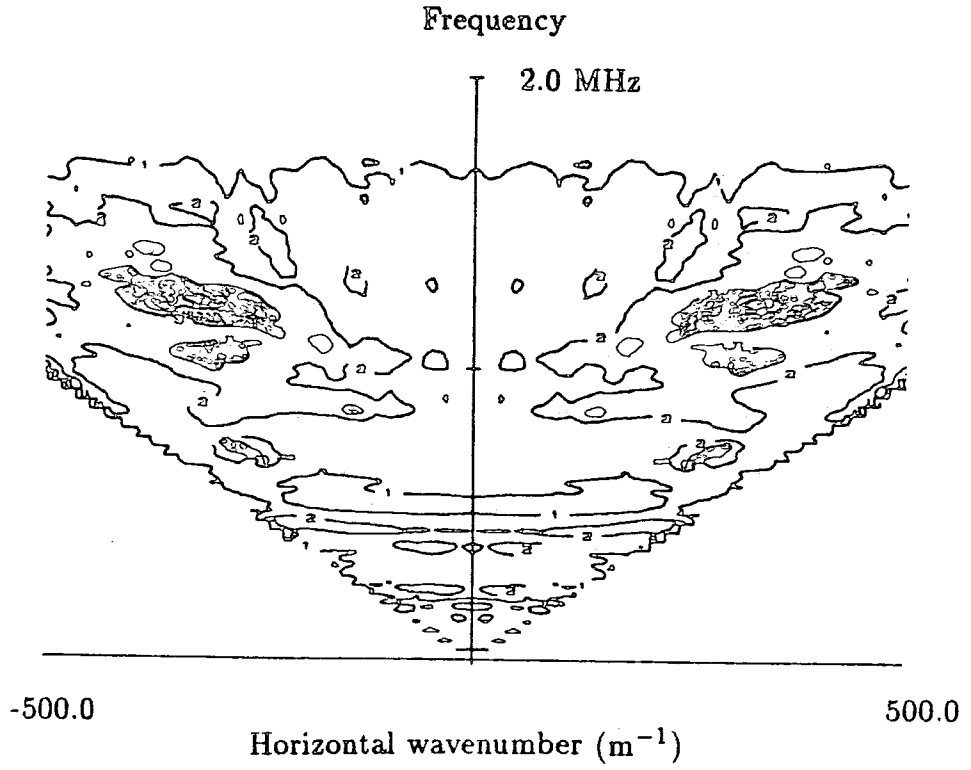

Figure 4.10. F-k directional deconvolution filter. There are five contour levels at equal increments of amplitude. High amplitudes (above amplitude 3) are shaded.

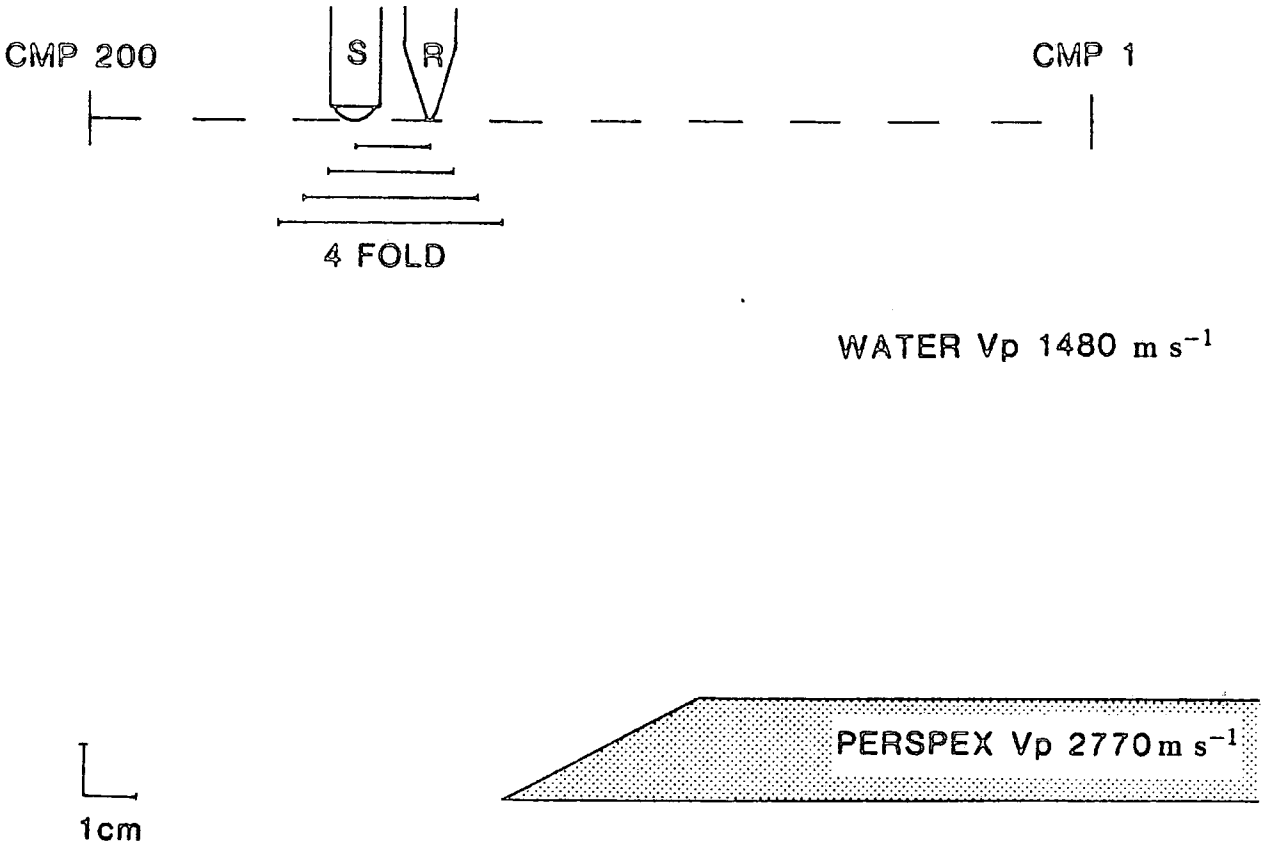

Figure 4.11. Dataset 1. Scale drawing of the physical model experiment.

4.12. The reflection from the top of the perspex is horizontal at the right of the figure, at a two-way traveltime of 0.156 ms, and the reflection from the sloping face of the wedge is displaced down-dip, at the left. The near-horizontal arrival at a two-way traveltime of 0.18 ms, which dips slightly to the right between the toe and top of the wedge, is a mode-converted wave. Efficient P-S conversion occurs on the slope of the wedge because of the large angle of incidence. The converted S-wave is reflected from the base of the model and is converted back to a P-wave when transmitted through the top of the perspex. Shear wave velocity in perspex is slightly less than P-wave velocity in water, so the reflection is nearly horizontal. The P-wave reflection from the bottom of the perspex is not horizontal below the sloping face of the wedge because of 'velocity pull-up'. Part of the diffraction hyperbola from the toe of the wedge is evident at the lower right of the figure.

The four constant-offset sections were migrated separately using a constant velocity of 1480 m s^{-1}, both with directional deconvolution and with signature deconvolution using the filter designed for the vertically travelling waveform. Only a limited window of interest was migrated. Source take-off angles to consider in the migration were calculated using the formula from section 3.5.1. In order to minimise 'discretisation noise', the maximum frequency tolerable in the data was calculated using the approximate formula from section 3.3.2. High-cut filtering to this frequency (0.8 MHz) would have limited the bandwidth of the data, so trials were performed with less stringent high-cut filters. The high-cut filter chosen involved a compromise between bandwidth and noise. Migration and deconvolution parameters are summarised in table 4.2.

The result of migrating the constant-offset section of figure 4.12 using directional deconvolution is shown in figure 4.13.a, and the result using conventional signature deconvolution in 4.13.b. The final four-fold stacks of the migrated constant-offset sections are shown in figure 4.14. The first reflector is the top of the perspex and is correctly positioned. The second reflector, with about half the time-dip of the first, is the primary reflection from the base of the perspex. It is still affected by velocity pull-up because prestack migration was done with

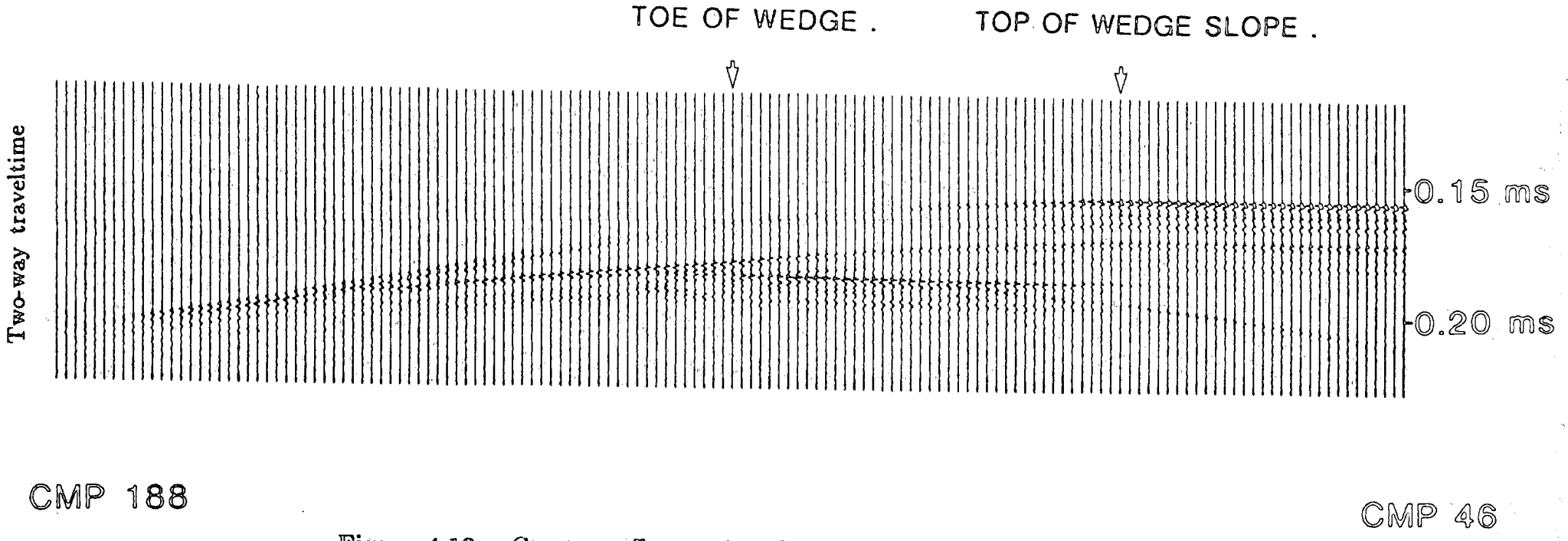

Figure 4.12. Constant-offset section obtained with a source-receiver offset of 3.5cm from the experiment shown in figure 4.11.

Source take-off angles.

Maximum angle:	46°
Deconvolution increment:	2°

Migration velocities.

1480.0 m s^{-1}

Input data.

Sampling interval:	0.25 μs
Bandpass filter:	trapezoidal
Corner frequencies:	0.1, 0.2, 1.0, 1.2 MHz

Constant-offset sections.

Number.	Offset(cm).
Offset # 1:	1.5
Offset # 2:	2.5
Offset # 3:	3.5
Offset # 4:	4.5

Table 4.2. Dataset 1. Directional deconvolution combined with prestack migration parameters.

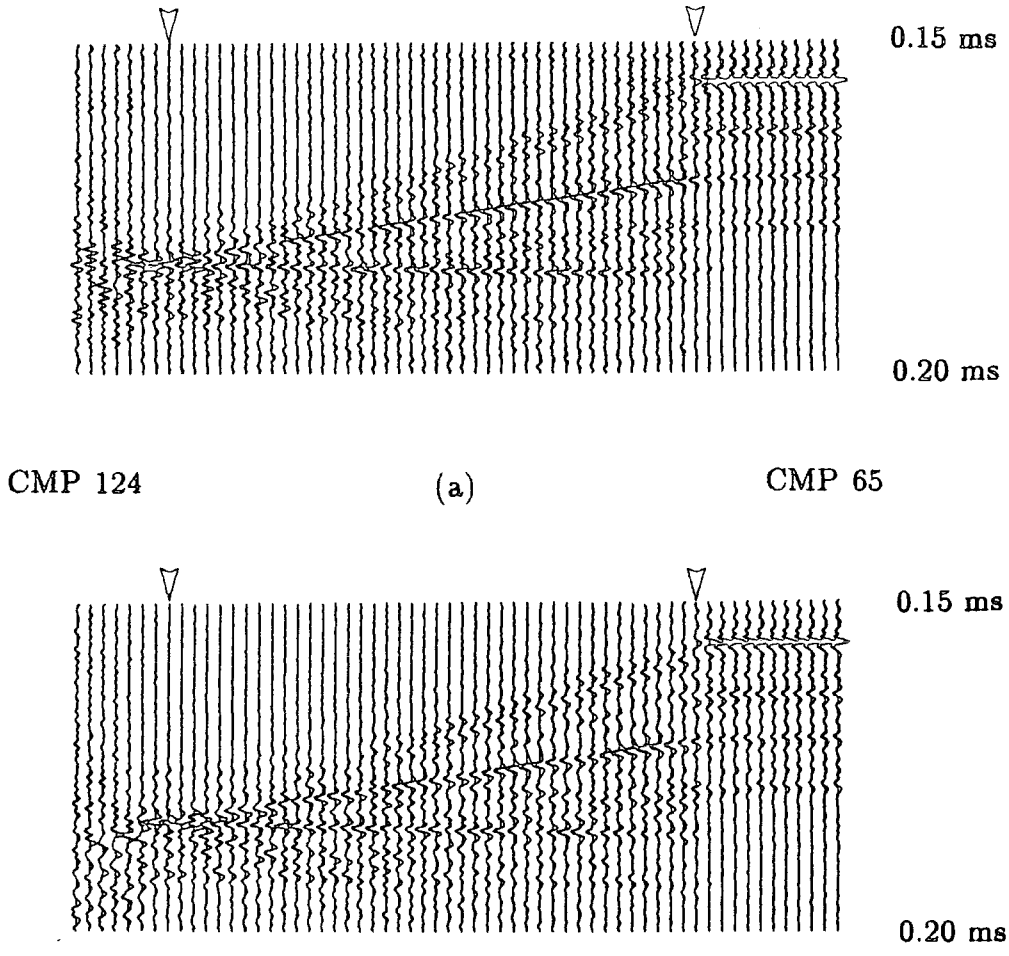

Figure 4.13. A limited window of the constant-offset section shown in figure 4.12 after prestack migration, (a) using directional deconvolution and (b) using standard signature deconvolution. Arrows mark the extent of the wedge slope. Traces have been normalised to constant energy.

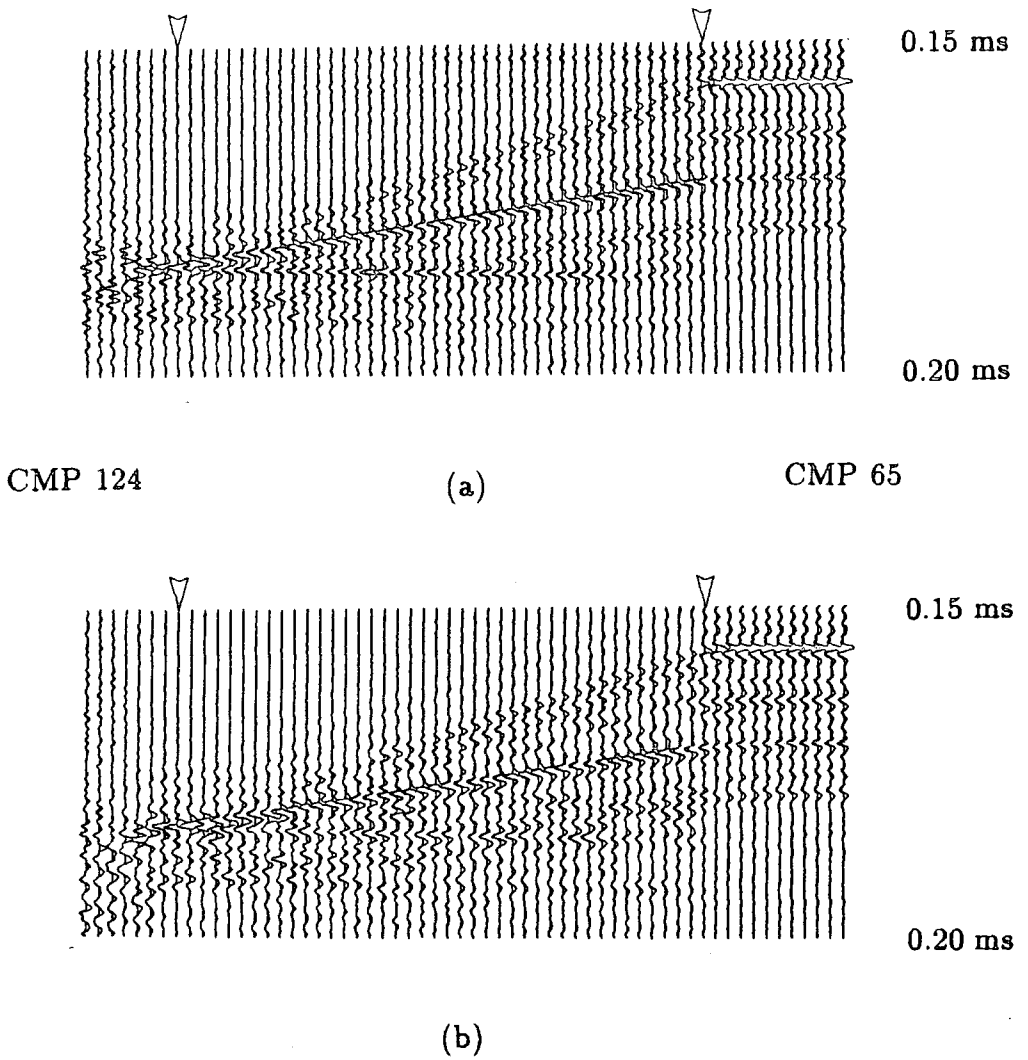

Figure 4.14. Four-fold stacked section (a) using directional deconvolution and (b) using standard signature deconvolution. Arrows mark the extent of the wedge slope. Traces were normalised to constant energy before stack.

constant velocity. The third event, which dips slightly to the right, is the mode converted reflection from the base of the perspex which travels as a shear wave within the perspex. The polarity of the second and third reflections is the opposite of the reflection from the top of the perspex, as would be expected. The noise beyond the toe of the wedge has been amplified by normalisation of the energy in each trace before stack.

The section resulting from directional deconvolution (figure 4.14.a) shows higher resolution and better reflector continuity than the conventionally deconvolved section (figure 4.14.b). The reflection from the horizontal top of the perspex is only correctly deconvolved to a narrow zero-phase wavelet for the directionally deconvolved section. Later reflectors are more continuous in figure 4.14.a than 4.14.b because wavelets are deconvolved correctly, regardless of reflector dip, and the section is not contaminated by noise resulting from incorrect deconvolution. The reflection from the sloping face of the wedge is not adequately deconvolved on either section. This is because the reflected waveform, as seen on the constant-offset section (figure 4.12), is not the same as the appropriate angular signature which was recorded with the test-rig, and then used for filter design. This is due to a problem with the repeatability of transducer signatures.

4.6 Physical model dataset 2

Dataset 2 was acquired over a 10° perspex wedge model. Two hundred 24 fold CMP gathers were acquired at a CMP spacing of 0.5 mm with an offset increment of 1.0 mm. The smallest offset was 1.5 cm. The small offset increment was used to ensure that common-receiver gathers were adequately spatially sampled.

The f-k method of directional deconvolution (chapter II) is applied to common-receiver gathers. A 24-fold common-receiver gather with a reflection from the sloping part of the wedge is shown in figure 4.15.a. The reflected waveform changes across the gather because the source take-off angle is greater at longer offsets. Directivity effects are more subtle than for dataset 1, as the re-

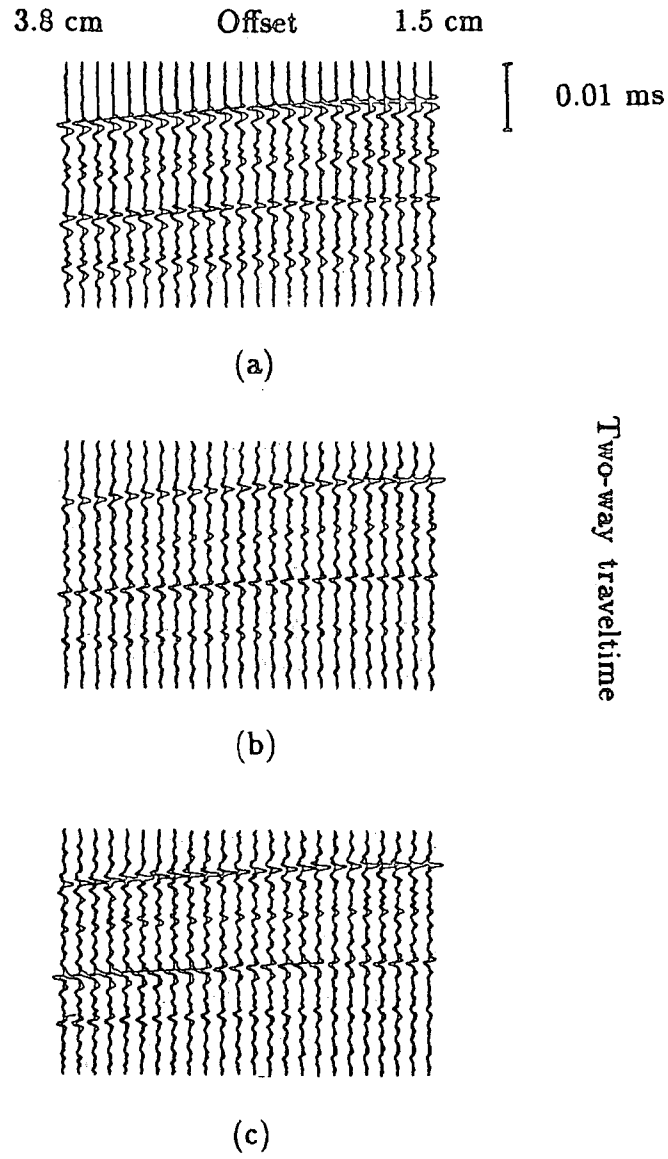

Figure 4.15. Dataset 2. A common-receiver gather, (a) raw, (b) after standard signature deconvolution and (c) after f-k directional deconvolution.

flector dip is less. Signature deconvolution using a filter designed for the vertically travelling wavelet does not deconvolve the longer offset traces correctly (figure 4.15.b). Figure 4.15.c shows the result of f-k directional deconvolution which was performed by a complex multiplication of the f-k transform of the gather (figure 4.15.a) with the f-k filter (figure 4.10). In order to alleviate problems associated with data edges (section 2.3), edges of the gather were tapered to zero over three traces, and the gather was padded with blank traces to make a 64-fold gather before deconvolution. The taper was removed after deconvolution, and the padding traces were discarded. High frequencies have been restored on the long-offset traces.

In order to compare the f-k and prestack migration methods of directional deconvolution, the complete dataset was resorted to common-receiver gathers, f-k directional deconvolution was applied to each gather, data were resorted to constant-offset sections and each constant-offset section was migrated. Prestack migration was also applied to raw constant-offset sections, both with directional deconvolution (chapter III) and with standard signature deconvolution. Only long-offset traces of this dataset exhibit significant directivity (figure 4.15). Figure 4.16 shows a long-offset constant-offset section (offset 3.6 cm) after prestack migration and the three types of deconvolution. There are only subtle differences between the three sections, because directional deconvolution and standard deconvolution both perform well for small take-off angles (compare figures 4.8 and 4.9). The directionally deconvolved sections (figure 4.16.a and b) are similar, and both have higher frequency content than the section with standard signature deconvolution (figure 4.16.c). The two directionally deconvolved sections should be identical if the two techniques are equivalent. Differences in the two sections are due to implementation of the methods, for example the discrete deconvolution increment used for the prestack migration method (section 3.4), and the interpolation used for mapping filters to the f-k domain (section 2.1.2).

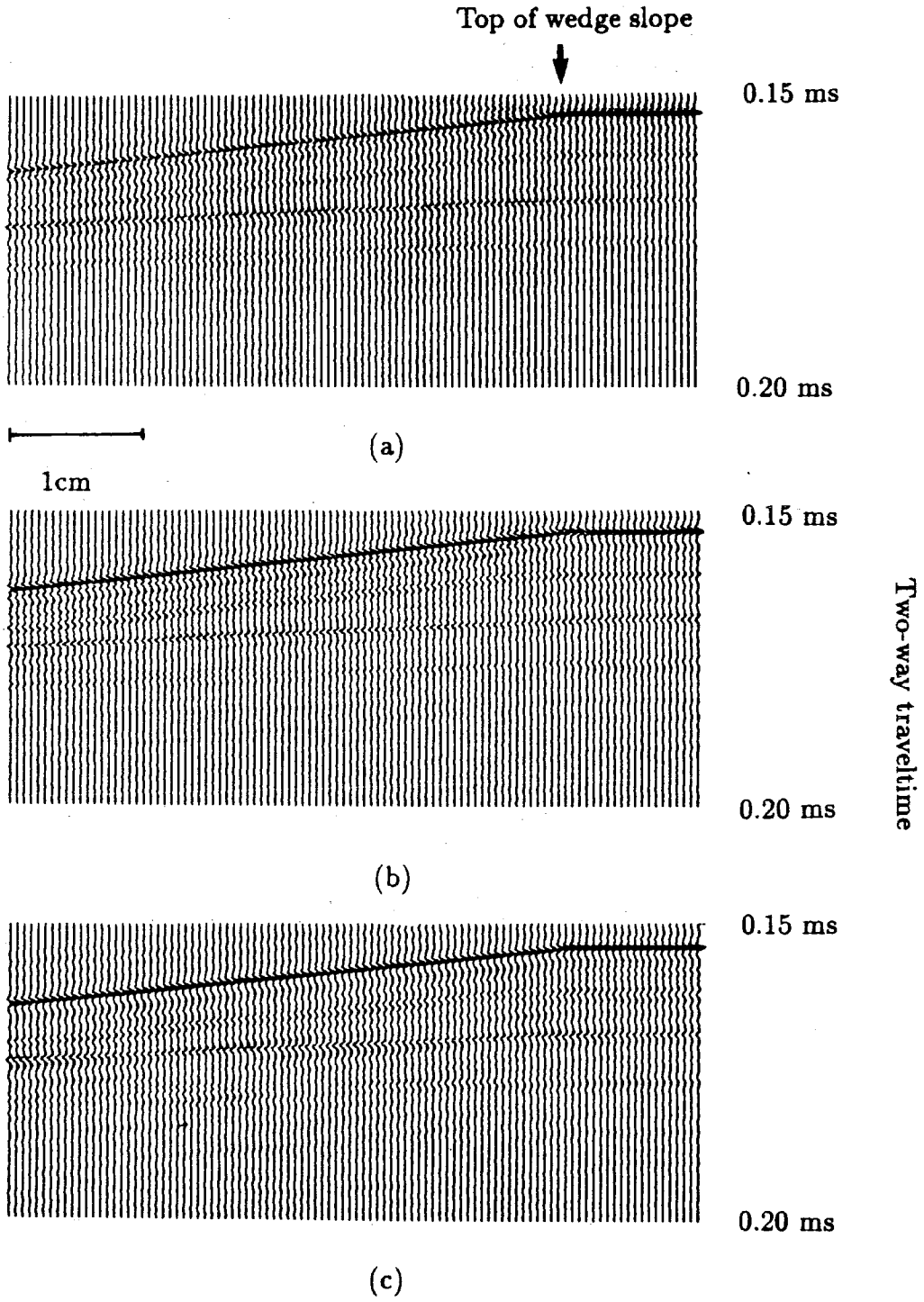

Figure 4.16. A limited window of a constant-offset section (offset 3.6 cm) after prestack migration (a) using f-k directional deconvolution before migration, (b) using directional deconvolution combined with prestack migration and (c) using standard signature deconvolution. Traces have been normalised to constant energy.

4.7 Conclusion from physical model data

Physical model data acquired over simple models have proved to be useful for evaluating directional deconvolution. Directional deconvolution improves reflector continuity and resolution.

Chapter V

Directional Deconvolution of Data from the Southern North Sea

5.1 Introduction

F-k directional deconvolution (chapter II) was applied to real data by Hubbard et al.(1984). The method requires no modifications for real data, but the need for spatial interpolation is a major shortcoming. In this chapter the application of directional deconvolution combined with prestack migration to two reflection datasets from the Southern North Sea is described. It was necessary to modify the basic method in order to apply it to data which have been recorded over variable velocity media. The results are used to assess whether reflection data benefit from directional deconvolution.

5.2 Requirements for a real dataset

Having tested the method of directional deconvolution combined with prestack migration on physical model data, the next step was to evaluate the method on real data. In order to do this effectively, it was necessary for the real datasets to fulfil two main requirements: there had to be significant directivity in the data, and the dataset had to be suitable for prestack time migration.

5.2.1 Significant directivity in the data

The effect of directional deconvolution depends on the amount of source directivity in the data. The amount of directivity depends on the size of the source array, the frequency content of the data, and reflector and acquisition geometries.

- The source radiation pattern for a single marine source element (point source), only has directivity due to the free surface ghost. For an array of point

sources, the directivity increases as the length of the array increases (chapter I). Data acquired with a 'super-long' array (Ursin, 1978) will be highly directional. Such data are not representative of seismic reflection data acquired in oil exploration. Most marine data acquired in the last twenty years have used source arrays with an in-line dimension of about 50 m.

- Source directivity is most evident at high frequencies. If high frequency signals are generated and recorded, directivity is most apparent.

- Reflection events exhibit directivity if energy has left the source at large take-off angles from the vertical. Directivity in reflection data is thus dependent on acquisition and reflector geometry. If very long source-receiver offsets are recorded, source directivity will be most evident on long offset traces.

A dataset exhibiting substantial directivity (with an unusually long source array, exceptionally high frequency content, steeply dipping reflectors and long source-receiver offsets), would be expected to show most benefit from directional deconvolution. However, to evaluate directional deconvolution as a method for general application, it was felt necessary to see how typical data benefit from directional deconvolution. Thus datasets which were likely to exhibit source directivity, but were not unusually directive were chosen for the tests.

5.2.2 Suitability for 2-D prestack 'time' migration

The directional deconvolution used here is incorporated in a 2-D prestack time migration algorithm (chapter III). Extensions of the basic method to 3-D data, and to depth migration are discussed in chapter VI, but these have not been implemented. To test the basic method, a dataset suitable for 2-D time migration was needed.

2-D migration assumes that all reflections have come from within the recording plane. The seismic section must thus be a 'dip-line'. Out-of-plane reflections

would be migrated incorrectly, and would be directionally deconvolved with filters designed for the in-line source signatures.

In the prestack migration scheme described in chapter III, the medium overlying the reflector was assumed to be of constant velocity. For application to real data, the scheme was extended to a velocity function which varied with depth only, i.e. a horizontally-stratified medium. This is known as 'time' migration (Schneider, 1978). For a medium with strong lateral velocity variations, 'depth' migration is needed to account fully for ray bending. If the medium has lateral velocity variations, time migration causes events to be mislocated, and directional deconvolution fails to account fully for ray bending.

5.3 Dataset A

5.3.1 Introduction

Dataset A was acquired by Horizon Exploration Limited in 1985 (line HEX 85-008). It is part of a non-exclusive survey in the southern North Sea. The acquisition parameters are shown in table 5.1 . The source array consisted of 16 Sodera S80 waterguns, with an in-line dimension of 50 m.

The data have been processed by Horizon Exploration Ltd. A migrated section is shown in figure 5.1, and the processing parameters in table 5.2. The section has two geologically distinct regions. To the right of shotpoint 400 (figure 5.1), there is a sequence of horizontal reflectors at two-way traveltimes less than 1.5 s, and a sequence of Carboniferous reflectors dipping to the left of the figure below 1.9 s. To the left of shotpoint 400 is a structural feature which is seen more clearly on other lines in the survey. It is a salt wall whose strike is oblique to the recording direction. The salt is from the Zechstein cycles in the Permian strata, which are represented between two-way traveltimes of 1.5 s and 1.9 s at shotpoint 400. Reflections from the dipping beds to the left of shotpoint 400 are from out of the recording plane, so this part of the section is not suitable for 2-D migration. An area to the right of shotpoint 400 was chosen for study.

HORIZON EXPLORATION LTD.
(NON EXCLUSIVE SURVEY)

FIELD PARAMETERS

Recorded by Horizon Exploration Ltd Contract Number 84-222

Party/Vessel D.V. Pacific Horizon Date January 1985

Positioning Primary - Pulse 8+Sonar Secondary - Sat Nav

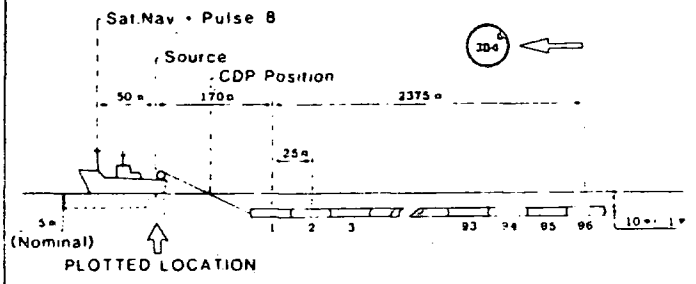

SEISMIC SOURCE

Type	Sodera vetergun
No guns	16
Capacity	1200 cu.ins
Pressure	2000 p.s.i.
Shot interval	25m
Array dimensions	2x50m

RECEIVERS

Number of stations	96
Station interval	25m
Array type	Linear
Type	Litton
Number per station	30
Array length	25m

RECORDING SYSTEM

Type	DFS V	Low cut filter	0Hz
Gain	f.P.P.	Slope	18dB/oct
Format	SEG B	High cut filter	130Hz
Record length	5s	Slope	72dB/oct
Sample interval	2ms		

Record polarity Increase in pressure recorded as negative numbers on tape

Table 5.1. Dataset A. Acquisition parameters.

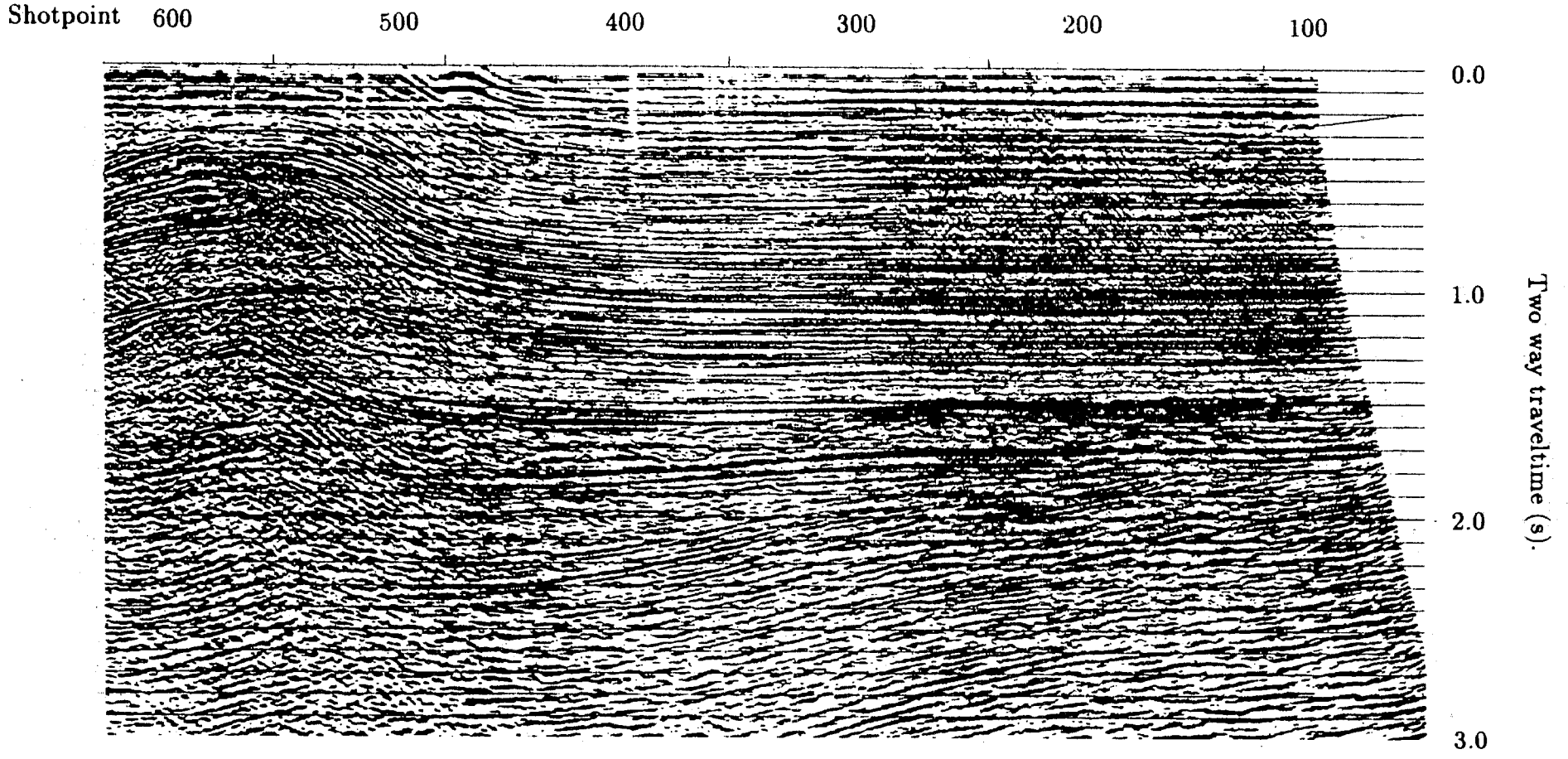

Figure 5.1. Dataset A. 48-fold migrated section (processed by Horizon Exploration Ltd.). Processing parameters are given in table 5.2.

PROCESSING SEQUENCE

Processing record length 8 seconds - sample rate 4 ms

1	Demultiple amplitude compensation	540/s to 3 0s
2	Resample	To 4ms
3	S O D To correction	-400ms
4	Signature deconvolution	Archived near field signature output, minimum phase ,
5	Edit gather	96 trace 40 fold no shaping
6	Deconvolution	See below
7	N M O correction	
8	Mute	See taper as
9	Scaling	Using 500ms windows
10	C D P Stack	48 fold weighting proportional to offset
11	FK filter	Dips ± 6ms/trace no dipback
12	Deconvolution	See below
14	Minimum to zero phase conversion	300 - 2000ms
15	Zero phase deconvolution	See below
16	Bandpass filter	See below
17	Scaling	Base level.window 0 - 5000ms
18	Running mix	1:3:1 Weighting of traces
19	Datum correction	+10ms
13	Migration:	Finite differences 100% stacking velocities 4ms window

T_0 defined as peak of watergun implosion

Datum correction : Shot and streamer depth at water velocity

Velocity analysis by : UNIVEL at 3Km intervals

Velocity function interpolation : Time -Linear
Space-Linear at equal times

FILTER PARAMETERS

DECONVOLUTION BEFORE STACK

Design window	Trace 1	300 - 3500ms		
	Trace 60	2400 - 3700ms		
Prediction distance	36ms			
Operator length	200ms			
Application window	Trace 1	300 - 5000ms	Trace 8	600 - 5000ms
	Trace 6	300 - 5000ms	Trace 96	2400 - 5000ms

DECONVOLUTION AFTER STACK

Design window	300 - 3500ms
Prediction distance	36ms
Operator length	200ms
Application window	0 - 5000ms

ZERO PHASE DECONVOLUTION

Design windows :	200 - 2000ms
	1000 - 3000ms
Application windows :	0 - 1400ms
	1000 - 5000ms

Low cut slope (dB/oct)	Filter (Hz)	High cut slope (dB/oct)
36	15 - 80	72
36	15 - 70	72

Overlap zone (ms) 400

Percentage white noise 1.0%

Length of auto-correlation (ms) 400

Number of channels used in averaging 11

BANDPASS FILTER

Centre frequencies are 3dB down points

Transition is continuous between specified times and passbands

Application time :	1500	2000	2500	3500
Centre frequencies (Hz) :	15 - 70 12	60 12 - 50 10 - 10		
Slopes (dB/oct) :	18	24 18	24 18	24 18 24

Table 5.2. Horizon Exploration Ltd. processing parameters.

5.3.2 Source array directivity

The Horizon Exploration Ltd watergun array consisted of two parallel sub-arrays which were deployed one width of the recording vessel apart. Each sub-array consisted of eight Sodera S80 waterguns, with an in-line dimension of 50 m. Tree et al.(1986) show that the minimum separation of S80 waterguns in an array should be 2.5 m. At separations larger than this, they may be considered to be point sources for the purpose of far-field signature calculation. This criterion is satisfied for the Horizon array. The far-field source array signatures were calculated using Horizon Exploration computer software. The ghost effect was included. Signatures were calculated for the in-line direction in 4° increments. Source take-off angles vary from horizontal towards the ship (−90°), to horizontal away from the ship (+90°). Selected far-field signatures are shown in figure 5.2. The amplitude spectrum of each signature is also displayed. The signatures show a decrease in energy and a change in wavelet shape as source take-off angle increases. Signatures radiated at take-off angles of 18° and greater are affected significantly (figure 5.2). Thus events on the section which have been radiated at source take-off angles of greater than 18° will exhibit significant source directivity.

Directional source signatures may be mapped on to the f-k plane as described in chapter II. The f-k spectrum for the Horizon Exploration array (figure 5.3) has a notch at a horizontal wavenumber of 0.0175 m^{-1}. This is the value which was calculated in chapter I for an array of eight point sources distributed evenly over 50 m. At a take-off angle of 18° this notch corresponds to a frequency of 80 Hz. This is at the upper end of the source signature bandwidth, so as a rule-of-thumb it may be said that directivity becomes apparent at take-off angles where the notch is within the useful bandwidth.

A desired output for directional source signature deconvolution, which must be the same for source signatures radiated at all take-off angles, was chosen as discussed in chapter IV. Filters were designed to avoid excessive noise amplification at all frequencies and take-off angles. This was achieved by choosing a

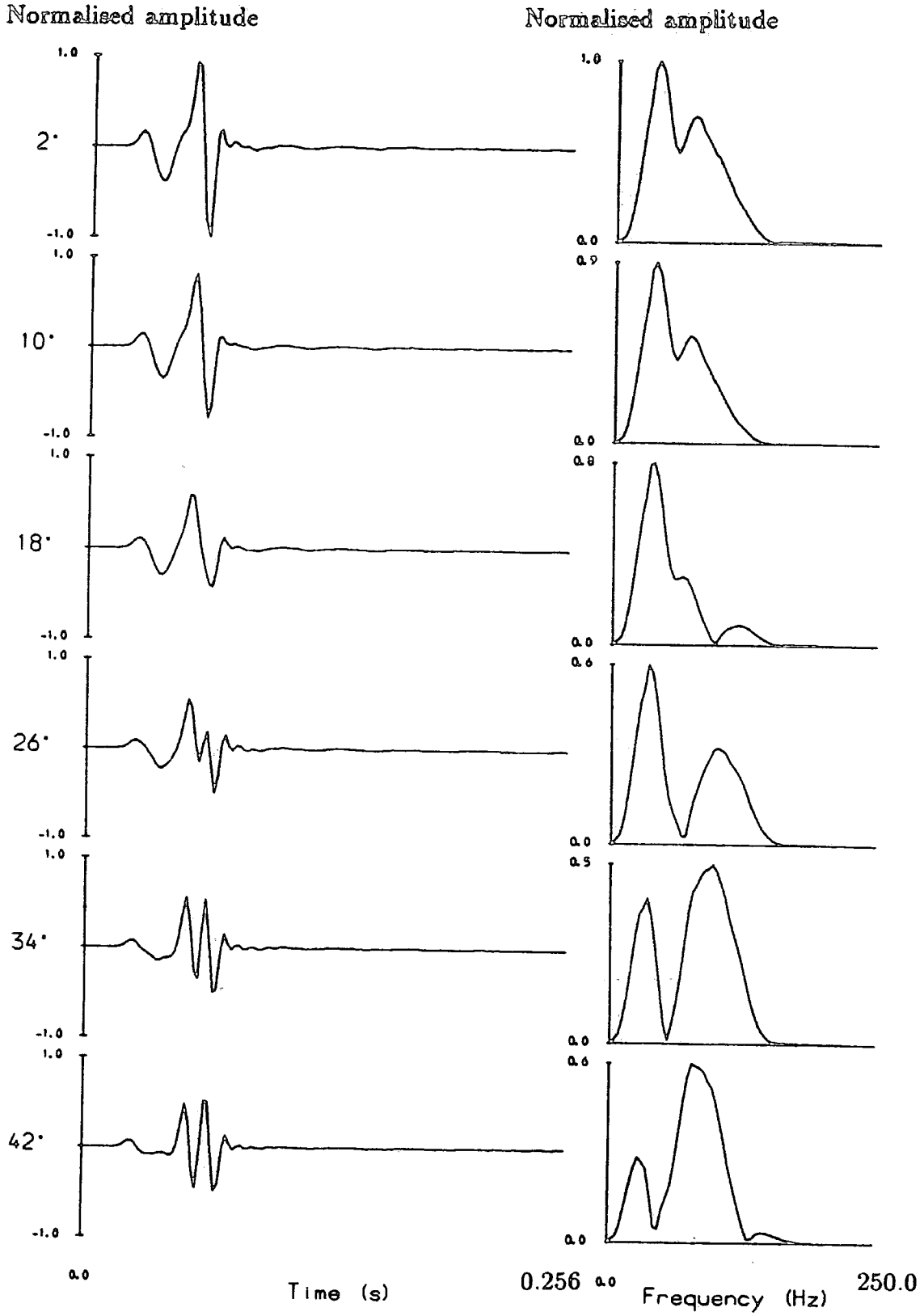

Figure 5.2. Far-field source signatures and amplitude spectra. Take-off angle varies from 2° to 42° from vertical.

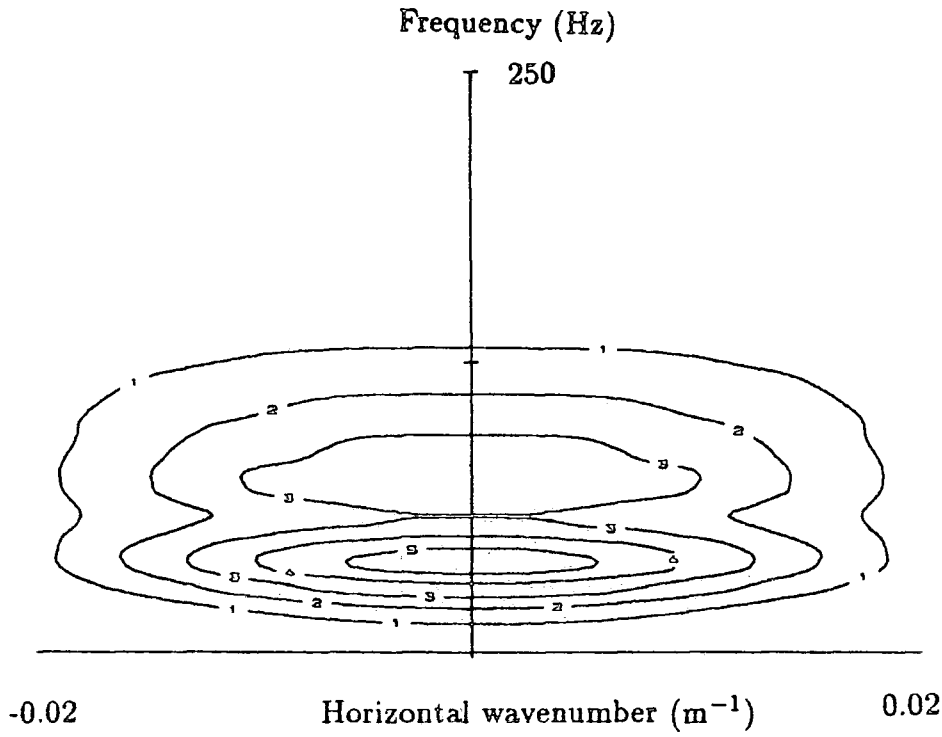

Figure 5.3. F-k source spectrum. There are five contour levels at equal increments of amplitude (5 is the highest amplitude).

desired output which was similar in spectral content to the source signatures, time domain filter design and the addition of 'white noise'. The desired output had the same amplitude for all take-off angles. The amplitude spectrum of the desired output for directional deconvolution of dataset A was chosen to be a smoothed version of the spectrum of the vertically travelling signature. A smooth amplitude spectrum means that the output wavelet is short in time. A minimum-phase wavelet was used, as predictive deconvolution was to be applied at a later stage. Filter design is summarised in table 5.3. Deconvolution filters for selected source signatures (figure 5.2) are shown in figure 5.4, and figure 5.5 shows the output obtained when the filters are applied to the signatures. For comparison, the output obtained when the signatures are deconvolved with the filter designed for the near-vertically travelling wavelet (2°) are shown in figure 5.6. Thus figures 5.5 and 5.6 can be used to compare the result of directional deconvolution with standard signature deconvolution. Differences are most evident for angular source signatures of 18° and greater.

5.3.3 Directivity effects

Directivity will be evident in the data if reflected energy has been radiated at large source take-off angles. Ray-tracing is useful for assessing the range of source take-off angles present. A depth model was needed for data in the region between shotpoints 100 and 400. As the medium is horizontally stratified, an approximate depth model was calculated using the formula of Dix (1955). Interval velocities were calculated from the results of stacking velocity analysis. If V_a and V_b are the r.m.s velocities at the top and bottom of an interval respectively, and t_a and t_b are the corresponding normal incidence traveltimes, the interval velocity, V_{int}, is given by

$$V_{int} = \left[\frac{\left({V_b}^2 t_b - {V_a}^2 t_a \right)}{(t_b - t_a)} \right]^{\frac{1}{2}}$$

Desired output.

Amplitude spectrum:	smoothed 0° signature spectrum.
Phase spectrum:	minimum phase.
Amplitude variation with take-off angle:	none.

Filter design.

Domain:	time domain.
Filter length:	0.256 s.
Lag of desired output:	0.128 s.
White noise:	1.0%

Table 5.3. Dataset A. Directional deconvolution filter design.

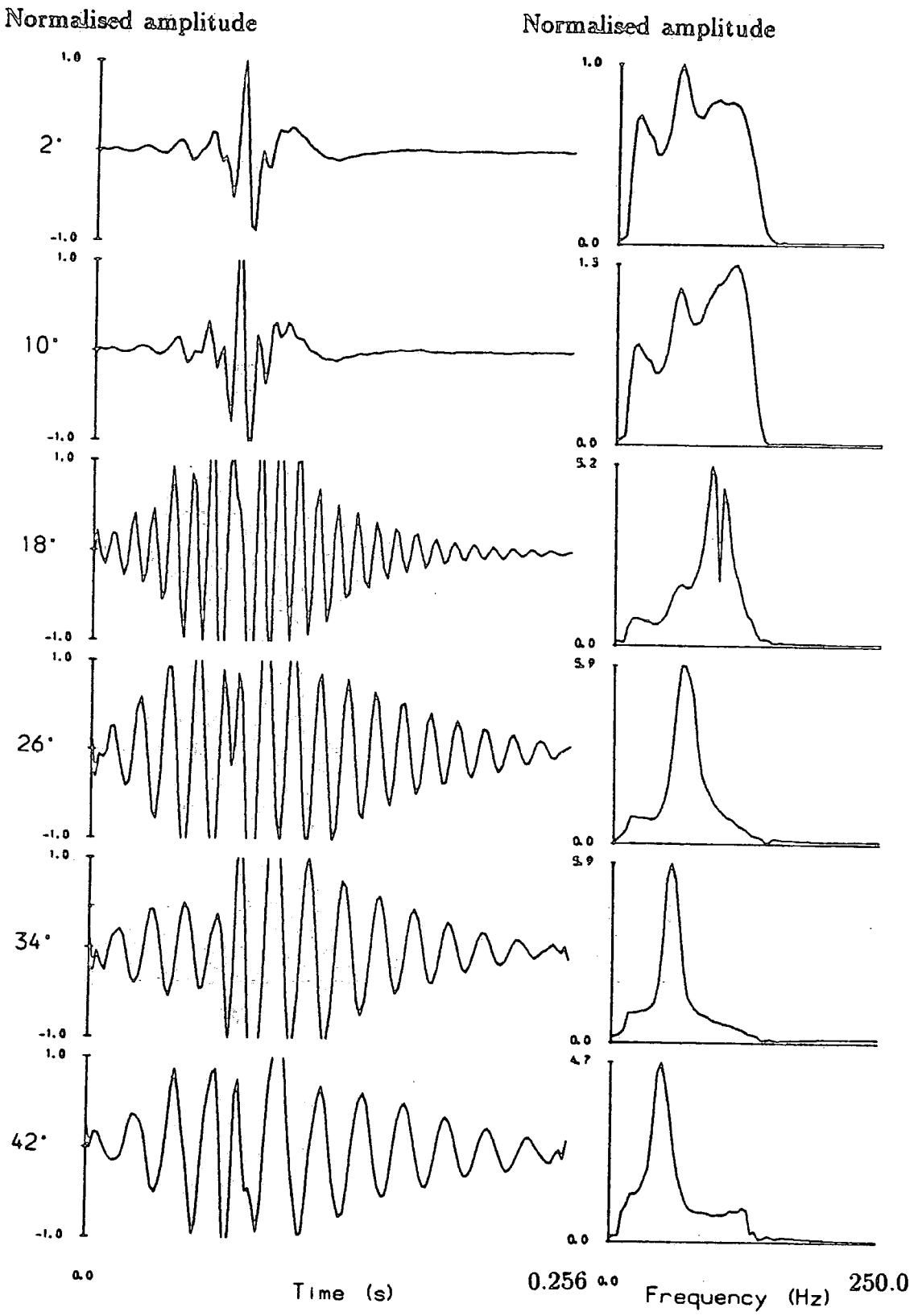

Figure 5.4. Directional deconvolution filters designed for the far-field signatures shown in figure 5.2.

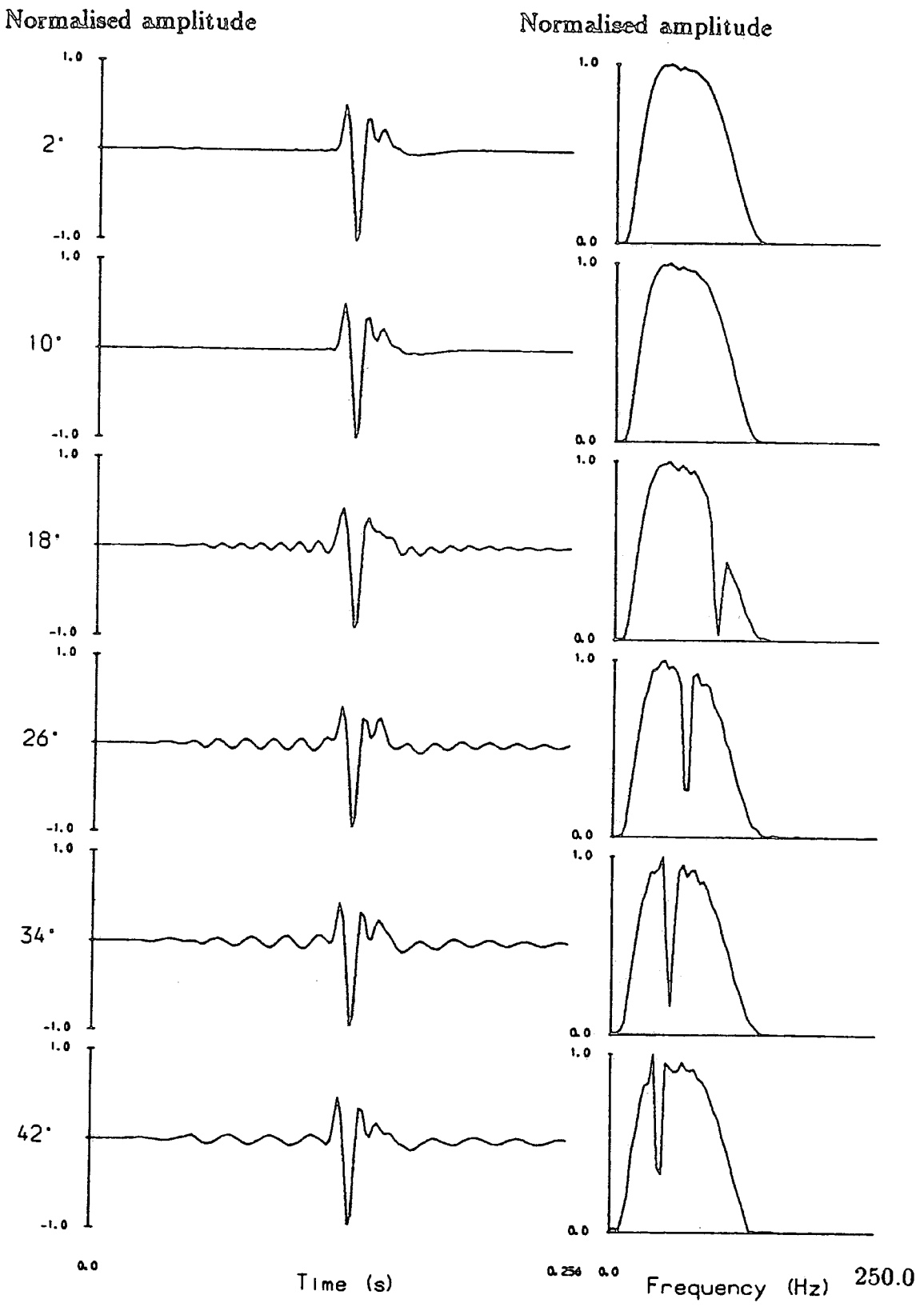

Figure 5.5. Actual outputs when the directional deconvolution filters (figure 5.4) were applied to the source signatures (figure 5.2).

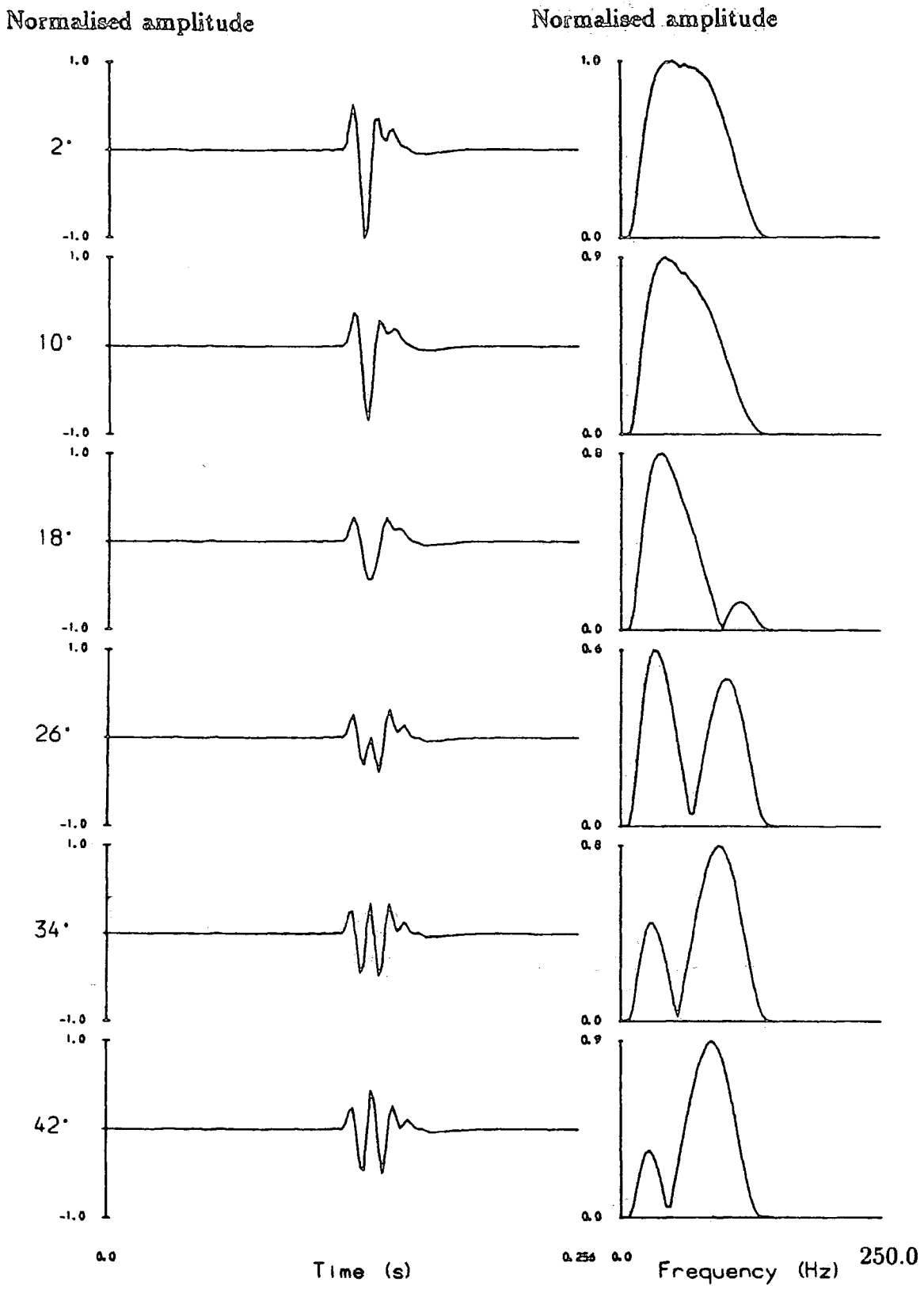

Figure 5.6. Actual outputs when the deconvolution filter designed for the near-vertical travelling signature (top of figure 5.4) was applied to the source signatures (figure 5.2).

A depth model was calculated using the traveltime and calculated interval velocity for each time interval of the velocity analysis. The resulting depth model is only approximate (e.g. Dubose, 1988), but is adequate for assessing directivity. Well-velocity data could be used to constrain the depth model. Unfortunately, there is only one released well in the area of the survey, and it is some distance from this seismic profile.

The approximate depth model and selected raypaths are shown in figure 5.7. Ray-tracing was performed with the GeoQuest 'Advanced Interpretive Modelling System' (AIMS). A real CMP gather (figure 5.8.a) contains large amplitude refracted events which are not modelled by ray-tracing, and hence are not seen on a synthetic gather (figure 5.8.b). By measuring source take-off angles on the raypath diagram (figure 5.7), the angles corresponding to each reflection event on the CMP gather may be estimated. Only events which have originated from source take-off angles of greater than 18° will show significant directivity. Such events are present at large offsets and short traveltimes on the CMP gather. Superimposed on the synthetic CMP gather (figure 5.8.b) is the mute zone. Events most affected by directivity lie within this mute zone. Events in the 'useful' part of the gather, i.e. not in the mute zone, have been radiated at small source take-off angles (less than 20°), and hence exhibit little directivity.

Ray bending has a major effect on limiting the amount of directivity evident in the data. Down-going rays are refracted away from the vertical due to the increase in interval velocity with depth. Thus the source take-off angle for a raypath to any reflection point is less than if the raypath were linear.

Ray-tracing has shown that there is little directivity in dataset A. Directional deconvolution is expected to have a small effect.

5.3.4 Directional deconvolution combined with prestack migration

Kirchhoff summation migration assumes that the medium is of constant velocity. It may be extended to a horizontally-statified medium by using r.m.s

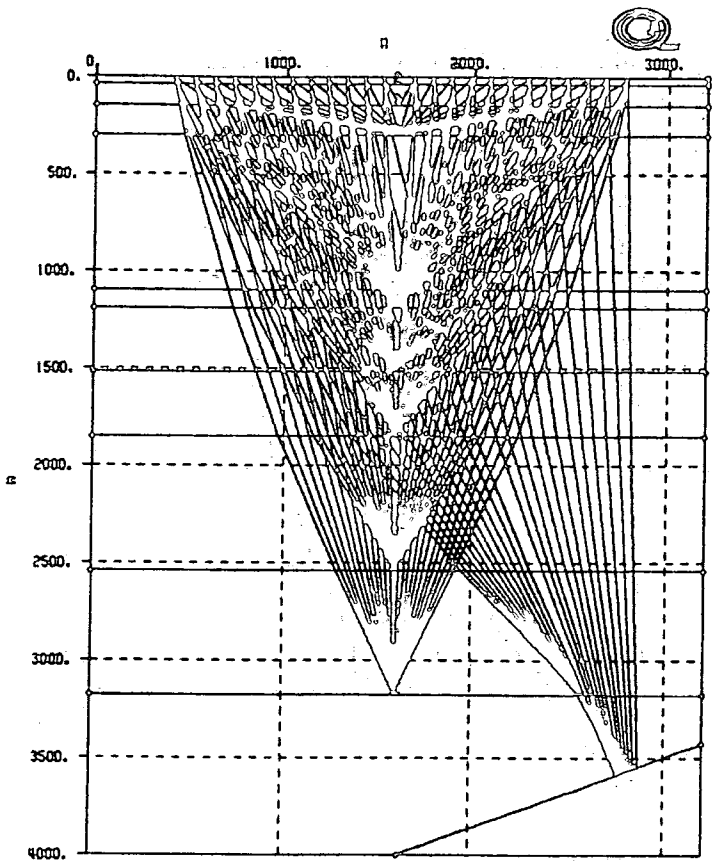

Figure 5.7. Dataset A. Raypath diagram. Depth model was derived from stacking velocities.

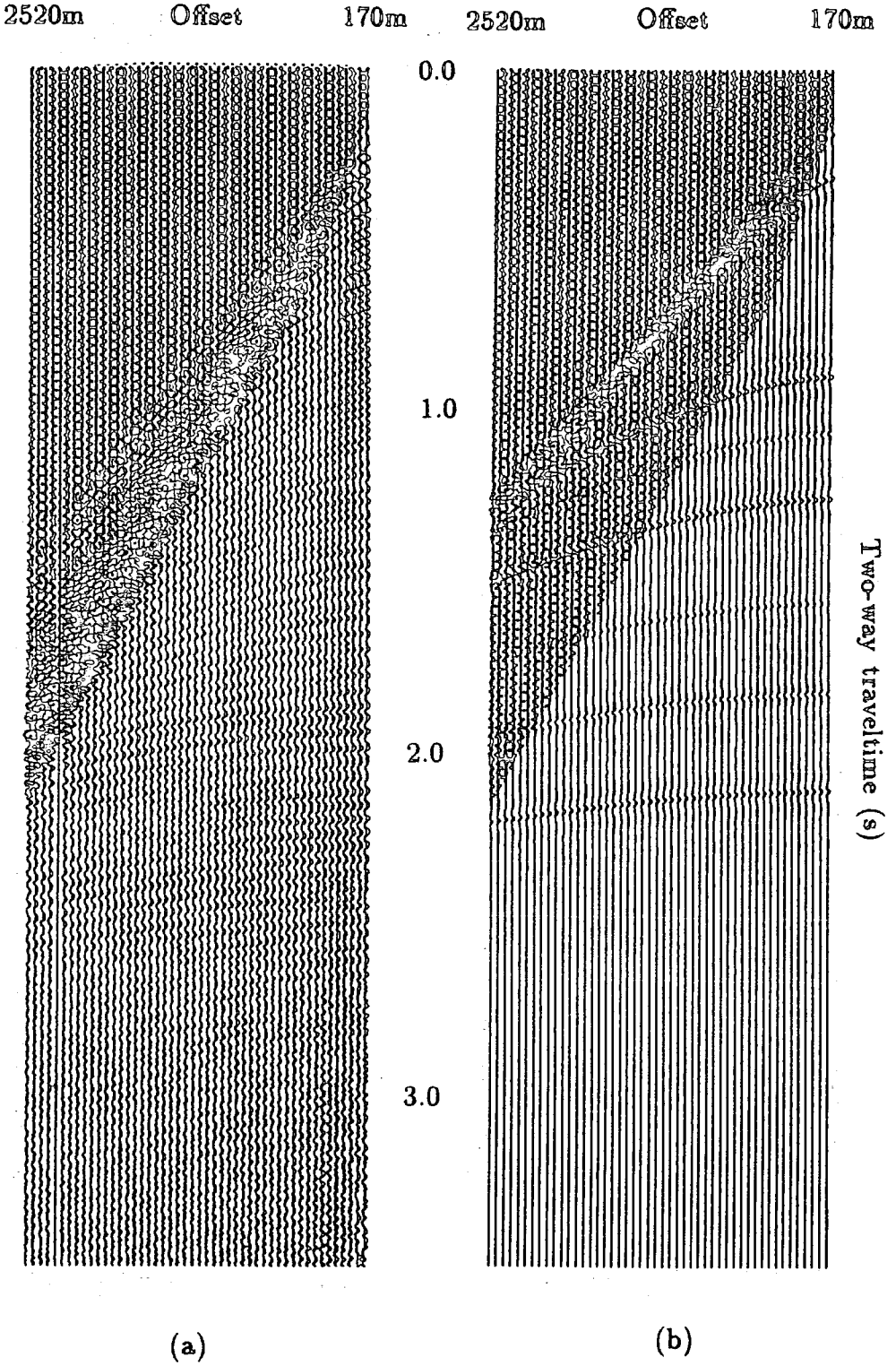

Figure 5.8. 48-fold CMP gathers, (a) real and (b) synthetic.

velocities (Schneider, 1978). Ray bending is ignored. This approximation is valid for rays which travel at a small angle to the vertical. The angle depends on the inhomogeneity of the medium. Values of 45° (Western Geophysical brochure) and 60° (Schneider, 1978) have been reported. Kirchhoff summation migration may therefore be used to image a reflector whose dip is less than a given angle and which is overlain by a horizontally-stratified medium.

The linear raypath assumption in Kirchhoff migration leads to errors when directional deconvolution is incorporated. Figure 5.9 uses the results from ray-tracing to demonstrate how the true source take-off angle and the take-off angle assuming a linear raypath to the reflection point are related. Angles have been measured from raypath plots (e.g. figure 5.7), and only arrivals from the 'useful' part of the data have been considered. The relationship depends on velocity structure. For this dataset there is an approximately linear relationship. A simple 'linear correction factor' may be applied when using the 'directional deconvolution combined with prestack migration' scheme (chapter III). During implementation of the scheme, the dataset is deconvolved with a filter designed for a particular source take-off angle. For a constant-velocity medium, the portion of migration summation operator to apply is determined by this angle. For a curved ray, the true take-off angle is related to the linear raypath take-off angle by the 'linear correction factor'. Thus, the angle used to determine position on the migration operator, which assumes a linear raypath, is the filter angle multiplied by the correction factor. The linear correction factor is 1.7 for this dataset.

The basic prestack migration and directional deconvolution algorithm (chapter III) has been modified to allow the use of r.m.s velocities and a linear correction factor (Appendix A).

5.3.5 Processing

The results of ray-tracing show that there is little evidence of source direc-

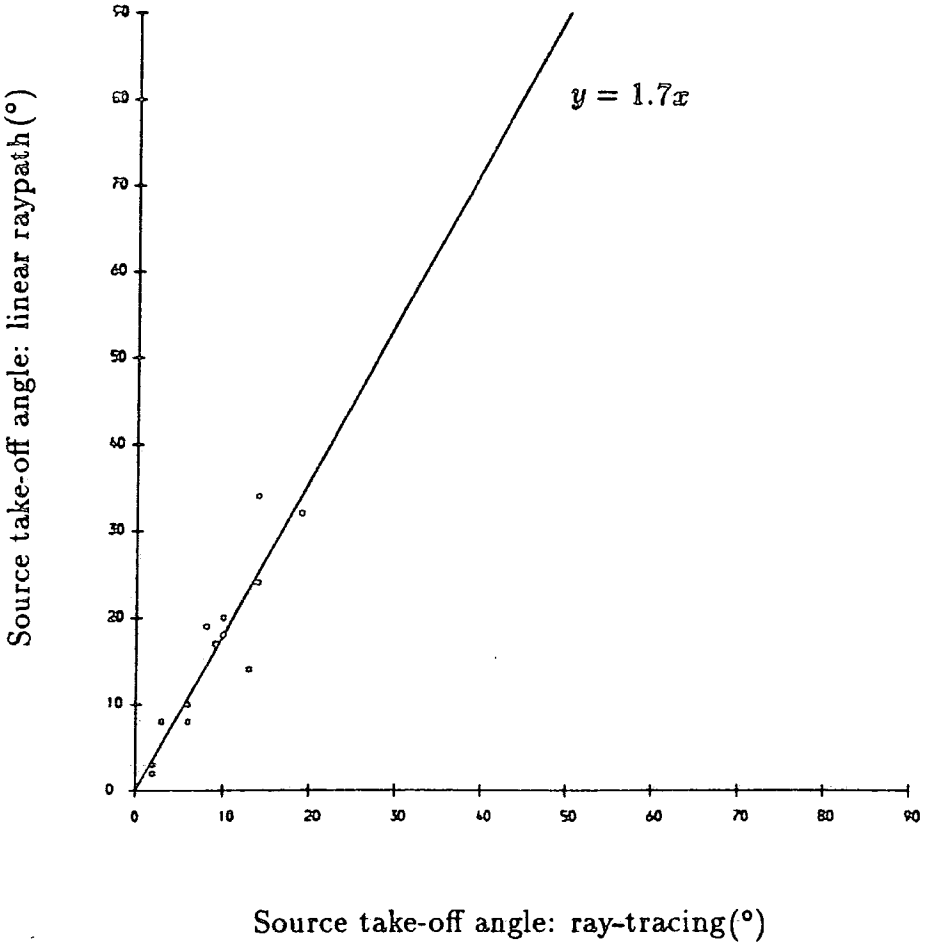

Figure 5.9. Graph of source take-off angles calculated from ray-tracing, against source take-off angles which assume linear raypaths to reflection points.

tivity in this dataset. It was useful to process the dataset, firstly as test data for the software, and also to determine if this hypothesis was correct. Processing parameters for directional deconvolution combined with prestack migration are given in table 5.4.

The maximum source take-off angle either side of the vertical, which defines the extent of the migration summation operator, is 28°. This angle is based on the results of ray-tracing, which indicate that the maximum angle which needs to be considered is 20°. The extra 8° allows for errors in the modelling, and for tapering at the ends of the migration operator (section 3.3.3). If a larger range of take-off angles were considered, this would be equivalent to extending the summation operator, which would result in a noisier section and longer computer run time. Considering a more limited range of take-off angles would prevent shallow or dipping reflectors from being fully migrated.

To economise on computing time and expense full 48-fold processing has not been performed. Only a limited window has been has been migrated, and only 12 constant-offset sections processed. The full processing sequence is summarised in table 5.5.

Each of the 12 constant-offset sections was processed separately, both with and without directional deconvolution. When processed without directional deconvolution, standard signature deconvolution was performed. All other processing of the sections was identical to enable a valid comparison. Processing parameters are similar to those used by Horizon Exploration Ltd (table 5.2).

5.3.6 Results and conclusions

Figure 5.10 shows the sixth constant-offset section after processing to stage 3 of the processing sequence (table 5.5). Figure 5.10.b has been processed using standard signature deconvolution before prestack migration, and figure 5.10.a using directional deconvolution combined with prestack migration. The mute

Source take-off angles.

Maximum angle:	28°
Deconvolution increment:	4°
Linear correction factor:	1.7

Migration velocities.

100% stacking velocities: SP 296.5

Input data.

Sampling interval:	2 ms
Bandpass filter:	trapezoidal
Corner frequencies:	10, 20, 60, 80 Hz
Migration window:	shotpoints 293-352
	traveltime 0.2-2.4 s

Constant-offset sections.

Number.	Offset(m).
Offset # 1:	170
Offset # 6:	1170
Offset # 12:	2370

Table 5.4. Dataset A. Directional deconvolution combined with prestack migration parameters.

Each constant-offset section.

1. Prestack migration: with either directional deconvolution or standard signature deconvolution.
2. Resample to 4 ms.
3. Newman filter.
4. Predictive deconvolution: see below
5. Bandpass filter: see below.

Stack.

6. Sections normalised by energy.
7. 12-fold stack.

Post-stack processing.

8. Predictive deconvolution: see below.
9. Bandpass filter: see below.

Display.

- Trace equalisation by energy.
- Reduction of dynamic range: $\pm\sqrt{amplitude}$ (Claerbout, 1985).
- Variable area wiggle.

Predictive deconvolution.

Prediction lag.	36 ms
Filter length.	200 ms
White noise.	1.0%

Bandpass filter.

Trapezoidal.	
Corner frequencies.	10, 20, 60, 80 Hz

Table 5.5. Dataset A. Complete processing sequence and display parameters.

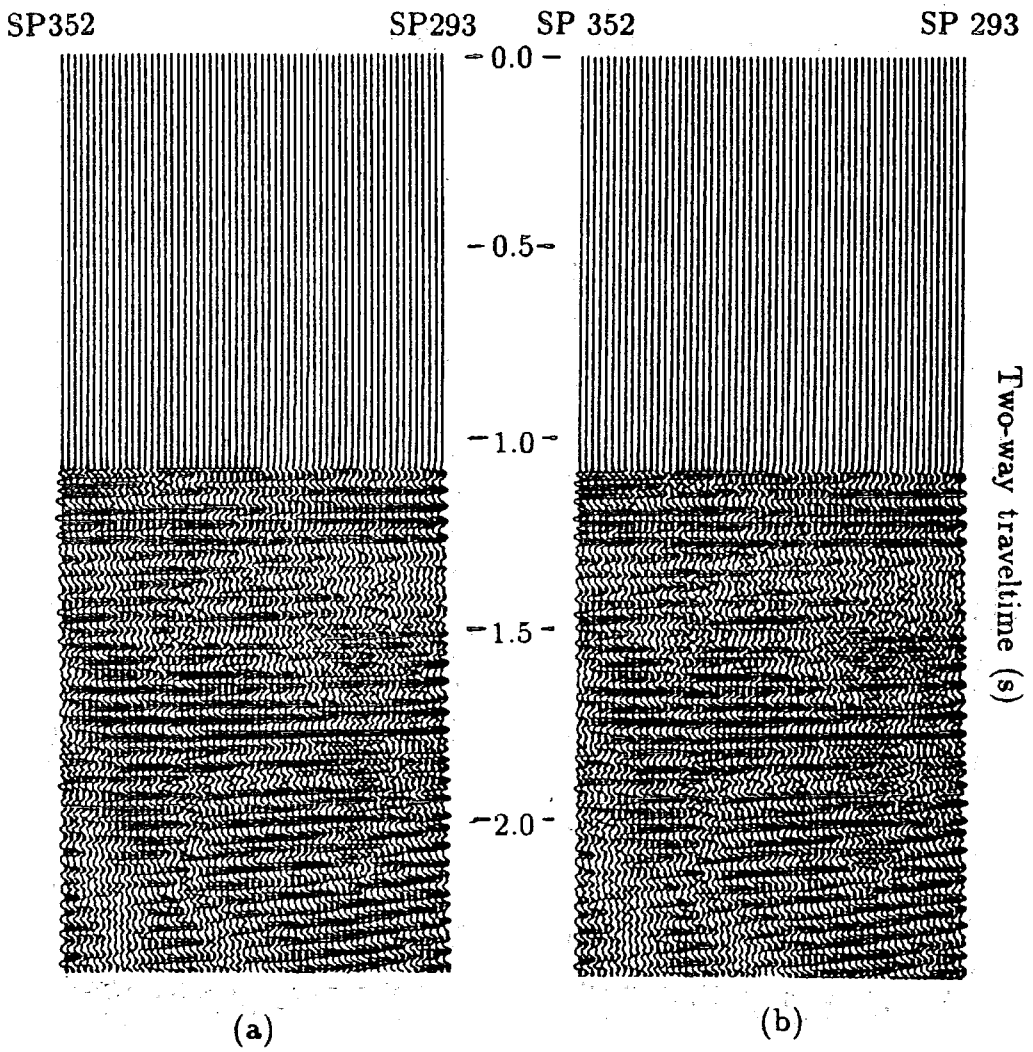

Figure 5.10. A limited window of the sixth constant-offset section (offset 1170m) after prestack migration: (a) using directional deconvolution and (b) using standard signature deconvolution. Processing and display parameters are given in tables 5.4 and 5.5.

zone extends to a two-way traveltime of 1.1 s for this offset. There is little difference between the two sections.

In figure 5.11, the same two sections have been processed to stage 5 (table 5.5), i.e. with predictive deconvolution. Predictive deconvolution has suppressed the 'ringing' nature of the sections, but there is still little difference between them.

The fully processed 12-fold stacked sections are shown in figure 5.12. There are only minor differences between the section processed using standard deconvolution (figure 5.12.b) and that processed using directional deconvolution (figure 5.12.a).

The final section (figure 5.12.a) is superimposed on the stacked section which was processed by Horizon Exploration Ltd (figure 5.1) in figure 5.13. The sections tie together well, which shows that the migration software is functioning correctly. Differences are due to additional processing parameters used by Horizon Exploration Ltd, particularly the time-varying filtering.

As predicted by ray-tracing, directional deconvolution has had little effect on this dataset. Although the source array is directional (figure 5.2), arrivals exhibiting source directivity lie in the mute zone of the data. The next test dataset has a similar sized source array and similar recording geometry to dataset A. However, the reflector geometry is more complex, and this has a major effect on source directivity effects in the data.

5.4 Test Dataset B

5.4.1 Introduction

Dataset B was acquired by Seismic Profilers A.S. in October 1982 (line SP88-48-76). It is part of a Merlin Geophysical (now GECO) non-exclusive survey in the Southern North Sea. The acquisition parameters are given in table 5.6.

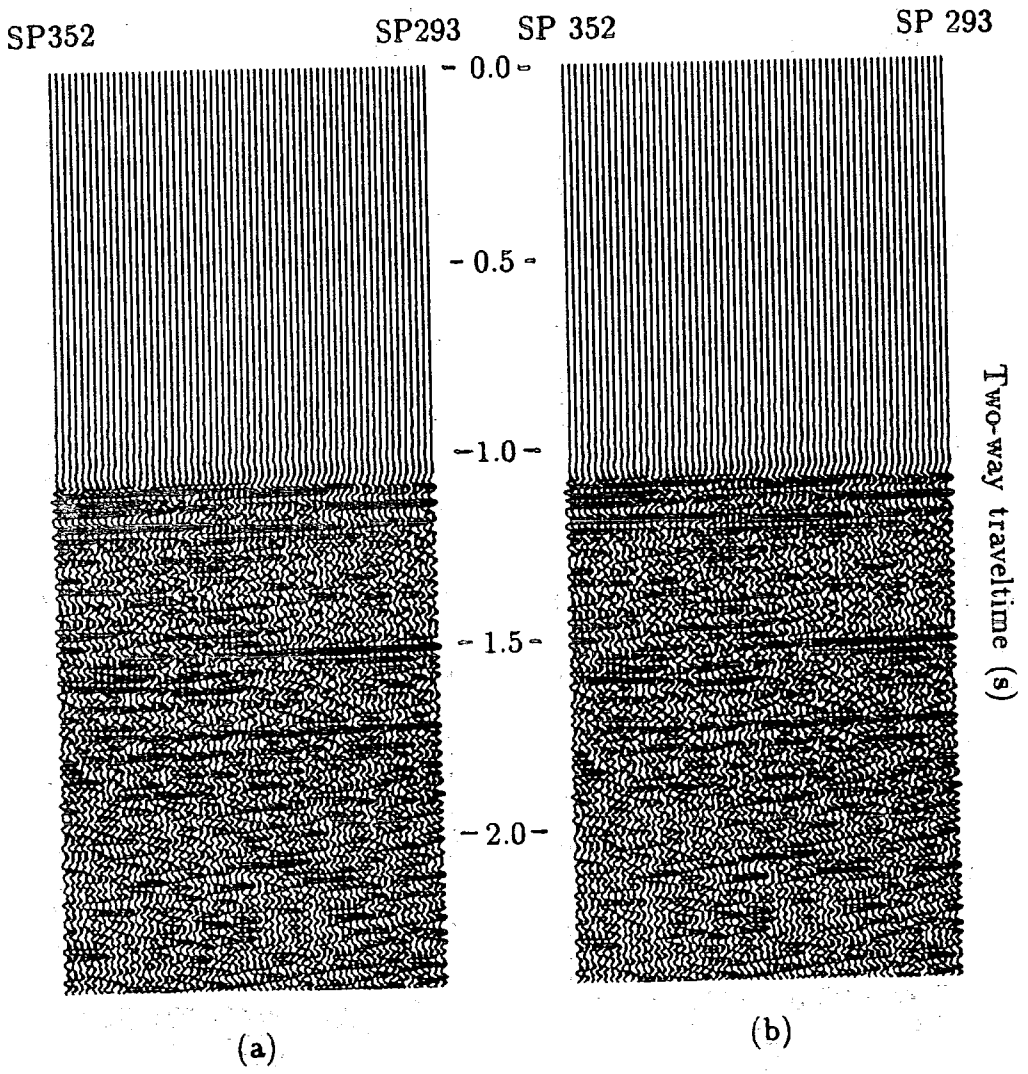

Figure 5.11. The same sections as figure 5.10 after predictive deconvolution and bandpass filtering. Processing and display parameters are given in tables 5.4 and 5.5.

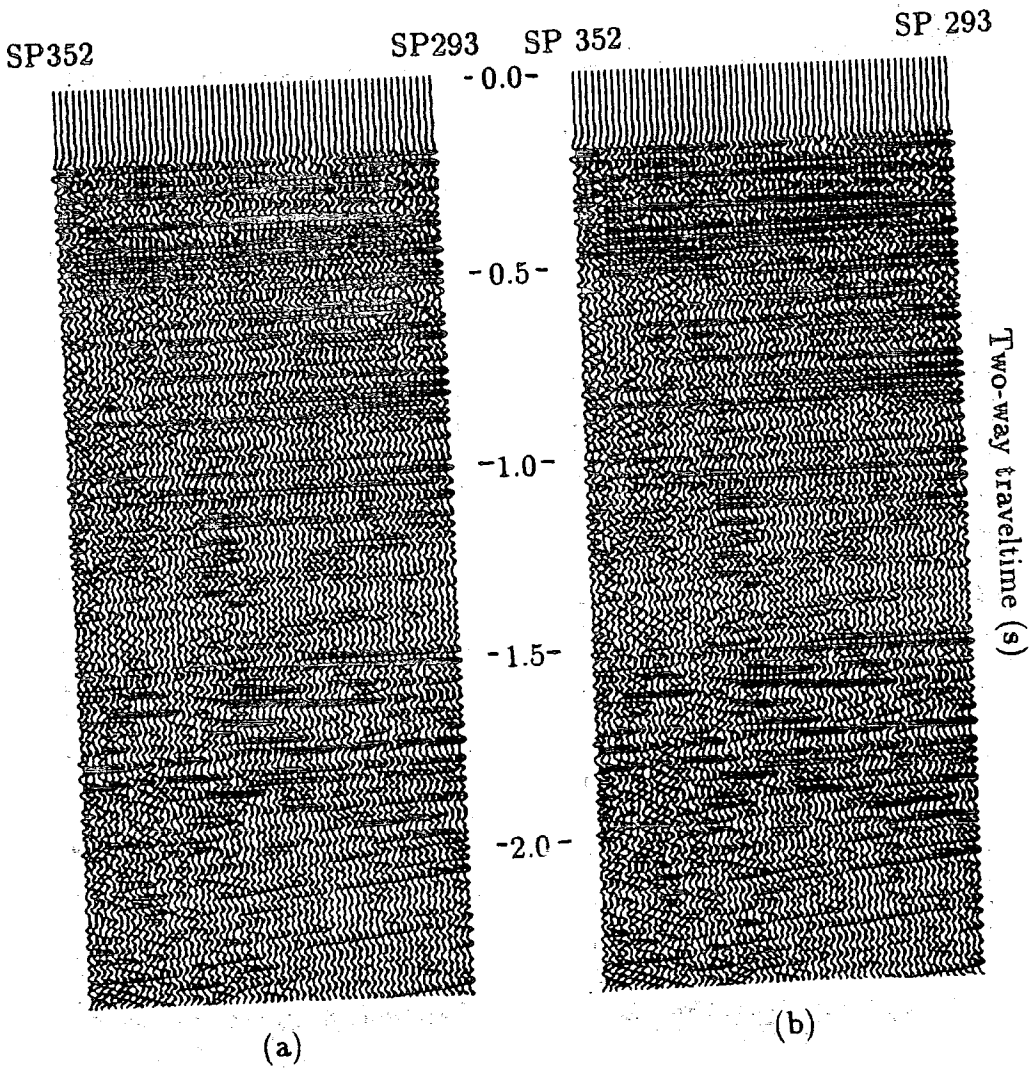

Figure 5.12. 12-fold stacked sections: (a) using directional deconvolution and (b) using standard signature deconvolution. Processing and display parameters are given in tables 5.4 and 5.5.

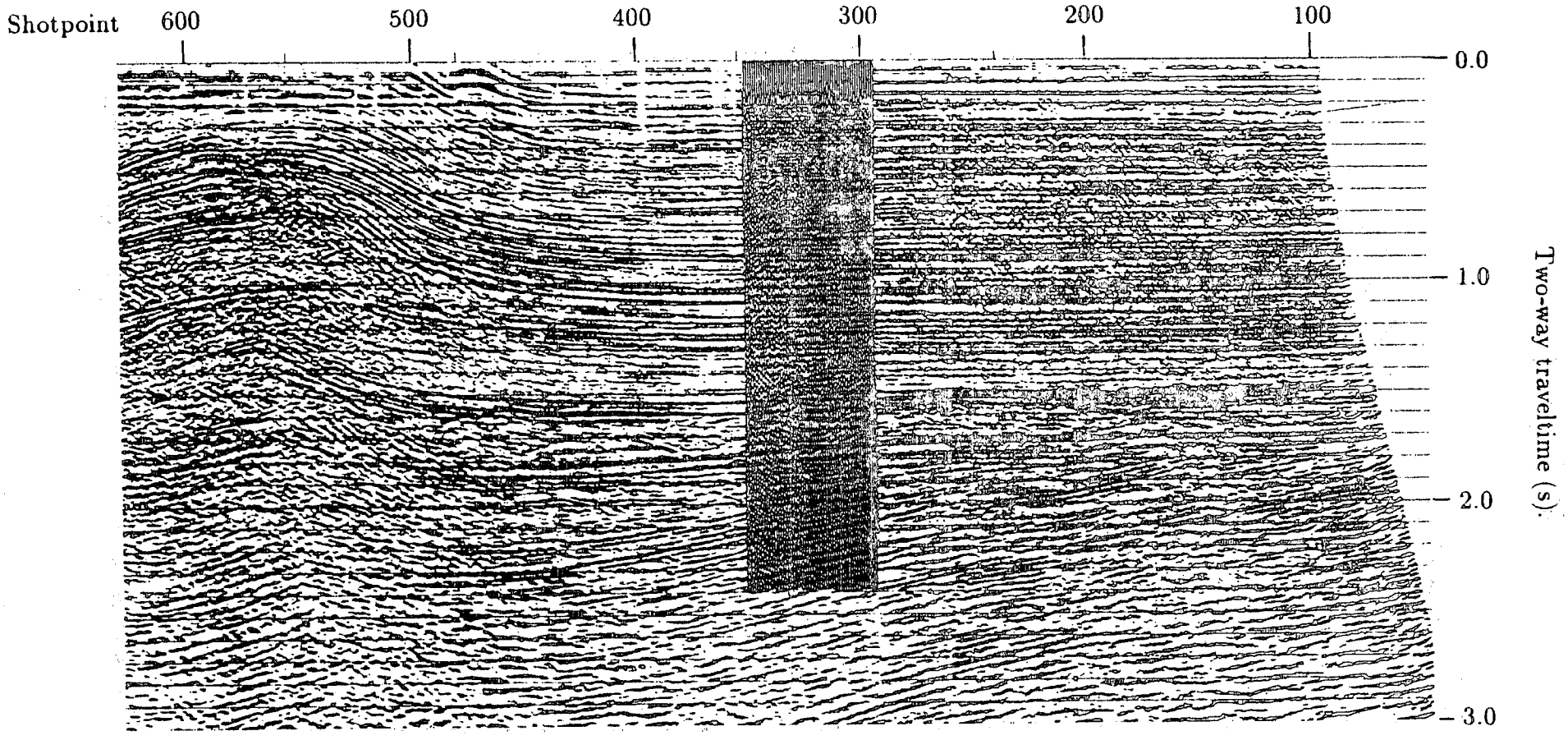

Figure 5.13. The 12-fold stacked window (figure 5.13.a) superimposed on the 48-fold stacked section processed by Horizon Exploration Ltd (figure 5.1).

MERLIN

EXPLORATION SERVICES

NON-EXCLUSIVE SURVEY

NOT TO BE SOLD OR TRADED WITHOUT THE PERMISSION
OF MERLIN GEOPHYSICAL LTD.

ACQUISITION

SHOT BY:	SEISMIC PROFILERS A.S. MV LIV PROFILER OCTOBER 1982
ENERGY SOURCE:	
TYPE	AIRGUN ARRAY
VOLUME	5560 CU. INS.
PRESSURE	2000 PSI
AVERAGE SOURCE DEPTH	5M
SHOTPOINT INTERVAL	25M
RECEIVING ARRANGEMENT:	
FOLD OF RECORDING	48
NUMBER OF GROUPS	96
AVERAGE CABLE DEPTH	9M
GROUP INTERVAL	25M
INSTRUMENTATION:	
RECORDING SYSTEM	OFS V
GAIN TYPE	I.F.P.
LOW CUT FILTER	8(18) HZ (DB/OCT)
HIGH CUT FILTER	90(72) HZ (DB/OCT)
RECORD FORMAT	SEG B
RECORD LENGTH	6S
SAMPLE RATE	4MS
POSITIONING SYSTEM	
PRIMARY: PULSE 8	SECONDARY: SATNAV/LORAN C

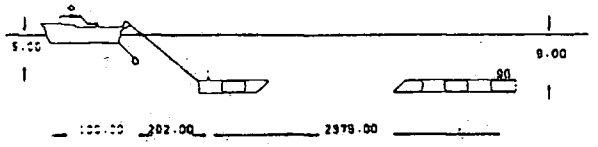

Table 5.6. Dataset B. Acquisition parameters.

The data were reprocessed in 1988 by Merlin Geophysical. A migrated 48-fold stacked section is shown in figure 5.14, and the processing parameters in table 5.7. The main structural feature on the section is a salt dome. Reflectors dip steeply on the flanks of the salt dome at shotpoint 200 at a two-way traveltime of 0.8 s (figure 5.14). Ray-tracing shows that these steeply dipping reflections originated from energy leaving the source at large take-off angles. These reflectors should thus benefit from directional deconvolution. The medium overlying the steep reflectors is not horizontally stratified. If there are strong lateral velocity variations, 'time' migration mislocates events.

5.4.2 Source array directivity

The airgun array is described in figure 5.15. It consists of four identical sub-arrays. Far-field source signatures have been calculated using the method of 'notional signatures' (Ziolkowski et al., 1982), by which far-field signatures are synthesised from near-field measurements. Near-field hydrophone signatures were supposed to have been recorded at the start of the survey. Unfortunately these appear to be erroneous. Instead, near-field signatures from trials carried out by Seismic Profilers in December 1983 were used. The trials used the same recording vessel as for the survey, but only one sub-array was used. It is assumed that other sub-arrays in the array have no effect on 'notional' signatures. 'Notional' signatures were calculated using Merlin Geophysical Software, which has the standard dimensions of the Seismic Profilers sub-array built in. The far-field signatures were then calculated by superposition of the 'notional' signatures. The free surface ghost was included in the calculations. In-line, far-field source signatures were calculated in 1° increments from $-90°$ (towards the boat) to $+90°$ (away from the boat). Selected far-field signatures are shown in figure 5.16.

A desired output for the deconvolution was chosen, and filters designed. Figures 5.17 to 5.19 show selected filters, the results of directional deconvolution and the results from standard signature deconvolution. Filter design is summarised in table 5.8. The desired output varies in energy with take-off angle in a similar

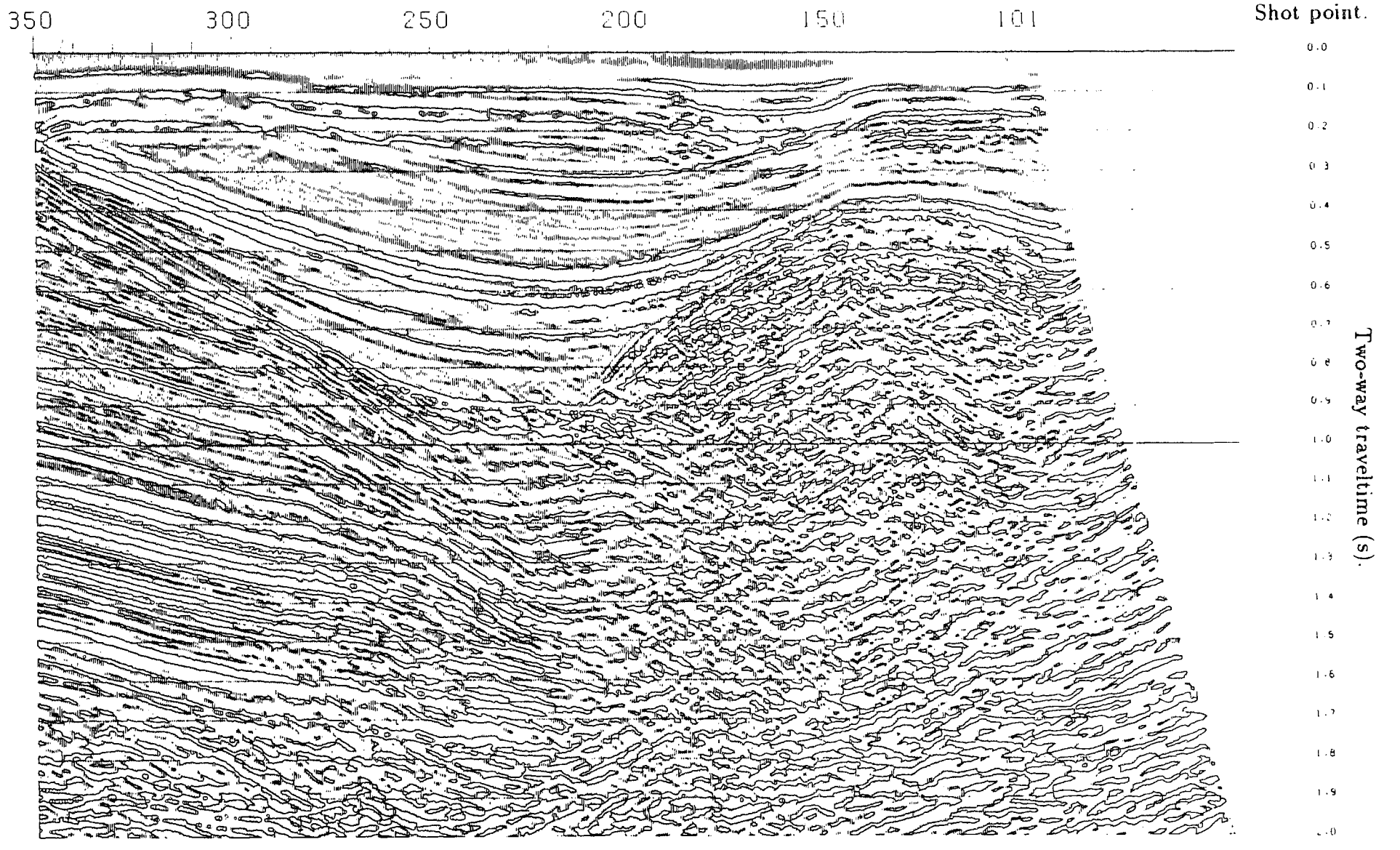

Figure 5.14. Dataset B. 48-fold migrated section (processed by Merlin Geophysical). Processing parameters are given in table 5.7.

1. DEMULTIPLE:	
2. COMMON CDP GATHER:	
3. SOURCE SIGNATURE COMPENSATION:	
INPUT	FARFIELD SIGNATURE DERIVED FROM NEAR FIELD RECORDINGS
DESIRED OUTPUT	MINIMUM PHASE GAUSSIAN WAVELET
4. AMPLITUDE BALANCE:	
EXPONENTIAL GAIN	+17 DB/SEC. 0.00 TO 1.40S
	+12 DB/SEC. 1.40 TO 2.45S
	+4 DB/SEC. 2.45 TO 5.00S
5. DECONVOLUTION BEFORE STACK:	
TYPE	LEAST SQUARES PREDICTIVE
	ZONE 1 / ZONE 2
MAXIMUM PREDICTION LAG	100MS / 100MS
MINIMUM PREDICTION LAG	12MS / 24MS
AUTOCORRELATION WINDOW	
NEAR TRACE	400-1600MS / 1400-3900MS
FAR TRACE	2200-5000MS / 2200-5000MS
APPLICATION START TIME	
NEAR TRACE	0MS / 1200MS
FAR TRACE	0MS / 2200MS
(CONTOURED: SPECIFIED FOR LINE SP82-48-12 SP 101)	
WIDTH OF MERGE ZONE	300MS
6. AMPLITUDE BALANCE:	
WHOLE TRACE EQUALISATION	
7. FK DOMAIN MULTIPLE ATTENUATION:	
VELOCITY DERIVATION	"MERVEL" VELOCITY ANALYSES
8. AMPLITUDE BALANCE:	
WHOLE TRACE EQUALISATION	
EXPONENTIAL GAIN	-17 DB/SEC. 0.00 TO 1.40S
	-12 DB/SEC. 1.40 TO 2.45S
	-4 DB/SEC. 2.45 TO 5.00S
9. NMO CORRECTION:	
VELOCITY DERIVATION	"MERVEL" VELOCITY ANALYSES
ANALYSIS LOCATION	EVERY 2 KM
10. STACK:	
TYPE	STANDARD MEAN AMPLITUDE CDP
COVERAGE	6000%
11. SPACE VARIANT GEOMETRICAL DIVERGENCE COMPENSATION:	
SCALAR COMPUTED FROM	$T(V_T)^2/(V_0)^2$
12. STATIC CORRECTIONS:	
GUN AND CABLE	+10MS
13. FK DOMAIN FILTER:	
ATTENUATION ZONE	DATA DIPS OF +/-7 TO +/-20 MS/TR
SCALAR WITHIN DIP LIMITS	0.1
14. DECONVOLUTION AFTER STACK:	
TYPE	LEAST SQUARES PREDICTIVE
	ZONE 1 / ZONE 2
MAXIMUM PREDICTION LAG	100MS / 100MS
MINIMUM PREDICTION LAG	12MS / 24MS
AUTOCORRELATION WINDOW	400-1600MS / 1200-3900MS
APPLICATION START TIME	0MS / 1200MS
(CONTOURED: SPECIFIED FOR LINE SP82-48-12 SP 101)	
WIDTH OF MERGE ZONE	300MS
16. MIGRATION:	
TYPE	FK DOMAIN WITH RESIDUAL FINITE DIFFERENCE WAVE EQUATION
TIME STEP	24MS
MIGRATION VELOCITY DERIVATION	100% STACKING VELOCITIES
18. FK DOMAIN FILTER:	
ATTENUATION ZONE	DATA DIPS OF +/-6 TO +/-20 MS/TR
SCALAR WITHIN DIP LIMITS	0.2

17. TIME VARIANT FILTER:

FILTERS LINEARLY INTERPOLATED IN TIME CUTOFFS AND SLOPES SPECIFIED AT -3 DB POINT	TIME (MS)	LOW CUT HZ (DB/OCT)	HIGH CUT
	4	15(24)	80(36)
	1400	10(24)	60(36)
	2000	7(24)	50(36)
	3000	7(24)	40(36)
	5000	7(24)	35(36)

20. AMPLITUDE BALANCE:	
WHOLE TRACE EQUALISATION	
GENERAL AMPLITUDE TREND ANALYSIS AND COMPENSATION	
ROBUST AGC	1000MS WINDOW

DISPLAY

DEVICE	SCITEX LASER PLOTTER
BIAS	0%
GAIN	+9 DB
POLARITY	COMPRESSION=NEGATIVE=TROUGH
DATUM PLANE	SEA LEVEL
SHOTPOINT LOCATION	SOURCE POSITION

Table 5.7. Merlin Geophysical processing parameters.

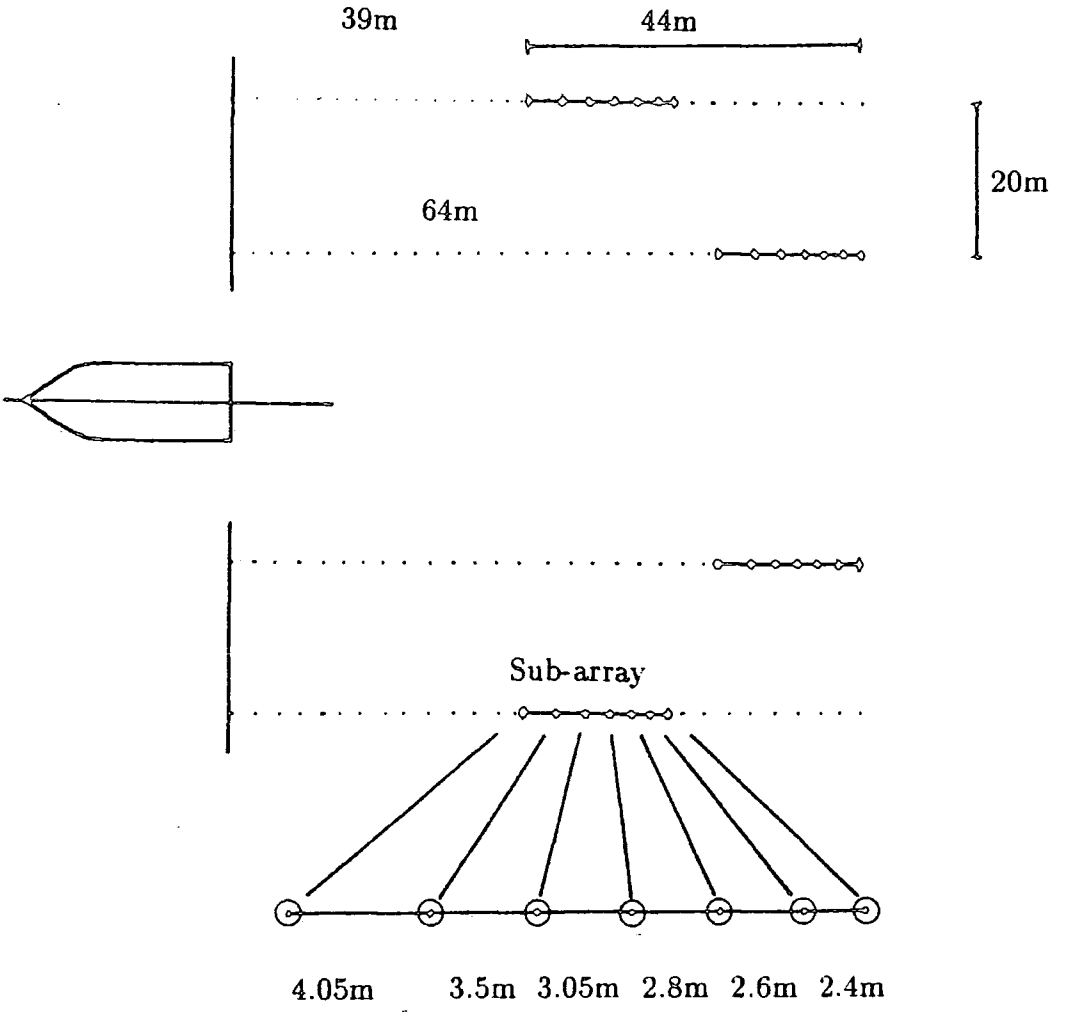

Gun size 465 305 191 145 114 96 75 cu. ins.

Total volume 5560 cu. ins.

Figure 5.15. Seismic Profilers A.S. airgun array. Plan view.

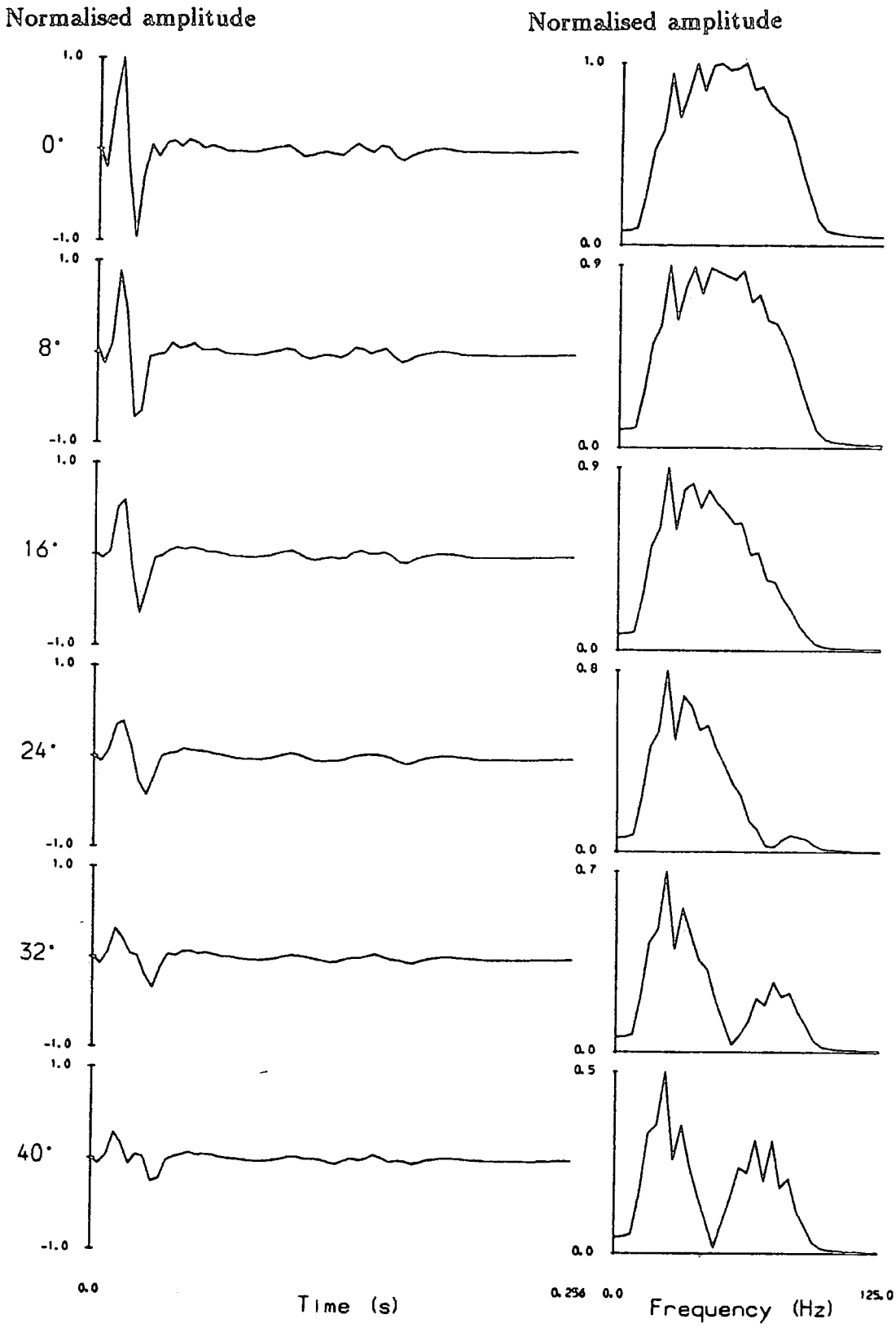

Figure 5.16. Far-field source signatures and amplitude spectra. Take-off angle varies from 0° to 40° from vertical.

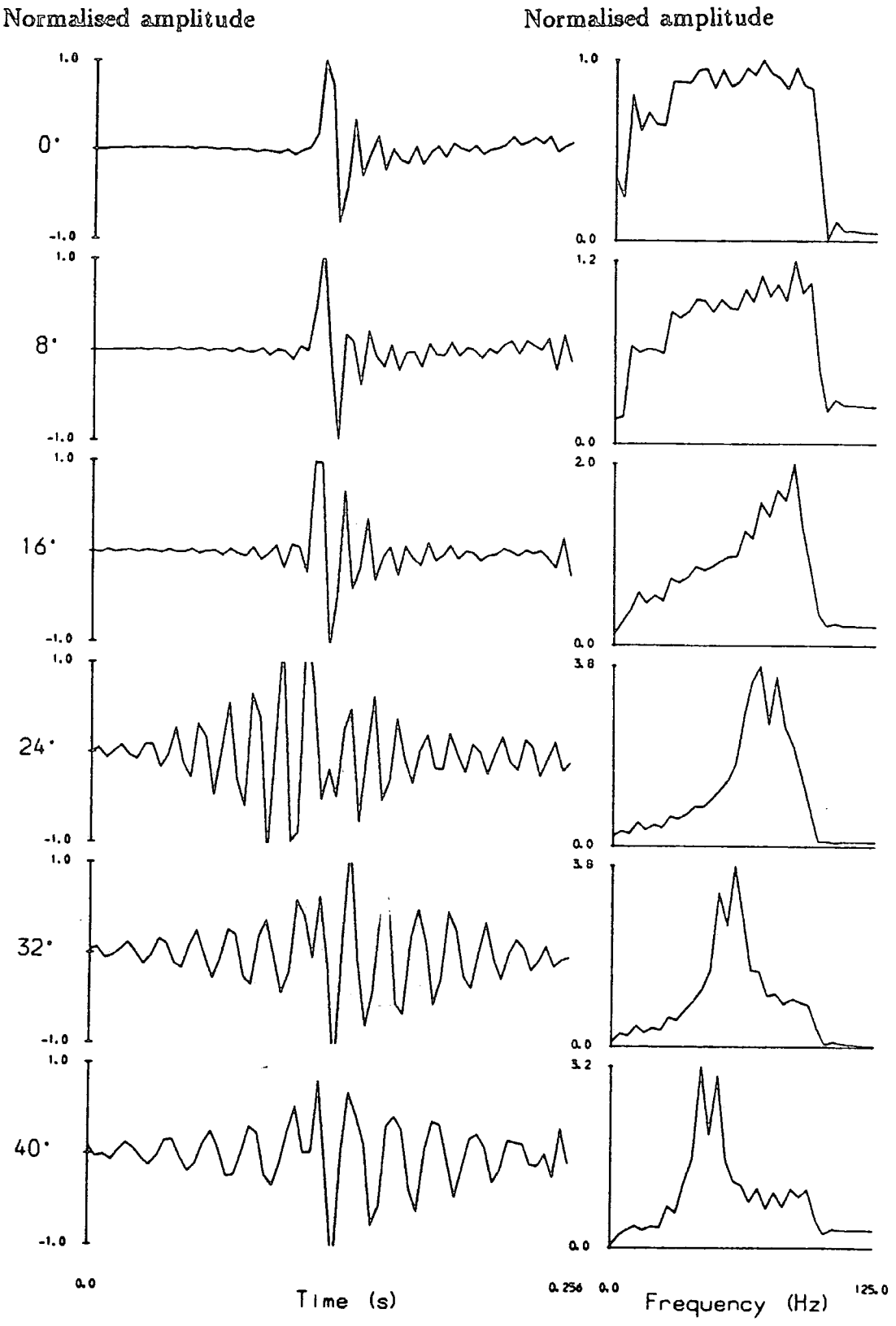

Figure 5.17. Directional deconvolution filters designed for the far-field signatures shown in figure 5.16.

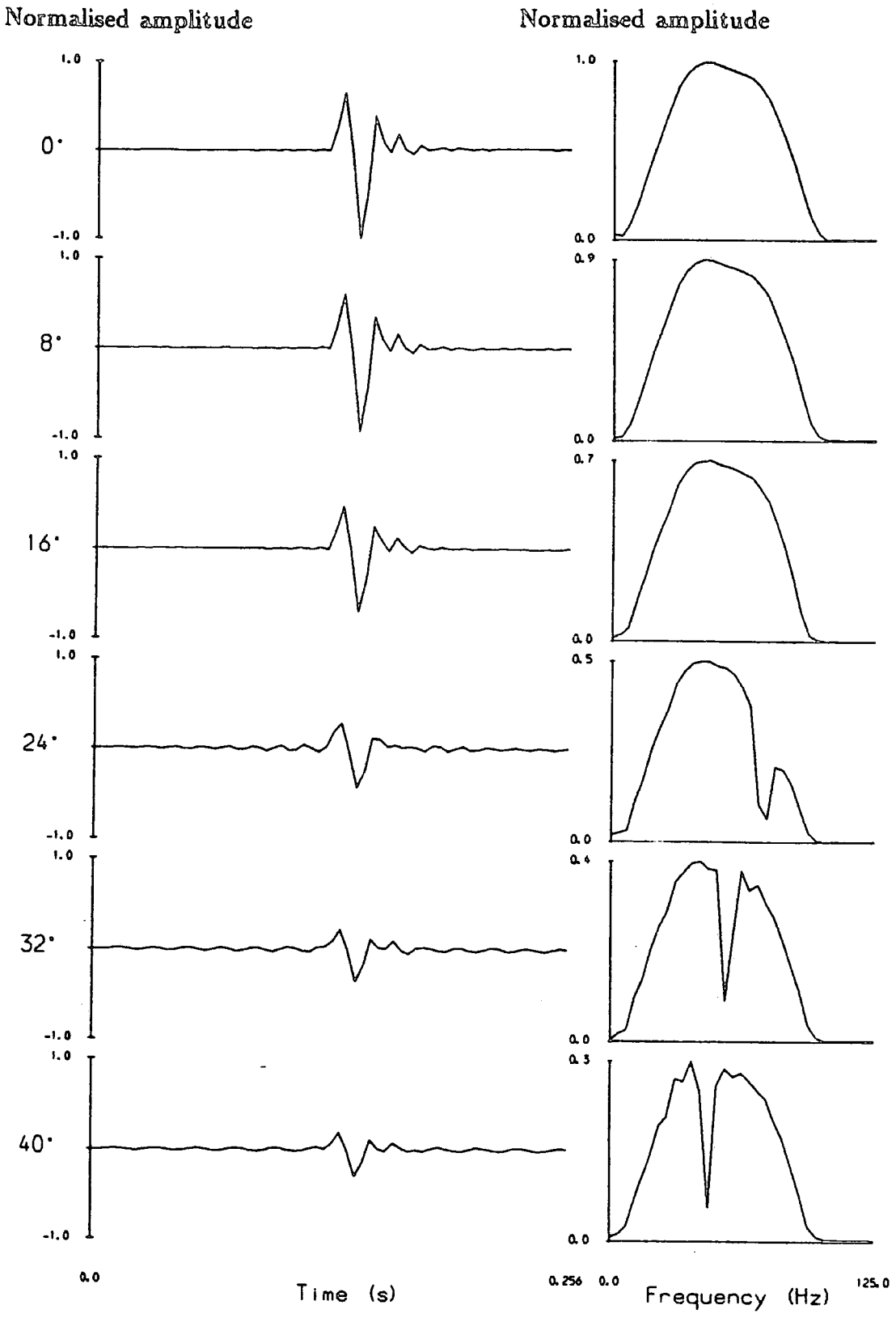

Figure 5.18. Actual outputs when the directional deconvolution filters (figure 5.17) were applied to the source signatures (figure 5.16).

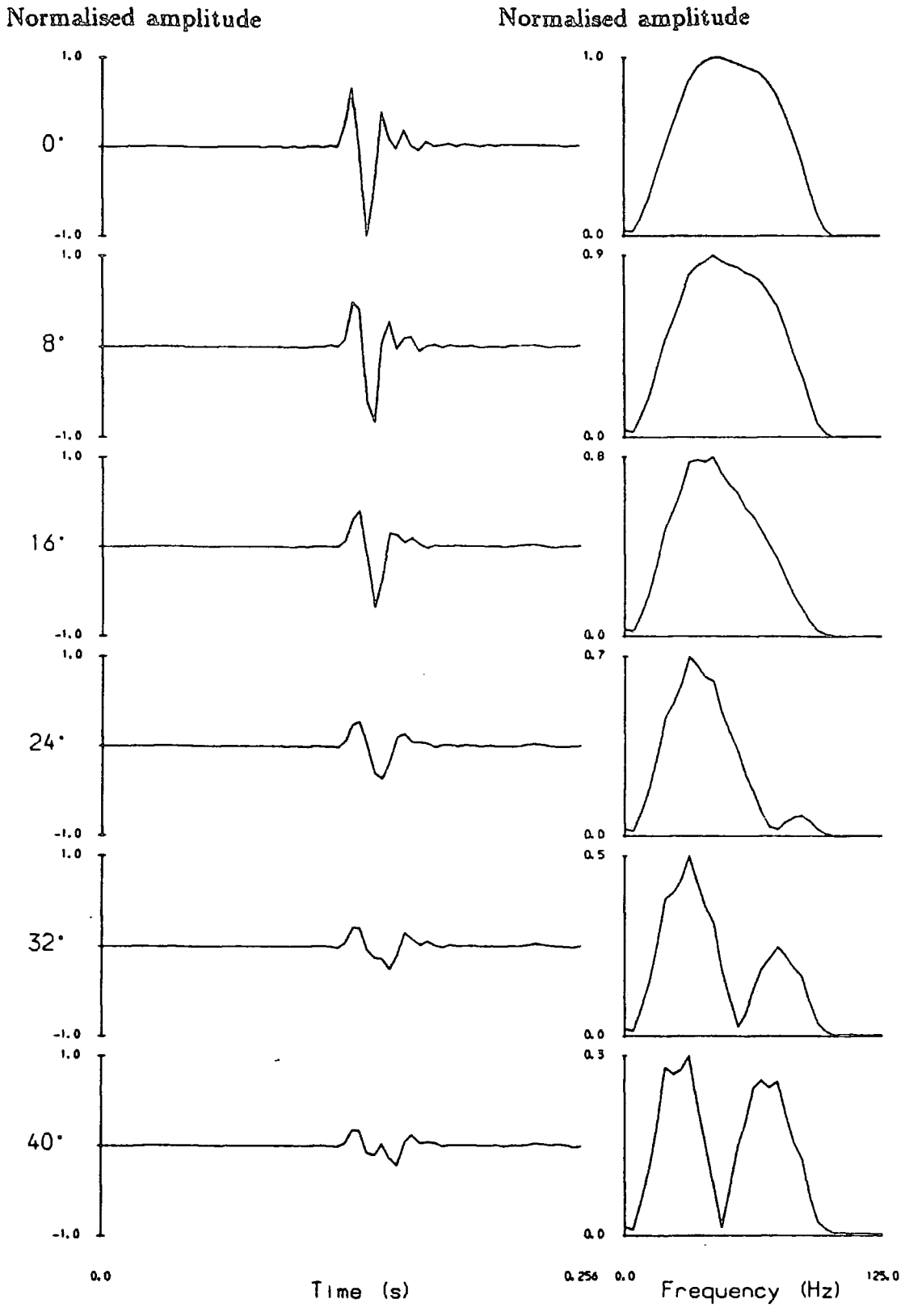

Figure 5.19. Actual outputs when the deconvolution filter designed for the near-vertical travelling signature (top of figure 5.17) was applied to the source signatures (figure 5.16).

Desired output.

Amplitude spectrum:	smoothed 0°signature spectrum.
Phase spectrum:	minimum phase.
Amplitude variation with take-off angle:	similar to source array

Filter design.

Domain:	time domain.
Filter length:	0.256 s.
Lag of desired output:	0.128 s.
White noise:	1.0%

Table 5.8. Dataset B. Directional deconvolution filter design.

nature to the source array. For dataset A (section 5.3.2), the desired output was uniform for all take-off angles, and this lead to deconvolution filters having large amplification at large take-off angles (figure 5.4). Filters designed for large take-off angles were not used for dataset A because energy originating from such angles was not present in the data. For dataset B, it was necessary to use filters designed for large take-off angles. The desired output was tapered so that these filters would not cause excessive noise amplification. The directivity of the source array is similar to that of the source array used for dataset A. Directivity is most apparent for take-off angles larger than 16°.

5.4.3 Directivity effects

Ray-tracing has been performed using an approximate depth model. Calculation of the depth model assumes a horizontally-stratified medium. The depth model is thus unreliable. Results of the modelling are shown in figures 5.20 and 5.21.b, with a real CMP gather (figure 5.21.a) for comparison. Arrivals from steep dips on the flanks of the salt dome originate from large source take-off angles and lie in the 'useful' (unmuted) part of the gather. Thus, there appears to be more directivity in this dataset than in datatset A.

An approximate 'correction factor' for ray bending is needed (section 5.3.4). Figure 5.22 shows the relationship between the source take-off angle from ray-tracing and the source take-off angle which assumes a linear raypath to the reflection point. A larger range of take-off angles has been considered than for dataset A (compare with figure 5.9). The linear correction factor is 1.4 for this dataset.

5.4.4 Processing

Processing parameters for directional deconvolution combined with prestack migration are summarised in table 5.9. Table 5.10 shows the full processing sequence.

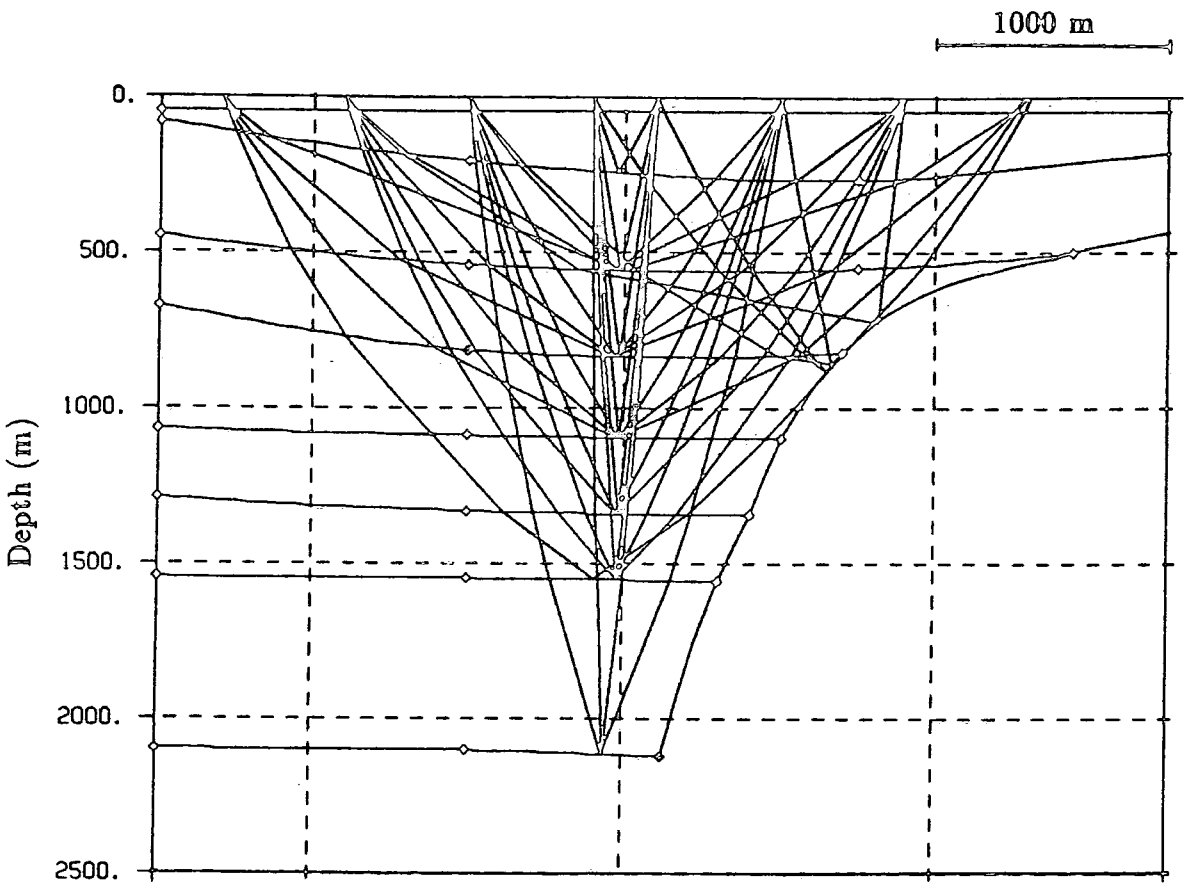

Figure 5.20. Dataset B. Raypath diagram. Depth model was derived from stacking velocities.

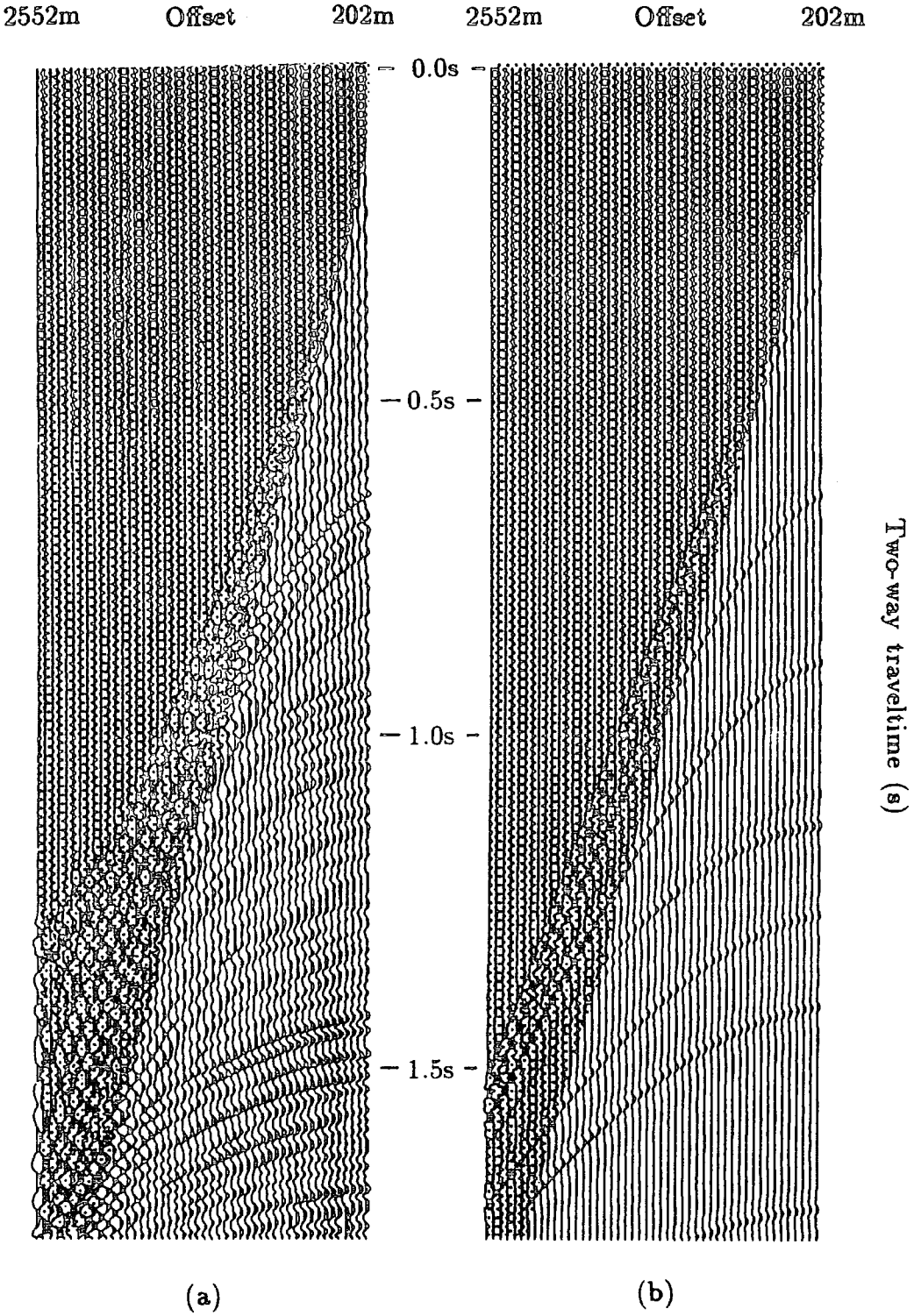

Figure 5.21. 48-fold CMP gathers, (a) real and (b) synthetic.

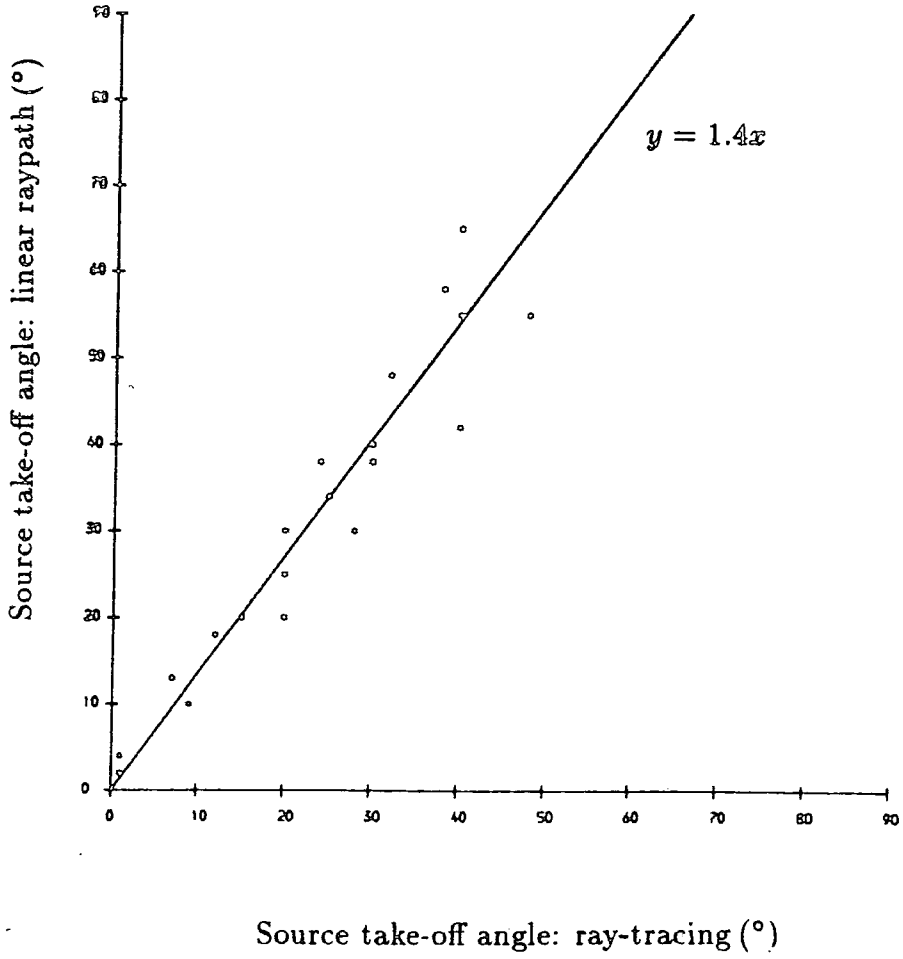

Figure 5.22. Graph of source take-off angles calculated from ray-tracing, against source take-off angles which assume linear raypaths to reflection points.

Source take-off angles.

Maximum angle:	44°
Deconvolution increment:	4°
Linear correction factor:	1.4°

Migration velocities.

100% stacking velocities: SP 263.

Input data.

Sampling interval:	4 ms
Bandpass filter:	trapezoidal
Corner frequencies:	10, 20, 80, 100 Hz
Migration window:	shotpoints 147-264
	traveltime 0.05-1.20 s

Constant-offset sections.

Number.	Offset(m).
Offset # 1:	202
Offset # 2:	402
Offset # 3:	602

Table 5.9. Dataset B. Directional deconvolution combined with prestack migration parameters.

Each constant-offset section.

1. Prestack migration: with either directional deconvolution or standard signature deconvolution.
2. Newman filter.
3. Predictive deconvolution: see below
4. Bandpass filter: see below.

Stack.

5. Sections normalised by energy.
6. 3-fold stack.

Post-stack processing.

7. Predictive deconvolution: see below.
8. Bandpass filter: see below.

Display.

- Trace equalisation by energy.
- Reduction of dynamic range: $\pm\sqrt{amplitude}$ (Claerbout, 1985).
- Variable area wiggle.

Predictive deconvolution.

Prediction lag.	12 ms
Filter length.	100 ms
White noise.	1.0%

Bandpass filter.

Trapezoidal.	
Corner frequencies.	10,20,80,100 Hz

Table 5.10. Dataset B. Complete processing sequence and display parameters.

5.4.5 Results: discretisation noise

Figure 5.23.a shows the middle of the three constant-offset sections, after processing to stage 2 of the processing sequence (table 5.10). The migrated section is very noisy. Migration noise, and methods of noise reduction, were discussed in chapter III. If the noise is 'discretisation noise', three methods of noise reduction were suggested, high-cut filtering, truncation of the migration operator, and spatial interpolation.

- One of the main aims of directional deconvolution is to preserve high frequencies. High-cut filtering of the input data is thus counter-productive.

- Migration operator truncation has been incorporated into the prestack migration scheme whereby the summation operator is only applied if the time-moveout per trace of the operator is less than half the period of the maximum frequency being considered (section 3.3.2). The full range of take-off angles specified will not be used if this criterion is disobeyed. For this dataset the maximum frequency of interest is 80 Hz and the spatial sampling interval is 50 m. Figure 5.23.b shows the same migrated section as figure 5.23.a, but the truncated migration operator was used. The noise is reduced but the steeply dipping reflectors are not imaged. This is because truncating the migration operator limits the maximum dip which can be migrated. Trace interpolation is needed.

- Trace interpolation was discussed in chapter II. The need for spatial interpolation is a major shortcoming of the f-k directional deconvolution method because spatial interpolation is expensive and difficult to perform. Two methods are available to reduce the spatial sampling of a constant-offset section which overcome these difficulties: (i) interpolation by insertion of dead traces before migration, and (ii) interleaving of adjacent constant-offset sections.

  (i) Bolondi et al.(1982) describe how 'dip moveout' (DMO) may be used as an interpolator. DMO is a prestack partial migration, which is im-

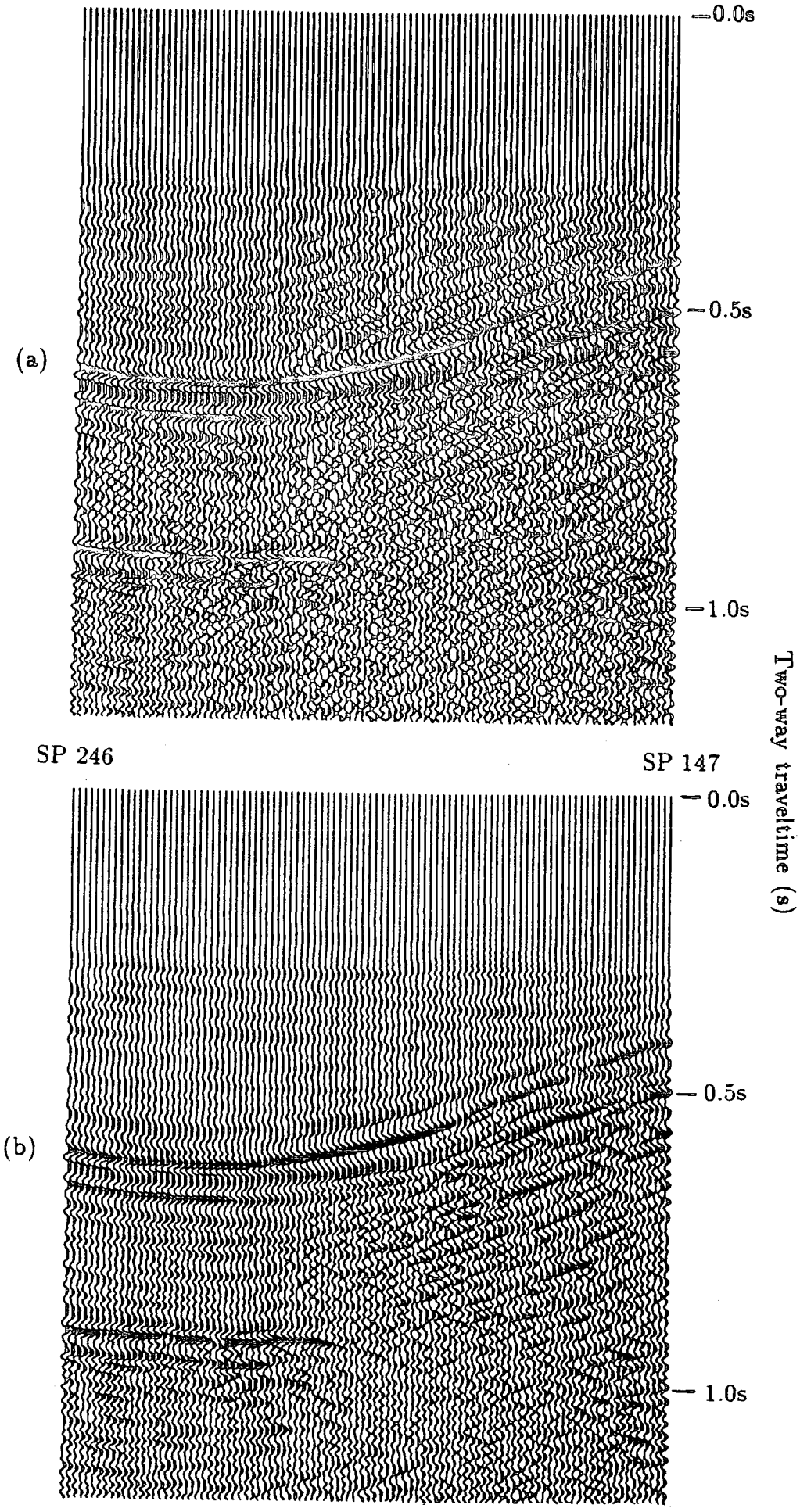

Figure 5.23. A limited window of the second constant-offset section (offset 402m) after prestack migration with standard signature deconvolution using (a) complete migration operators and (b) truncated migration operators. Display parameters are given in table 5.10.

plemented in a similar manner to full prestack migration. To perform interpolation, blank traces are inserted between adjacent traces on the constant-offset section before migration. Migration will 'smear' energy across these dead traces, which will appear as 'live' traces after migration. Deregowski (1986) notes that an even better interpolation is obtained if some form of crude interpolation is performed on the dead traces before migration. A simple average of adjacent traces is suggested. Interpolation by this method will perform well if the data are not spatially aliased. If data are spatially aliased, interpolation will occur along apparent aliased dips as well as true dips, so an alternative method is needed.

(ii) Spatial sampling of a constant-offset section is determined by the shot interval. The common midpoints on a constant-offset section are also separated by the shot interval. The common midpoints of an adjacent constant-offset section (i.e. the next largest or smallest offset) will be displaced by half the receiver spacing. Thus, if adjacent constant-offset sections are interleaved, spatial sampling is halved, and all traces are in their true spatial positions. An NMO correction is required to account for the two different offsets. Moveout is small, hence this is relatively insensitive to velocity errors and invalid NMO assumptions.

The former of the two interpolation methods was used for this dataset because less computation is required. Before migration each constant-offset section was padded with blank traces to halve the spatial sampling interval, and a simple linear interpolation was performed. Thus the processing sequence (table 5.10) now has an additional interpolation stage before stage 1. A portion of the second constant-offset section, corresponding to the migration window, is displayed in figure 5.24.a, before interpolation, and in 5.24.b after linear interpolation. After prestack migration, using the truncated migration operator, the steeply dipping reflectors are now imaged (figure 5.25.b). Migration noise has been suppressed (compare with figure 5.23.a).

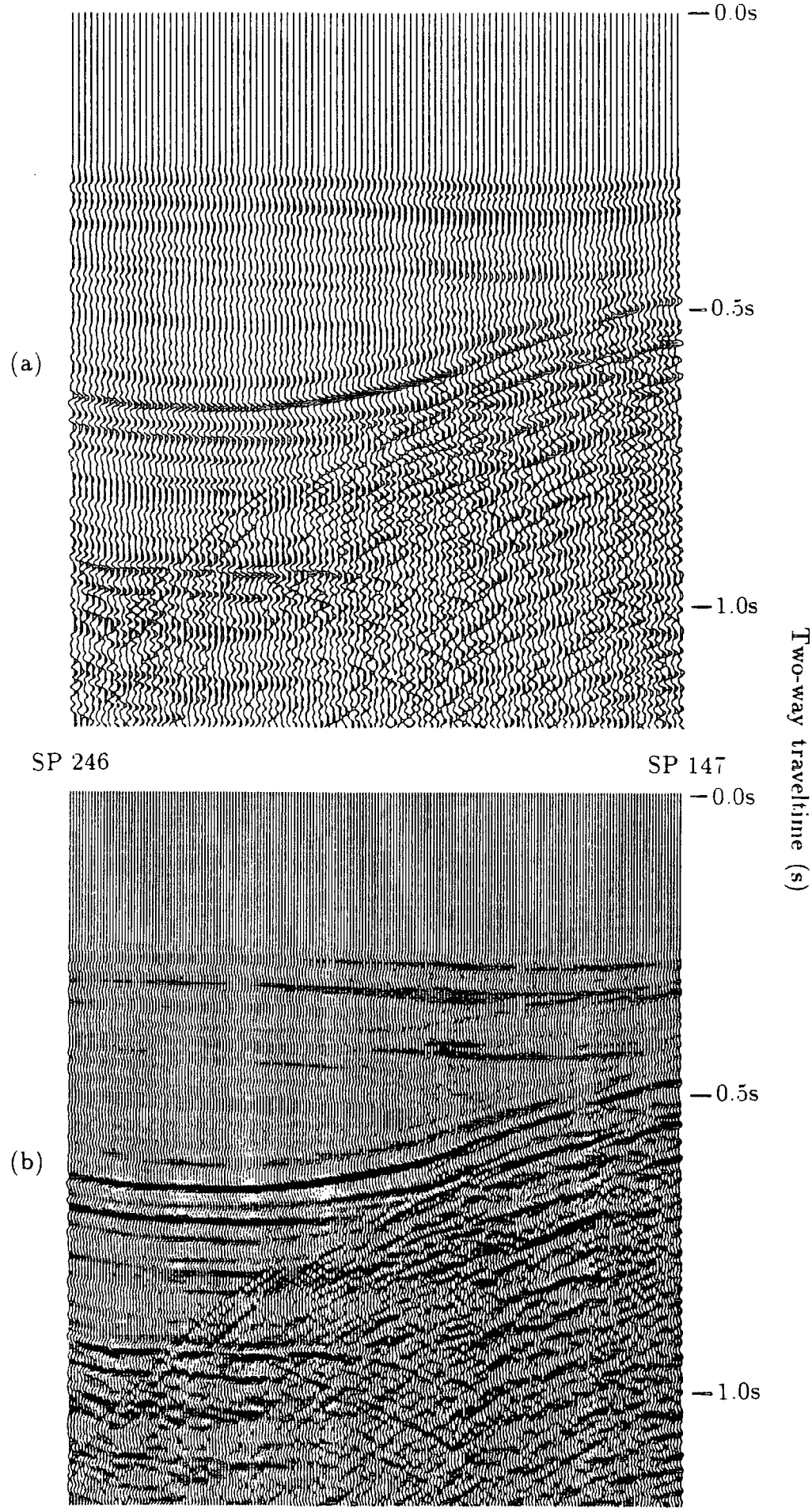

Figure 5.24. A limited window of the second constant-offset section before migration. (a) Original 25m shot spacing. (b) 12.5m shot spacing simulated by crude spatial interpolation. Display parameters are given in table 5.10.

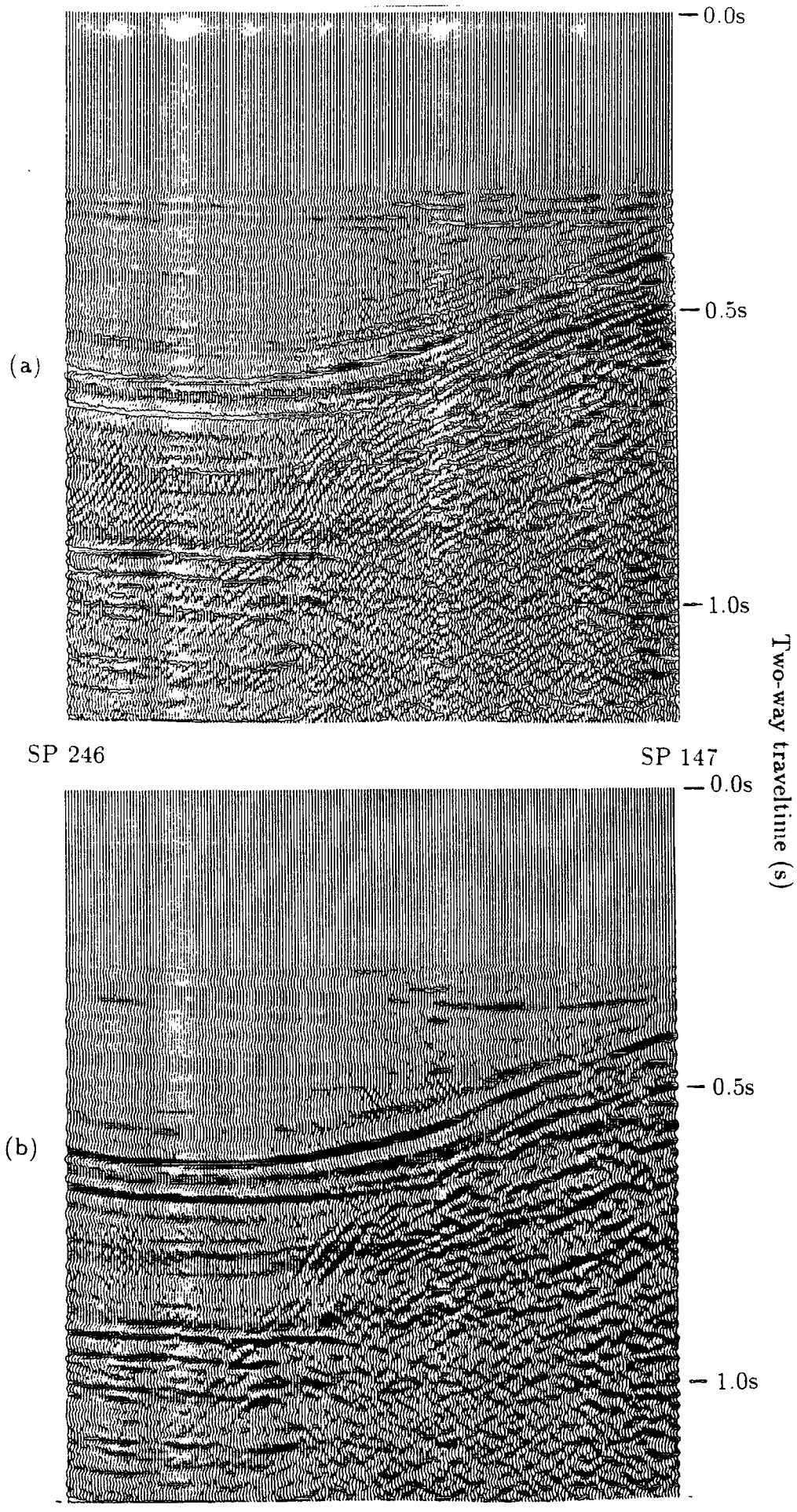

Figure 5.25. A limited window of the second constant-offset section after prestack migration: (a) using directional deconvolution and (b) using standard signature deconvolution. Processing and display parameters are given in tables 5.9 and 5.10.

A comparison of directional deconvolution (figure 5.25.a) and standard signature deconvolution (figure 5.25.b) may now be made. Both sections have been processed to stage 2 of the sequence (table 5.10). The directionally deconvolved section (figure 5.25.a) has high frequency content, but is noisy. Directional deconvolution has amplified high frequency components of the reflected signal and of the noise. Because high frequencies have been amplified in the directionally deconvolved section, 'discretisation' noise is greater. After predictive deconvolution and bandpass filtering (figure 5.26), i.e processing to stage 4 (table 5.10), the difference in frequency content is still apparent. Shallow and dipping reflectors are most affected. This is seen more clearly on the 3-fold stacked sections (figure 5.27). The section processed with directional deconvolution (figure 5.27.a) is superior to the conventionally processed section (figure 5.27.b) because shallow and dipping reflectors are more continuous and are better resolved. Examples are: the events at a traveltime of 0.55 s at SP 246 and 0.38 s at SP 147, which are only clearly seen to be two reflectors on the directionally deconvolved section; and the events at a traveltime of 0.47 s at SP 147 which continue to the steeply dipping reflections at a traveltime of 0.7 s at SP 195. The steeply dipping reflectors, however, are not adequately imaged. Migration velocities must be checked.

5.4.6 Results: velocity analysis

The 3-fold stacked section with standard signature deconvolution and prestack migration (figure 5.27.b) is superimposed on the 48-fold Merlin section (figure 5.14) in figure 5.28. The two sections appear to be similar, indicating that the prestack migration algorithm is functioning correctly.

Prestack migration may be used as a velocity analysis tool (Gardner et al., 1974). If the migration velocity field is equal to the actual velocity field, migration of different constant-offset sections yields the same result. If there are errors in the velocity field, reflections are misplaced by different amounts for each constant-offset section. This principle may be used for velocity analysis in several different ways. Each constant-offset section may be migrated with a

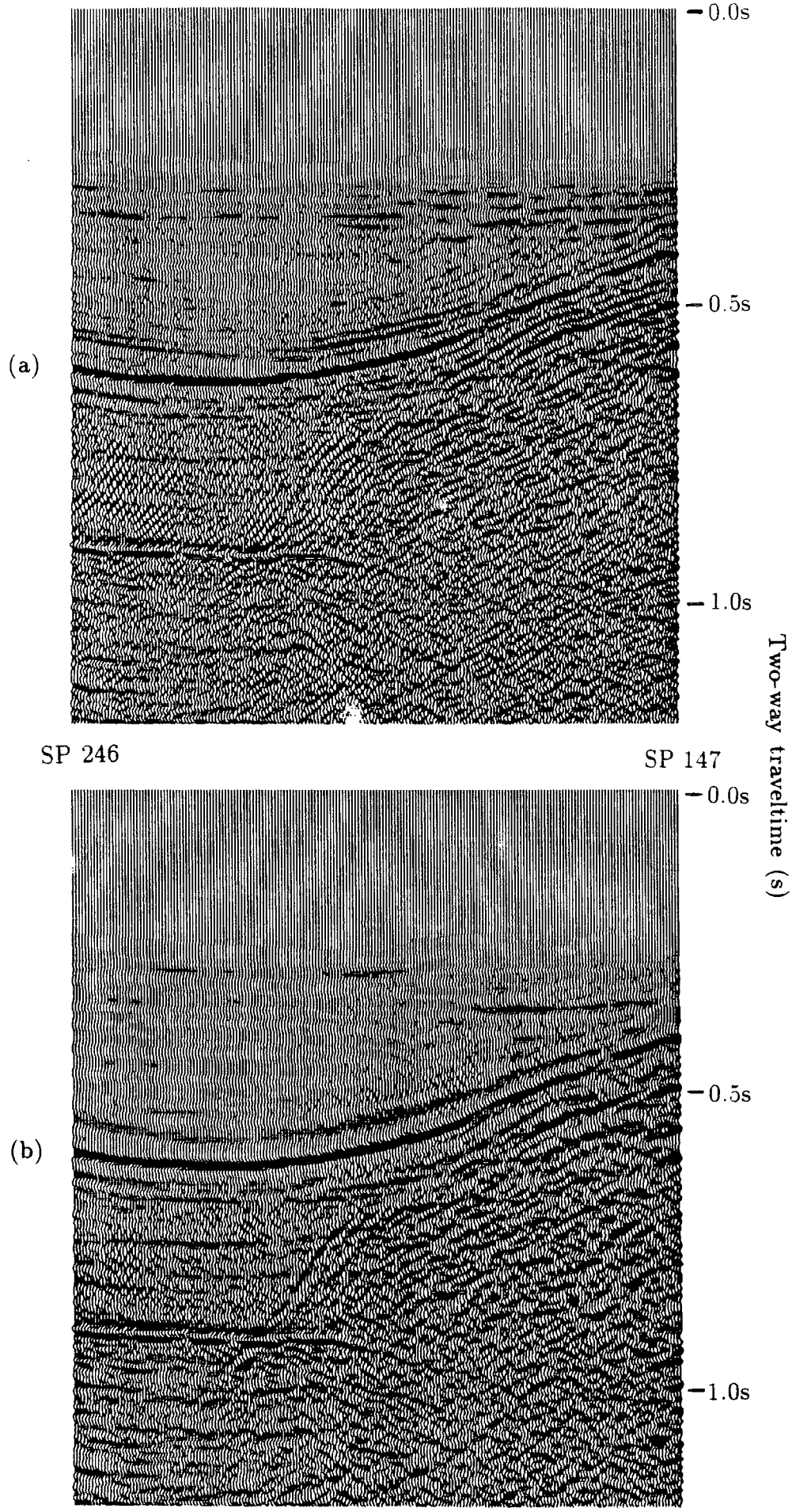

Figure 5.26. The same sections as figure 5.25 after predictive deconvolution and bandpass filtering. Processing and display parameters are given in tables 5.9 and 5.10.

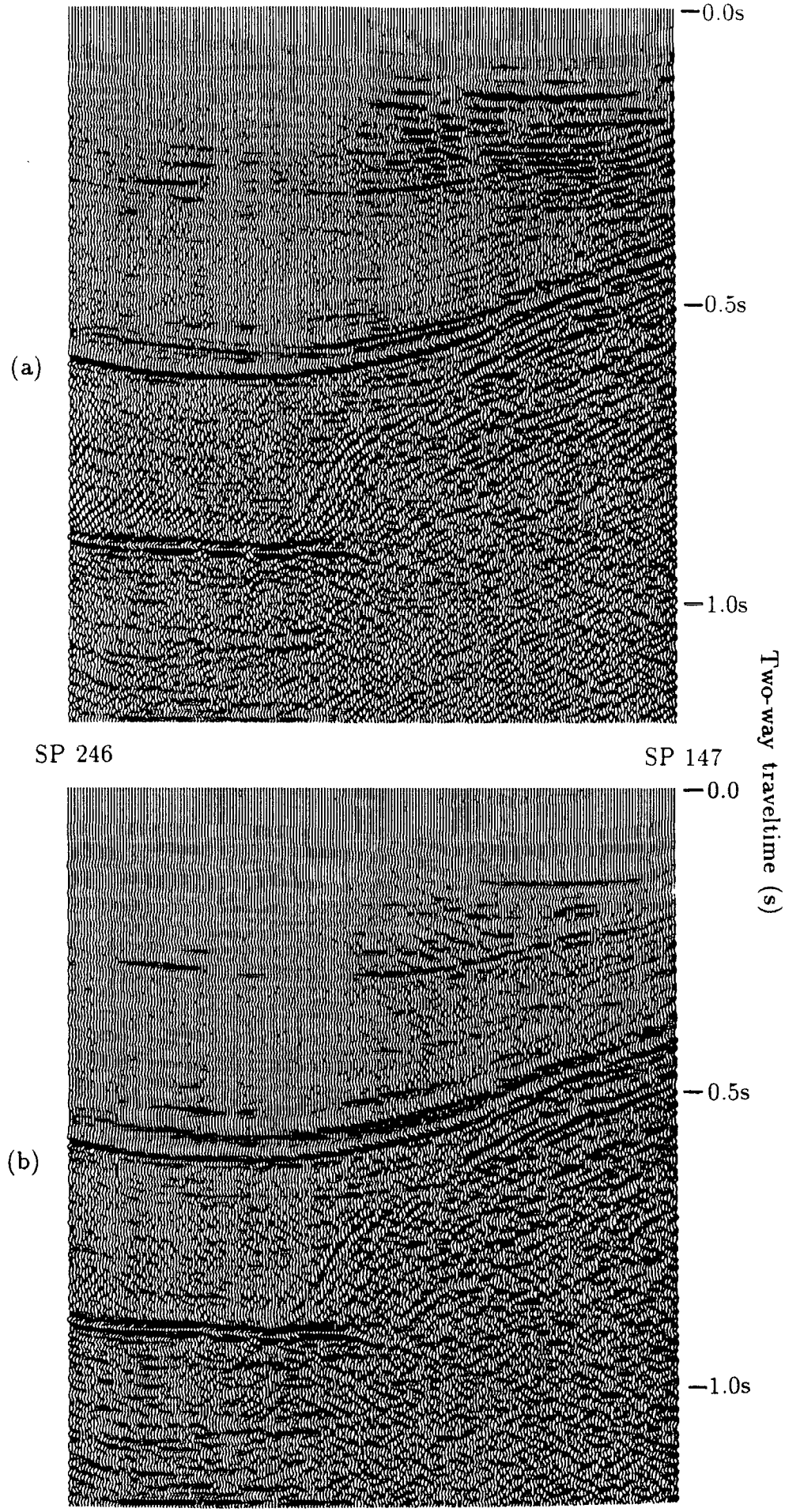

Figure 5.27. 3-fold stacked sections: (a) using directional deconvolution and (b) using standard signature deconvolution. Processing and display parameters are given in tables 5.9 and 5.10.

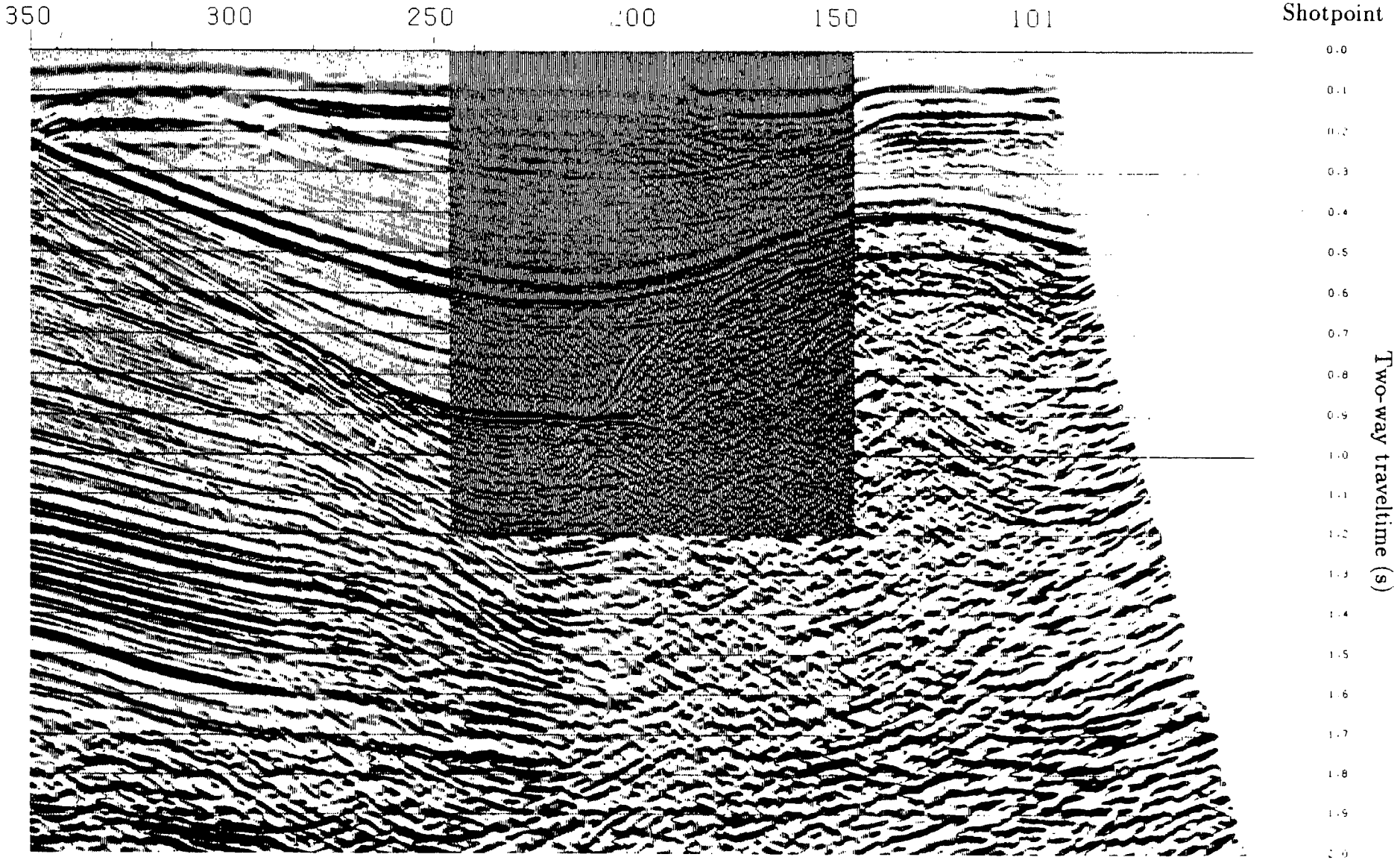

Figure 5.28. The 3-fold stacked window (figure 5.27.a) superimposed on the 48-fold stacked section processed by Merlin Geophysical (figure 5.14).

range of velocities. Sections migrated with the same velocity function are then stacked, and the best stack chosen (Fowler, 1984). This method is very computer intensive. An alternative method is to migrate each constant-offset section with only one velocity field, and then to re-sort the data into CMP gathers. Errors in the velocity field will be apparent as reflector moveout. Residual NMO may be applied to the CMP gathers (Al-Yahya, 1986), residual migration may be performed (Black et al., 1985), or the constant-offset sections could be re-migrated using an updated velocity field.

The three migrated constant-offset sections, which are stacked in figure 5.27.a, are shown re-sorted in to 3-fold CMP gathers in figure 5.29. Eighteen CMPs, located at regular intervals of the migration window, are displayed. Residual moveout can be seen on most reflectors. The moveout varies laterally for a given traveltime (e.g. reflector at 0.9 s), which shows that there is lateral variation in velocity. The migration algorithm (Appendix A) uses only a single velocity function. For this processing (table 5.9), the stacking velocities from shotpoint 263 were used. The steeply dipping reflectors are the most interesting for the evaluation of directional deconvolution. A velocity function appropriate for the migration of these reflectors was needed.

Stacking velocities are dip dependent (Levin, 1971), but migration velocities are not. Consider a plane dipping reflector (dip α) below a uniform velocity overburden of velocity V. The stacking velocity V_{stack}, obtained from velocity analysis (Taner and Koehler, 1969), is related to the medium velocity by

$$V_{stack} = \frac{V}{\cos \alpha}$$

Thus migration velocity is less than stacking velocity, when the stacking velocity has been calculated for arrivals from a dipping reflector.

Migration was performed with a range of velocity functions. Functions used were a percentage of stacking velocities. As an example, the 3-fold stacked section

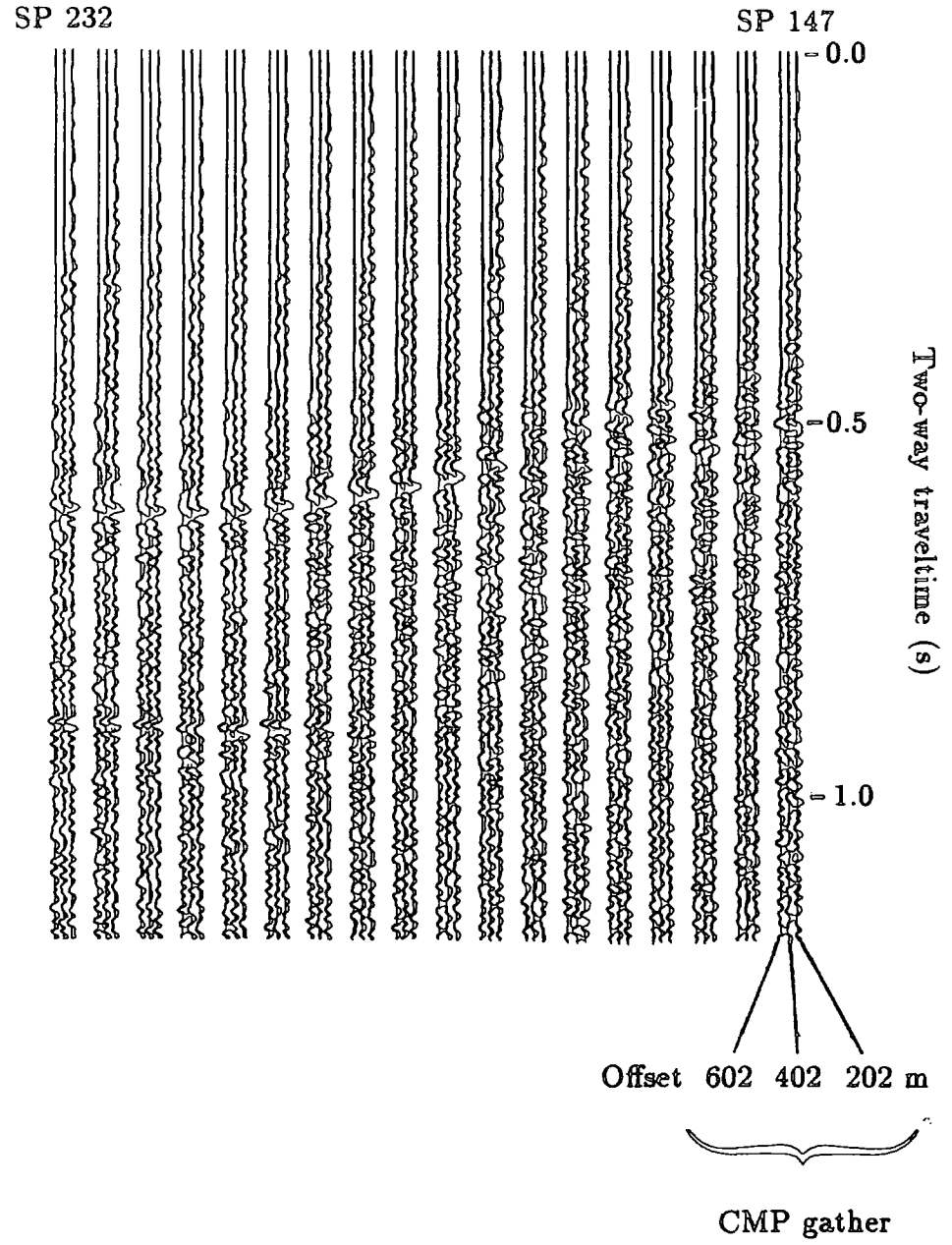

Figure 5.29. Eighteen 3-fold CMP gathers, resorted from the three migrated sections, which are shown stacked in figure 5.27.a.

and re-sorted CMP gathers for processing using 90% of the stacking velocity function are shown in figures 5.30 and 5.31. The steeply dipping reflectors were not adequately imaged in any of the trials.

5.4.7 Migration of steep dips

Prestack migration was derived for a constant-velocity medium in chapter III. In this chapter (section 5.3.4), the method has been extended to a horizontally stratified-medium by using r.m.s velocities. The r.m.s approximation is poor for steeply dipping reflectors because ray bending is ignored. A more advanced method is needed.

For steeply dipping reflectors, and wide-angle reflection data, rays travel at a large angle to the vertical. 'Depth' migration is needed. Kirchhoff depth migration uses ray-tracing to define migration summation operators (e.g. McMechan and Fuis, 1987). Ray bending is fully accounted for, and steep dips may be imaged. This method, which is very expensive, is discussed further in chapter VI.

A novel migration method, which does account for ray bending, is described by Zhu (1988). Analytical formulae for zero-offset Kirchhoff migration may be found for certain one-dimensional velocity functions. This overcomes the need for numerical ray-tracing, and hence is cheaper. An example is that of a medium with a linear increase in velocity with depth, namely

$$V(z) = V_0 + kz$$

where V_0 is the velocity at the surface and k is the velocity gradient. For such a medium, raypaths are circular arcs. Directional source signature deconvolution may be incorporated into linear velocity-depth Kirchhoff prestack migration by considering the geometry of raypaths (Telford et al., 1976). To define the migration summation operator, consider raypaths to a point diffractor (figure 5.32).

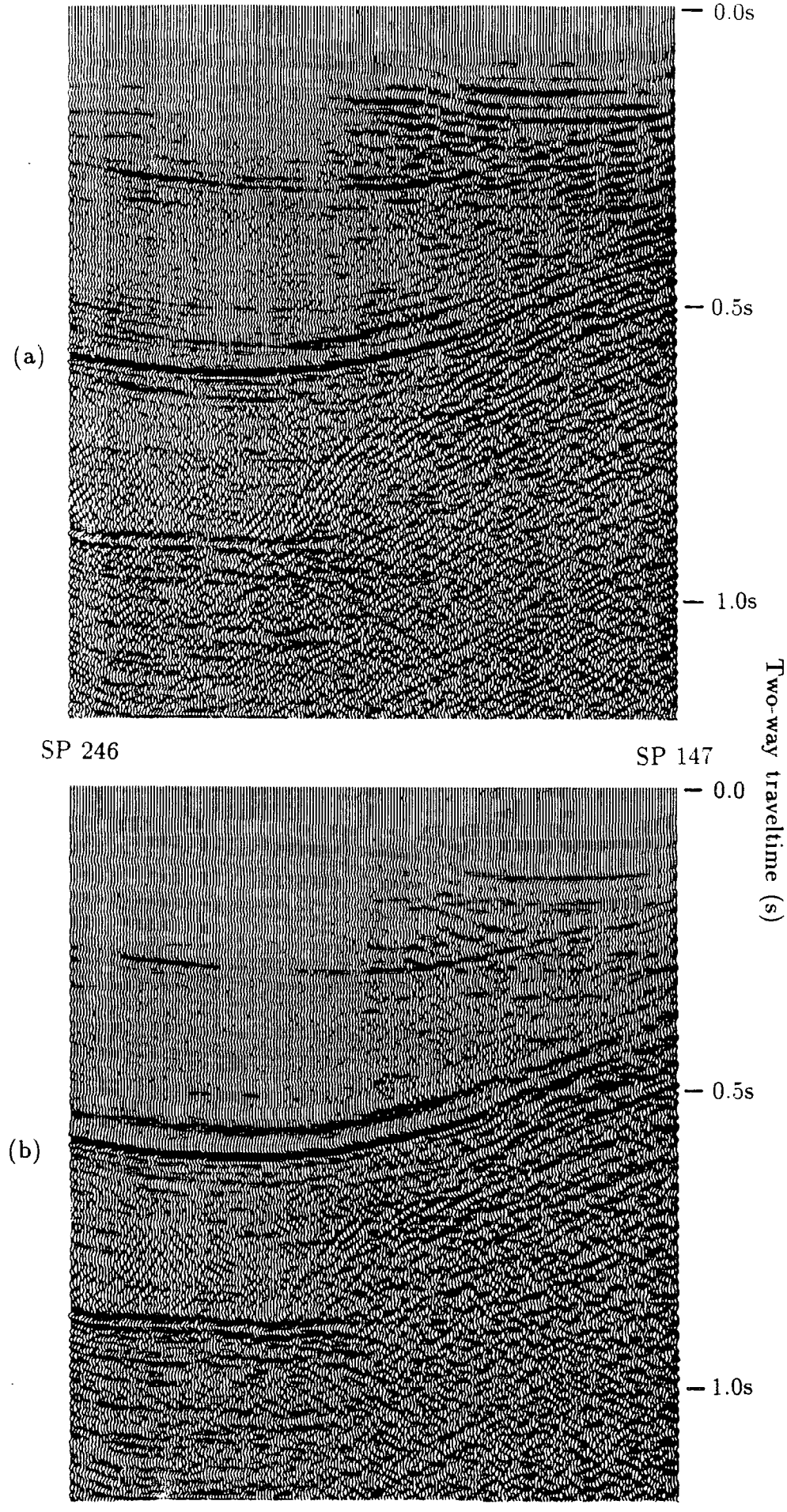

Figure 5.30. 3-fold stacked sections: (a) using directional deconvolution and (b) using standard signature deconvolution. 90 % stacking velocities were used as migration velocities. Other processing and display parameters are given in tables 5.9 and 5.10.

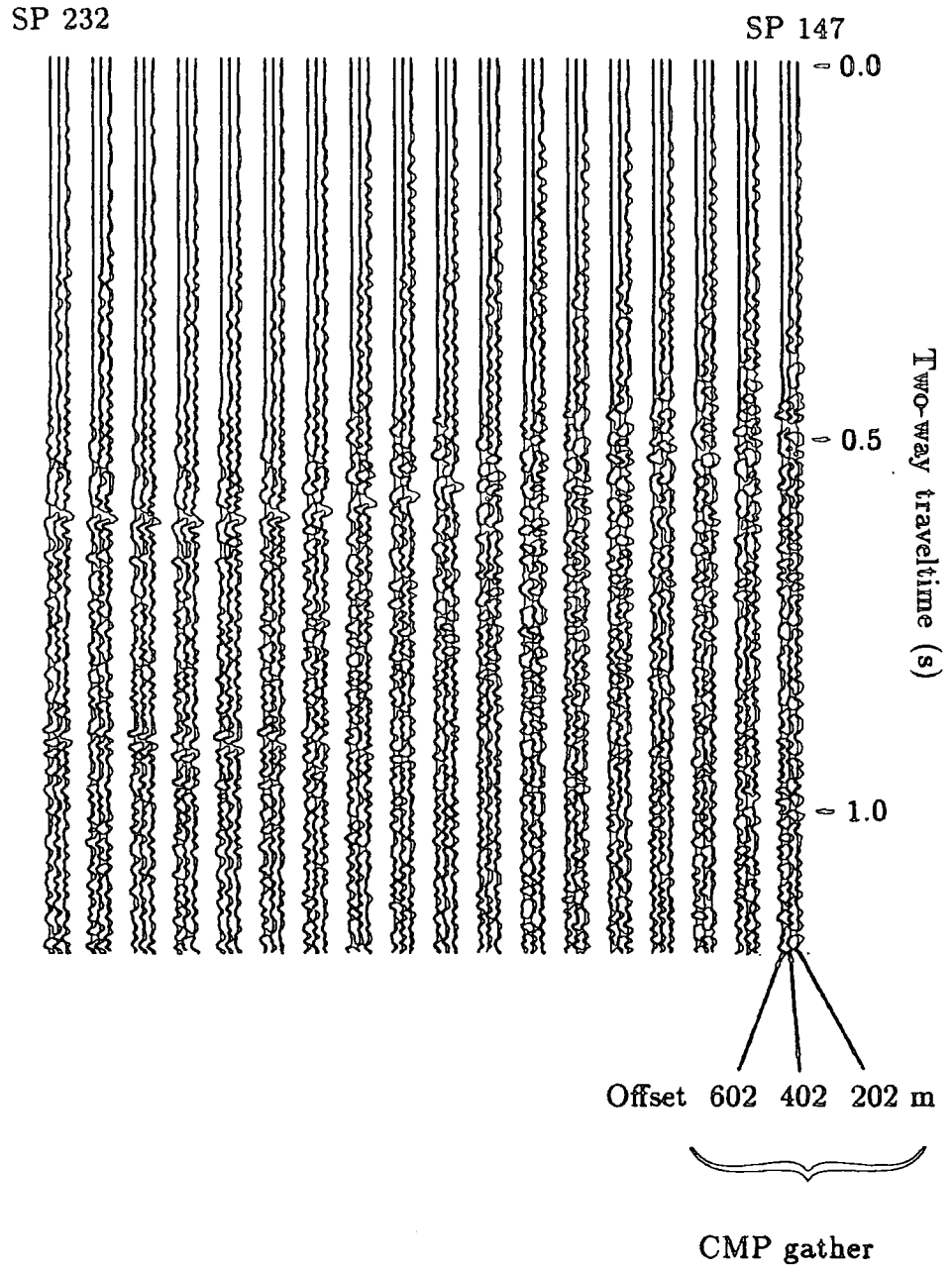

Figure 5.31. Eighteen 3-fold CMP gathers, resorted from the three migrated sections, which are shown stacked in figure 5.30.a.

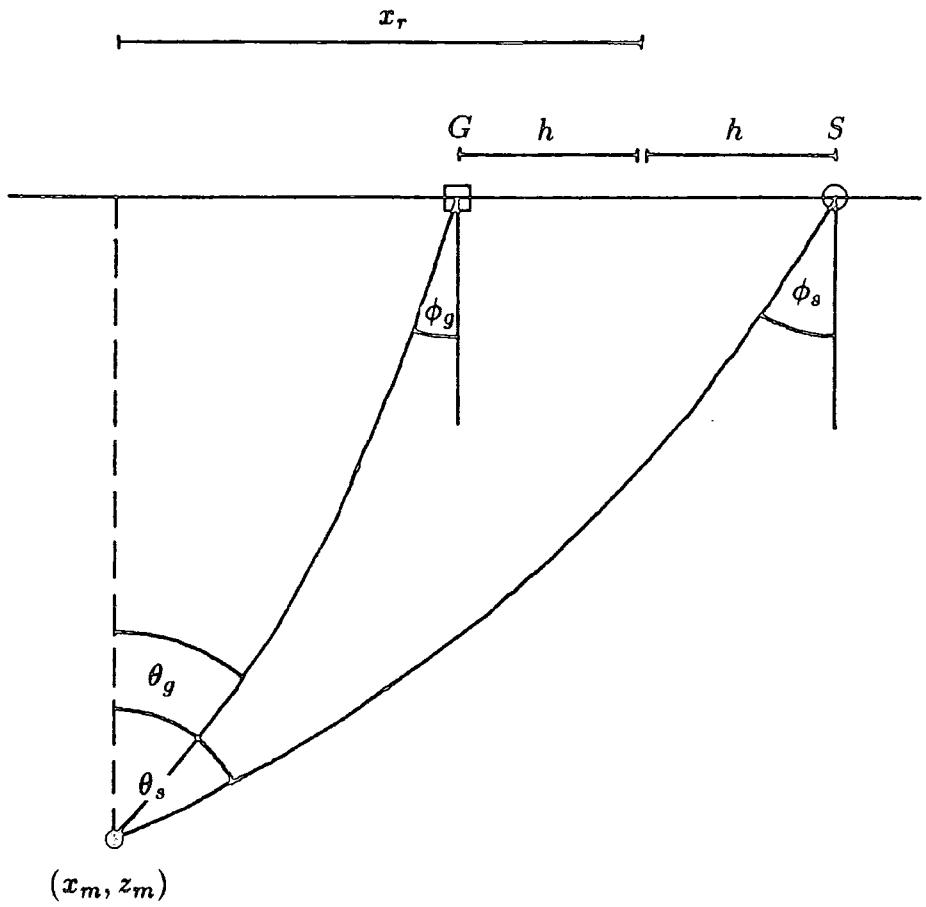

Figure 5.32. Geometry of raypaths to a point diffractor (at (x_m, z_m)). The velocity of the medium varies linearly with depth.

This is how constant velocity prestack migration was derived (figure 3.6). Traveltime to a point on the migration operator at an offset x_r from the apex of the operator is given by the sum of the travetimes from the source, t_s, and from the receiver t_g, to the point diffractor. First consider the source raypath.

The migration summation operator is applied as a function of source take-off angle ϕ_s (chapter III). The ray parameter for the source raypath, p_s, is given by

$$p_s = \frac{\sin \phi_s}{V_0}$$

Now

$$(x_r + h) = \frac{1}{p_s k}(\cos \phi_s - \cos \theta_s)$$

(Telford et al., 1976), therefore

$$\cos \theta_s = cos\phi_s - p_s k(x_r + h)$$

Thus θ_s is calculated if the source take-off angle is specified and the velocity function is known. Using results from Telford et al.(1976),

$$t_s = \frac{1}{k} \log \left(\frac{tan\frac{\theta_s}{2}}{tan\frac{\phi_s}{2}} \right)$$

and

$$z_m = \frac{1}{p_s k}(\sin \theta_s - sin\phi_s)$$

Thus t_s and z_m are calculated. Now consider the receiver raypath.

$$(x_r - h) = \frac{1}{p_g k}(\cos\phi_g - \cos\theta_g)$$

and

$$z_m = \frac{1}{p_g k}(\sin\theta_g - sin\phi_g)$$

The ray parameter for the receiver raypath p_g, is given by

$$p_g = \frac{\sin\phi_g}{V_0}$$

so

$$(x_r - h) = \frac{V_0}{k\sin\phi_g}(\cos\phi_g - \cos\theta_g) \qquad 5.1$$

and

$$z_m = \frac{V_0}{k\sin\phi_g}(\sin\theta_g - sin\phi_g) \qquad 5.2$$

Equations 5.1 and 5.2 are solved simultaneously for ϕ_g giving

$$\sin\phi_g = \sqrt{\frac{4k^2(x_r - h)^2 V_0^2}{((z_m k + V_0)^2 - V_0^2 + k^2(x_r - h)^2)^2 + 4k^2(x_r - h)^2 V_0^2}}$$

θ_g is calculated from

$$\cos\theta_g = \cos\phi_g - p_g k(x_r - h)$$

so the receiver raypath traveltime may be calculated from

$$t_g = \frac{1}{k} \log \left(\frac{tan\frac{\theta_g}{2}}{tan\frac{\phi_g}{2}} \right)$$

Thus the total traveltime to the diffractor is calculated as

$$t_s + t_g$$

The algorithm for directional deconvolution combined with prestack migration has been modified to allow a linear variation of velocity with depth (Appendix A). The migration summation operators are applied as a function of source take-off angle (chapter III), and are calculated as above. Rays beyond their turning point (i.e θ_g or θ_s greater than 90°) are not considered.

Unfortunately, the velocity-depth function for dataset B (figure 5.33), is not a simple linear increase of velocity with depth. Interval velocities have been calculated from stacking velocities using the Dix (1955) formula. The model of a linear variation of velocity with depth is thus a poor approximation for the whole section. The steeply dipping reflectors, at a two way traveltime of 0.85 s at shotpoint 205, are the most interesting for directional deconvolution. If a linear velocity-depth function could be 'targeted', so that reflectors at this traveltime were correctly imaged, directional deconvolution could be evaluated. For 'time' migration, the shape of the Kirchhoff summation operator at any traveltime is governed by the r.m.s velocity for that traveltime (section 5.3.4). Thus, if a linear velocity-depth function were used which gave the correct r.m.s velocity at the target traveltime, the shape of the migration operator should be similar to the 'time' migration operator, and hence the migration should be similar. The shape of the linear velocity-depth operator will be different on the flanks of the operator, because ray bending is accounted for. Thus, steep dips should be imaged more clearly. The r.m.s velocity to a given traveltime is known approximately from

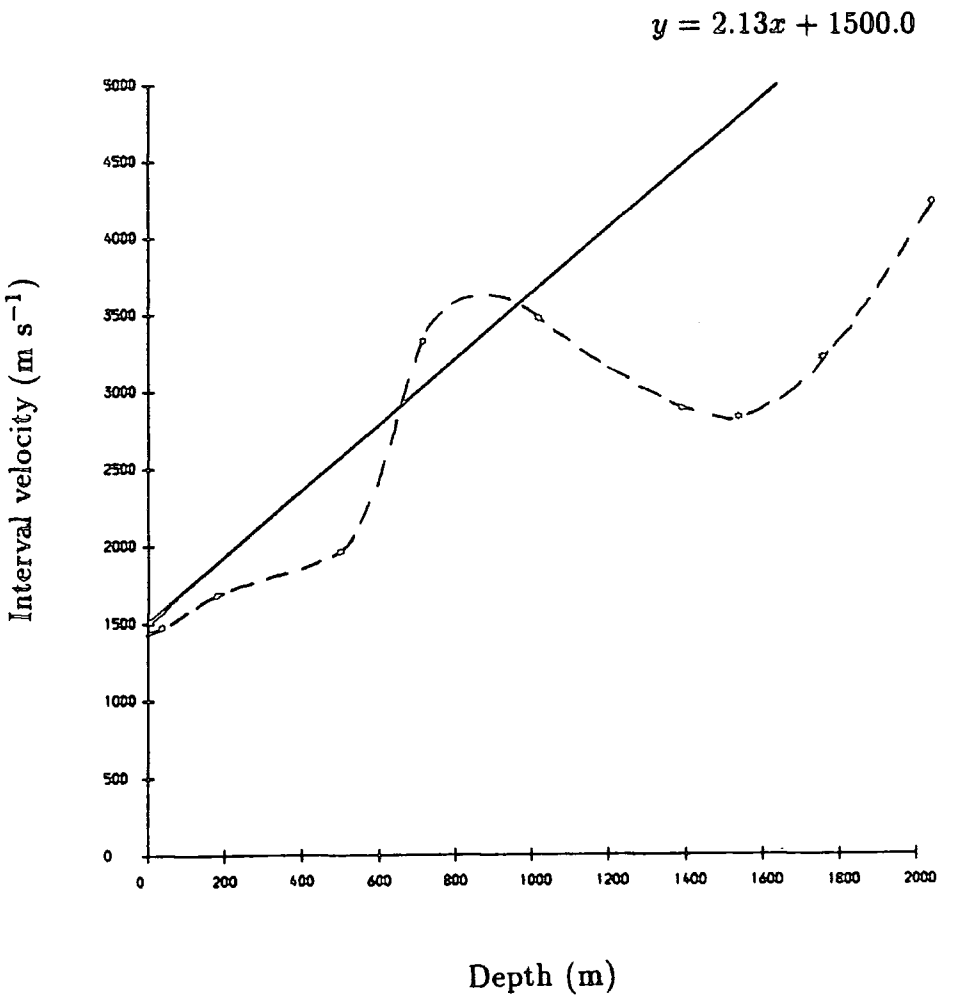

Figure 5.33. Velocity-depth function for dataset B (dashed line). Interval velocities were derived from stacking velocities. A linear velocity-depth function is superimposed on the graph.

velocity analysis. The r.m.s velocity for a one-way traveltime t_m is defined as (Al-Chalabi, 1979)

$$V_{rms}^2 = \frac{1}{t_m} \sum_{k=1}^{n} {V_k}^2 t_k \qquad 5.3$$

For a continuous velocity function, equation 5.3 can be expressed in integral form

$$V_{rms}^2 = \frac{1}{t_m} \int_0^{t_m} V^2(t)\, dt$$

To calculate $V(t)$ given a linear velocity-depth function $V(z) = V_0 + kz$

$$dt = \frac{dz}{V(z)} = \frac{dz}{V_0 + kz}$$

$$t_m = \int_0^{z_m} \frac{dz}{V_0 + kz} = \frac{1}{k} ln \frac{V_0 + kz_m}{V_0}$$

Rearranging

$$V_0 + kz_m = V_0 e^{kt_m}$$

so

$$V(t) = V_0 e^{kt}$$

Hence

$$V_{rms}^2 = \frac{1}{t_m} \int_o^{t_m} \left(V_0 e^{kt}\right)^2 dt$$

Solving and rearranging

$$2kt_m V_{rms}^2 - {V_0}^2 \left(e^{2kt_m} - 1\right) = 0 \qquad 5.4$$

Formula 5.4 can be solved for V_0 and k which define the linear velocity-depth function to be used. For the steeply dipping reflectors, the r.m.s velocity is 2520 m s^{-1} and the two-way traveltime is 0.85 s. Choosing a velocity at the surface of 1500 m s^{-1}, the velocity gradient is 2.13 s^{-1}. The linear velocity-depth function to use is thus

$$V(z) = 1500 + 2.13z \text{ m s}^{-1}$$

where the units of z are metres.

This velocity-depth function is superimposed on figure 5.33.

The results of processing the second constant-offset section to stage 4 of the processing sequence (table 5.10), both with and without directional deconvolution, are shown in figure 5.34. The steeply dipping reflectors are imaged more clearly here than in the section where conventional Kirchhoff migration was used (figure 5.26). The 3-fold stacked sections (figure 5.35) show a similar improvement (compare with figure 5.27). The directionally deconvolved section (figure 5.35.a), shows the greater improvement, because the source take-off angle in the migration algorithm, which is used to select the deconvolution filter, is now calculated using a curved raypath. Thus the approximate correction factor (section 5.3.4) is no longer necessary. Directional deconvolution (figure 5.35.a) has improved the frequency content and continuity of the steeply dipping reflectors compared to standard deconvolution (figure 5.35.b). An example is the event at a traveltime of 0.47 s at SP 147 which continues to the steeply dipping events at a traveltime of 0.7 s at SP 195. The directionally deconvolved section is noisier.

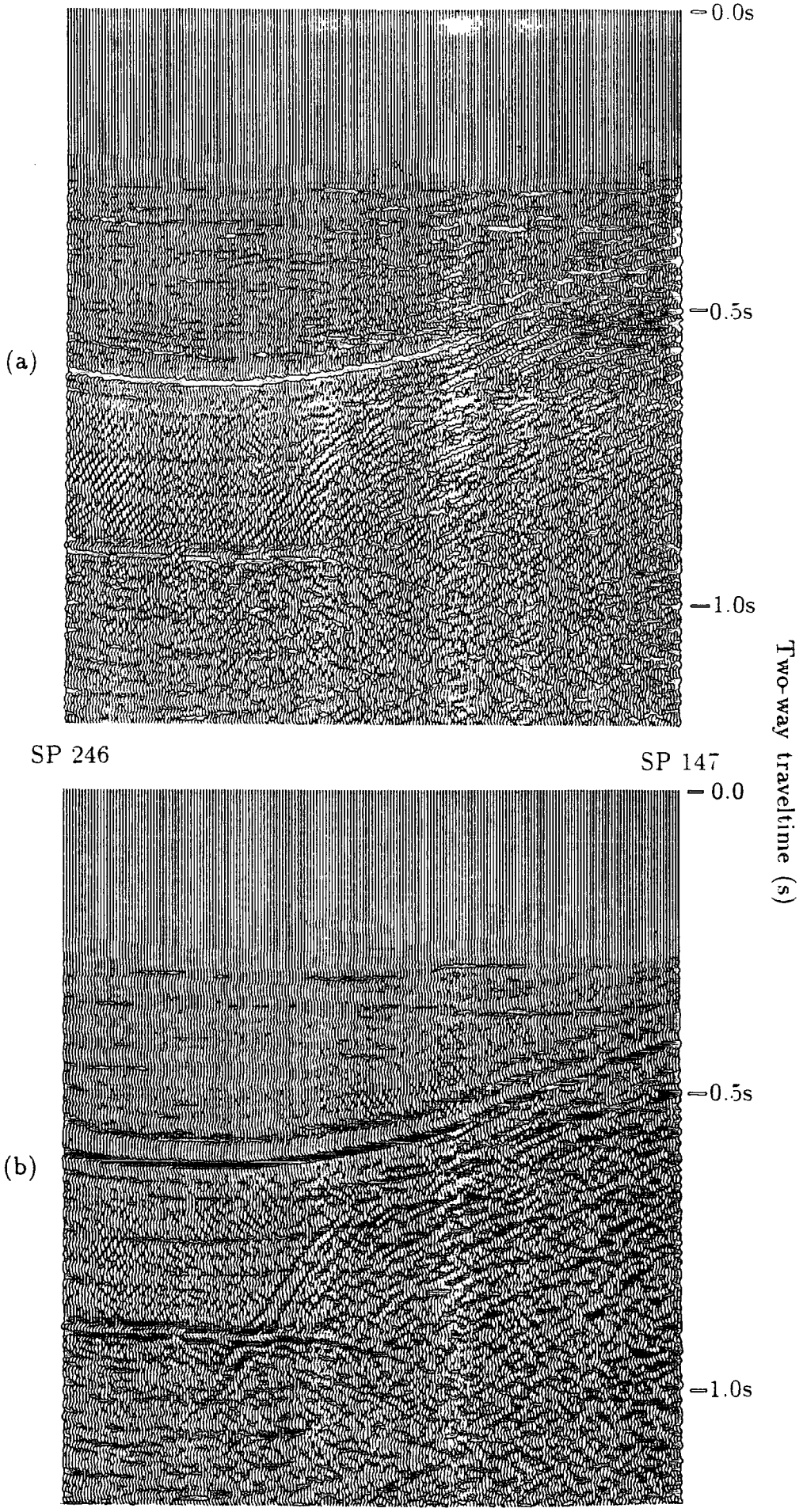

Figure 5.34. A limited window of the second constant-offset section after prestack migration, predictive deconvolution and bandpass filtering: (a) using directional deconvolution and (b) using standard signature deconvolution. A linear velocity-depth model was used. Other processing and display parameters are given in tables 5.9 and 5.10.

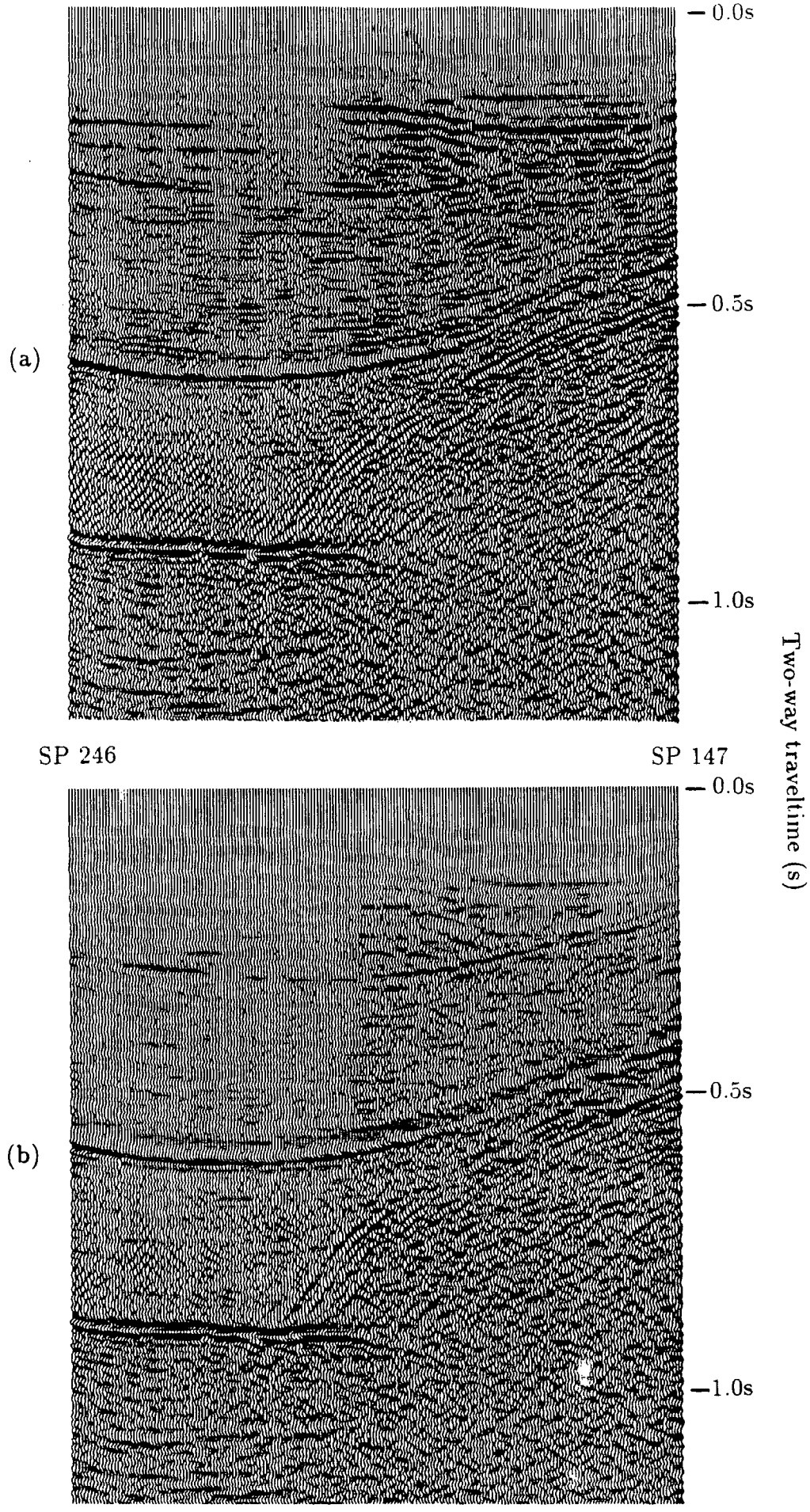

Figure 5.35. 3-fold stacked sections: (a) using directional deconvolution and (b) using standard signature deconvolution. A linear velocity-depth model was used. Other processing and display parameters are given in tables 5.9 and 5.10.

The linear velocity-depth function was 'targeted', so that reflectors at two-way traveltimes of about 0.85 s would be migrated correctly. Re-sorted CMP gathers after migration with a linear velocity-depth function (figure 5.36) are similar to re-sorted CMP gathers for conventional Kirchhoff migration (figure 5.29) for these traveltimes. Unfortunately the steeply dipping reflectors are of low amplitude and are not visible on the CMP gathers, so it is uncertain whether they are migrated correctly. The section could have been migrated with a range of linear velocity-depth functions and the best image chosen. This was not thought to be necessary because the 'targetting' method has shown that migration is improved when ray bending is considered, and that directional deconvolution is superior to conventional signature deconvolution for this dataset. Full 'depth' migration would be needed to image all reflectors correctly.

5.4.8 Conclusions

Dataset B benefits from directional deconvolution. Improvements are greatest for shallow and dipping reflectors (figures 5.27 and 5.35).

Prestack migration may be used for velocity analysis (section 5.4.6). The present algorithm (Appendix A) is limited in that only a single velocity function can be used. This is adequate for demonstrating the technique.

Standard Kirchhoff migration does not image steeply dipping reflectors correctly, so an alternative method which honours ray bending is needed (section 5.3.7). Kirchhoff migration for a velocity function which increases linearly with depth overcomes the need for numerical ray-tracing, and may be 'targeted' to image given reflectors. Steeply dipping reflectors benefit substantially from directional deconvolution (figure 5.35).

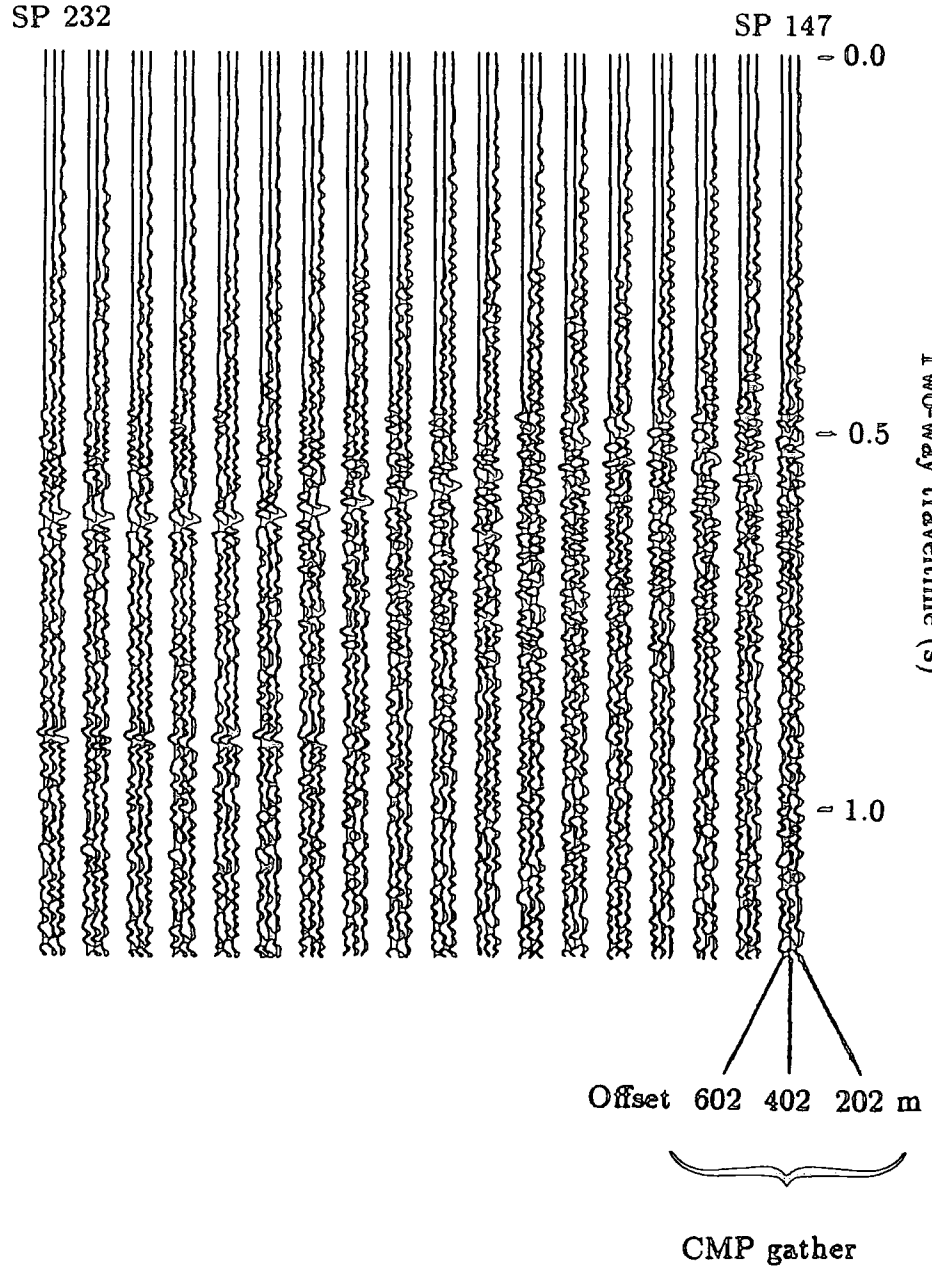

Figure 5.36. Eighteen 3-fold CMP gathers, resorted from the three migrated sections, which are shown stacked in figure 5.35.a.

Chapter VI

Conclusions and Discussion

6.1 Directional deconvolution methods

The aim of directional source signature deconvolution is to remove the effects of source directivity. Directivity is due to the use of source arrays and to the surface ghost (chapter I). Two methods of directional deconvolution have been described. The f-k method (chapter II) has been demonstrated on physical model data (chapter IV), having previously been applied to real data by Hubbard et al.(1984). The new prestack migration method (chapter III) has been applied to both model (chapter IV) and to real (chapter V) data. Both methods are capable of performing directional deconvolution under ideal conditions. Such conditions were provided by the physical model datasets because spatial sampling was tailored to each method and the velocity structure was simple and known. For real data, practical considerations determine which of the two methods can be used.

6.1.1 F-k directional deconvolution

Application of f-k directional deconvolution is relatively straightforward. Sorting and filter application are time consuming, but relatively little effort is needed once the deconvolution filter has been designed. The major problem with the method is due to spatial aliasing. Reflections in a common-receiver gather are usually spatially aliased for common acquisition geometries. Spatial interpolation is necessary, and is difficult to perform and expensive.

6.1.2 Directional deconvolution combined with prestack migration

Prestack migration which was applied to data from the Southern North Sea in

section 5.4.4 was the simplest form of migration, 'time' migration. Ray bending was neglected, so an approximate correction factor was needed for deconvolution. The 'linear velocity-depth' method (section 5.4.7), accounts for ray bending, so improved migration and improved deconvolution of steep dips resulted. The depth model for the latter method was, however, only approximate. Further work could extend the method of directional deconvolution combined with prestack migration to full prestack 'depth' migration, dip moveout (DMO), 3-D data, and time-varying deconvolution.

- Gray (1986) describes an efficient ray-tracing depth migration technique into which directional deconvolution could be incorporated. For Kirchhoff migration, each subsurface point is considered to be a point diffractor. Migration summation operators are calculated by considering traveltimes along rays to diffractors. For 'depth' migration, numerical ray-tracing is used to calculate traveltimes through a complex overburden. In Gray's (1986) method, traveltimes are computed for zero-offset (post-stack) migration by shooting rays downwards from the earth's surface. A fan of rays is shot to a depth z, and traveltimes are interpolated between rays as necessary. For calculating traveltimes to the next depth point, $z + \delta z$, information stored for the rays at z can be used to calculate the extra short ray segment. For prestack migration, fans of rays are shot from both source and receiver positions. Directional deconvolution can be incorporated efficiently, because a fan of rays shot downwards from the source position may be defined by source take-off angle. Thus, when the constant-offset section is deconvolved for a particular take-off angle (section 3.3) only rays radiated at that angle may be considered.

- Prestack depth migration used as a velocity analysis method is not feasible at present, because of massive computer requirements. Prestack time migration is also still in its infancy as a velocity analysis method (section 5.4.6). The most common prestack migration method is a partial prestack migration method, dip moveout (DMO) (Deregowski and Rocca, 1981). DMO attempts

to overcome limitations of the CMP method without needing a detailed velocity field, and at low cost. For a constant-velocity medium, DMO followed by post-stack migration is equivalent to prestack migration. DMO and prestack migration impulse responses are thus related by the post-stack migration impulse response, which is a circular arc (figure 6.1). Directional deconvolution could be incorporated into a Kirchhoff DMO scheme (Deregowski, 1985) in a similar manner to a Kirchhoff prestack migration scheme because of this simple geometrical relationship.

- So far, only 2-D data have been considered. Prestack migration of 3-D data is not done routinely. However, the basic method of directional deconvolution combined with prestack migration, and the extensions described above (depth migration and DMO), could be extended to 3-D data.

- Time-varying deconvolution can also be incorporated into the basic method. Deconvolution filters have been designed using far-field source signatures. These signatures change as they travel through the earth because of attenuation. High frequencies are attenuated preferentially, so deeper reflections have lower frequency content. If an attenuation model is known, deconvolution filters can be designed to compensate for loss of high frequencies at depth. These time-varying filters could be applied in the directional deconvolution method.

The main problem with directional deconvolution combined with prestack migration is that prestack migration must be performed. Prestack migration is expensive, the velocity field must be known and migration noise is a problem for steeply dipping reflectors because of spatial sampling considerations. The latter two problems are soluble (sections 5.3.6 and 5.3.5 respectively). The remaining problem, cost, a problem with both directional deconvolution methods, is acceptable if it is justified by the results.

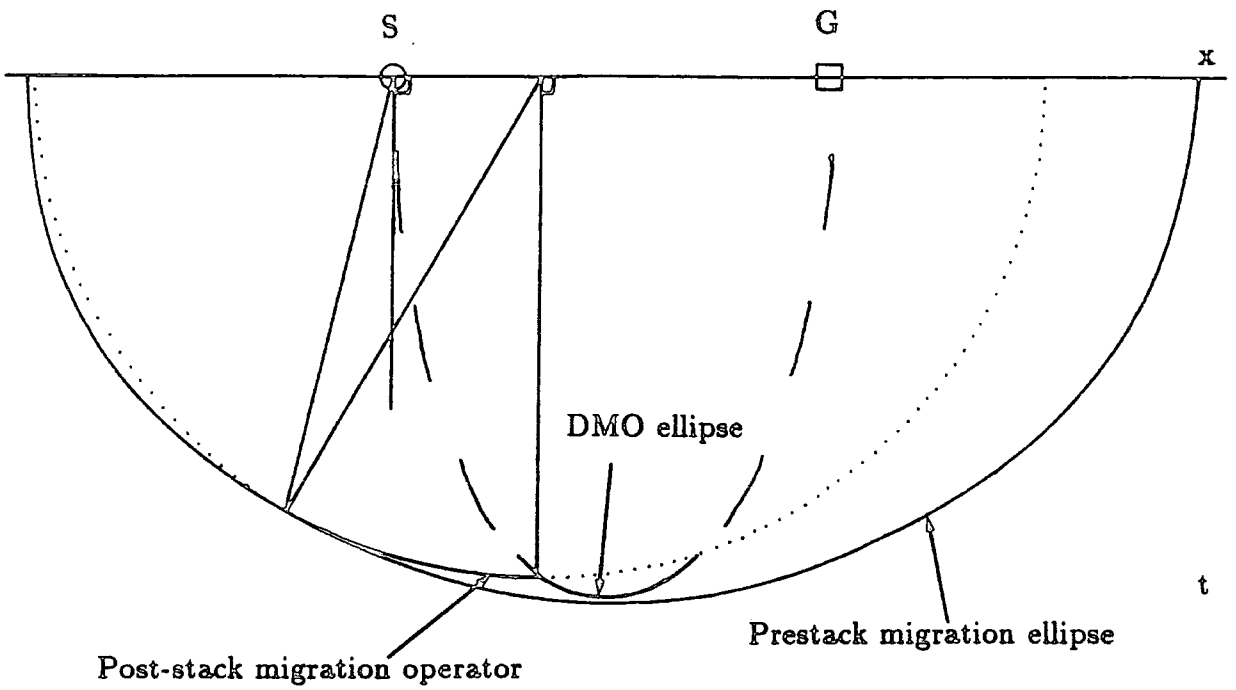

Figure 6.1. Relationship between the DMO ellipse, the prestack migration ellipse and the post-stack migration operator for a constant-velocity medium.

6.2 Results of directional deconvolution

Reflectors in dataset B (section 5.4) were more continuous and had higher frequency content after directional deconvolution. Dataset A was virtually unaffected by directional deconvolution (section 5.3). These results were predicted by ray-tracing (sections 5.4.3 and 5.3.3 respectively). The amount of source directivity evident in primary reflected data is dependent on a number of factors: the in-line dimension of the source array; frequency content of the data; depth of the target; ray bending; offset; the mute zone and reflector dip. For 'directional' data, directional deconvolution will improve the quality of reflections and the results of subsequent processing will show the benefit (chapter I).

Directional deconvolution is not without disadvantages. Data are noisier because directional deconvolution amplifies noise at notch frequencies. To avoid excessive noise amplification, directional deconvolution cannot fully synthesise a point source. Residual directivity will affect reflectors and subsequent processing.

Whether or not to perform directional deconvolution is ultimately a question of cost. Ideally, sections would be processed with and without directional deconvolution, and the interpreter would have both available.

6.3 Source arrays

If data are acquired with a directional source array, directional deconvolution is unable to synthesise a point source. This is because of notches in the source spectrum and because data are recorded with finite spatial sampling. Directional deconvolution is also imperfect because it is based on a simple convolutional model. The model is too simple because source signatures are altered as they travel through the earth by attenuation. Thus directional deconvolution cannot fully convert data recorded with a directional array to point source equivalent data.

Primary reflected data are affected adversely by the use of long source arrays.

This can be illustrated by synthetic modelling (Loveridge et al., 1984), by the application of directional deconvolution (chapter V), and by experiments where a profile is acquired using both long and short source arrays (Brummitt, 1989). Directional deconvolution is unable to fully compensate for directivity, so source arrays with a short in-line dimension should be used when possible. For 3-D data, wide arrays will adversely affect cross-line reflections, so source arrays with short cross-line and in-line dimensions should be used.

Long source arrays are used when suppression of coherent noise in the field is of paramount importance (section 1.6.1), and most data acquired in the 1970s and early 1980s were acquired using long source arrays. For such data directional deconvolution is desirable.

References

Al-Chalabi, M. 1979. Velocity determination from seismic reflection data. In: *Developments in Geophysical Exploration Methods-1.* A.A.Fitch (ed.), 1-68, Applied Science Publishers, London.

Al-Yahya, K. 1986. Velocity Analysis using Prestack Migration. Presented at the 56th meeting of the SEG, Houston.

Angona, F.A. 1960. Two-dimensional modelling and its application to seismic problems. *Geophysics*, 25, 468-482.

Bardan, V. 1987. Trace interpolation in seismic data processing. *Geophysical Prospecting*, 35, 343-358.

Black, J.L., McMahon, I.T., Meinardus, H.A. and Henderson, I. 1985. Application of Prestack Migration and Dip Moveout. Presented at the 55th meeting of the SEG, Washington.

Bolondi, G., Loinger, E. and Rocca, F. 1982. Offset continuation of seismic sections. *Geophysical Prospecting*, 30, 813-828.

Bracewell, R.N. 1979. *The Fourier Transform and its Applications (second edition).* McGraw-Hill, New York.

Brigham, E.O. 1974. *The Fast Fourier Transform.* Prentice-Hall, Englewood Cliffs, N.J.

Brummitt, J.G. 1989. Source directivity and its effects on resolution and signature deconvolution. *First Break*, 7, 17-24.

Červený, V., Popov, M. and Pšenčík, I. 1982. Computation of wave fields in inhomogeneous media - Gaussian beam approach. *Geophysical Journal of the Royal Astronomical Society*, 70, 109-128.

Červený, V., Molotkov, I. and Pšenčík, I. 1977. *Ray Method in Seismology.* Univerzita Karlova, Praha.

Christie, P.A.F., Hughes, V.J. and Kennett, B.L.N. 1983. Velocity filtering of seismic reflection data. *First Break*, 1(3), 9-24.

Claerbout, J.F. 1985. *Imaging of the earth's interior.* Blackwell Scientific Publications, Oxford.

Clement, W.G. 1973. Basic principles of two-dimensional digital filtering. *Geophysical Prospecting*, 21, 125-145.

Cooley, J.W. and Tukey, J.W. 1965. An algorithm for the machine calculation of complex Fourier series. *Maths Computation*, 19, 297-301.

Confurius, A. 1987. *Angular-Dependent Deconvolution of Seismic CMP Data in Frequency-Wavenumber Space.* Report number 1987-20, Delft University of Technology.

Deregowski, S.M. 1985. An Integral Implementation of Dip Moveout. Presented at the 47th meeting of the EAEG, Budapest.

Deregowski, S.M. 1986. What is DMO? *First Break*, 4(7), 7-24

Deregowski, S.M. and Rocca, F. 1981. Geometrical optics and wave theory of constant-offset sections in layered media. *Geophysical Prospecting*, 29, 374-406.

Devey, M.G. 1979. *Derivation of the Migration Integral.* BP technical note TN451, Exploration and Production Department.

Dix, C.H. 1955. Seismic velocities from surface measurements. *Geophysics*, 20, 68-86.

Dragoset, W.H., Hargreaves, N. and Larner, K. 1987. Air-gun source instabilities. *Geophysics*, 52, 1229-1251.

DuBose, Jnr., J.B. 1988. A technique for stabilising interval velocities from the Dix equation. *Geophysics*, 53, 1241-1243.

Eiken, O. 1987. Comment on 'Extended marine arrays versus simulated extended arrays' by M.M.Roksandić. *Geophysical Prospecting*, 35, 932-933.

Embree, P., Burg, J.P. and Backus, M.M. 1963. Wide-band velocity filtering - the pie-slice process. *Geophysics*, 28, 948-974.

Fowler, P. 1984. Velocity Independent Imaging of Seismic Reflectors. Presented at the 54th meeting of the SEG, Atlanta.

Fuchs, K. and Müller, G. 1971. Computation of synthetic seismograms with the reflectivity method and comparison with observation. *Geophysical Journal*, 23, 417-433.

Gardner, G.H.F., French, W.S. and Matzuk, T. 1974. Elements of migration and velocity analysis. *Geophysics*, 39, 811-825.

Giles, B.F. and Johnston, R.C. 1973. System approach to air-gun array design. *Geophysical Prospecting*, 21, 77-101.

Gray, S.H. 1986. Efficient traveltime calculations for Kirchhoff migration. *Geophysics*, 51, 1685-1688.

Hale, D. 1982. *Q-Adaptive Deconvolution.* Stanford Exploration Project, Report number 30, 133-158.

Hampson, G. 1987. The relationship of pre-stack apparent velocity filtering to the symmetry of the CMP stack response. *First Break*, 5, 359-377.

Hatton, L., Worthington, M.H. and Makin, J. 1986. *Seismic Data Processing: Theory and Practice.* Blackwell Scientific Publications, Oxford.

Hood, P. 1981. Migration. In: *Developments in Geophysical Exploration Methods-2.* A.A.Fitch (ed.), 151-230, Applied Science Publishers, London.

Hosken, J.W.J. 1979. *Improvements in the Practice of 2-D Diffraction Stack Migration.* BP internal report no. EPR/R 1247, Exploration and Production Department.

Howson, C.D. 1982. *An Evaluation of a New Method of Computing Synthetic Seismograms.* M.Sc. Thesis. University of Durham.

Hubbard, T.P., Sugrue, M.J., Sandham, W.A. and Booth, E.A. 1984. Marine Source and Receiver Deghosting and Array Inversion in f-k Space. Presented at the 46th meeting of the EAEG, London.

Jain, S. and Wren, A.E. 1980. Migration before stack - procedure and significance. *Geophysics*, 45, 204-212.

Jovanovitch, D.B., Sumner, R.D. and Akins-Easterlin, S.L. 1983. Ghosting and marine signature deconvolution: a prerequisite for detailed seismic interpretation. *Geophysics*, 48, 1468-1485.

Jurkevics, A. and Wiggins, R. 1984. A critique of seismic deconvolution methods. *Geophysics*, 49, 2109-2116.

Kelly, K.R., Ward, R.W., Treitel, S. and Alford, R.M. 1976. Synthetic seismograms: a finite difference approach. *Geophysics*, 41, 2-27.

Kennett, B.L.N. and Harding, A.J. 1985. Is ray theory adequate for reflection seismic modelling? (A survey of modelling methods). *First Break*, 3(1), 9-14.

Ku, C.C., Telford, W.M. and Lim, S.H. 1971. The use of linear filtering in gravity problems. *Geophysics*, 36, 1174-1203.

Kuhn, M.J. 1979. Acoustical imaging of source receiver coincident profiles. *Geophysical Prospecting*, 27, 62-77.

Larner, K., Chambers, R., Yang, M., Lynn, W. and Wai, W. 1983. Coherent noise in marine seismic data. *Geophysics*, 48, 854-886

Larner, K., Hale, D., Zinkham, S.M. and Hewlitt, C. 1982. Desired seismic characteristics of an air gun source. *Geophysics*, 47, 1273-1284.

Levin, F.K. 1971. Apparent velocity from dipping interface reflections. *Geophysics*, 36, 510-516.

Lindsey, J.P. 1960. Elimination of seismic ghost reflections by means of a linear filter. *Geophysics*, 25, 130-140.

Loveridge, M.M. 1985. *Marine Seismic Source Signatures, Directivity and the Ghost.* Ph.D. dissertation, University of Oxford.

Loveridge, M.M., Parkes, G.E., Hatton, L. and Worthington, M.H. 1984. Effects of marine source array directivity on seismic data and source signature deconvolution. *First Break*, 2(7), 16-22.

Lynn, W. and Larner, K. 1989. Effectiveness of wide marine seismic source arrays. *Geophysical Prospecting*, 37, 181-207.

March, D.W. and Bailey, A.D. 1983. A review of the two-dimensional transfrom and its use in seismic processing. *First Break*, 1(1), 9-21.

McDonald, J.A., Gardner, G.H.F. and Hilterman, F.J. 1983. *Seismic Studies in Physical Modelling.* International Human Resources Development Corporation, Boston.

McMechan, G.A. and Fuis, G.S. 1987. Ray equation migration of wide-angle reflections from southern Alaska. *Journal of Geophysical Research*, 92, 407-420.

Mooney, H.M. 1983. Synthetic seismograms for body waves: an overview. *First Break*, 1(12), 9-20.

Neidell, N.S. and Taner, M.T. 1971. Semblance and other coherency measures for multichannel data. *Geophysics*, 36, 482-497.

Newman, P. 1975. Amplitude and Phase Properties of a Digital Migration Process. Presented at the 37th meeting of the EAEG, Bergen.

Peacock, K.L. and Treitel, S. 1969. Predictive deconvolution: theory and practice. *Geophysics*, 34, 155-169.

Purnell, G.W. 1986. Observations of wave velocity and attenuation in two-phase media. *Geophysics*, 51, 2193-2199.

Roberts, G.A. and Goulty, N.R. 1988. Directional deconvolution of the seismic source signature combined with prestack migration. *First Break*, 6, 247-253.

Robinson, E.A. and Treitel, S. 1980. *Geophysical Signal Analysis.* Prentice-Hall, Englewood Cliffs, N.J.

Roksandić, M.M. 1986. Extended marine source arrays versus simulated extended arrays. *Geophysical Prospecting*, 34, 1154-1166.

Safar, M.H. 1976. Efficient design of airgun arrays. *Geophysical Prospecting*, 24, 773-787.

Safar, M.H. 1985. On the improvement in penetration achieved by using extended marine source arrays. *Geophysical Prospecting*, 33, 359-368.

Schneider, W.A. 1978. Integral formulation for migration in two and three dimensions. *Geophysics*, 43, 49-76.

Sharp, R.J., Peacock, J.H. and Goulty, N.R. 1985. Ultrasonic Seismic Modelling System. Presented at the 47th meeting of the EAEG, Budapest.

Sheriff, R.E. 1984. *Encyclopedic Dictionary of Exploration Geophysics (second edition).* SEG, Tulsa.

Society of Exploration Geophysicists. 1980. *Digital tape standards.* SEG, Tulsa.

Stolt, R.H. and Benson, A.C. 1986. *Seismic Migration Theory and Practice.* Handbook of geophysical exploration, section 1- Seismic Exploration, Vol. 5, K. Helbig and S. Treitel (eds.). Geophysical Press, Amsterdam.

Suprajitno, M. and Greenhalgh, S.A. 1985. Separation of upgoing and downgoing waves in vertical seismic profiling by contour-slice filtering. *Geophysics*, 50, 950-962.

Taner, M.T. and Koehler, F. 1969. Velocity spectra - digital computer derivation and applications of velocity functions. *Geophysics*, 34, 859-881.

Tatham, R.H., Goolsbee, D.V., Massell, W.F. and Nelson, H.R. 1983. Seismic shear-wave observations in a physical model experiment, *Geophysics*, 48, 688-701.

Telford, W.M., Geldart, L.P., Sheriff, R.E. and Keys, D.A. 1976. *Applied Geophysics.* Cambridge University Press, Cambridge.

Tree, E.L., Lugg, R.D. and Brummitt, J.G. 1986. Why waterguns? *Geophysical Prospecting*, 34, 302-329.

Trorey, A.W. 1977. Diffractions for arbitrary source-receiver locations. *Geophysics*, 42, 1177-1182.

Ursin, B. 1978. Attenuation of coherent noise in marine seismic exploration using very long arrays. *Geophysical Prospecting*, 26, 722-749.

Van der Schans, G.A. and Ziolkowski, A.M. 1983. Angular-Dependent Signature Deconvolution. Presented at the 53rd meeting of the SEG, Las Vegas.

Wapenaar, C.P.A. and Berkhout, A.J. 1987. Three-dimensional target-oriented pre-stack migration. *First Break*, 5, 217-227.

Waters, K.H. 1978. *Reflection Seismology: a Tool for Energy Resource Exploration.* John Wiley and sons inc, New York.

Western Geophysical. 1987. *Prestack Frequency-Wavenumber (f-k) Migration.* Western Geophysical brochure.

Yilmaz, O. 1987. *Seismic Data Processing.* Investigations in Geophysics, Vol. 2, E.B. Neitzel(ed.). SEG, Tulsa.

Zhu, T. 1988. Ray-Kirchhoff migration in inhomogeneous media. *Geophysics*, 53, 760-768.

Ziolkowski, A., Parkes, G.E., Hatton, L. and Haughland, T. 1982. The signature of an airgun array: computation from near field measurements including interactions. *Geophysics*, 47, 1413-1421.

Appendix A

Computer software

A suite of computer programs has been written to evaluate directional deconvolution on physical model and real data.

Sotware is implemented on the NUMAC (Northern Universities Multiple Access Computer) Amdahl 470/V8 mainframe, which uses the MTS (Michigan Terminal System) operating system. All programs are written in the Fortran 77 programming language. The IBM VS Fortran compiler is used. MTS system subroutines are used for magnetic tape operations, and two external subroutine libraries are used extensively: *GHOST80 (Culham laboratory), a graphical library and *NAG (Numerical Algorithms Group, Oxford), a numerical algorithm library.

There are three main software catagories: general seismic plotting and processing; f-k directional deconvolution, and directional deconvolution combined with prestack migration. The two main directional deconvolution programs are listed in this appendix. Brief descriptions of other main programs are given.

A.1 General seismic plotting and processing

SEISPL. Seismic trace plotting and interactive time series analysis. Adapted from NCBPLOT (J.S.Thatcher).

SEISFK. F-k plotting and processing.

DEDES. Interactive design of desired output for deconvolution.

DEPRO. Design of directional signature deconvolution filters.

Three subroutine libraries are used by these programs:

TSASUB. Time series analysis (A.N.Bowen).

SUBS1 and **SUBS2.** General purpose and tape handling (J.S.Thatcher).

Synthetic modelling was performed with the GeoQuest AIMS (Advanced Interprtive Modelling System) package.

A.2 F-k directional deconvolution

FKFIL. Transform time domain deconvolution filters (output from DEPRO) to frequency domain.

FKMAP. Map deconvolution filters (output from FKFIL) on to the f-k plane (section 2.1.2). A NAG spline is used for the one-dimensional interpolation.

FKPRO. f-k directional deconvolution (figure 2.4). Sorts CMP gathers to common-receiver gathers. Prepares gathers by spatial tapering, D.C. removal and padding with zero traces. Deconvolution by complex multiplication of f-k transform of gather with filter (output from FKMAP). See program listing.

A.3 Directional deconvolution combined with prestack migration

DDANG. Calculate angular limits necessary to migrate reflections up to a given dip, for a constant-velocity medium (section 3.5.1).

DDFIL. Transform time domain filters (output from DEPRO) to frequency domain and write headers.

DDPSM1. Prestack migration with a choice of deconvolution types (section 3.5.2). See program listing.

DDPSM2. Modified version of DDPSM1. Linear velocity-depth variation (section 5.4.7) See program listing.

DDNEW. Apply Newman filter in the frequency domain (section 3.2.2).

```
      PROGRAM FKPRO
C*****************************************************************************
C
C DESCRIPTION:
C
C Application of f-k directional deconvolution to CMP data from SEGY
C tape. Stages are
C
C : sort to common-receiver gathers (incl. mute and DC removal)
C : 2-D FFT each common-receiver gather
C : complex multiplication with f-k filter (output from FKMAP)
C : inverse 2-D FFT
C : output: 1. selected constant-offset sections to file for comparison
C               with prestack migration directional deconvolution.
C           2. selected common-receiver gathers before and after
C               directional deconvolution.
C
C CONTROL FILE:
C
C       !!!!!!!!! all (10X,I4) format !!!!!!!!!!!!!
C
C       NGATH --- no. of common-receiver gathers to process
C       NFOLD --- fold ( = no. of 0's per CMP gather)
C       NSKIP --- no. of gathers to skip at start of tape
C       NMUTE --- no. of samples to mute at start of traces
C       NSWR  --- no. of samples to output
C       NLAG  --- no. of samples lag of Desired output for filter design
C       NPLOT --- no. of common-rec. gathers to output (before and after)
C                 max=5 (defined in DIMENSION statement)
C       NPLAR(1)------
C         :       ----- common-receiver gather 0 (range 1-NGATH)
C       NPLAR(NPLOT)--
C
C       NOFF  --- no. of constant offset profiles to output after decon.
C                 max=5 (defined in DIMENSION statement)
C       NOFFAR(1) ----
C         :         --- constant-offset section 0 (range 1-NFOLD)
C       NOFFAR(NOFF)--
C
C  LOGICAL UNIT NUMBERS:
C
C       2   = control file
C       3   = f-k filter (output from FKMAP)
C       4   = output common-receiver gathers
C       10          =
C        :          =  output constant-offset sections
C       10+(NOFF-1) =
C
C size of 2-D FFT
C
      PARAMETER (NROWS=64,NSAMS=2048)
C
      IMPLICIT REAL*8(A-H,O-Z)
      DIMENSION X(NROWS,NSAMS),Y(NROWS,NSAMS),WORK(3*NSAMS+1),ND(2)
     &          ,NOFFAR(5),NPLAR(5)
      COMPLEX COMFIL(NROWS,NSAMS/2+1)
C
C read control file
C
      READ(2,1000) NGATH
      READ(2,1000) NFOLD
      READ(2,1000) NSKIP
      READ(2,1000) NMUTE
      READ(2,1000) NSWR
      READ(2,1000) NLAG
      READ(2,1000) NPLOT
      DO 500 I=1,NPLOT
         READ(2,1000) NPLAR(I)
 500  CONTINUE
      READ(2,1000) NOFF
      DO 200 I=1,NOFF
         READ(2,1000) NOFFAR(I)
 200  CONTINUE
 1000 FORMAT(10X,I4)
C
C parameters for nag fft
C
      NDIM  = 2
      ND(1) = NROWS
      ND(2) = NSAMS
      N     = ND(1)*ND(2)
      LWORK = 6145
      IFAIL = 0
C
      IPLOT = 1
      NYQ = NSAMS/2+1
C
C-----------------------------------------------------------------------
C loop over common-rec gathers
C-----------------------------------------------------------------------
C
      DO 100 IGATH=1,NGATH
         PRINT*,IGATH
C
C initialize arrays
C
         DO 300 J=1,NSAMS
            WORK(J) = 0.0D0
            DO 400 K=1,NROWS
               X(K,J) = 0.0D0
               Y(K,J) = 0.0D0
 400        CONTINUE
 300     CONTINUE
C
C sort to common-receiver gather
C
         CALL SORT(IGATH,X,NFOLD,NROWS,NSAMS,NMUTE,WORK,NSKIP)
C
C output this gather ?
C
         IF (IGATH.EQ.NPLAR(IPLOT)) THEN
            DO 600 I = 1,NFOLD
               WRITE(4) (X(I,J),J = 1,NSAMS)
 600        CONTINUE
         ENDIF
C
C nag 2-d fft
C
         CALL C06FJF(NDIM,ND,N,X,Y,WORK,LWORK,IFAIL)
C
```

```
C complex multiplication
C
        CALL CMULT(X,Y,NROWS,NYQ,IGATH,COMFIL,NSAMS)
C
C inverse 2-d fft
C
        CALL INVFFT(X,Y,NROWS,NYQ,NSAMS,NDIM,ND,N,WORK,LWORK,IFAIL)
C
C lag compensation and spatial ramp removal
C
        DO 800 I=1,NFOLD
           DO 900 J=1,NSWR
              IF(J+NLAG.LE.NSAMS) THEN
                IF (I.EQ.1.OR.I.EQ.NFOLD) X(I,J) = 2*X(I,J)
                X(I,J) = X(I,J+NLAG)
              ELSE
                X(I,J) = 0.0
              ENDIF
 900       CONTINUE
 800     CONTINUE
C
C output this gather ?
C
        IF (IGATH.EQ.NPLAR(IPLOT)) THEN
           DO 700 I=1,NFOLD
              WRITE(4) (X(I,J),J=1,NSWR)
 700       CONTINUE
           IPLOT = IPLOT+1
        ENDIF
C
C write offsets to constant-offset sections
C
         CALL OFFWRI(NOFF,NOFFAR,X,NROWS,NSWR)
C
C-------------------------------------------------------------------------
C
 100  CONTINUE
      END
C
      SUBROUTINE SORT(IGATH,X,NFOLD,NROWS,NSAMS,NMUTE,WORK,NSKIP)
C*************************************************************************
C
C DESCRIPTION:
C
C Reads SEGY tape (MTS system subroutine)
C Sorts CMP to common-receiver gathers.
C Removes dc, spatial taper and mute
C
C Cannot cope with multiple tapes (yet) !!!!!!!!!!
C
      IMPLICIT REAL*8(A-H,O-Z)
      DIMENSION X(NROWS,NSAMS),WORK(NSAMS)
      REAL*4 R4TEMP(7048)
      CHARACTER*1 FILE(8432),TRH(240)
      INTEGER*2 NBYTRH,NBYDAT,NBYFIL,LEN
C
      EQUIVALENCE (FILE(1),TRH(1)),(FILE(241),R4TEMP(1))
C
C parameters for mts tape read
C
      INPCHN = 1
      NBYTRH = 240
      NBYDAT = 4*2048
      NBYFIL = NBYTRH+NBYDAT
      LEN    = 5
C
C skip SEG-Y headers and unwanted gathers
C
      IF (IGATH.EQ.1) THEN
         CALL CNTRL('FSR 1',LEN,INPCHN)
         CALL CNTRL('FSR 1',LEN,INPCHN)
         DO 700 I=1,NSKIP
            DO 800 J=1,NFOLD
               CALL CNTRL('FSR 1',LEN,INPCHN)
 800        CONTINUE
 700     CONTINUE
         PRINT*,'HEADERS AND GATHERS SKIPPED'
      ENDIF
C
C-------------------------------------------------------------------------
C loop over traces in gather
C-------------------------------------------------------------------------
C
      DO 100 I=1,NFOLD
         DO 200 J=1,I-1
            CALL CNTRL('FSR 1',LEN,INPCHN)
 200     CONTINUE
C
C read data block
C
         CALL READ(FILE,NBYFIL,0,LNUM,INPCHN)
         DO 400 J=1,NSAMS
            WORK(J) = DBLE(R4TEMP(J))
 400     CONTINUE
C
C remove DC, spatial taper,  and mute
C
         CALL REMAV(NSAMS,WORK,DC)
         DO 600 J=NMUTE+1,NSAMS
            IF (1.EQ.1.OR.I.EQ.NFOLD) WORK(J) = WORK(J)/2.
            X(I,J) = WORK(J)
 600     CONTINUE
C
         DO 300 J=I+1,NFOLD
            CALL CNTRL('FSR 1',LEN,INPCHN)
 300     CONTINUE
C-------------------------------------------------------------------------
 100  CONTINUE
C-------------------------------------------------------------------------
C
C rewind tape to prepare for next call
C
      DO 500 I=1,NFOLD*(NFOLD-1)
         CALL CNTRL('BSR 1',LEN,INPCHN)
 500  CONTINUE
C
      RETURN
      END
C
      SUBROUTINE CMULT(X,Y,NROWS,NYQ,IGATH,COMFIL,NSAMS)
```

```
C*********************************************************************
C
C DESCRIPTION:
C
C F-k mulitplication.
C On first call (IGATH.EQ.1) reads in filter
C
      IMPLICIT REAL*8(A-H,O-Z)
      DIMENSION X(NROWS,NYQ),Y(NROWS,NYQ),TEMP1(1025),TEMP2(1025)
      COMPLEX COMFIL(NROWS,NYQ),COMBUF,COMRES
      SAVE COMFIL
C
C read filter
C
      IF (IGATH.EQ.1) THEN
         READ(3) IIII
         DO 100 I=1,NROWS
            READ(3) (TEMP1(J),J=1,NYQ)
            READ(3) (TEMP2(J),J=1,NYQ)
            DO 200 J=1,NYQ
               COMFIL(I,J) = CMPLX(SNGL(TEMP1(J)),SNGL(TEMP2(J)))
 200        CONTINUE
 100     CONTINUE
      ENDIF
C
C complex multiplication
C
      SCALE = SQRT(FLOAT(NSAMS*NROWS))
      DO 300 J=1,NYQ
         DO 400 I=1,NROWS
            COMBUF = CMPLX(SNGL(X(I,J)),SNGL(Y(I,J)))
            COMRES = COMBUF*COMFIL(I,J)
            X(I,J) = SCALE*DBLE(REAL(COMRES))
            Y(I,J) = SCALE*DBLE(AIMAG(COMRES))
 400     CONTINUE
 300  CONTINUE
C
      RETURN
      END
C
      SUBROUTINE INVFFT(X,Y,NROWS,NYQ,NSAMS,NDIM,ND,N,WORK,LWORK,IFAIL)
C*********************************************************************
C
C DESCRIPTION:
C
C Inverse 2-D FFT.
C
      IMPLICIT REAL*8(A-H,O-Z)
      DIMENSION X(NROWS,NSAMS),Y(NROWS,NSAMS),WORK(3*NSAMS+1),ND(2)
C
C mirror quadrants to restore symmetry
C
      DO 100 I=NYQ+1,NSAMS
         DO 200 J=1,NROWS
            IF (J.EQ.1) THEN
               X(J,I) = X(J,(NSAMS-I+2))
               Y(J,I) = -Y(J,(NSAMS-I+2))
            ELSE
               X(J,I) = X((NROWS-J+2),(NSAMS-I+2))
               Y(J,I) = -Y((NROWS-J+2),(NSAMS-I+2))
            ENDIF
 200     CONTINUE
 100  CONTINUE
C
C nag 2-d inverse fft
C
      CALL C06GCF(Y,N,IFAIL)
      CALL C06FJF(NDIM,ND,N,X,Y,WORK,LWORK,IFAIL)
      CALL C06GCF(Y,N,IFAIL)
C
      RETURN
      END
C
      SUBROUTINE OFFWRI(NOFF,NOFFAR,X,NROW,NSAMS)
C*********************************************************************
C
C DESCRIPTION:
C
C Outputs constant-offset sections
C
      IMPLICIT REAL*8(A-H,O-Z)
      DIMENSION X(NROWS,NSAMS),NOFFAR(5)
C
      DO 100 I=1,NOFF
         NTR = NOFFAR(I)
         WRITE(9+I) (X(NTR,J),J=1,NSAMS)
 100  CONTINUE
C
      RETURN
      END
```

```
      PROGRAM DDSPM1
*************************************************************************
C
C DESCRIPTION:
C
C Prestack Kirchhoff migration of a constant-offset section with directional
C deconvolution, standard signature deconvolution or no deconvolution.
C Assumes constant velocity: interpolates velocity from velocity/time pairs.
C
C CONTROL FILE:
C
C !!!!!!!!!!!!!!!!!!!!!!!!!!!!!!!!!!!!!!!!!!!!!!!!!!!!!!!!!!!!!!!!!!!!!!!
C !!       all variables preceeded by 10 comment characters          !!
C !!                 except TITLEs                                   !!
C !!!!!!!!!!!!!!!!!!!!!!!!!!!!!!!!!!!!!!!!!!!!!!!!!!!!!!!!!!!!!!!!!!!!!!!
C
C  variable    description                                    format
C ------------------------------------------------------------------
C
C    ANGRAN     angular  range from vertical (degrees)       (F7.2)
C    ASNELL     approximate linear  correction factor        (F7.2)
C
C diagnostic printout-----------------------------------------------
C
C    IDIAGN     0 = none  NOT WORKING                        (I4)
C               1 = some  NOT WORKING
C               2 = lots  NOT WORKING
C
C  array--------------------------------------------------------------
C
C    TITLE      not used                                     (A10)
C    NXINT      number of input traces                       (I4)
C    NYINT      number of samples on input traces            (I4)
C    XINT       spatial sample interval (metres)             (F7.2)
C    YINT       temporal sample interval (ms)                (F7.2)
C
C  migrated array-----------------------------------------------------
C
C    TITLE      not used                                     (A10)
C    NTRC       number of traces in migration window         (I4)
C    TRCST      x corrdinate of first traces                 (F7.2)
C    SAMINC     output temporal sample interval              (F7.2)
C    STNOB      sample number to start migration window      (F7.2)
C    OBS        number of samples in migration window        (F7.2)
C
C  velocity-----------------------------------------------------------
C
C    NVEL       number of time/velocity pairs                (I4)
C
C      NVEL     pairs of twtt/rms-velocity                   (F7.2,F7.2)
C
C const os---------------------------------------------------------
C
C    TITLE:     TANK  -  model or real data from SEGY tape   (A10)
C               SEED  -  seed with wavelets from file
C               UNF   -  constant-offset section from file
C
C    C          half source-receiver offset (m)              (F7.2)
C                 +ve : line shot in source direction
C                 -ve : line shot in rec. direction
C
C
C   if TITLE = TANK
C
C    NFOLD      fold                                         (I4)
C    NOFF       trace number of constant-offset section      (I4)
C    NSKIP      number of unwanted gathers at tape start     (I4)
C
C    NSOD       number of samples to skip for S.O.D          (I4)
C
C   if TITLE = SEED
C
C    NTEMP      number samples in wavelet                    (I4)
C    NPNTS      number of occurences of wavelet              (I4)
C         NPNTS           pairs of
C    LSTART,MSTART    x coordinate and sample number         (I4,I4)
C
C   if TITLE = UNF
C
C    no parameters needed
C
C docon-------------------------------------------------------------
C
C    IDECO      0 - no deconvolution
C               1 - directional deconvolution                (I4)
C               2 - signature deconvolution
C    IBAND      1 - bandpass filter                          (I4)
C   if IBAND = 1
C    F1         low cut frequency                            (F7.2)
C    F2         low corner frequency                         (F7.2)
C    F3         high corner frequency                        (F7.2)
C    F4         high cut frequency                           (F7.2)
C   if IDECO = 1
C    DECINC     angular deconvolution increment              (F7.2)
C
C-------------------------------------------------------------------
C
C LOGICAL UNIT NUMBERS:
C
C     1 = tape (SEGY) or file containing test wavelet
C     2 = output file
C    14 = controlfile
C
C   if deconvolving needs:
C
C    16 = temporary store for real part of FFT of deconvolved output
C    17 = temporary store for im   part of FFT of deconvolved output
C   (18 = angular deconvolution filters - FILE NAME DEFINED IN OPEN
C                                         STATEMENT)
C
C*************************************************************************
C
C maximum size of arrays: NTRACS traces, NSAMS samples NFFT samples in FFT
C
      PARAMETER (NSAMS=512,NTRACS=440,NFFT=2048)
C
      REAL*4 VALINT(NTRACS,NSAMS),TRACE2(NTRACS,NSAMS),F(NFFT)
     &      ,TVELAR(20),VELAR(20),S(NFFT),FFTEMR(NFFT),FFTEMI(NFFT)
     &      ,NSHIFT(40,NSAMS),TWTT(NSAMS)
      INTEGER*2 LENMTS
      CHARACTER*10 TITLE,TITDA
```

```
C
      PI    = 3.14159265
      PI2   = PI/2.0
C
C initialise arrays
C
      DO 880 I=1,NSAMS
         DO 881 J=1,NTRACS
            TRACE2(J,I) = 0.0
            VALINT(J,I) = 0.0
 881     CONTINUE
 880  CONTINUE
      DO 882 I=1,NFFT
         FFTEMR(I) = 0.0
         FFTEMI(I) = 0.0
         F(I)      = 0.0
         S(I)      = 0.0
 882  CONTINUE
C
C read controlfile
C
      CALL RDCFIL(ANGRAN,ASNELL,IDIAGN,NXINT,NYINT,XINT,YINT,NTRC,TRCST
     &           ,SAMINC,STNOB,OBS,NVEL,TVELAR,VELAR,C,TITDA,N1,N2,N3
     &           ,NSOD,IDECO,DECINC,IBAND,F1,F2,F3,F4
     &           ,JANS,NTRCS,TRACE2,NTRACS,NSAMS,F)
      TRCINC = XINT
      NSTNOB = 1+NINT(STNOB/SAMINC)
      NOBS   = 1+NINT(OBS/SAMINC)
      SAMINC = SAMINC/2.0
      NENNOB = NSTNOB+NOBS-1
      NTRST  = NINT(TRCST/TRCINC)
      XMAX = (NXINT-1)*XINT
      YMAX = (NYINT-1)*YINT
      ANT = 1./(2*F3)
C
C printout log
C
      CALL PROUT(ANGRAN,ASNELL,IDIAGN,NXINT,NYINT,XINT,YINT,NTRC
     &          ,TRCST,NTRST
     &          ,NSTNOB,NOBS,TRCINC,SAMINC,NENNOB,NVEL,TVELAR
     &          ,VELAR,C,TITDA,N1,N2,N3,NSOD
     &          ,IDECO,DECINC,IBAND,F1,F2,F3,F4,JANS,NTRCS)
C
C FFT of constant-offset section and bandpass (and weighting)
C
      CALL SINTAB(NFFT,S)
      SIGNI  = -1.0
      DO 430 I=1,NXINT
         DO 431 J=1,NSAMS
            FFTEMR(J) = SQRT(REAL(J))*TRACE2(I,J)
  431    CONTINUE
         CALL FFTA(NFFT,FFTEMR,FFTEMI,SIGNI,S)
         WRITE(16) (FFTEMR(K),K=1,NFFT)
         WRITE(17) (FFTEMI(K),K=1,NFFT)
         IF (I.EQ.1.OR.I.EQ.NXINT) THEN
            PRINT*,' FFT @ ',I
         ENDIF
  430 CONTINUE
      MFFT  = NFFT/2+1
      FNYQ = 1./(2.*YINT)
      DF    = FNYQ/FLOAT(MFFT)
      IF (IBAND.EQ.1) THEN
         DO 547 I=1,MFFT
            F(I) = DF*FLOAT(I)
 547     CONTINUE
         DO 548 I=2,MFFT
            IF (F1.GE.F(I-1).AND.F1.LE.F(I))    JJ=I-1
            IF (F2.GE.F(I-1).AND.F2.LE.F(I))    J =I-1
            IF (F3.GE.F(I-1).AND.F3.LE.F(I))    K =I-1
            IF (F4.GE.F(I-1).AND.F4.LE.F(I))    KK=I-1
 548     CONTINUE
      ENDIF
C
C open direct access file for angular filters
C
      IF (IDECO.NE.0) OPEN (18,FILE='GANGFIL',STATUS='OLD'
     &                      ,ACCESS='DIRECT',RECL=17000)
C
C perform bandpass filtering only or 1-d decon
C
      IF (IDECO.EQ.0.AND.IBAND.EQ.1) THEN
         CALL BAND(TRACE2,NTRACS,NXINT,NSAMS,S
     &             ,FFTEMR,FFTEMI,NFFT,JJ,KK,J,K)
      ELSE IF (IDECO.EQ.2) THEN
         ANGFIL = 0.0
         CALL DECON(TRACE2,NTRACS,NXINT,NSAMS,ANGFIL,S
     &              ,FFTEMR,FFTEMI,NFFT,JJ,KK,J,K,IBAND)
      ENDIF
C
C preliminary sort
C
      CALL PRESRT(NSHIFT,ANGRAN,IDECO,DECINC,NSTNOB,NENNOB,NVEL
     &           ,TVELAR,VELAR,C,XINT,SAMINC,IANGRA,IDECIN,ASNELL)
C
C angular window parameters
C
      RANGRA = ASNELL*ANGRAN*PI/180.0
      CORNER = RANGRA*4.0/5.0
      MCOUNT = 0
C
C-----------------------------------------------------------------------
C main loops
C-----------------------------------------------------------------------
C
      DO 700 MANG = IANGRA,-IANGRA+IDECIN,-IDECIN
         PRINT*,'MANG ',MANG,'--------------------'
         MCOUNT = MCOUNT+1
         IF (IDECO.EQ.1) THEN
            ANGFIL = FLOAT(MANG)-FLOAT(IDECIN)/2.0
            CALL DECON(TRACE2,NTRACS,NXINT,NSAMS,ANGFIL
     &                 ,S,FFTEMR,FFTEMI,NFFT,JJ,KK,J,K,IBAND)
         ENDIF
         ICALL = 1
         DO 200 I=NSTNOB,NENNOB
            INOB = I-NSTNOB+1
            NSHMA = NSHIFT(MCOUNT,INOB)
            NSHMI = NSHIFT(MCOUNT+1,INOB)
            B = (I-1)*SAMINC
            CALL VELCAL(B,NVEL,TVELAR,VELAR,VEL,ICALL)
            BDEPTH = B*VEL
```

```
            DO 554 NSH = NSHMA,NSHMI+1,-1
               XSHIFT = FLOAT(NSH)*XINT
               CALL ELLIP(BDEPTH,XSHIFT,C,VEL,YELLIP,ALPHA)
               IF (MCOUNT.EQ.1.AND.NSH.EQ.NSHMA) GOTO 5540
               IF (ABS(YELLIP-TWTT(I)).GT.ANT) GOTO 5540
               IF (YELLIP.LT.0.0.OR.YELLIP.GT.YMAX) GOTO 5540
               CALL WEIGHT(ALPHA,CORNER,RANGRA,YELLIP,AMPLIT)
               DO 650 N=1,NTRC
                  NXELL= NTRST+N+NSH-1
                  IF (NXELL.GE.1.AND.NXELL.LE.NXINT) THEN
                     CALL INTERP(NXELL,YELLIP,TRACE2,NTRACS
     &                           ,NSAMS,XINT,YINT,VALUE)
                     VALUE = VALUE*AMPLIT
                     VALINT(N,1) = VALINT(N,I)+VALUE
                  ENDIF
 650           CONTINUE
 5540          TWTT(I) = YELLIP
 554        CONTINUE
 200     CONTINUE
 700  CONTINUE
C
C weight and write migrated array to file
C
      DO 411 I=1,NTRC
         DO 412 J=1,NENNOB
            VALINT(I,J) = J*VALINT(I,J)
  412    CONTINUE
         WRITE(2) (VALINT(I,J),J=1,NENNOB)
  411 CONTINUE
C
      STOP
      END
C
      SUBROUTINE ELLIP(Y,X,C,VEL,TWT,ALPHA)
C*************************************************************************
C
C DESCRIPTION:
C
C 1. calculates take-off angle for given X shift
C 2. calculates twtt for X shift
C
      PI = 3.14159265
      PI2 = PI/2.0
C
C calculate alpha
C
      XCOORD = X
      W = XCOORD+C
      IF (W.NE.0.0) THEN
         TAL = Y/W
         IF (TAL.LT.0.0) THEN
            ALPHA = ATAN(TAL)+PI
         ELSE
            ALPHA = ATAN(TAL)
         ENDIF
      ELSE
         ALPHA = PI2
      ENDIF
      ALPHA = PI2-ALPHA
C
C calculate twtt
C
      YSQ = Y*Y
      TWT = 1.0/VEL*(SQRT((X-C)**2+YSQ)+SQRT((X+C)**2+YSQ))
C
      RETURN
      END
C
      SUBROUTINE INTERP(NXELL,SY,TRACE2,NTRACS,NSAMS,XINT,YINT,SVALUE)
C*************************************************************************
C
C DESCRIPTION:
C
C    1. x coordinate passed as an integer number of tracos
C    2. interpolates  a value for y (time) coordinate using NAG
C         bicubic-spline
C    3. returns value interpolated from TRACE2
C
      REAL*4 TRACE2(NTRACS,NSAMS)
      REAL*8 XGRID(4),YGRID(4),B(8),C(8),WRK(40),Y,VALUE
C
      VALUE = 0.0D0
      SVALUE = 0.0
      L = NXELL
C
C interpolation for time
C
      NYELL = INT(SY/YINT)+1
      MMIN = NYELL-1
      MMAX = NYELL+2
C
C XGRID = independant variable for nag call i.e time
C
      XGRID(1) = DBLE((MMIN-1)*YINT)
      DO 100 I=1,4
         XGRID(I) = XGRID(1)+DBLE((I-1)*YINT)
         YGRID(I) = DBLE(TRACE2(L,(MMIN+I-1)))
 100  CONTINUE
C
C nag spline
C
      IFAIL = 0
      CALL E01BAF(4,XGRID,YGRID,B,C,8,WRK,40,IFAIL)
      Y = DBLE(SY)
      CALL E02BBF(8,B,C,Y,VALUE,IFAIL)
      IF (IFAIL.NE.0) PRINT*,'NAG ERROR $$$$$$$$$$$$$$$$$$$$$$$$$$$$$$$$'
      SVALUE = SNGL(VALUE)
C
      RETURN
      END
C
      SUBROUTINE CONSTO(TRACE2,NCHR,NSAMR,NFOLD,NOFF,NGATH,NSKIP,NSOD)
C*************************************************************************
C
C DESCRIPTION:
C
C reads SEGY CMP tape using MTS system subroutine
C outputs constant-offset section
C
C SOURCE: Stefan Thatcher
```

```
C
      INTEGER*2 NBYTRH,NBYDAT,NBYFIL,LEN
      CHARACTER*1 FILE(6240),TRH(240),CREPLY
      REAL*4 TRACE2(NCHR,NSAMR),R4TEMP(2048)
C
      EQUIVALENCE (FILE(1),TRH(1)),(FILE(241),R4TEMP(1))
C
      INPCHN = 1
      NCHN = NFOLD
      LEN = 5
C
C wind tape over the REEL IDENTIFICATION blocks
C
      CALL CNTRL('FSR 1', LEN, INPCHN)
      CALL CNTRL('FSR 1', LEN, INPCHN)
C
C skip unwanted gathers
C
      DO 61 I=1,NSKIP
         IF (I.EQ.1.OR.I.EQ.NSKIP) THEN
            PRINT*,'SKIPPED  ',I
         ENDIF
         DO 62 J=1,NCHN
            CALL CNTRL('FSR 1',LEN,1)
 62      CONTINUE
 61   CONTINUE
C
C loop for number of traces
C
      DO 746 NTRAC=1,NGATH
         IF (NTRAC.EQ.1.OR.NTRAC.EQ.NGATH) THEN
            PRINT*,'     READ      ',NTRAC
         ENDIF
         DO 10 J = 1, NOFF-1
            CALL CNTRL('FSR 1', LEN, 1)
 10      CONTINUE
         CALL READ(FILE,NBYFIL,0,LNUM,INPCHN)
         CALL REMAV(NSAMR,R4TEMP,DC)
         DO 21 J = 1 , NSAMR
            TRACE2(NTRAC,J)=R4TEMP(J+NSOD)
 21      CONTINUE
         DO 30 J=NOFF+1,NCHN
            CALL CNTRL('FSR 1', LEN, 1)
 30      CONTINUE
 746  CONTINUE
C
C rewind tape
C
      CALL REWIND(1)
      RETURN
      END
C
      SUBROUTINE DECON(TRACE2,NTRACS,NXINT,NSAMS,ANGFIL,S,FFTEMR,FFTEMI
     &                 ,NFFT,J2,K2,J1,K1,IBAND)
C*********************************************************************
C
C DESCRIPTION:
C
C  1. reads correct filter for angle from direct access file (18)
C  2. performs deconvolution  by complex multiplication  of filter
C              with raw data ( ffts read from 16,17)
C  3. bandpass filters
C  4. writes to TRACE2 incorporating lag
C
      REAL*4 TRACE2(NTRACS,NSAMS),S(NFFT),FFTEMR(NFFT),FFTEMI(NFFT)
     &         ,FFILR(2048),FFILI(2048)
C
      REWIND 16
      REWIND 17
C
C read FFILR/I from direct access file -- ANGFILD
C
      NR = 14+NINT(ANGFIL/4.0)
      PRINT*,'       DECON FILTER NO.   ',NR
      READ(18,REC=NR) ANGLE,LAG,(FFILR(I),I=1,NFFT)
     &                          ,(FFILI(I),I=1,NFFT)
      PRINT*,'                   ANGLE ',ANGLE
C
C complex multiplication
C
      MFFT = NFFT/2+1
      DO 100 I=1,NXINT
         READ(16) (FFTEMR(J),J=1,MFFT)
         READ(17) (FFTEMI(J),J=1,MFFT)
         DO 200 J=1,MFFT
            FFTR = FFTEMR(J)
            FFTI = FFTEMI(J)
            FFTEMR(J) = FFTR*FFILR(J)-FFTI*FFILI(J)
            FFTEMI(J) = FFTR*FFILI(J)+FFTI*FFILR(J)
 200     CONTINUE
C
C bandpass?
C
         IF (IBAND.EQ.1) THEN
            CALL HANN(FFTEMR,MFFT,J2,K2,J1,K1)
            CALL HANN(FFTEMI,MFFT,J2,K2,J1,K1)
         ENDIF
C
C inverse FFT
C
         DO 201 J=MFFT+1,NFFT
            FFTEMR(J) = FFTEMR(NFFT-J+2)
            FFTEMI(J) = -FFTEMI(NFFT-J+2)
 201     CONTINUE
         SIGNI=1.0
         CALL FFTA(NFFT,FFTEMR,FFTEMI,SIGNI,S)
         DO 300 K=1,NSAMS
            IF (K+LAG.LT.NSAMS) THEN
               TRACE2(I,K) = FFTEMR(K+LAG)
            ELSE
               TRACE2(I,K) = 0.0
            ENDIF
 300     CONTINUE
 100  CONTINUE
C
      RETURN
      END
C
      SUBROUTINE BAND(TRACE2,NTRACS,NXINT,NSAMS,S,FFTEMR,FFTEMI
     &                ,NFFT,J2,K2,J1,K1)
```

```
C*********************************************************************
C
C DESCRIPTION:
C
C  1. bandpass filters
C  2. writes to TRACE2
C
      REAL*4 TRACE2(NTRACS,NSAMS),S(NFFT),FFTEMR(NFFT),FFTEMI(NFFT)
C
      REWIND 16
      REWIND 17
C
      MFFT = NFFT/2+1
      DO 100 I=1,NXINT
         READ(16) (FFTEMR(J),J=1,MFFT)
         READ(17) (FFTEMI(J),J=1,MFFT)
         CALL HANN(FFTEMR,MFFT,J2,K2,J1,K1)
         CALL HANN(FFTEMI,MFFT,J2,K2,J1,K1)
         DO 201 J=MFFT+1,NFFT
            FFTEMR(J) = FFTEMR(NFFT-J+2)
            FFTEMI(J) = -FFTEMI(NFFT-J+2)
 201     CONTINUE
         SIGNI=1.0
         CALL FFTA(NFFT,FFTEMR,FFTEMI,SIGNI,S)
         DO 300 K=1,NSAMS
            TRACE2(I,K) = FFTEMR(K)
 300     CONTINUE
 100  CONTINUE
C
      RETURN
      END
C
C
      SUBROUTINE RDCFIL(ANGRAN,ASNELL,IDIAGN,NXINT,NYINT,XINT,YINT
     &                  ,NTRC,TRCST,SAMINC
     &                  ,STNOB,OBS,NVEL,TVELAR,VELAR,C,TITDA,N1,N2,N3
     &                  ,NSOD,IDECO,DECINC,IBAND,F1,F2,F3,F4
     &                  ,JANS,NTRCS,TRACE2,NTRACS,NSAMS,TEMP)
C*********************************************************************
C
C DESCRIPTION:
C
C reads control file
C
      REAL*4 TRACE2(NTRACS,NSAMS),TEMP(NSAMS),TVELAR(20),VELAR(20)
      CHARACTER*10 TITLE,TITDA
C
 993  FORMAT(10X,F7.2)
 994  FORMAT(10X,I4)
 995  FORMAT(A10)
 997  FORMAT(10X,F7.2,F7.2)
C
      READ(14,993)     ANGRAN
      READ(14,993)     ASNELL
C
C diagnostic printout ?
C
      READ(14,994)     IDIAGN
C
C input array parameters
C
      READ(14,995)      TITLE
      READ(14,994)      NXINT
      READ(14,994)      NYINT
      READ(14,993)       XINT
      READ(14,993)       YINT
                         YINT=YINT*0.001
C
C migrated output window
C
      READ(14,995)      TITLE
      READ(14,994)       NTRC
      READ(14,993)      TRCST
      READ(14,993)     SAMINC
                       SAMINC=SAMINC*0.001
      READ(14,993)      STNOB
                        STNOB=STNOB*0.001
      READ(14,993)        OBS
                          OBS=OBS*0.001
C
      READ(14,994)       NVEL
      DO 100 I=1,NVEL
         READ(14,997) TVELAR(I),VELAR(I)
         TVELAR(I) = TVELAR(I)*0.001
 100  CONTINUE
C
C input data
C
      READ(14,995)      TITDA
      READ(14,993)          C
      IF (TITDA.EQ.'TANK') THEN
         READ(14,994)   NFOLD
         READ(14,994)    NOFF
         READ(14,994)   NSKIP
         READ(14,994)   NSOD
         NGATH = NXINT
         N1    = NFOLD
         N2    = NOFF
         N3    = NSKIP
         PRINT*,'CALLING CONSTO'
         CALL CONSTO(TRACE2,NTRACS,NSAMS,NFOLD,NOFF,NGATH,NSKIP,NSOD)
         PRINT*,'OUT OF CONSTO'
         PRINT*,' '
      ELSE IF (TITDA.EQ.'SEED') THEN
         READ(14,994)   NTEMP
         READ(14,994)   NPNTS
         READ(1) (TEMP(I),I=1,NTEMP)
         DO 842 I=1,NPNTS
            READ(14,227) LSTART,MSTART
 227        FORMAT(10X,I4,I4)
            DO 843 J=1,NTEMP
               TRACE2(LSTART,MSTART+J) = TEMP(J)
 843        CONTINUE
 842     CONTINUE
         N1 = NTEMP
         N2 = NPNTS
      ELSE
         DO 844 I=1,NXINT
            READ(1) (TRACE2(I,J),J=1,NYINT)
 844     CONTINUE
```

```
      ENDIF
C
C deconvolution
C
      READ(14,994)      IDECO
      READ(14,994)      IBAND
      IF (IBAND.EQ.1) THEN
         READ(14,993) F1
         READ(14,993) F2
         READ(14,993) F3
         READ(14,993) F4
      ENDIF
      IF (IDECO.EQ.1) THEN
         READ(14,993) DECINC
      ENDIF
C
      RETURN
      END
C
      SUBROUTINE PROUT(ANGRAN,ASNELL,IDIAGN,NXINT,NYINT,XINT,YINT
     &                ,NTRC,TRCST
     &                ,NTRST,NSTNOB,NOBS,TRCINC,SAMINC,NENNOB,NVEL
     &                ,TVELAR,VELAR,C,TITDA,N1,N2,N3,NSOD
     &                ,IDECO,DECINC,IBAND,F1,F2,F3,F4,JANS,NTRCS)
C*********************************************************************
C
C DESCRIPTION:
C
C printout log of input file etc
C
       REAL*4 TVELAR(NVEL),VELAR(NVEL)
       CHARACTER*10 TITDA
C
       PRINT*,'Angle range '
       PRINT*,'------------'
       PRINT*,' limited to ',ANGRAN,' degrees take off angle'
       PRINT*,' '
       PRINT*,ASNELL,' linear correction for snells law'
       PRINT*,' '
       PRINT*,'Migrated output'
       PRINT*,'---------------'
       PRINT*,'  X  : ',NTRC,' traces spaced at  ',TRCINC,'m  starting'
       PRINT*,'     at ',TRCST ,' m',' i.e trace no ',NTRST
       PRINT*,' '
       PRINT*,' Time: ',NOBS,' samples at ',SAMINC,'s  sample interval'
       PRINT*,'                              one way traveltime'
       PRINT*,'     window starts at  sample',NSTNOB,' ends at ',NENNOB
       PRINT*,' '
       PRINT*,' '
       PRINT*,'Input'
       PRINT*,'-----'
       PRINT*,'  X  : ',NXINT,' traces at  ',XINT,' m spacing '
       PRINT*,'  Y  : ',NYINT,' samples at ',YINT,' s sample interval'
       PRINT*,'       ',NSOD,' samples to skip to correct to SOD'
       PRINT*,' '
       PRINT*,'Velocity '
       PRINT*,'--------'
       PRINT*,NVEL,' time / velocity pairs'
       PRINT*,' '
       DO 100 I=1,NVEL
         PRINT*,I,'         ',TVELAR(I),' s  ',VELAR(I),' m/s'
100    CONTINUE
       IF (TITDA.EQ.'TANK') THEN
        PRINT*,' '
        PRINT*,'CONSTOFF PARAMS '
        PRINT*,'---------------'
        PRINT*,'OFFSET  ',C
        PRINT*,'NFOLD   ',N1
        PRINT*,'NOFF  which single offset to read  ',N2
        PRINT*,'NGATH no of gathers .traces in constoff sect  ',NXINT
        PRINT*,'NSKIP any gathers to skip ?  ',N3
        PRINT*,' '
       ELSE IF (TITDA.EQ.'SEED') THEN
        PRINT*,'TEST DATA'
        PRINT*,'**********'
        PRINT*,'HALF OFFSET ',C
        PRINT*,' '
        PRINT*,'signal has ',N1,' samples'
        PRINT*,'input array seeded with ',N2,' signals'
       ELSE
        PRINT*,'input array read from unformatted file'
       ENDIF
       IF (IBAND.EQ.1) THEN
        PRINT*,' '
        PRINT*,'BANDPASS  ',F1,' > ',F2,' > ',F3,' > ',F4,' Hz'
        PRINT*,' '
       ELSE
        PRINT*,' '
        PRINT*,'NO BANDPASSING'
        PRINT*,' '
       ENDIF
      IF (IDECO.EQ.1) THEN
         PRINT*,' '
         PRINT*,'------ DECON ---------'
         PRINT*,' angular increment  ',DECINC
         PRINT*,' '
       ELSE IF (IDECO.EQ.2) THEN
         PRINT*,' '
         PRINT*,'1-D DECON'
         PRINT*,' '
       ELSE IF (IDECO.EQ.0) THEN
         PRINT*,' '
         PRINT*,'NO DECON'
         PRINT*,' '
       ENDIF
C
        RETURN
        END
C
      SUBROUTINE PRESRT(NSHIFT,ANGRAN,IDECO,DECINC,NSTNOB,NENNOB
     &             ,NVEL,TVELAR,VELAR,C,XINT,SAMINC,IANGRA,IDECIN,ASNELL)
C*********************************************************************
C
C DESCRIPTION:
C
C calculates which part of summation operator to use when each
C angular deconvolution filter is used
C
      REAL*4 NSHIFT(40,NENNOB),TVELAR(NVEL),VELAR(NVEL)
C
```

```
      PI = 3.14159265
C
      IF (IDECO.EQ.1) THEN
         IDECIN = NINT(DECINC)
         IANGRA = NINT(ANGRAN/DECINC)
         IF (FLOAT(IANGRA).LT.ANGRAN/DECINC) THEN
            IANGRA = (IANGRA+1)*IDECIN
         ELSE
            IANGRA = IANGRA*IDECIN
         ENDIF
         ANGRAN = FLOAT(IANGRA)
      ELSE
         IANGRA = NINT(ANGRAN)
         IDECIN = 2*IANGRA
      ENDIF
      PRINT*,' '
      PRINT*,'NEW ANGLES '
      PRINT*,'  ANGRAN ',ANGRAN
      PRINT*,'  IANGRA ',IANGRA
      PRINT*,'  IDECIN ',IDECIN
      PRINT*,' '
      PRINT*,'  corresponding max. straight line angle = '
     &                  ,IANGRA*ASNELL
      MCOUNT = 0
C
C calculate part of migration operator for each angular increment
C
      DO 550 MANG = IANGRA,-IANGRA,-IDECIN
         MCOUNT = MCOUNT+1
         PRINT*,MCOUNT,' MANG ',MANG
         ANGL = ASNELL*FLOAT(MANG)*PI/180.0
         ICALL =1
         DO 551 LDEPTH = NSTNOB,NENNOB
            DEPTH = FLOAT(LDEPTH-1)
            OWT = DEPTH*SAMINC
            CALL VELCAL(OWT,NVEL,TVELAR,VELAR,VEL,ICALL)
            IF (MCOUNT.EQ.1) THEN
               IF (LDEPTH.EQ.NSTNOB.OR.LDEPTH.EQ.NENNOB)
     &            PRINT*,LDEPTH,'          ',VEL
            ENDIF
            XSHIFT = OWT*VEL*TAN(ANGL)-C
            NXSH = NINT(XSHIFT/XINT)
            NSHIFT(MCOUNT,LDEPTH-NSTNOB+1) =NXSH
            IF (LDEPTH.EQ.NSTNOB.OR.LDEPTH.EQ.NENNOB) THEN
               PRINT*,'          NXSH ',NXSH
            ENDIF
  551    CONTINUE
  550 CONTINUE
C
      RETURN
      END
C
      SUBROUTINE WEIGHT(ALPHA,CORNER,RANGRA,YCOORD,AMPLIT)
C*********************************************************************
C
C DESCRIPTION:
C
C applys weighing across angular apeture
C
C
      PI  = 3.14159265
      PI2 = PI/2.0
C
      IF (ABS(ALPHA).LT.CORNER) THEN
         AMPLIT = COS(ALPHA)
      ELSE IF(ABS(ALPHA).GE.CORNER.AND.ABS(ALPHA).LT.RANGRA) THEN
         AMPLIT = (0.5+0.5*COS(5.*PI*ALPHA/RANGRA))*COS(CORNER)
      ELSE
         AMPLIT = 0.0
      ENDIF
C
      RETURN
      END
C
      SUBROUTINE VELCAL(OWT,NVEL,TVELAR,VELAR,VEL,ICALL)
C*********************************************************************
C
C DESCRIPTION:
C
C linear interpolation of velocities between given values
C
C
      REAL*4 TVELAR(NVEL),VELAR(NVEL)
C
      TWT = 2*OWT
      DO 100 I=ICALL,NVEL
         IF (TWT.GE.TVELAR(I).AND.TWT.LT.TVELAR(I+1)) THEN
            THETA = (VELAR(I+1)-VELAR(I))/(TVELAR(I+1)-TVELAR(I))
            VEL = VELAR(I)+(TWT-TVELAR(I))*THETA
            ICALL = I
            RETURN
         ENDIF
  100 CONTINUE
      PRINT*,'PROBLEM IN VELCAL'
C
      RETURN
      END
C
      SUBROUTINE FFTA(LX, X, Y, SIGNI, S)
C*********************************************************************
C
C DESCRIPTION:
C
C FFT using the Cooley-Tukey algorithm
C
C SOURCE:  Claerbout,  modified by Tim Hardman 1985.
C
      REAL*4 X(LX), Y(LX), S(LX)
C
      SC = 1.0
      IF (SIGNI .LT. 0.0) SC = 1.0 / LX
      NN = LX / 2
      N = LX / 4
      J = 1
      DO 30 I = 1, LX
         IF (I .GT. J) GO TO 10
         TEMPX = X(J) * SC
         TEMPY = Y(J) * SC
         X(J) = X(I) * SC
         Y(J) = Y(I) * SC
```

```
      X(I) = TEMPX
      Y(I) = TEMPY
10    M = NN
20    IF (J .LE. M) GO TO 30
      J = J - M
      M = M / 2
      IF (M .GE. 1) GO TO 20
30    J = J + M
      L = 1
      NL = NN
40    ISTEP = 2 * L
      IND = 1
      DO 100 M = 1, L
         INDN = IND - N - 1
         IF (INDN) 50, 60, 70
50       WX = S(1 - INDN)
         WY = S(IND) * SIGNI
         GO TO 80
60       WX = 0.
         WY = SIGNI
         GO TO 80
70       WX = -S(INDN + 1)
         WY = S(N + 1 - INDN) * SIGNI
80       DO 90 I = M, LX, ISTEP
            TEMPX = WX * X(I + L) - WY * Y(I + L)
            TEMPY = WX * Y(I + L) + WY * X(I + L)
            X(I + L) = X(I) - TEMPX
            Y(I + L) = Y(I) - TEMPY
            X(I) = X(I) + TEMPX
90          Y(I) = Y(I) + TEMPY
100      IND = IND + NL
      L = ISTEP
      NL = NL / 2
      IF (L .LT. LX) GO TO 40
C
      RETURN
      END
C
      SUBROUTINE SINTAB(LX, S)
C*********************************************************************
C
C DESCRIPTION:
C
C sine table generation
C   S(I)=SIN(2*PI*(I-1/)/LX)   I=1,2,....,LX/4+1
C
C   where LX=2**INTEGER and is the number of points in the time series
C
C SOURCE: Alan Nunns, modified by Tim Hardman 1985.
C
      REAL*4 S(LX)
C
      N1 = LX / 4 + 1
      ARG = 0.0
      DELARG = 0.6283185307179586E01 / LX
      DO 10 I = 1, N1
         S(I) = SIN(ARG)
         ARG = ARG + DELARG
10    CONTINUE
C
      RETURN
      END
C
      SUBROUTINE HANN(X, N, JJ, KK, J, K)
C*********************************************************************
C
C DESCRIPTION:
C
C applies a Hanning bandpass window
C
C SOURCE Tim Hardman
C
      REAL*4 X(N)
      NN = N - 1
      PI2 = 0.62831853071796E01
C
      IF (JJ .EQ. 1) GO TO 20
C
      DO 10 I = 2, JJ
10    X(I - 1) = X(I - 1) * 0.0
C
20    IF (J .EQ. JJ) GO TO 40
C
      CON1 = PI2 / FLOAT(2*(J - JJ))
      DO 30 I = JJ, J
      ARG = FLOAT(I - JJ) * CON1
      X(I) = X(I) * 0.5 * (.1+01 - COS(ARG))
30    CONTINUE
40    IF (K .EQ. KK) GO TO 60
C
      CON2 = PI2 / FLOAT(2*(KK - K))
      DO 50 I = K, KK
         ARG = FLOAT(KK - I) * CON2
50    X(I) = X(I) * 0.5 * (.1+01 - COS(ARG))
C
60    IF (KK .EQ. N) GO TO 80
C
      DO 70 I = KK, NN
70       X(I + 1) = X(I + 1) * 0.0
C
80    RETURN
      END
C
      SUBROUTINE REMAV(N,X,DC)
C*********************************************************************
C
C DESCRIPTION
C
C removes DC from time series
C
      REAL*4 X(N)
C
      DN=FLOAT(N)
      DC=0.0
C
      DO 10 I=1,N
10    DC=X(I)+DC
C
      DC=DC/DN
C
```

```
      DO 20 I=1,N
20    X(I)=X(I)-DC
C
      RETURN
      END
```

```
      PROGRAM DDPSM2
*****************************************************************************
C
C DESCRIPTION:
C
C Prestack Kirchhoff migration of a constant-offset section with directional
C deconvolution, standard signature deconvolution, or no deconvolution.
C A linear velocity-depth function is used.
C
C !!!!!!!!!!!!!!!!!!!!!!!!!!!!!!!!!!!!!!!!!!!!!!!!!!!!!!!!!!!!!!!!!!!!!!!!
C !                                                                         !
C ! A MODIFIED VERSION OF DDPSM1. ONLY THOSE ROUTINES WHICH ARE            !
C ! MODIFIED ARE LISTED HERE. OTHER SUBROUTINES ARE IDENTICAL TO           !
C !                    THOSE IN DDPSM1                                      !
C !    routines ELLIP and VELCAL are not needed                             !
C !                                                                         !
C !                                                                         !
C !!!!!!!!!!!!!!!!!!!!!!!!!!!!!!!!!!!!!!!!!!!!!!!!!!!!!!!!!!!!!!!!!!!!!!!!
C
C CONTROL FILE:
C
C  variable    description                                    format
C-----------------------------------------------------------------------
C
C  ANGRAN      see DDSPM1
C  VSURF       velocity at surface                            (F7.2)
C  VGRAD       velocity gradient                              (F7.2)
C
C diagnostic
C array
C etc
C
C !!!! AS FOR DDSPM1 EXCEPT  !!!!!!!!!!!!!!!!!!!!!!!!!!!!!!!!!!!!!!!!!!!!
C
C decon-------------------------------------------------------------------
C
C !!! N.B NEED DECINC FOR ALL MIGRATIONS (unlike DDPSM1)
C
C         DECINC angular increment                            (F7.2)
C
C-----------------------------------------------------------------------
C
C*****************************************************************************
C
      PARAMETER (NSAMS=512,NTRACS=440,NFFT=2048)
C
      REAL*4 VALINT(NTRACS,NSAMS),TRACE2(NTRACS,NSAMS),F(NFFT)
     &      ,S(NFFT),FFTEMR(NFFT),FFTEMI(NFFT)
     &      ,NSHIFT(40,NSAMS),TWTT(NSAMS)
      INTEGER*2 LENMTS,NCOUNT(NSAMS)
      CHARACTER*10 TITLE,TITDA
C
      PI    = 3.14159265
      PI2   = PI/2.0
C
C initialise arrays
C
      DO 880 I=1,NSAMS
         NCOUNT(I) = 0
         DO 881 J=1,NTRACS
            TRACE2(J,I) = 0.0
            VALINT(J,I) = 0.0
  881    CONTINUE
  880 CONTINUE
      DO 882 I=1,NFFT
         FFTEMR(I) = 0.0
         FFTEMI(I) = 0.0
         F(I)      = 0.0
         S(I)      = 0.0
  882 CONTINUE
C
C read controlfile
C
      CALL RDCFIL(ANGRAN,VSURF,VGRAD,IDIAGN,NXINT,NYINT,XINT,YINT,NTRC
     &           ,TRCST
     &           ,SAMINC,STNOB,OBS,C,TITDA,N1,N2,N3
     &           ,NSOD,IDECO,DECINC,IBAND,F1,F2,F3,F4
     &           ,JANS,NTRCS,TRACE2,NTRACS,NSAMS,F)
      TRCINC = XINT
      NSTNOB = 1+NINT(STNOB/SAMINC)
      NOBS   = 1+NINT(OBS/SAMINC)
      SAMINC = SAMINC/2.0
      NENNOB = NSTNOB+NOBS-1
      NTRST  = NINT(TRCST/TRCINC)
      XMAX = (NXINT-1)*XINT
      YMAX = (NYINT-1)*YINT
      ANT = 1./(2*F3)
C
C     printout log
C
      CALL PROUT(ANGRAN,VSURF,VGRAD,IDIAGN,NXINT,NYINT,XINT,YINT,NTRC
     &          ,TRCST,NTRST
     &          ,NSTNOB,NOBS,TRCINC,SAMINC,NENNOB
     &          ,C,TITDA,N1,N2,N3,NSOD
     &          ,IDECO,DECINC,IBAND,F1,F2,F3,F4,JANS,NTRCS)
C
C FFT of constant-offset section and bandpassing (and weighting)
C
      CALL SINTAB(NFFT,S)
      SIGNI  = -1.0
      DO 430 I=1,NXINT
         DO 431 J=1,NSAMS
            FFTEMR(J) = SQRT(REAL(J))*TRACE2(I,J)
  431    CONTINUE
         CALL FFTA(NFFT,FFTEMR,FFTEMI,SIGNI,S)
         WRITE(16) (FFTEMR(K),K=1,NFFT)
         WRITE(17) (FFTEMI(K),K=1,NFFT)
         IF (I.EQ.1.OR.I.EQ.NXINT) THEN
            PRINT*,' FFT 0 ',I
         ENDIF
  430 CONTINUE
      MFFT  = NFFT/2+1
      FNYQ = 1./(2.*YINT)
      DF    = FNYQ/FLOAT(MFFT)
      IF (IBAND.EQ.1) THEN
         DO 547 I=1,MFFT
            F(I) = DF*FLOAT(I)
  547    CONTINUE
         DO 548 I=2,MFFT
            IF (F1.GE.F(I-1).AND.F1.LE.F(I))    JJ=I-1
```

```
            IF (F2.GE.F(I-1).AND.F2.LE.F(I))     J =I-1
            IF (F3.GE.F(I-1).AND.F3.LE.F(I))     K =I-1
            IF (F4.GE.F(I-1).AND.F4.LE.F(I))     KK=I-1
 548      CONTINUE
      ENDIF
C
C open direct access file for angular filters
C
      IF (IDECO.NE.0) OPEN (18,FILE='GANGFIL',STATUS='OLD'
     &                      ,ACCESS='DIRECT',RECL=17000)
C
C perform bandpass filtering only or 1-d decon
C
      IF (IDECO.EQ.0.AND.IBAND.EQ.1) THEN
         CALL BAND(TRACE2,NTRACS,NXINT,NSAMS,S
     &            ,FFTEMR,FFTEMI,NFFT,JJ,KK,J,K)
      ELSE IF (IDECO.EQ.2) THEN
          ANGFIL = 0.0
          CALL DECON(TRACE2,NTRACS,NXINT,NSAMS,ANGFIL,S
     &              ,FFTEMR,FFTEMI,NFFT,JJ,KK,J,K,IBAND)
      ENDIF
C
C preliminary sort
C
      CALL PRESRT(NSHIFT,ANGRAN,VSURF,VGRAD,IDECO,DECINC,NSTNOB,NENNOB
     &                          ,C,XINT,SAMINC,IANGRA,IDECIN,ASNELL)
C
C angular window params
C
      RANGRA = ANGRAN*PI/180.0
      CORNER = RANGRA*4.0/5.0
      MCOUNT = 0
C
C-----------------------------------------------------------------------
C main loops
C-----------------------------------------------------------------------
C
      DO 700 MANG = IANGRA,-IANGRA+IDECIN,-IDECIN
         PRINT*,'MANG ',MANG,'----------------------'
         MCOUNT = MCOUNT+1
         IF (IDECO.EQ.1) THEN
            ANGFIL = FLOAT(MANG)-FLOAT(IDECIN)/2.0
            CALL DECON(TRACE2,NTRACS,NXINT,NSAMS,ANGFIL
     &                ,S,FFTEMR,FFTEMI,NFFT,JJ,KK,J,K,IBAND)
         ENDIF
         ICALL = 1
         DO 200 I=NSTNOB,NENNOB
            INOB = I-NSTNOB+1
            NSHMA = NSHIFT(MCOUNT,INOB)
            NSHMI = NSHIFT(MCOUNT+1,INOB)
            IF (NSHMA.EQ.9999.OR.NSHMI.EQ.9999) GOTO 200
            NCOUNT(I) = NCOUNT(I)+1
            B = (I-1)*SAMINC
            Z = VSURF/VGRAD*(EXP(VGRAD*B) 1.0)
            VZ = VSURF+VGRAD*Z
            VSURSQ = VSURF*VSURF
            VGRASQ = VGRAD*VGRAD
            DO 554 NSH = NSHMA,NSHMI+1,-1
               XSHIFT = FLOAT(NSH)*XINT
C tt source
               XSOU = XSHIFT+C
               XSOUSQ = XSOU*XSOU
               FAC = 4*VGRASQ*XSOUSQ*VSURSQ
               BOT = ((Z*VGRAD+VSURF)**2-VSURSQ+VGRASQ*XSOUSQ)**2
               ANGS = SQRT(FAC/(FAC+BOT))
               IF (ABS(ANGS).GT.1.0) GOTO 554
               ANGS = ASIN(ANGS)
               ANGZ = VZ*SIN(ANGS)/VSURF
               IF (ABS(ANGZ).GT.1.0) GOTO 554
               ANGZ = ASIN(ANGZ)
               TS = 1.0/VGRAD*LOG(ABS(TAN(ANGS/2.0)/TAN(ANGZ/2.0)))
C tt rec
               XREC = XSHIFT-C
               XRECSQ = XREC*XREC
               FAC = 4*VGRASQ*XRECSQ*VSURSQ
               BOT = ((Z*VGRAD+VSURF)**2-VSURSQ+VGRASQ*XRECSQ)**2
               ANGR = SQRT(FAC/(FAC+BOT))
               IF (ABS(ANGR).GT.1.0) GOTO 554
               ANGR = ASIN(ANGR)
               ANGZ = VZ*SIN(ANGR)/VSURF
               IF (ABS(ANGZ).GT.1.0) GOTO 554
               ANGZ = ASIN(ANGZ)
               TR = 1.0/VGRAD*LOG(ABS(TAN(ANGR/2.0)/TAN(ANGZ/2.0)))
C twt
               YELLIP = ABS(TR)+ABS(TS)
C
               IF (NCOUNT(I).EQ.1.AND.NSH.EQ.NSHMA) GOTO 5540
               IF (ABS(YELLIP-TWTT(I)).GT.ANT) GOTO 5540
               IF (YELLIP.LT.0.0.OR.YELLIP.GT.YMAX) GOTO 554
               ALPHA = ANGS
               CALL HEIGHT(ALPHA,CORNER,RANGRA,YELLIP,AMPLIT)
               DO 650 N=1,NTRC
                  NXELL= NTRST+N+NSH-1
                  IF (NXELL.GE.1.AND.NXELL.LE.NXINT) THEN
                     CALL INTERP(NXELL,YELLIP,TRACE2,NTRACS
     &                          ,NSAMS,XINT,YINT,VALUE)
                     VALUE = VALUE*AMPLIT
                     VALINT(N,I) = VALINT(N,I)+VALUE
                  ENDIF
 650           CONTINUE
 5540          TWTT(I) = YELLIP
 554        CONTINUE
 200     CONTINUE
 700  CONTINUE
C
C weight and write migrated array to file
C
      DO 411 I=1,NTRC
         DO 412 J=1,NENNOB
            VALINT(I,J) = J*VALINT(I,J)
 412     CONTINUE
         WRITE(2) (VALINT(I,J),J=1,NENNOB)
 411  CONTINUE
C
      STOP
      END
C
      SUBROUTINE RDCFIL(ANGRAN,VSURF,VGRAD,IDIAGN,NXINT,NYINT,XINT,YINT
     &                 ,NTRC,TRCST,SAMINC
     &                 ,STNOB,OBS,C,TITDA
```

```
     &                  ,N1,N2,N3
     &                  ,NSOD,IDECO,DECINC,IBAND,F1,F2,F3,F4
     &                  ,JANS,NTRCS,TRACE2,NTRACS,NSAMS,TEMP)
C*****************************************************************
C
C DESCRIPTION:
C
C reads control file
C
      REAL*4 TRACE2(NTRACS,NSAMS),TEMP(NSAMS)
      CHARACTER*10 TITLE,TITDA
C
 993  FORMAT(10X,F7.2)
 994  FORMAT(10X,I4)
 995  FORMAT(A10)
 997  FORMAT(10X,F7.2,F7.2)
C
      READ(14,993)    ANGRAN
      READ(14,993)     VSURF
      READ(14,993)     VGRAD
C
C diagnostic printout ?
C
      READ(14,994)    IDIAGN
C
C input array parameters
C
      READ(14,995)     TITLE
      READ(14,994)     NXINT
      READ(14,994)     NYINT
      READ(14,993)      XINT
      READ(14,993)      YINT
                        YINT=YINT*0.001
C
C migrated output window
C
      READ(14,995)     TITLE
      READ(14,994)      NTRC
      READ(14,993)     TRCST
      READ(14,993)    SAMINC
                      SAMINC=SAMINC*0.001
      READ(14,993)     STNOB
                       STNOB=STNOB*0.001
      READ(14,993)       OBS
                         OBS=OBS*0.001
C
      READ(14,995)     TITDA
      READ(14,993)         C
      IF (TITDA.EQ.'TANK') THEN
         READ(14,994)   NFOLD
         READ(14,994)    NOFF
         READ(14,994)   NSKIP
         READ(14,994)   NSOD
         NGATH = NXINT
         N1    = NFOLD
         N2    = NOFF
         N3    = NSKIP
         PRINT*,'CALLING CONSTO'
         CALL CONSTO(TRACE2,NTRACS,NSAMS,NFOLD,NOFF,NGATH,NSKIP,NSOD)
         PRINT*,'OUT OF CONSTO'
         PRINT*,' '
      ELSE IF (TITDA.EQ.'SEED') THEN
         READ(14,994)   NTEMP
         READ(14,994)   NPNTS
         READ(1) (TEMP(I),I=1,NTEMP)
         DO 842 I=1,NPNTS
            READ(14,227) LSTART,MSTART
 227        FORMAT(10X,I4,I4)
            DO 843 J=1,NTEMP
               TRACE2(LSTART,MSTART+J) = TEMP(J)
 843        CONTINUE
 842     CONTINUE
         N1 = NTEMP
         N2 = NPNTS
      ELSE
         DO 844 I=1,NXINT
            READ(1) (TRACE2(I,J),J=1,NYINT)
 844     CONTINUE
      ENDIF
C
      READ(14,994)     IDECO
C
      READ(14,994)     IBAND
      IF (IBAND.EQ.1) THEN
         READ(14,993) F1
         READ(14,993) F2
         READ(14,993) F3
         READ(14,993) F4
      ENDIF
C
         READ(14,993) DECINC
C
      READ(14,995) TITLE
      READ(14,994) JANS
C
      IF (JANS.NE.1) THEN
         READ(14,994) NTRCS
      ENDIF
C
      RETURN
      END
C
      SUBROUTINE PROUT(ANGRAN,VSURF,VGRAD,IDIAGN,NXINT,NYINT,XINT,YINT
     &                  ,NTRC,TRCST
     &                  ,NTRST,NSTNOB,NOBS,TRCINC,SAMINC,NENNOB
     &                  ,C,TITDA,N1,N2,N3,NSOD
     &                  ,IDECO,DECINC,IBAND,F1,F2,F3,F4,JANS,NTRCS)
C*****************************************************************
C
C DESCRIPTION:
C
C printout parameters
C
       CHARACTER*10 TITDA
C
       PRINT*,'Angle range '
       PRINT*,'------------'
       PRINT*,' limited to ',ANGRAN,' degrees take off angle'
       PRINT*,' '
       PRINT*,VSURF,' VELOCITY AT SURFACE '
```

```
      PRINT*,VGRAD,' VELOCITY GRADIENT   '
      PRINT*,' '
      PRINT*,'Migrated output'
      PRINT*,'---------------'
      PRINT*,'  X  : ',NTRC,' traces spaced at  ',TRCINC,'m  starting'
      PRINT*,'     at ',TRCST ,' m',' i.e trace no ',NTRST
      PRINT*,' '
      PRINT*,' Time: ',NOBS,' samples at ',SAMINC,'s  sample interval'
      PRINT*,'                              one way traveltime'
      PRINT*,'     window starts at  sample',NSTNOB,' ends at ',NENNOB
      PRINT*,' '
      PRINT*,' '
      PRINT*,'Input'
      PRINT*,'-----'
      PRINT*,'  X  : ',NXINT,' traces at  ',XINT,' m spacing '
      PRINT*,'  Y  : ',NYINT,' samples at ',YINT,' s sample interval'
      PRINT*,'       ',NSOD,' samples to skip to correct to SOD'
      PRINT*,' '
C
      IF (TITDA.EQ.'TANK') THEN
       PRINT*,' '
       PRINT*,'CONSTOFF PARAMS '
       PRINT*,'---------------'
       PRINT*,'OFFSET  ',C
       PRINT*,'NFOLD   ',N1
       PRINT*,'NOFF  which single offset to read  ',N2
       PRINT*,'NGATH no of gathers .traces in constoff sect  ',NXINT
       PRINT*,'NSKIP any gathers to skip ?  ',N3
       PRINT*,' '
      ELSE IF (TITDA.EQ.'SEED') THEN
       PRINT*,'TEST DATA'
       PRINT*,'**********'
       PRINT*,'HALF OFFSET ',C
       PRINT*,' '
       PRINT*,'signal has ',N1,' samples'
       PRINT*,'input array seeded with ',N2,' signals'
      ELSE
       PRINT*,'input array read from unformatted file'
      ENDIF
C
      IF (IBAND.EQ.1) THEN
       PRINT*,' '
       PRINT*,'BANDPASS  ',F1,' > ',F2,' > ',F3,' > ',F4,' Hz'
       PRINT*,' '
      ELSE
       PRINT*,' '
       PRINT*,'NO BANDPASSING'
       PRINT*,' '
      ENDIF
C
      IF (IDECO.EQ.1) THEN
         PRINT*,' '
         PRINT*,'------ DECON ----------'
         PRINT*,' angular increment  ',DECINC
         PRINT*,' '
      ELSE IF (IDECO.EQ.2) THEN
         PRINT*,' '
         PRINT*,'1-D DECON'
         PRINT*,' '
      ELSE IF (IDECO.EQ.0) THEN
         PRINT*,' '
         PRINT*,'NO DECON'
         PRINT*,' '
       ENDIF
C
        RETURN
        END
C
      SUBROUTINE PRESRT(NSHIFT,ANGRAN,VSURF,VGRAD,IDECO,DECINC,NSTNOB
     &                  ,NENNOB,C,XINT,SAMINC,IANGRA,IDECIN,ASNELL)
C*********************************************************************
C
C DESCRIPTION:
C
C calculates which part of operator to use when each angular
C deconvolution filter is used.
C
C
C
      REAL*4 NSHIFT(40,NENNOB)
C
      PI = 3.14159265
C
         IDECIN = NINT(DECINC)
         IANGRA = NINT(ANGRAN/DECINC)
         IF (FLOAT(IANGRA).LT.ANGRAN/DECINC) THEN
            IANGRA = (IANGRA+1)*IDECIN
         ELSE
            IANGRA = IANGRA*IDECIN
         ENDIF
         ANGRAN = FLOAT(IANGRA)
      PRINT*,' '
      PRINT*,'NEW ANGLES '
      PRINT*,'  ANGRAN ',ANGRAN
      PRINT*,'  IANGRA ',IANGRA
      PRINT*,'  IDECIN ',IDECIN
      PRINT*,' '
      MCOUNT = 0
      DO 550 MANG = IANGRA,-IANGRA,-IDECIN
         MCOUNT = MCOUNT+1
         PRINT*,MCOUNT,' MANG ',MANG
         ANGS = FLOAT(MANG)*PI/180.0
         ICALL =1
         DO 551 LDEPTH = NSTNOB,NENNOB
            DEPTH = FLOAT(LDEPTH-1)
            OWT = DEPTH*SAMINC
            Z = VSURF/VGRAD*(EXP(VGRAD*OWT)-1.0)
            VZ = VSURF+VGRAD*Z
            ANGZ = VZ*SIN(ANGS)/VSURF
            IF (ABS(ANGZ).GT.1.0) THEN
               NXSH =9999
               GOTO 5000
            ENDIF
            ANGZ = ASIN(ANGZ)
            RAYPAR = SIN(ANGS)/VSURF
            IF (RAYPAR.NE.0.0) THEN
               XSHIFT = 1.0/(RAYPAR*VGRAD)*(COS(ANGS)-COS(ANGZ))
            ELSE
               XSHIFT = 0.0
            ENDIF
```

```
            XSHIFT = XSHIFT-C
            NXSH = NINT(XSHIFT/XINT)
 5000       NSHIFT(MCOUNT,LDEPTH-NSTNOB+1) =NXSH
            IF (LDEPTH.EQ.NSTNOB.OR.LDEPTH.EQ.NENNOB) THEN
               IF (MCOUNT.EQ.1) THEN
                  PRINT*,LDEPTH,'INT. VEL  ',VZ
               ENDIF
               PRINT*,'          NXSH ',NXSH
            ENDIF
 551     CONTINUE
 550  CONTINUE
C
      RETURN
      END
```